



Woodham, Emma (2017) *Investigating the role of the Rho GTPase Cdc42 in the migration and invasion of the melanocyte lineage*. PhD thesis.

<http://theses.gla.ac.uk/8195/>

Copyright and moral rights for this work are retained by the author

A copy can be downloaded for personal non-commercial research or study, without prior permission or charge

This work cannot be reproduced or quoted extensively from without first obtaining permission in writing from the author

The content must not be changed in any way or sold commercially in any format or medium without the formal permission of the author

When referring to this work, full bibliographic details including the author, title, awarding institution and date of the thesis must be given

Enlighten:Theses
<http://theses.gla.ac.uk/>
theses@gla.ac.uk



Investigating the Role of the Rho GTPase Cdc42 in the Migration and Invasion of the Melanocyte Lineage

Emma Woodham

Cancer Research UK Beatson Institute

Thesis submitted for Degree of Doctor of
Philosophy

February 2017



University
of Glasgow

Abstract

Cell migration plays a central role during organismal development, and is essential for wound healing and immune cell defence in multicellular organisms. The ability of cells to move is largely underpinned by the actin cytoskeleton, which can be rapidly and dynamically assembled and disassembled in response to a host of intrinsic and extrinsic signals. To produce coordinated movement, the cell exerts a fine level of control over the actin cytoskeleton. Loss of control can lead to the development of many types of disease, including cancer. We therefore strive to discover the complex and multifaceted mechanisms controlling cell migration and invasion, in order to understand how and why cells move. This knowledge will help us to understand and explain important biological processes, and help us develop novel therapeutics for many types of disease.

During recent decades, one family of proteins have emerged as master regulators of the actin cytoskeleton. These are the Rho family of GTPases, which are small molecular switches controlled by guanine nucleotide hydrolysis. In their active state, they can affect a whole host of signalling pathways. The discovery of the classic family members Rac1, Cdc42 and RhoA, and their downstream targets revolutionised the way we understand cell migration. The individual molecular pathways downstream of Cdc42, Rac1 and other Rho GTPases are well documented, but we know surprisingly little about how these pathways are coordinated when cells move in a complex environment *in vivo*.

To further understand the role of Rho GTPases *in vivo*, we used the melanoblast journey through the developing mouse embryo as a model. In the developing embryo, melanoblasts originate from the neural crest, and must traverse the dermis to reach the epidermis of the skin and hair follicles where they become melanocytes. We previously established that Rac1 signals via SCAR/WAVE and Arp2/3 to effect pseudopod extension and migration of melanoblasts in skin. Here, we show that RhoA is redundant in the melanocyte lineage, but Cdc42 controls multiple motility systems independently of Rac1. Cdc42 null mice displayed a severe loss of pigmentation, and melanoblasts showed cell cycle progression, migration and cytokinesis defects. However, unlike Rac1 knockouts, Cdc42 null melanoblasts were elongated and displayed large, bulky pseudopods

with active actin dynamics. Despite assuming a shape usually associated with fast motility, Cdc42 knockout melanoblasts migrated slowly and inefficiently in the epidermis, with nearly static pseudopods.

By performing global RNA-sequencing on cultured primary melanocytes, we revealed alterations in expression of adhesion and lysosomal pathways in the absence of Cdc42. This correlated with fewer, less dynamic integrin-based adhesions in these cells along with a delay in cell spreading. In addition, in-depth molecular analysis revealed a mislocalisation of active myosin and branched actin regulators in Cdc42 null cells. Therefore, while Rac1 has a very specific role in signalling to branched actin network generation, we believe that Cdc42 coordinates multiple systems, such as actin polymerisation, adhesion dynamics and contractility, to achieve efficient migration.

In addition, we highlight a key role for Cdc42 in the invasion, but not the migration or proliferation of melanoma cells. We demonstrate that partial knockdown of Cdc42 in B16F10 melanoma cells does not lead to significant morphology changes, nor does it affect their 2D migration or proliferation. Surprisingly however, we demonstrate that these cells are less able to invade into *in vitro* invasion assays.

Declaration

I declare that all of the work in this thesis was performed personally. No part of this work has been submitted for consideration as part of any other degree or award.

Acknowledgements

Firstly I would like to thank my supervisor Laura Machesky for giving me the opportunity to undertake a PhD under her guidance. She is an exceptional role model and was always enthusiastic towards my work. I appreciate the respect and guidance she provided me with over the last four years and I am very thankful to have been her student. I would also like to thank Cancer Research UK for funding my work and providing me with a fantastic environment to complete my research training.

I am also extremely grateful to my fellow lab members. This work would not have been possible with their constant help and guidance, particularly the post-doctoral researchers Ben Tyrrel, Nikki Paul and Karthic Swamanithan and our Scientific Officer Heather Spence, whom I worked closely with. They, along with the other group members past and present were always generous with their time and willing to answer my questions. Special thanks also goes to my advisor Robert Insall and his lab for their helpful discussions and support. I also would like to thank my summer student Shelly Scribner, who carried out some of this work. The Machesky and Insall groups are not just colleagues, but extremely close friends, never failing to put a smile on my face during difficult times, usually with lots of cake! I would particularly like to thank Clelia Amato for daily warm Italian greetings and hugs, and fellow students Micheala Mrschtik and Evangelos Giampazolias for sharing this experience with me. I am also extremely grateful for the lovely support staff at the Beatson, for making it a warm and friendly place to work. I particularly want to thank Margaret O'Prey not only for training me at the imaging facility, but for being a great friend.

Completing this PhD was a huge challenge for me, one which I wouldn't have managed without fantastic friends. I firstly want to thank Marie Indahl and Alix Healey for being the best flatmates, never failing to cheer me up during the evenings, I will always remember our time at Broomhill. I am also grateful to Fiona Macleod, Aisling O'Conner and many others for their friendship and good times during the last four years. And to my best friends Katherin Shippin and Olivia Duthie, for your love and kindness during particularly difficult times, for always being there for me, encouraging and believing in me.

I am also hugely grateful to my parents Colin and Mary, and to my brother Gordon for everything you have done for me. Also my Uncles, Grandparents and wider family for your support and belief in me and what I can achieve. I would finally like to express my gratitude to my boyfriend Anthony. For his love and support during the years we spent apart to complete my PhD, for making me happy no matter what.

I would like to dedicate this thesis to my Grandad, Dr Anthony Arthur Woodham, who sadly passed away at the beginning of my PhD.



Publications

WOODHAM, E. F.*, PAUL, N.P.*, TYRRELL, B., SPENCE, H.J., SCRIBNER, M.R., GIAMPAZOLIAS, E., HEDLEY, A., CLARK, W., KAGE, F., MARSTON, D.J., HAHN, K.M., TAIT, S.W.G, LARUE, L., BRAKEBUSCH, C., INSALL, R.H., & LAURA M. MACHESKY. Coordination by Cdc42 of actin, contractility and adhesion for melanoblast movement in mouse skin. (Current Biology, in press)

GIAMPAZOLIAS, E., ZUNINO.B., DHAYADE, S., LOPEZ, J., ICHIM, G., PROICS, E., RUBIO-PATINO,C., FORT, L., YATIM, N., WOODHAM, E.F., OROZCO, S., LECIS, D., MACHESKY, L.M., MILLING, S., OBERST, A., RICCI, J.E., RYAN, K., BLYTH, K., & STEPHEN W.G. TAIT. Mitochondrial permeabilisation engages NFκB and anti-tumour activity under caspase-deficient conditions. (Revisions ongoing, Nature Cell Biology)

TYRRELL, B. J., WOODHAM, E. F., SPENCE, H. J., STRATHDEE, D., INSALL, R. H. & MACHESKY, L. M. 2016. Loss of strumpellin in the melanocytic lineage impairs the WASH Complex but does not affect coat colour. *Pigment Cell Melanoma Res.*

WOODHAM, E. F. & MACHESKY, L. M. 2014. Polarised cell migration: intrinsic and extrinsic drivers. *Curr Opin Cell Biol*, 30, 25-32.

LI, A., MORTON, J. P., MA, Y., KARIM, S. A., ZHOU, Y., FALLER, W. J., WOODHAM, E. F., MORRIS, H. T., STEVENSON, R. P., JUIN, A., JAMIESON, N. B., MACKAY, C. J., CARTER, C. R., LEUNG, H. Y., YAMASHIRO, S., BLYTH, K., SANSOM, O. J. & MACHESKY, L. M. 2014. Fascin is regulated by slug, promotes progression of pancreatic cancer in mice, and is associated with patient outcomes. *Gastroenterology*, 146, 1386-96 e1-17

Abbreviations

Arp2/3	Actin related protein 2/3
ARPC1-5	Actin related protein 2/3 complex subunit 1-5
Brdu	5-Bromo-2'-deoxyuridine
BSA	Bovine serum albumin
Cdc42	Cell division control protein 42 homolog
CDKN2	Cyclin dependent kinase inhibitor
COPI	Coat protein 1
Cre	Cre recombinase
DAPI	4',6-diamidino-2-phenylindole
DCT	Dopachrome tautomerase
DMEM	Dulbecco's modified eagle medium
DMSO	Dimethyl sulfoxide
DRF	Diaphanous-related formins
ECM	Extracellular matrix
EEA1	Early endosomal antigen 1
EMT	Epithelial to mesenchymal transition
Ena/VASP	Enabled/vasodilator-stimulated phosphoprotein
ERK	Extracellular signal-regulated kinase
FAK	Focal adhesion kinase
FBS	Foetal Bovine Serum
FLIM	Fluorescence lifetime imaging microscopy
FRET	Fluorescence resonance energy transfer
GAPDH	Glyceraldehyde 3-phosphate dehydrogenase
GDI	Guanine nucleotide dissociation inhibitor
GDP	Guanosine diphosphate
GEF	Guanine nucleotide exchange factor
GAP	GTPase activating protein
GFP	Green fluorescent protein
GSK3B	Glycogen synthase kinase 3 beta
GTP	Guanosine triphosphate
HBSS	Hank's Buffered Salt Solution
HBS	HEPES buffered saline
HCl	Hydrochloric acid

IQGAP	Ras GTPase-activating-like protein
Kit	Kit receptor tyrosine kinase
KitL	Kit ligand
mDia	mouse Diaphanous-related formin
MITF	Microphthalmia-associated transcription factor
MLC	Myosin light chain
MMP	Matrix metalloproteinase
MRCK	Myotonic dystrophy kinase-related Cdc42-binding kinase
MTOC	Microtubule organising centre
NC	Neural crest
NPF	Nucleation promoting factor
WASH	WASP and SCAR homologue
WASP	Wiskott-Aldrich syndrome protein
N-WASP	Neural Wiskott-Aldrich syndrome protein
OHT	4-hydroxytamoxifen
Pak	p21 activated kinase
PAR1	Partitioning defective 1
PAR3	Partitioning defective 3
PBS	Phosphate Buffered Saline
PE	PBS/EDTA
PFA	Paraformaldehyde
Rac	Ras-related C3 botulinum toxin substrate
Pax3	Paired domain and homeodomain-containing transcription factor
Rho	Ras homolog gene family
RhoA	Ras homolog gene family member A
ROCK	Rho kinase
RTK	Receptor tyrosine kinase
SCP	Schwann cell precursor
Sox10	SRY (sex determining region Y)-box 10
TAE	Tris-acetate-EDTA
TAZ	Transcriptional coactivator with a PDZ-binding domain
TE	Tris-EDTA
TBST	TBS Tween
VCAM-1	Vascular cell adhesion protein 1

WASP	Wiskott-Aldrich syndrome protein
WAVE	WASP family verprolin homologous
Wnt3a	Wnt family member 3a
YAP	Yes associated protein
X-Gal	5-bromo-4-chloro-3-indolyl- β -D-galactopyranoside

Table of Contents

Abstract	ii
Declaration	iv
Acknowledgements	v
Publications	vii
Abbreviations	viii
List of Figures and Tables	xiv
1 Introduction.....	1
1.1 Cell migration modes and the actin cytoskeleton	1
1.1.1 The cytoskeleton and cell movement	1
1.1.2 Actin Polymerisation	1
1.1.3 2D cell migration	2
1.1.4 3D cell migration	8
1.1.5 Adhesions and cell migration	11
1.1.6 The actin cytoskeleton and cancer metastasis.....	13
1.2 The Rho GTPase family and Cdc42.....	17
1.2.1 The Rho GTPase family	17
1.2.2 Rho GTPases coordinate cell migration	20
1.3 Cdc42 in cell migration.....	24
1.3.1 Cdc42 activation and effectors.....	24
1.3.2 Cdc42 and polarity	25
1.3.3 Cdc42 and mammalian cell division	28
1.3.4 Cdc42 in invasion and cancer	29
1.4 Melanoblasts and the melanocyte lineage.....	31
1.4.1 Melanoblast specification	32
1.4.2 The melanoblast journey	34
1.4.3 Melanoblasts from Schwann cells: a second wave.....	38
1.4.4 Melanoblasts to melanoma.....	40
2 Materials and Methods	43
2.1 Materials.....	43
2.1.1 Reagents and solutions	43
2.1.2 Antibodies and Dyes	45
2.1.3 Kits.....	46
2.1.4 DNA Constructs.....	47
2.1.5 Oligos	47
2.1.6 RNA Sequences	47
2.2 Methods	48
2.2.1 Mouse strains and genotyping.....	48
2.2.2 Cell culture	49
2.2.3 SDS-PAGE and western blotting	51
2.2.4 Immunofluorescent staining of cells and immunohistochemistry	52
2.2.5 Cloning and molecular biology.....	54
2.2.6 Embryo study techniques.....	55
2.2.7 Cell biology techniques	57
2.2.8 RNA Sequencing.....	61
3 Investigating the Role of Cdc42 in Melanoblast Migration and Proliferation.....	64
3.1 Introduction and aims	64
3.2 Results	66
3.2.1 Loss of Cdc42 in the melanocyte lineage leads to coat colour defects, suggesting migration and proliferation defects	66
3.2.2 Loss of RhoA in the melanoblast lineage does not lead to coat colour defects.....	69

3.2.3	Cdc42-null melanoblasts fail to fully populate the developing mouse embryo before birth	69
3.2.4	Cdc42 controls melanoblast cell-cycle progression and cytokinesis	79
3.2.5	Cdc42 is not required for melanoblasts to cross the basement membrane into the epidermis	81
3.2.6	Loss of Cdc42 uncouples actin dynamics and pseudopod extension from migration	84
3.2.7	Loss of Cdc42 and Rac1 from the melanoblast lineage leads to death at birth and a reduction in melanoblast number	94
3.3	Discussion	97
3.3.1	Cdc42 is necessary for melanoblast population of the developing embryo before birth	97
3.3.2	Cdc42 controls melanoblast proliferation by promoting S phase entry and aiding cytokinesis	98
3.3.3	Loss of Cdc42 uncouples actin dynamics and pseudopod extension from migration	99
3.3.4	Loss of RhoA in the melanoblast lineage does not lead to coat colour defects.	100
3.3.5	Rac1 and Cdc42 double knockout melanoblasts fail to populate the developing embryo.....	100
3.4	Summary	101
4	Investigating the Role of Cdc42 in Melanocyte Migration and Proliferation	102
4.1	Introduction and aims	102
4.2	Results	103
4.2.1	Knock-down of Cdc42 in cultured melanocytes leads to migration and proliferation defects.....	103
4.2.2	Isolation of an inducible Cdc42 knockout primary melanocyte cell line	103
4.2.3	Primary melanocytes require Cdc42 for efficient pseudopod extension and ruffling	107
4.2.4	Expression levels of Cdc42 effectors and other actin regulators is unchanged in knockout cells	114
4.2.5	Cdc42 controls the localisation of P-MLC in primary melanocytes.....	117
4.2.6	Cdc42 controls the activation and nuclear accumulation of YAP, but not its response to serum starvation.....	119
4.2.7	Knockout protrusions are not solely dependent on microtubules, formins or Arp2/3 to form	122
4.2.8	Cdc42 promotes G1 to S transition and is necessary for efficient cytokinesis in melanocytes.....	124
4.3	Discussion	130
4.3.1	Cdc42 is essential for normal pseudopod dynamics and migration in melanocytes, as in their melanoblast precursors	130
4.3.2	Cdc42 coordinates the regulators of branched actin networks, but not the activation of Rac1	130
4.3.3	Cdc42 controls cell contractility by directing the location of myosin light chain phosphorylation	131
4.3.4	Cdc42 controls YAP nuclear accumulation but abrogation of YAP signalling does not affect melanocyte morphology	132
4.3.5	Knockout protrusions are not dependent on microtubules, Arp2/3 or formins to extend	133
4.3.6	Cdc42 promotes G1 to S transition and controls cytokinesis in melanocytes.....	134
4.4	Summary	135
5	Cdc42, Melanocyte Gene Expression and Coordination of Adhesion Dynamics	137
5.1	Introduction and aims	137

5.2 Results	138
5.2.1 RNA sequencing of Cdc42 knockout melanocytes reveals global changes in diverse signalling networks	138
5.2.2 Cdc42 controls melanocyte adhesion number, size and lifetime	146
5.2.3 Defects in adhesion and filopodia formation delay the spreading of Cdc42 knockout cells	149
5.3 Discussion	155
5.3.1 Loss of Cdc42 alters the expression of diverse signalling pathways including up-regulation of lysosomal proteins	155
5.3.2 Cdc42 controls the expression of genes involved in focal adhesion pathways..	156
5.3.3 Cdc42 controls adhesion formation and dynamics to support migration and spreading	157
5.4 Summary	160
6 Investigating the role of Cdc42 in Melanoma Migration and Invasion	161
6.1 Introduction and aims	161
6.2 Results	162
6.2.1 Knockdown of Cdc42 in B16F10 melanoma cells does not effect cell morphology, migration or proliferation.....	162
6.2.2 Cdc42 knockdown slows the invasion on B16F10 melanoma cells.....	166
6.3 Discussion	169
6.3.1 B16F10 Melanoma migration and proliferation are not affected by Cdc42 knockdown	169
6.3.2 Cdc42 aids melanoma cell invasion	169
6.4 Summary	170
7 Conclusions and Future Directions	171
7.1 Conclusions	171
7.1.1 Cdc42 and Rac1 have important and distinct roles during the melanoblast journey, but RhoA is not required	171
7.1.2 Cdc42 coordinates the spatial positioning of key actin regulators to facilitate migration	173
7.1.3 Cdc42 promotes G1 to S cell cycle transition and cytokinesis.....	173
7.1.4 Cdc42 coordinates adhesion dynamics and actin polymerisation to drive migration	174
7.1.5 Cdc42 aids melanoma invasion	175
7.2 Future Directions	175
7.2.1 How do melanoblasts achieve orchestrated population of the developing embryo?.....	175
7.2.2 Is the lysosomal network affected in Cdc42 knockout melanocytes?.....	177
7.2.3 Which pathways link Cdc42 to adhesion dynamics?	180
7.2.4 Does Cdc42 control invasion <i>in vivo</i> ?	182
8 References	183
9 Appendix	193

List of Figures and Tables

Figure 1.1 Actin polymerisation geometry controls the formation of different actin based structures for motility.....	3
Figure 1.2 Cell Migration in 2D	5
Figure 1.3 Cells use diverse migration modes to navigate 3D environments.....	9
Figure 1.4 Integrin-based adhesions and signalling	14
Figure 1.5 The metastatic cascade	16
Figure 1.6 The Rho GTPase family	19
Figure 1.7 The GTPase activation cycle	21
Figure 1.8 Rho GTPases coordinate cell migration.....	23
Figure 1.9 Cdc42 integrates multiple signalling inputs into diverse cellular effects	26
Figure 1.10 Cdc42 and invasion	30
Figure 1.11 Melanoblast specification and migration during mouse embryonic development.....	33
Figure 1.12 Melanoblast population of the developing embryo.....	35
Figure 1.13 Melanoblasts use pseudopods to migrate between keratinocytes ...	37
Figure 1.14 The peripheral nerve: a novel melanoblast source during development.....	39
Figure 1.15 Melanoma Progression	41
Figure 3.1 Loss of Cdc42 in the melanoblast lineage leads to coat colour defects in adult mice	67
Figure 3.2 Melanocytes are not present in the hair follicles of hypopigmented areas	68
Figure 3.3 Deletion of RhoA from the melanoblast lineage does not result in any coat colour defects.....	70
Figure 3.4 Gene strategy to achieve melanoblast-specific expression of β -galactosidase to track the melanoblast journey	71
Figure 3.5 Loss of Cdc42 does not affect melanoblast number at E11.5	73
Figure 3.6 Cdc42 controls the number and position of melanoblasts around the belly at E13.5.....	74
Figure 3.7 Cdc42 controls the number and position of melanoblasts down the developing limb at E13.5	75
Figure 3.8 Cdc42 controls the number and position of melanoblasts around the belly at E15.5.....	77
Figure 3.9 Cdc42 controls the number and position of melanoblasts down the developing limb at E15.5	78
Figure 3.10 Cdc42 null melanoblasts are in the cell cycle, but fewer are in S-phase	80
Figure 3.11 Loss of Cdc42 in melanoblasts and melanocytes leads to an extended division time due to a cytokinesis defect	82
Figure 3.12 Cdc42 knockout melanoblasts are able to cross from the dermis into the epidermis during development.	83
Figure 3.13 Gene strategy to achieve melanoblast specific expression GFP to image live melanoblast migration through skin.....	85
Figure 3.14 Cdc42 null melanoblasts have a striking elongated and bleb-like morphology as they move through the skin.....	86
Figure 3.15 Cdc42 null melanoblasts display less-dynamic pseudopods and have a 'bi-polar' morphology.....	88

Figure 3.16 Cdc42 null melanoblasts have an altered morphology and defects in pseudopod dynamics	89
Figure 3.17 Loss of Cdc42 in melanoblasts leads to less efficient migration	90
Figure 3.18 Gene strategy to achieve melanoblast-specific expression of Lifeact-GFP to image live actin dynamics	92
Figure 3.19 Actin bursts can be seen at the tips of knockout pseudopods	93
Figure 3.20 Gene strategy to achieve melanoblast targeted double knockout of both Rac1 and Cdc42	95
Figure 3.21 Loss of both Cdc42 and Rac1 in the melanoblast lineage leads to death at birth and many fewer melanoblasts at E15.5	96
Figure 4.1 Knockdown of Cdc42 by siRNA leads to an elongated cell morphology and slows proliferation	104
Figure 4.2 Cdc42 knockdown melanocytes have a severe migration defect	105
Figure 4.3 Generation of an inducible Cdc42 knockdown melanocyte cell-line	106
Figure 4.4 Cdc42 is lost at the protein level after 5 days of OHT treatment ...	108
Figure 4.5 Cdc42 knockout melanocytes fail to make lamellipods and have pseudopod and migration defects	109
Figure 4.6 Actin branching machinery is poorly localised in knockout melanocytes	111
Figure 4.7 Levels of active Rac1 are modestly enhanced in the absence of Cdc42	113
Figure 4.8 Transient expression of Cdc42-YFP in Cdc42 knockout cells rescues cell morphology changes	115
Figure 4.9 Protein levels of Cdc42 regulators and actin related proteins were not altered in the absence of Cdc42	116
Figure 4.10 Knockout melanocytes have the same levels of phosphorylated-MLC but is differently localised	118
Figure 4.11 YAP phosphorylation is increased in the absence of Cdc42 leading to a decrease in nuclear YAP	120
Figure 4.12 Knockdown of YAP in melanocytes does not mimic loss of Cdc42 .	121
Figure 4.13 Microtubules are not essential to support the long thin protrusions made by knockout melanocytes, but they contribute to their bipolar nature	123
Figure 4.14 Cdc42 knockout melanocytes do not rely on formins to form protrusions or spread	125
Figure 4.15 Knockout melanocytes can still spread in the presence of Arp2/3 inhibitor and cells are less bi-polar	126
Figure 4.16 Cdc42 is required for cell-cycle transition from G1 to S-phase	127
Figure 4.17 Cdc42 knockout melanocytes have an extended division time and cytokinesis defect	129
Figure 5.1 RNA sequencing of Cdc42 knockout melanocytes implicates Cdc42 in the expression of diverse signalling components	139
Figure 5.2 Genes involved in lysosomal networks are up-regulated in the absence of Cdc42	141
Figure 5.3 Genes involved in pathways in cancer and focal adhesion signalling are down-regulated in the absence of Cdc42	142
Figure 6.1 Cdc42 is successfully knockout-down in B16F10 melanoma shRNA cell lines	163
Figure 6.2 Knock-Down of Cdc42 does not change B16F10 melanoma cell morphology, proliferation or migration	164
Figure 6.3 Knock-down of Cdc42 does not impair the ability of B16F10 melanoma cells to close a wound	165

Figure 6.4 Knock-down of Cdc42 impairs the ability of B16F10 melanoma to invade into matrigel.....	167
Figure 6.5 Expression of Cdc42 shRNA impairs B16F10 melanoma cell invasion into Matrigel.....	168
Figure 7.1 Rac1 null and Cdc42 null melanoblasts have different morphologies but both migrate more slowly than wild-type melanoblasts.....	172
Figure 7.2 Rho GTPases act in a coordinated manner to achieve coordinated cell migration.....	176
Figure 7.3 Staining for various markers of the vesicular network reveals no gross abnormalities.....	178
Figure 7.4 Cdc42 null melanocytes have a large, highly acidic compartment and overall have a higher pH than control cells	181

Table 1 Reagents and solutions	43
Table 2 Antibodies and dyes.....	45
Table 3 Kits	46
Table 4 DNA constructs.....	47
Table 5 Oligos.....	47
Table 6 RNA sequences.....	47
Table 7 Mouse stains and genotyping	48

1 Introduction

1.1 Cell migration modes and the actin cytoskeleton

1.1.1 The cytoskeleton and cell movement

Cell movement plays an essential role in the life of single and multi-cellular organisms. For example, the simple amoeba *Dictyostelium discoideum* moves in order to seek nutrients and to aggregate during development. Cell movement has maintained this central role in organismal survival throughout evolution, with multicellular organisms relying on highly orchestrated cell migration programmes during development and throughout their adult life. In early stages of development, large sheets of cells must migrate and fold over each other to complete gastrulation and dorsal closure. As the organism continues to develop, cells from the neural crest lineage migrate large distances until they reach their destination (Huang and Saint-Jeannet, 2004). Cell motility is also required in adult life for the migration of many types of immune cells to aid in the immune response, and during wound healing. The cell's diverse cytoskeletal components underpin its ability to migrate. Providing the force behind migration is the actin cytoskeleton, which can be dynamically assembled and shaped by a diverse array of actin binding proteins (Insall and Machesky, 2009). However, cancer cells hijack this powerful system to help them spread to new areas of the body. Cancer metastasis is defined as one of the hallmarks of cancer (Hanahan and Weinberg, 2000), and is the most common cause of cancer related death (Sporn, 1996).

1.1.2 Actin Polymerisation

Polymerisation of actin monomers (G-actin) into filamentous actin (F-actin) provides protrusive force directly underneath the plasma membrane. F-actin is in a constant state of flux, with G-actin monomers being added at the barbed 'plus' end of the filament, antagonising depolymerisation at the 'minus' end (Pollard and Cooper, 2009). Polymerisation can be induced either by increasing the rate of monomer addition onto plus ends, severing filaments to create new barbed ends, or by nucleating new filaments. Clustering of monomers to create a new filament is called 'nucleation', and there is a kinetic barrier on this process. It is therefore aided by nucleation promoting factors (NPFs) that help

overcome this barrier by keeping the monomers and filament in direct proximity (Insall and Machesky, 2009)

When forming new filaments, the cell can extend linear filaments forming long straight filaments, or to nucleate a new filament on the side of an existing one, resulting in the formation of a new filament at a 70° angle to the existing one (Olson and Sahai, 2009). This choice, executed by the type of nucleation proteins recruited, will ultimately dictate cell shape and therefore motility. Stated simply, recruitment of formin homology proteins (FH) or members of the Ena/VASP family will lead to extension of linear filaments at the 'barbed' ends. With the help of actin bundling proteins such as fascin, these linear filaments can be grouped into slender actin structures called filopodia that protrude from the cell (Jacquemet et al., 2015) (Figure 1.1).

Alternatively, recruitment of the Arp2/3 complex to the sides of existing filaments leads to the formation of a branched network. This 7-member complex consists of two actin related proteins Arp2 and Arp3 and five non-Arp components, p41/ARPC1, p34/ARPC2, p21/ARPC3, P20/ARPC4 and p16/ARPC5, which was the first barbed end actin nucleation factor to be identified, which was plausible as an effector of leading edge protrusion (Machesky et al., 1994). This branched network supports the formation of wide thin membrane extensions called lamellipoda (Nobes and Hall, 1995) (Figure 1.1). In addition to these two basic geometric choices, other actin-binding proteins add an additional layer of control over the actin network, allowing it to be moulded dynamically depending on the cell's needs. For example, actin-severing proteins such as cofilin can increase the number of barbed ends by cleaving existing filaments (Devreotes and Horwitz, 2015). We are still discovering new actin binding proteins, and elucidating the roles of others in controlling this complex system.

1.1.3 2D cell migration

1.1.3.1 Coordinating migration in 2D

We have learnt much about how cell migration is coordinated by investigating

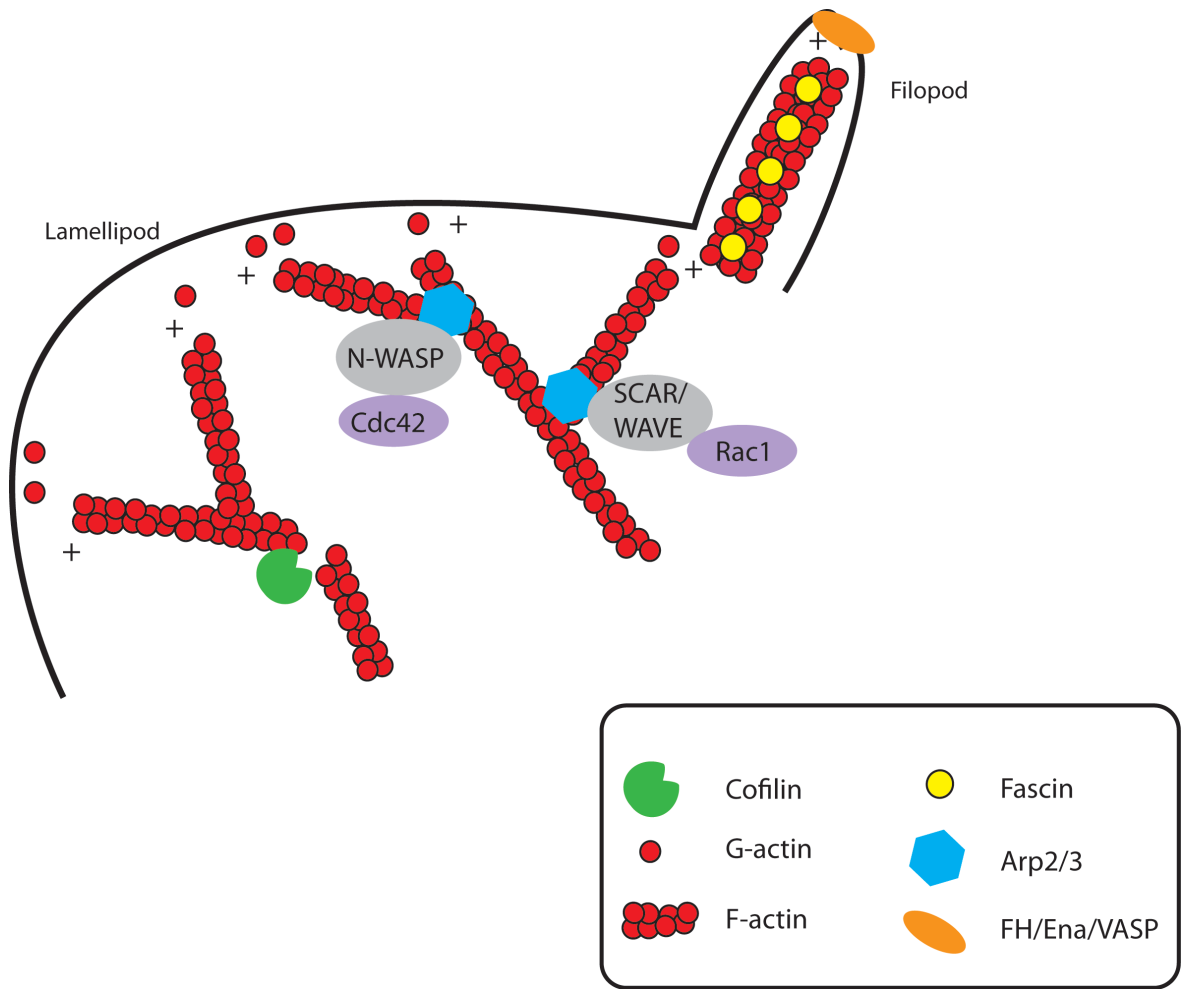


Figure 1.1 Actin polymerisation geometry controls the formation of different actin based structures for motility

F-actin filaments are polymerised from G-actin monomers underneath the membrane, generating protrusive force. The geometry of monomer addition and direction of filament growth are dependent on the nucleation promoting factor (NPF) that is recruited. Actin filaments are extended at the plus end in a linear fashion by members of the formin homology (FH) domain family, including Ena and VASP. These long actin filaments can then be bundled together by actin bundling proteins such as fascin, forming finger-like membrane protrusions called filopodia. Alternatively, monomers can be added to the side of filaments through recruitment of the Arp2/3 complex, resulting in filament extension at a 70° angle forming branched actin networks. The Arp2/3 complex requires the NPFs N-WASP or SCAR/WAVE to reach maximal activation. These NPFs are in turn activated by the Rho family GTPases Cdc42 or Rac1. Cleavage of actin filaments by cofilin creates new barbed ends for monomer addition.

cell migration along 2D surfaces. In this context, multiple cell types undergo a cycle of events to achieve efficient movement. First, the cell extends a lamellipod, driven by actin polymerisation below the membrane. It is essential that this extension is supported underneath by the formation of nascent adhesions that connect the cytoskeleton with the extracellular matrix (ECM) (Le Clainche and Carlier, 2008). These adhesions also form a positive feedback loop, encouraging extension of the protrusion (Ridley, 2015). The cell then creates force for translocation using myosin motors, moving the cell body and nucleus in the direction of travel. Finally, the cell must release adhesions at its rear as it moves forward. To achieve persistent and efficient movement these processes must be coordinated in time and space (Figure 1.2).

By studying cells moving in a 2D environment, we are beginning to unravel the complex mechanisms and protein families that control this process. Cells receive signals from their environment that provide migration cues in the form of chemoattractants, chemokines and growth factors. These signals bind to and activate receptors on the cell membrane, initiating signalling cascades that ultimately lead to moulding of the actin cytoskeleton and adhesion formation. The Rho family of GTPases are key convergence points for these signalling inputs. These molecular switches receive and integrate these signals into downstream responses by activating effector proteins (Raftopoulou and Hall, 2004). Rho GTPases can control actin polymerisation through activation of the WASP family of proteins. These proteins act as scaffolds, activating the Arp2/3 complex to generate branched actin filaments, forming lamellipodia. In addition, Rho GTPases can activate formin homology domain proteins and those from the Ena/VASP family to promote the extension of linear filaments, forming filopodia. These are the two key actin-based structures that cells utilise to migrate along a 2D substratum (Figure 1.1).

1.1.3.2 Lamellipodia

These actin based fan-like protrusions are used by many cell types to move and spread in 2D. Though it is difficult to assign formation of a structure to one Rho

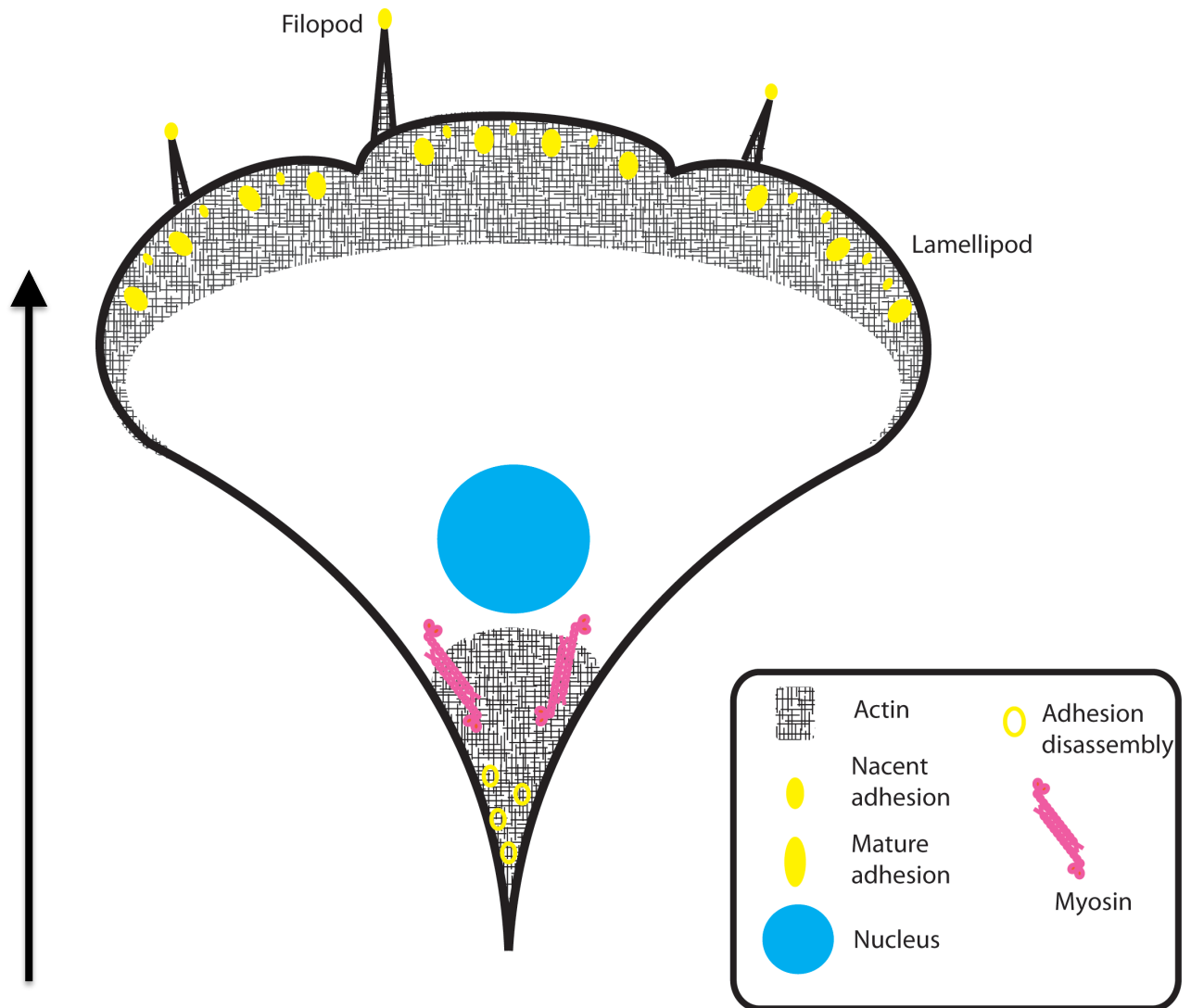


Figure 1.2 Cell Migration in 2D

Cells migrating in 2D adhere to the substratum on their ventral side. In order to migrate, cells progress through a migration cycle. Firstly, the cell extends a lamellipodium, a large thin fan-like protrusion which can often contain thin finger like protrusions called filopodia. These extending lamellipodia and filopodia are then supported underneath by nascent adhesions, which in time can mature into larger focal adhesions. To complete this cycle, the cell rear must retract through myosin contraction, and adhesions must be disassembled.

GTPase family member, lamellipodium formation is most commonly associated with Rac1 activity (Ridley and Hall, 1992). At the membrane, this GTPase can induce the formation of branched actin networks by activation of the Arp2/3 complex through the SCAR/WAVE complex, which is a member of the WASP family of nucleation promoting factors (NPFs) (Insall and Machesky, 2009). WASP proteins all contain a highly conserved C-terminal VCA domain that promotes the actin nucleating activity of the Arp2/3 complex. The SCAR/WAVE complex consists of five subunits, SCAR/WAVE, HSPC300, Abi, Nap1 and Cyfip, and is the major NPF to activate the Arp2/3 complex in lamellipodia. Like other WASP family members, it acts as a scaffold, bringing Arp2/3 and G-actin into close proximity. This interaction speeds up the addition of new monomers onto the filament. We are still trying to understand the factors controlling this complex, and recently Chen et al. reported a novel family of around 120 membrane proteins containing a sequence motif that binds to a conserved sequence on the complex. This interaction face appears to be key to the organisation and dynamics of the actin cytoskeleton (Chen et al., 2014). In addition, the Arp2/3 complex can also be activated by N-WASP, another WASP family member that is activated by the Rho GTPase Cdc42. This interaction also contributes to endocytic processes at the plasma membrane (Insall and Machesky, 2009).

1.1.3.3 Filopodia

Many cell types extend these thin, finger-like structures when migrating in 2D. Filopodia can vary in length, number and lifetime, and are highly dynamic structures. They can be seen as spiky membrane protrusions, but can also form within the boundary of the membrane as straight ridges. We are still in the early stages of understanding these beautiful and delicate structures, and have yet to fully explain their role in cell migration.

Filopodia are composed of parallel actin filaments, tightly bundled by the actin bundling proteins such as fascin (Jacquemet et al., 2015). In contrast to lamellipodia, filopodia are produced by polymerisation of linear filaments from their tip, consisting of the barbed filament ends proximal to the plasma membrane. As discussed earlier, linear filaments are extended by formin homology proteins or members of the Ena/VASP family. These catalyse addition of actin monomers to the barbed ends while remaining attached to the filament

end, at the same time preventing capping proteins from binding (Kovar and Pollard, 2004). The Rho GTPase Cdc42 is most commonly associated with the formation of filopodia. Cdc42 can activate formin homology domain proteins such as mDia1, 2 and 3 (Raftopoulou and Hall, 2004). Microinjection of Cdc42 under the plasma membrane has been shown to induce filopod formation (Nobes and Hall, 1995). However, filopodia have been reported in Cdc42 null cells (Czuchra et al., 2005) so it appears Cdc42 can induce filopodia, but is not absolutely required for their formation. Filopodia that arise within branched lamellipodial networks could form from the bundling of existing networks by various actin-binding proteins. It is unknown whether these structures have a different role than filopodia that extend beyond the membrane.

The parallel nature of the filaments in these structures allows molecular motors such as myosin-X (MYO10) to transport components such as receptors to the tip of the filopod (Jacquemet et al., 2015). In addition, adhesions have been seen at the base, shaft and tip of filopods, suggesting that these structures could be acting as antennae for the cell, feeling around the surrounding environment and somehow relaying back this information to the cell. It is possible for example that filopodia could sense both the topology and stiffness of the surroundings, suggested by work that shows that filopodia are important for haptotaxis and not chemotaxis (Johnson et al., 2015). In support of this hypothesis, filopodia are often seen during cell spreading. Cells could employ these structures to gain information about the environment as the cell settles. Alternatively, filopodia could function as support cables to aid advancement of the lamellipod during spreading. In this context, adhesions mature after advancement of the lamellipod, suggesting that adhesions under filopodia could be nascent adhesions, providing initial attachment before full cell spreading (Wong et al., 2014). These structures have also been seen in cells migrating in three-dimensional environments, which will be explored later in this chapter. In the future, it would be interesting to gain a deeper understanding of these structures, and unravel the mechanism by which they communicate back to the cell.

1.1.4 3D cell migration

1.1.4.1 Cell migration in 3D

Historically, studying cell migration in 2D environments has helped us build an understanding of how the cytoskeleton is coordinated and controlled. We now face the challenge of applying and adapting this knowledge to cell migration in 3D. The challenges cells face to navigate through a complex 3D environment are of course very different to those in 2D. Cells in 3D are surrounded by, and communicate with other cells or matrices. Often, cells must squeeze through tight spaces or tunnel their way through barriers to reach their destination. With the advances in *in vivo* imaging techniques and the design of *in vitro* 3D matrices, we are beginning to understand the different ways cells navigate through 3D environments. As in 2D, different cell types move in different ways through the 3D environment. However, two popular modes of migration are emerging in the field and have been termed ‘mesenchymal’ and ‘amoeboid’ migration (Petrie and Yamada, 2016). Mesenchymal migration is a term used to generally describe migration dependent on adhesion, which uses actin based protrusion at the front. Amoeboid is less dependent on adhesion formation and uses contractile force to drive migration.

1.1.4.2 3D cell migration, degrading vs squeezing

It is clear from imaging cells moving in 3D that they favour different types of protrusions to those used for 2D migration. As already discussed, cells migrating in 2D often display large fan-shaped protrusions called lamellipodia. These structures are not often seen in 3D, with cells favouring chunkier protrusions that shall be referred to here as pseudopods. Pseudopods are actin driven, and are characteristic of a cell displaying a ‘mesenchymal’ phenotype (Figure 1.3). Similarly to lamellipods, actin polymerisation and protrusive force in pseudopods can be driven through the Arp2/3 SCAR/WAVE pathway, under the control of Rac1 (Li et al., 2011). These pseudopods can possess degradative abilities through secretion of membrane bound metalloproteases (MMPs) that cleave the surrounding ECM (Figure 1.3) (Friedl and Wolf, 2003). Cells undergoing mesenchymal motility are elongated in the direction of migration, for example

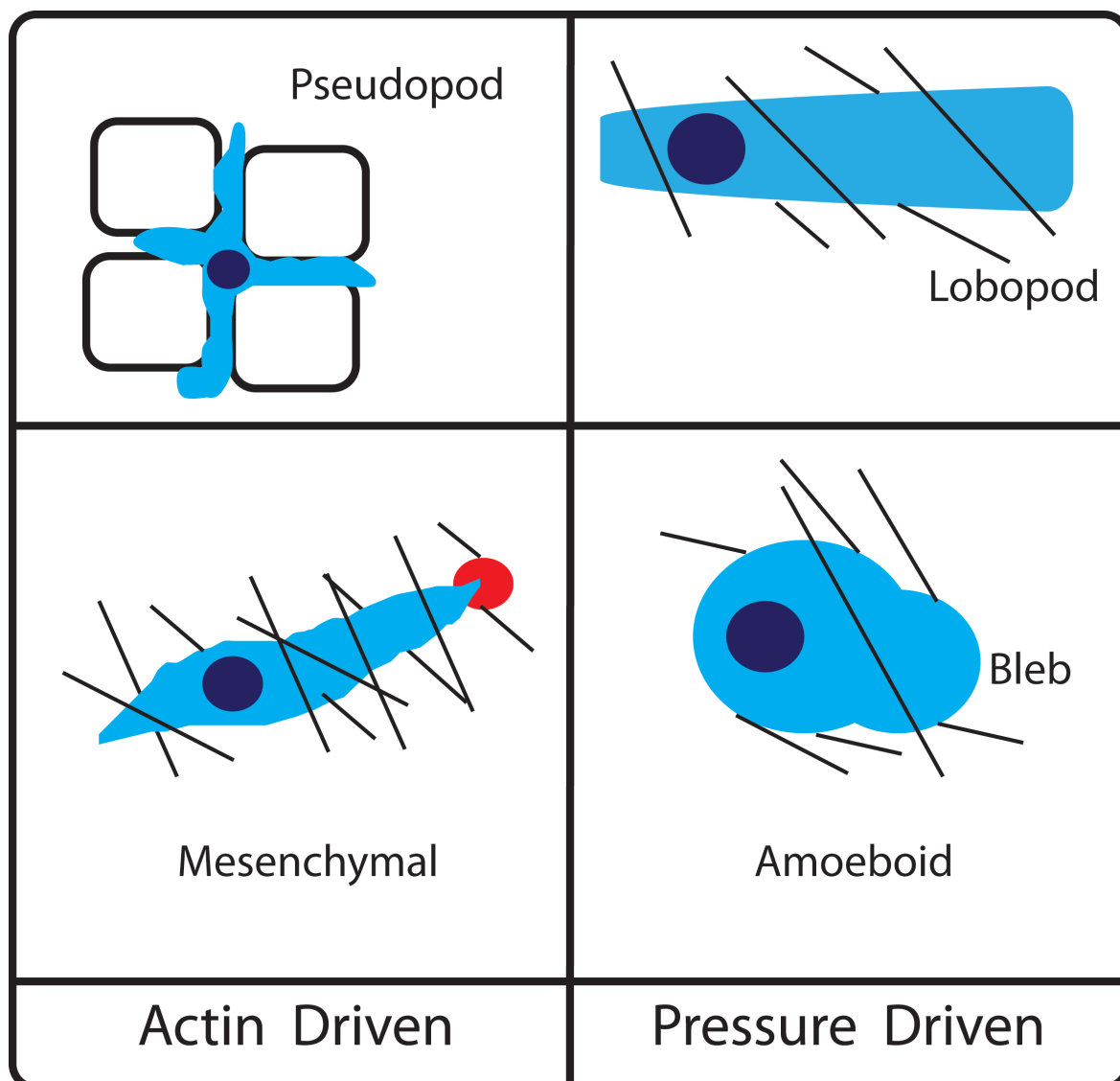


Figure 1.3 Cells use diverse migration modes to navigate 3D environments

The migration modes utilised by cells moving through three dimensions can be classified into actin driven and pressure driven. Cells migrating in an actin- dependent manner extend protrusions by actin polymerisation under the leading edge. For example, melanoblasts move through the developing embryo skin using actin-based pseudopods to squeeze between surrounding keratinocytes. The pseudopods of transformed or cancerous cells can acquire the ability to degrade the surrounding matrix (shown by black lines) by secreting matrix metalloproteinases (shown in red), which they use to hollow out a tunnel through which the cell can squeeze. This type of migration is displayed by MDA-MB-231 breast cancer carcinoma cells, and is thought to be classically mesenchymal. Cells can also navigate through the 3D environment independent of the protrusive force of the actin cytoskeleton. These cells migrate in a pressure-driven manner extending protrusions as a result of a build up of intracellular pressure. These modes of migration are more novel and less well understood, but are associated with elevated levels of Rho/ROCK signalling and myosin contraction. This migration mode is termed 'amoeboid migration'. A new type of protrusion has recently been associated with this protrusion, seen in fibroblasts, and have been termed 'lobopodia'.

MDA-MB-231 carcinoma cells (Yu et al., 2012). Filopodia appear to have an important function *in vivo* and can be seen extending from pseudopods and from sheets of cells (Li et al., 2014). Filopodia that extend from epithelial sheets during dorsal closure in flies appear to be crucial for efficient closure, with the filopods acting as a zip-like structure (Pickering et al., 2013). The expression of the actin bundling protein fascin is correlated with cancer invasion, suggesting that these structures could aid cancer cell invasion (Li et al., 2010).

However, cells can also move in 3D by primarily using force generated by contraction of the acto-myosin network. Initially, this migration mode termed 'amoeboid' migration was only thought to be utilised by a limited number of cell types; however, this mode of migration has now been seen in a diverse array of cell types. It is characterised by bubble-like protrusions that are driven by hydrostatic pressure (Figure 1.3) (Olson and Sahai, 2009). This mode is driven mainly by contractility generated by the GTPase Rho and its associated kinase ROCK. A new type of actin-dependent protrusion has been described, called 'lobopodial' protrusions. These protrusions have been seen in adherent fibroblasts, where they use intracellular pressure generated by acto-myosin contractility to extend a blunt, cylindrical protrusion (Figure 1.3) (Petrie et al., 2014). Interestingly, these cells are polarised and can sustain prolonged, directional movement.

A key study by Wolf et al. utilised degradable collagen lattices and nondegradable substrates with various pore sizes to study the parameters controlling migration through confined spaces (Wolf et al., 2013). They suggest that migration through 3D tissue is dependent on the cell's ability to deform and its capacity to degrade the ECM. The nucleus is highlighted as a key factor for migration of cells in 3D, and they hypothesise that a cell's success in traversing tight environments is its ability to deform the nucleus, the largest and most rigid organelle. When a deformation limit is reached, cells then depend on MMP mediated degradation to enlarge the pore in order to proceed.

It is likely that cells moving in 3D will use the most efficient migration method to proceed through the environment. Cells might therefore use aspects of 'mesenchymal' and 'amoeboid' motility, and these modes are better considered as a spectrum than two defined pathways. As actin regulators all partake in the

same feedback and feed-forward loops, it is unlikely that migration pathways are linear.

1.1.5 Adhesions and cell migration

Adhesions function as essential sites of contact between the intracellular cytoskeleton and the extracellular environment, containing multimolecular scaffolds and signalling complexes. Failure to establish functional adhesions can lead to disease, as they are essential during embryonic development, for tissue maintenance, host defence and homeostasis (Winograd-Katz et al., 2014). They are key to such a diverse array of processes as they provide the cell with information on its location, environment, adhesive state and matrix type. In addition to mediating the influx of signals from the environment, adhesions also provide a platform for the cell to signal to its environment in a bi-directional manner. Adhesions are fascinating and intricate structures, and we are still striving to understand the full range of adhesion components and the signalling networks surrounding these structures.

During migration, tiny nascent adhesions form underneath the advancing lamellipod, acting both to stabilise the protrusion and to facilitate migration (Swaminathan et al., 2016). As the cell advances and adhesions are put under tension, they can mature into larger focal or fibrillar adhesions (Gardel et al., 2010). These maturing adhesions facilitate polymerisation and retrograde flow of the actin cytoskeleton above to support the forward movement of the cells. We understand that this crosstalk between the polymerising actin above and the adhesion below must be subject to complex feedback and feed forward loops, but it still remains unclear exactly how this is coordinated

1.1.5.1 Integrin mediated adhesions and signalling

Adhesion complexes are most commonly built upon integrin heterodimers, which are the best characterised family of cell surface ECM receptors. Integrin heterodimers consist of non-covalently associated α and β subunits which are single pass type I transmembrane proteins. Various combinations of different integrin pairings bind to a diverse array of ECM components including fibronectin, laminin, collagen, thrombospondin, vitronectin, and to cell surface

adhesion molecules such as VCAM-1 (Humphries et al., 2006). Integrins can be described as allosteric receptors. Upon ligand binding, integrins can become activated by binding of activating proteins such as talin to the short cytoplasmic tail of the β integrin causing conformational changes (Outside-In signalling) (Calderwood, 2004) (Tadokoro et al., 2003). This binding and activation in turn leads to conformational changes in the integrin head groups, increasing integrin affinity for the ligand (Inside-out signalling). Multimolecular complexes then build on the cytoplasmic integrin tail, consisting of many different types of proteins including scaffold and signalling proteins, linking the adhesion site with the actin cytoskeleton.

In the past, many approaches have been taken to characterise the composition of adhesions, termed the 'integrin adhesome' but recent technological advances based on proteomics and advanced imaging techniques have begun to reveal the complexity of these structures. These approaches identify two- or three-fold more proteins than would be expected from the previous literature. Despite this complexity, a set of 'core' adhesion proteins is emerging, with the other non-canonical proteins often functioning in a cell-type manner and which are still being investigated (Horton et al., 2015, Humphries et al., 2015).

Members of the 'core' adhesome include talin, focal adhesion kinase (FAK), paxillin, vinculin, and α -actinin, which appear to commonly assemble around the tails of activated integrins (Harburger and Calderwood, 2009). As described earlier, talin functions to activate ligand bound integrins. It can only do this after it is freed from its autoinhibited head tail conformation by calpain-mediated proteolysis or by binding to phosphatidylinositol (4,5)-bisphosphate (PtdIns(4,5)P₂) (Calderwood, 2004, Goksoy et al., 2008). FAK, which can bind to talin and paxillin is a non-receptor tyrosine kinase and signalling scaffold regulated by phosphorylation. FAK contains a FERM domain, through which it can interact with the Arp2/3 complex (Serrels et al., 2007). Recently, this interaction has been shown to be necessary to couple nascent adhesions to lamellipodial actin (Swaminathan et al., 2016). Both FAK and the Arp2/3 complex can also bind to vinculin, which may also couple the actin cytoskeleton to adhesion sites (DeMali et al., 2002). Vinculin does not directly bind to β integrin tails but rather, through its interaction with other focal adhesion

proteins such as FAK, Arp2/3, α -actinin and paxillin, it plays an important role in adhesions. Vinculin null cells have spreading defects, enhanced adhesion turnover and migrate significantly faster (Ziegler et al., 2006). Paxillin is another signalling scaffold that is recruited in the early stages of adhesion formation (Deakin and Turner, 2008). It possesses many protein-protein interaction sequences, including leucine rich repeats, a proline rich region and LIM domains. Through these modules, this versatile scaffold can recruit many different types of proteins to the adhesion, including phosphatases, actin binding proteins and regulators of Rho GTPases. Together with the other components of the adhesome, these proteins mediate the 'inside-out' and 'outside-in' signalling associated with adhesions, making adhesions essential and versatile structures (Figure 1.4).

Disassembly of adhesions is crucial to achieve coordinated cell migration. Integrins are in a state of flux, constantly being turned over by internalisation by clathrin dependent and independent mechanisms. Integrins then enter recycling paths to be returned to the membrane, or can be sent for degradation (Bridgewater et al., 2012). In addition to disassembly, adhesions can also remodel or slide to new positions. Therefore, it is essential to have a fully functional endocytic trafficking system to connect adhesion assembly and disassembly loops. Integrin recycling is not only key in the coordination of 2D cell migration, but has also been shown to control the invasive ability of cancer cells (Yoon et al., 2005, Ramsay et al., 2007a) reviewed in (Ramsay et al., 2007b).

1.1.6 The actin cytoskeleton and cancer metastasis

1.1.6.1 Regulators of the actin cytoskeleton facilitate metastasis

Metastasis is the spread of cancer from its original site to secondary sites, and is the main cause of cancer related death (Sporn, 1996). In order to disseminate from the original tumour and colonise secondary sites, cancer cells must navigate through diverse environments seeking out space and nutrients. In the case of melanoma metastasis, Muinonen-Martin et al. have suggested that these cells metastasise by locally breaking down lysophosphatidic acid (LPA), thus

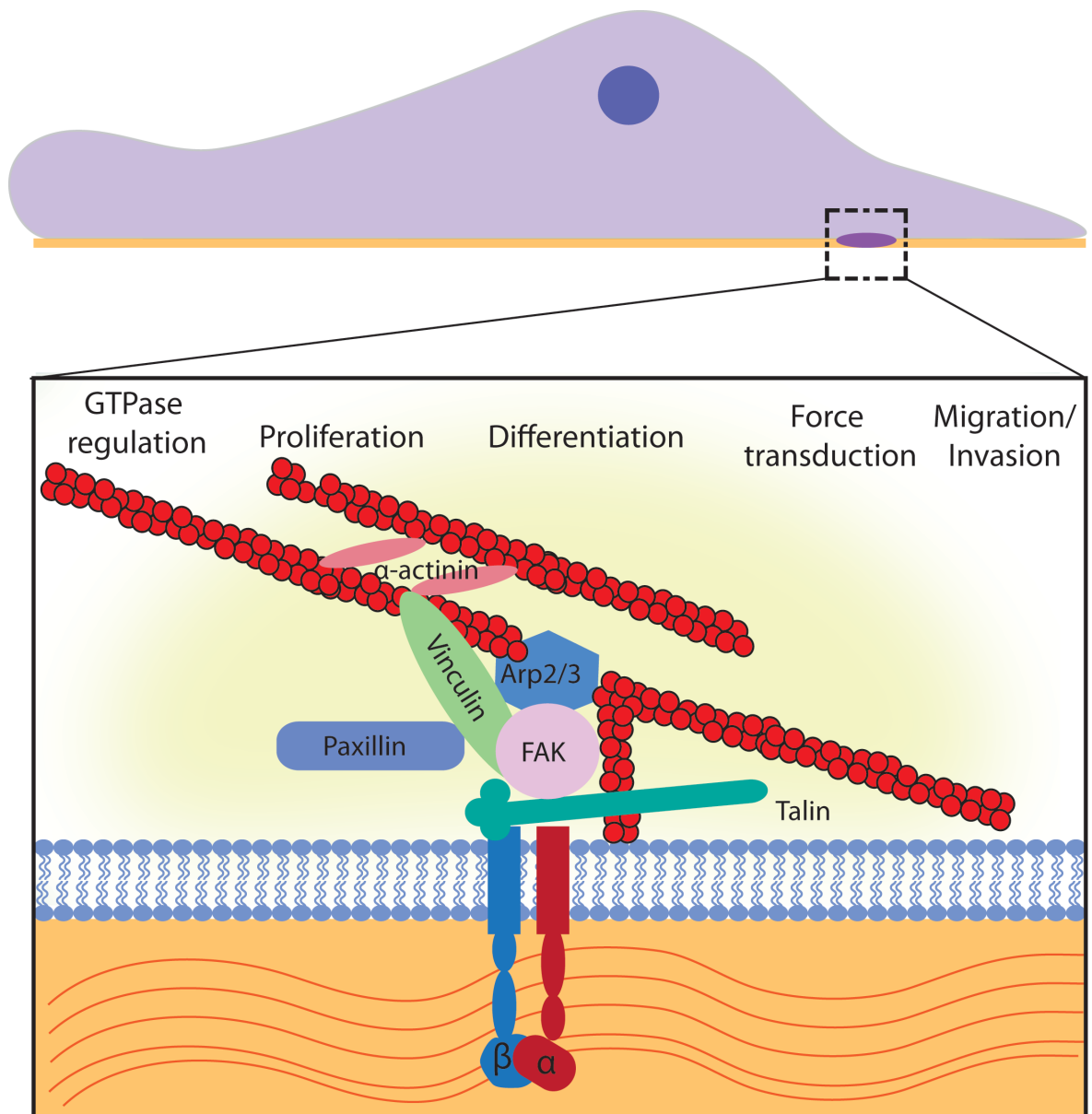


Figure 1.4 Integrin-based adhesions and signalling

Integrin-based adhesions are built around a heterodimeric pairing of α and β subunits bound to a ligand in the extracellular matrix such as fibronectin, laminin, collagen, thrombospondin or vitronectin. Integrins are then activated by proteins such as talin binding to the cytoplasmic tail of the β subunit, inducing conformational changes that strengthen the attachment of the integrin head with the ligand. Subsequently, a multi-molecular complex is built at this site consisting of large scaffold and signalling proteins. This schematic highlights 'core' adhesion proteins which appear to be commonly recruited to adhesion sites. The scaffold proteins FAK and vinculin interact with and recruit the Arp2/3 complex to adhesion sites, linking adhesion dynamics to actin polymerisation and membrane extension. The multi-domain scaffold paxillin is recruited early to adhesions and provides docking sites for many types of molecules including activators of GTPases. Alpha-actinin forms an anti-parallel rod-shaped dimer which bundles actin filaments at adhesion sites.

Creating a gradient (Muinonen-Martin et al., 2014). The metastatic journey is driven through aberrant regulation of multiple components of the actin cytoskeleton, which are normally tightly regulated. We are still uncovering the roles that different actin related proteins play in cancer cell movement in the hope of building a picture of how the actin cytoskeleton facilitates metastasis.

A whole host of actin regulators have been identified as mutated or mis-regulated in different types of cancer, including the classic GTPases Rac1, Cdc42 and RhoA. Also implicated are multiple actin binding proteins such as cofilin, profilin, gelsolin and actin nucleation promoting factors including N-WASP, WAVE1,2 and 3 and inducers of actin polymerisation Arp2/3 and Ena/VASP (Olson and Sahai, 2009). It is becoming clear that cancer cells hijack different aspects and components of migratory pathways to aid them at different times in their journey to new sites.

1.1.6.2 The metastatic cascade

We are still striving to fully understand what drives cancer cells to metastasise, and the paths which different types of cancers take to achieve this. Generally, cancer cells must first move out of the tumour, and invade towards the bloodstream or lymphatic system, which they use as a transport system to reach other organs. We are beginning to appreciate the complexity of the tumour environment, and its role in promoting metastasis. Tumours are complex entities, containing blood vessels, immune cells, fibroblasts, lymphocytes and ECM. The tumour cells are in close proximity and are constantly interacting with these components. It has been suggested that this interaction and the presence of other signalling molecules induces cancer cells to undergo epithelial-mesenchymal transition (EMT) (Thiery et al., 2009). This process involves de-regulation of cell-surface adhesion molecules such as E-cadherin and gene expression changes, resulting in the cell breaking free from their neighbouring cells and becoming more motile and invasive (Christofori and Semb, 1999). These changes allow the cells to break free from the tumour environment, and allow them to invade their way efficiently towards the bloodstream or lymphatic system (Figure 1.5).

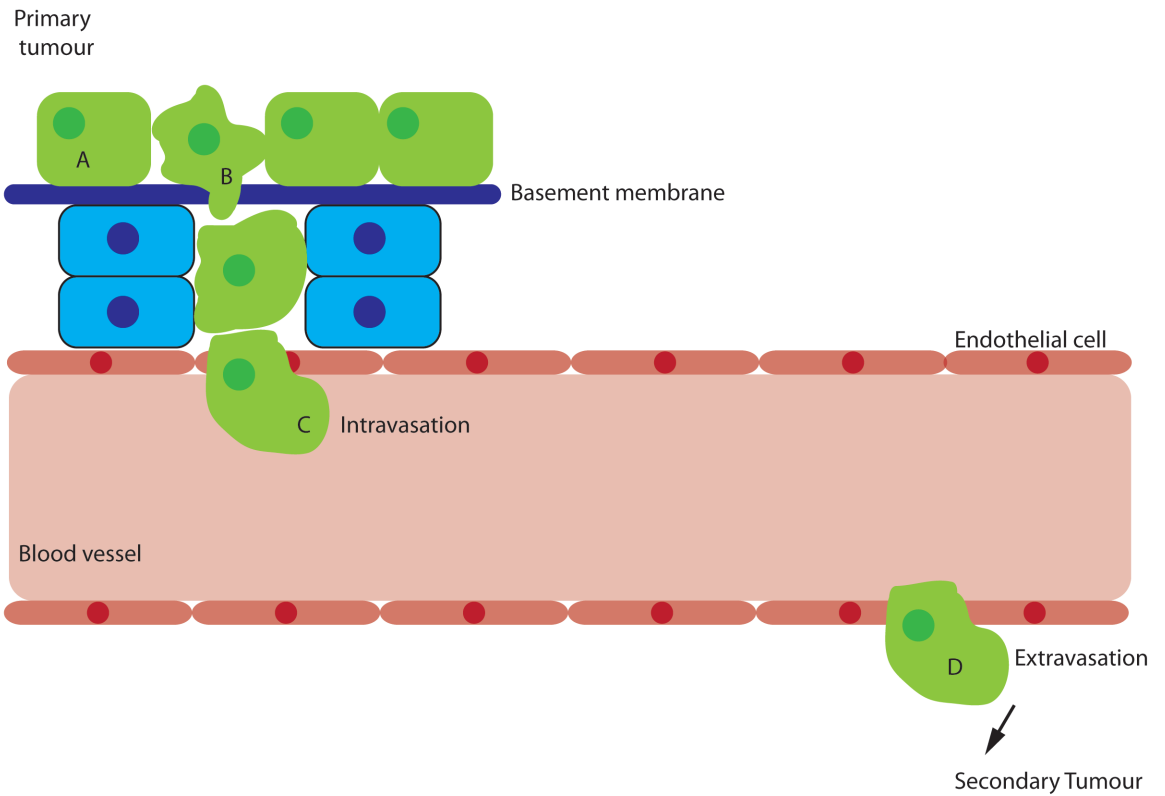


Figure 1.5 The metastatic cascade

Cancer spread is a multi-faceted process, where cancer cells break free from the original tumour, invade the surrounding matrix and spread to secondary sites using the blood or lymphatic system. Cells within the tumour gain migratory and invasive abilities through changes in gene expression, sometimes referred to as epithelial to mesenchymal transition (EMT) (A to B). Cells can then use actin-based ventral membrane protrusions called invadopodia to breach the basement membrane and invade through the surrounding matrix (B). Cells then intravasate into the blood and lymphatic systems to be transported through the body (C). At distant sites, a small proportion of circulating tumour cells extravasate, and colonise other organs forming a secondary tumour (D).

To enter the vasculature, cells need to degrade and re-model the ECM. To do this they use actin-based structures called invadopodia. These are ventral membrane protrusions composed of a variety of proteins including actin regulatory proteins, adhesion molecules and matrix degradation enzymes (Beaty and Condeelis, 2014). The actin bundling protein fascin is a key component of invadopodia, leading to their stabilisation (Li et al., 2010). These structures protrude into the surrounding matrix and secrete matrix-degrading proteases to locally degrade the ECM, forming a tunnel through which the cell can move. Once cancer cells have successfully entered the vasculature, called 'intravasation', they travel in the blood stream until they become lodged in capillary beds. Only a small proportion of circulating tumour cells endure this journey through the vasculature, as they must survive in an anchorage-independent manner and tolerate strong forces and immune cell surveillance (Steinert et al., 2014). The cancer cells then extravasate and begin to colonise the surrounding tissue.

1.2 The Rho GTPase family and Cdc42

1.2.1 The Rho GTPase family

As discussed so far in this chapter, cells can move using a diverse array of migration modes, utilising different types of actin-based structures to do so. These migration modes are the product of complex signalling networks, involving many factors. Remarkably however, one family of proteins appears to play a central role in regulating all modes of migration. This family is the Rho GTPases, a sub family of the Ras superfamily of GTPases, which also includes Ras, Rab, Arf and Ran (Etienne-Manneville and Hall, 2002). Rho GTPases act as signalling hubs, receiving signals from cell-surface receptors and a host of other pathways and transducing these cues into cytoskeletal rearrangements to facilitate cell migration and division. The small GTPases are generally 20-25 kDa and are highly conserved throughout evolution. They act as molecular switches, cycling between an active GTP bound state and an inactive GDP bound state. When active, they can proceed to activate a host of downstream signalling molecules (Nobes and Hall, 1999). The ability of GTPases to be easily and quickly controlled through many signalling inputs makes them ideal candidates to impart temporal-spatial information to the cell to induce a fast response by the cell. In

addition, activation of one GTPase can activate several distinct signalling pathways. This family has emerged as a master regulator of many aspects of cell migration, including actin polymerisation, adhesion formation and turnover, cell contractility and polarity.

1.2.1.1 Rho GTPase family members

Since their discovery over 20 years ago, the Rho family of GTPases has revolutionised our understanding of cell movement. Our understanding of the classic members Rac, Rho and Cdc42 began with 2D tissue-culture studies using fibroblasts, and injection of dominant-negative and constitutively active forms (Ridley and Hall, 1992, Nobes and Hall, 1995, Nobes and Hall, 1999). They noted that injection of active Rac induced membrane ruffling, as did Cdc42, but Cdc42 activation could also trigger filopodia assembly. Rho activation triggered focal adhesions and stress fibres, suggesting a role in cell contractility, and Cdc42 was seen to promote filopodia. Since this seminal work by Alan Hall and colleagues, we have developed a deeper understanding of this family, which we now know acts synergistically to control diverse aspects of cell migration.

20 members of the Rho GTPase family have been identified in mammals, with Rho, Rac and Cdc42 being the most highly conserved, present across eukaryotic species. Seven members have been identified in *Drosophila melanogaster*, five in *Caenorhabditis elegans* and fifteen in *Dictyostelium discoideum* (Raftopoulou and Hall, 2004). In mammals, there are groups of closely related Rho genes (RhoA, B and C) and also Rac genes (Rac1, 2 and 3). In addition, there are also splice variants of Cdc42 and Rac1 (Heasman and Ridley, 2008). The family can be classified into eight subfamilies (See Figure 1.6 adapted from (Heasman and Ridley, 2008)). The atypical Rho GTPases RhoBTB, Rnd, RhoU and RhoV and RhoH are all predominantly GTP bound and are therefore regulated by other pathways. Rho proteins can be post-translationally modified on their c-terminus by addition of a lipidic group by prenylation to allow interaction with membranes (Vega and Ridley, 2008).

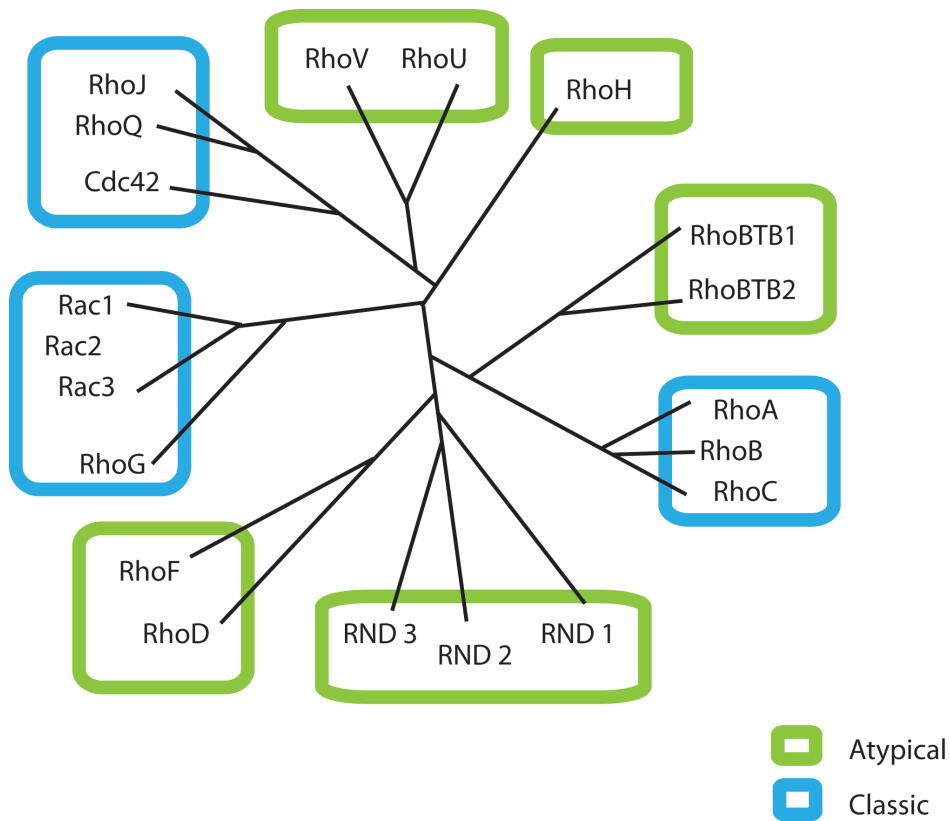


Figure 1.6 The Rho GTPase family

Phylogenetic tree based on the amino acid similarity between the 20 classic and atypical Rho GTPase family members. They fall into 8 subfamilies; GTPases Rho, Rac and Cdc42 and RhoF and RhoD families cycle between active GTP bound and inactive GDP bound forms. The atypical members include RhoBTB, Rnd, Rho, RhoV and RhoH. These proteins are predominantly GTP bound and appear to be regulated by alternative mechanisms such as degradation and post-translational modification.

Adapted from Heasman et al, (2008)

1.2.1.2 Controlling Rho GTPase activity

In order for Rho GTPase signalling to be effective, it must be tightly regulated. For this reason, the activity of Rho GTPases can be controlled in a number of ways through a host of signalling pathways. Generally, they are active when in the GTP bound form and inactive when bound to GDP. Exchange of nucleotides results in structural changes in two regions of the G protein called switch I and II (Morreale et al., 2000). Activation leads to a cascade of signalling through diverse effector proteins. Nucleotide status is controlled by guanine nucleotide exchange factors (GEFs) and GTPase activating proteins (GAPs). GEFs induce the exchange of GDP for GTP and GAPs catalyse the hydrolysis of GTP to GDP (Figure 1.7). The location and activation state of GAPs and GEFs are crucial to controlling GTPase behaviour. Some GAPs and GEFs are shared between Rho GTPases allowing synergistic control of their pathways. However, some GTPases have unique GAPs and GEFs, allowing specific control of these members and their associated signalling pathways. Identification of these factors is complex as they do not contain one common sequence motif; however, evidence suggests that there are over 60 GEFs and over 70 GAPs (Etienne-Manneville and Hall, 2002). As well as GAPs and GEFs, Rho GTPases are also subject to regulation by guanine nucleotide dissociation inhibitors (GDIs) which extract inactive GTPases from the membrane.

1.2.2 Rho GTPases coordinate cell migration

Having identified the Rho GTPases Rho, Rac and Cdc42 as integral players in the transduction of cytoskeletal rearrangements, the challenge we face is to understand what part each plays in the overall coordination of cell movement, and how they synergise to achieve this. We are still in the early stages of understanding the relationships between GTPases, and how they work together in 3D systems. It is clear however that GTPases are part of elaborate feedback and feed forward loops, making it difficult to extrapolate linear pathways linking a single GTPase to an output. However, this chapter will try to summarise which GTPases have been implicated to date in the formation of various structures required for migration.

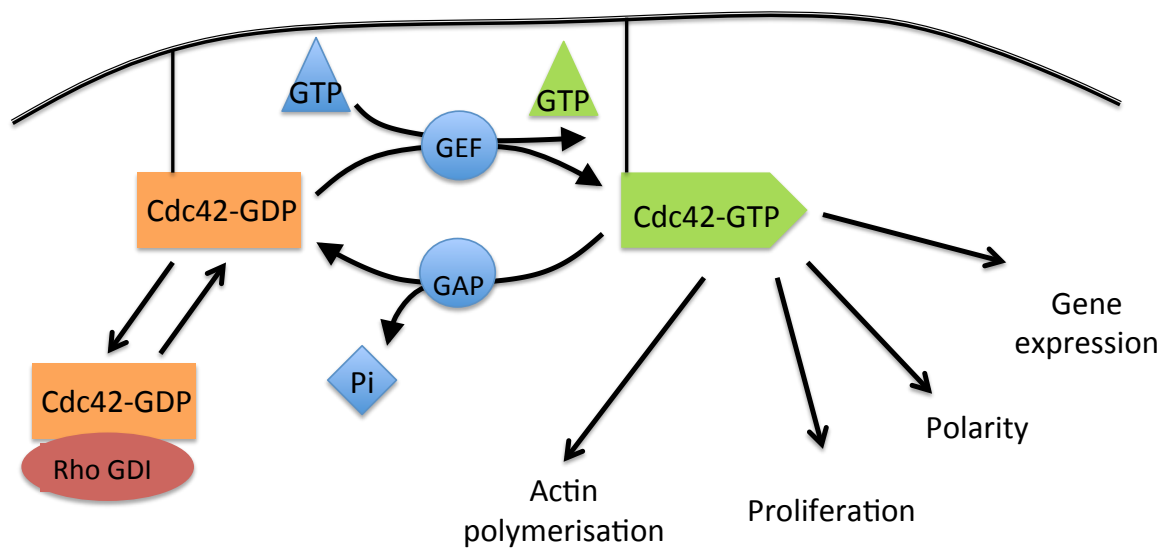


Figure 1.7 The GTPase activation cycle

Classical GTPases become activated upon the binding of GTP, mediated by guanine exchange factors (GEFs). When in their active form, GTPases control a host of signalling pathways, including actin polymerisation, proliferation, polarity and gene expression. GTPases are deactivated by guanine activating proteins (GAPs) which catalyse the hydrolysis of GTP to GDP in the binding pocket. Binding of Rho GDI prevents nucleotide exchange and membrane association.

The role of Rac has been studied extensively in 2D environments and recently some studies have emerged in 3D systems. Rac is a central player in the polymerisation of actin at the leading edge of the migrating cell. It achieves this through activation of the actin nucleation promoting factor Scar/WAVE, which activates the Arp2/3 complex resulting in branched filament polymerisation, as discussed earlier. Previous work in the lab has shown that Rac1 is required for the extension of long pseudopods by melanoblasts. Without Rac1, cells migrate poorly using short stubby protrusions (Li et al., 2011). Both Rac and Cdc42 can bind and activate the PAK family of Serine/Threonine kinases. These kinases can phosphorylate and activate LIM kinase, which can phosphorylate and inactivate cofilin, preventing filament severing. PAK kinases have also been linked to the turnover of focal adhesions. Adhesions are essential during cell migration, forming traction points through which the cell can generate force for migration, and acting as signalling hubs, connecting the cell to the surrounding ECM (Raftopoulou and Hall, 2004) (Figure 1.8).

In addition to activation of PAK kinases, Cdc42 has also been identified as master regulator of cell polarity through its interaction with the Par polarity complex. This complex ensures correct placement of the microtubule organising centre (MTOC) to allow growth of the microtubule cytoskeleton in the direction of migration to facilitate directed movement of vesicles to the leading edge (Etienne-Manneville, 2004). This pathway ensures directed and sustained migration, and will be discussed in more detail later on in this chapter. As discussed earlier, Cdc42 can also induce branched actin polymerisation via the Arp2/3 complex through activation of the actin nucleation promoter N-WASP (Figure 1.8). However, it is thought that Rac is the main activator of the Arp2/3 complex at the leading edge.

In contrast to Rac and Cdc42 which drive actin polymerisation and directionality, Rho has mainly been implicated in controlling contractility via the acto:myosin cytoskeleton. Through its effector kinase ROCK, RhoA can lead to phosphorylation of the regulatory myosin light chain subunit, opening up the

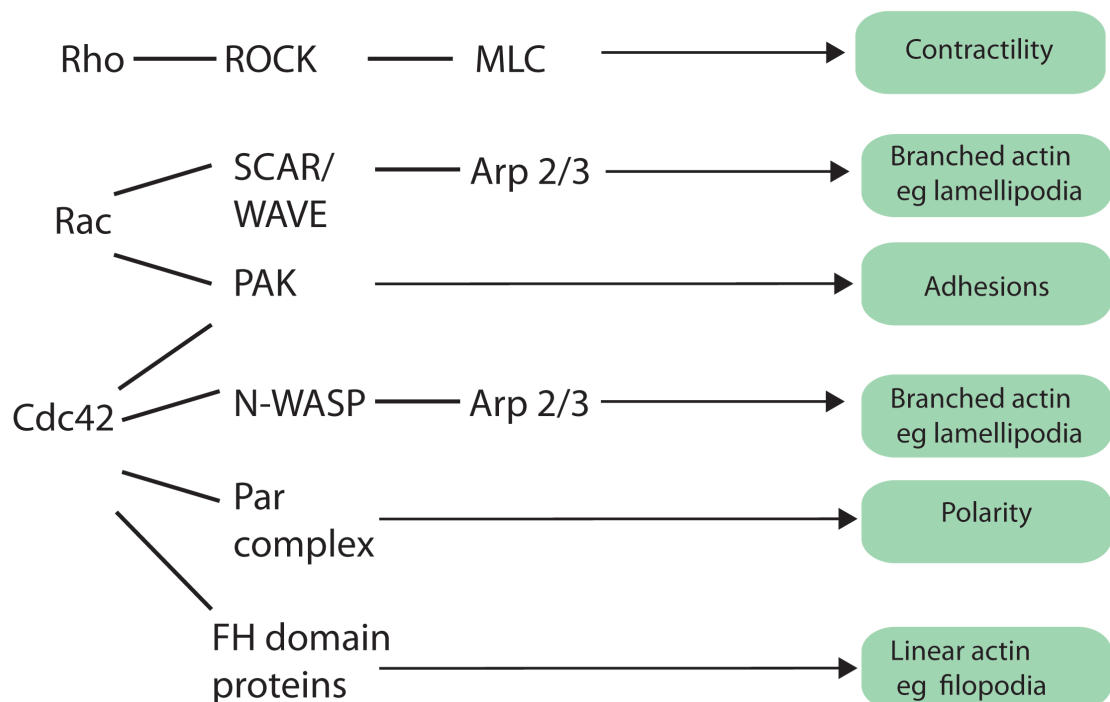
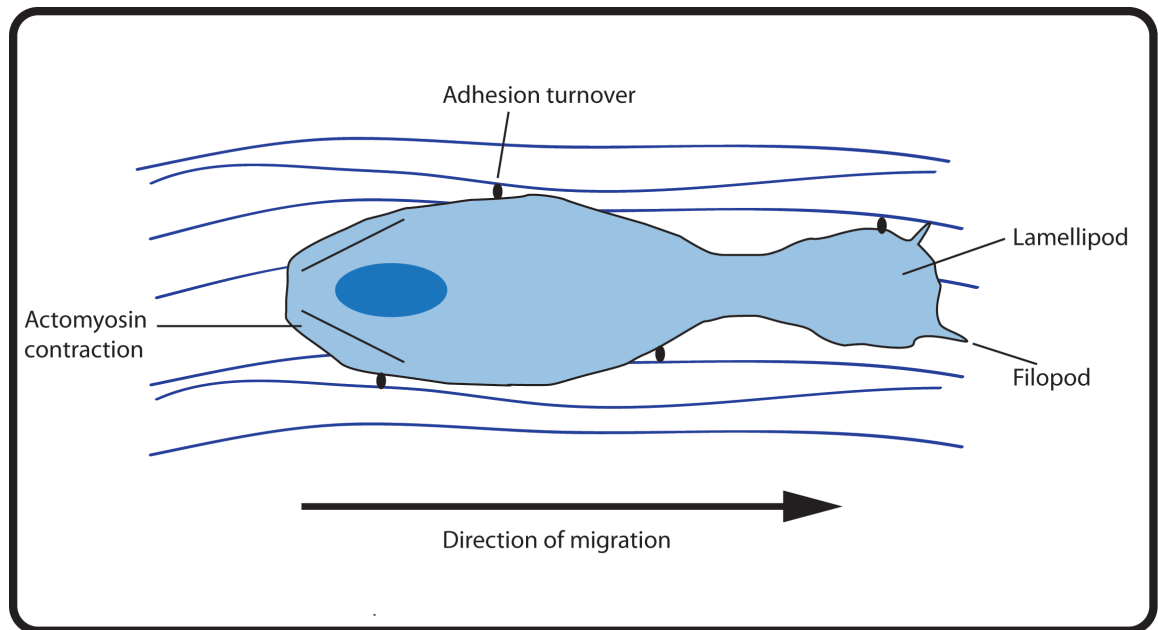


Figure 1.8 Rho GTPases coordinate cell migration

The classical Rho GTPases Rac1, Cdc42 and Rho dynamically coordinate the processes involved in cell migration, including actin polymerisation, contractility and adhesion turnover. Rapid and dynamic control over these processes is required to facilitate movement, and GTPases do this by controlling overlapping but unique signalling pathways. Rac1 is mainly associated with driving actin polymerisation at the leading edge through activation of the SCAR/WAVE and Arp2/3 complexes, driving pseudopod/lamellipod extension. Cdc42 can also stimulate actin polymerisation but via the N-WASP-Arp2/3 pathway, and is associated with filopod formation. In addition, Cdc42 and Rac can also control the activity of PAK kinases, which carry out many functions including control of adhesion turnover. Rho family GTPases are associated with controlling cell contractility through ROCK. ROCK can phosphorylate the myosin regulatory light chain (MLC) opening up myosin head groups to assist with actin filament sliding.

Adapted from Ridley et al (2015) and Raftopoulou et al (2004)

myosin motor to bind to actin filaments to allow contraction. Contraction is essential for movement of the cell body and for rear end retraction to allow cells to move forward (Mitchison and Cramer, 1996). This pathway plays a major role in bleb-based migration modes (Figure 1.8).

The contribution of each GTPase to different migration modes is dependent on the cell type and the environment. Fluorescence resonance energy transfer (FRET) imaging and fluorescence lifetime imaging (FLIM) using fluorescence based reporters for GTPase activity have helped forge new advances in our understanding of the localisation of GTPase activation (Kraynov et al., 2000). One such reporter has helped us gain a high-resolution picture of GTPase activation in motile HT1080 fibroscaroma cells, demonstrating that Cdc42 is active at the leading edge, whereas Rac is active slightly behind this (Itoh et al., 2002). Recently, reporters have evolved such that the activation levels of two GTPases can be studied simultaneously within the same cell (MacNevin et al., 2016). These types of reporters as well as photo-activatable probes (Wu et al., 2009) will be useful tools in elucidating the role of Rho GTPases in coordinated cell migration.

1.3 Cdc42 in cell migration

1.3.1 Cdc42 activation and effectors

Early insights into the function of the Rho GTPase Cdc42 showed that it was a crucial factor in bud site selection in yeast (Johnson and Pringle, 1990), and could induce the formation of actin cytoskeletal rearrangements and the formation of filopodia in mammalian cells (Nobes and Hall, 1995)). In the 20 years since its discovery we have come to recognise Cdc42 as a master regulator of the actin cytoskeleton, with an incredible capacity to influence a wide variety of cellular responses. This is in part due to its capacity to integrate signals from multiple pathways to activate many downstream effectors. Cdc42 has a lipid anchor, and active Cdc42 can be found at the plasma membrane of the leading edge, or at the Golgi (Raftopoulou and Hall, 2004). Activation of Cdc42 can occur through many signalling receptors, including those from the tyrosine kinase, G-protein, cytokine and integrin families (Sinha and Yang, 2008). Many GEFs are known to Activate Cdc42, including B-Pix, TIAM1 and Vav1,2 and 3

(Schmidt and Hall, 2002). As mentioned earlier, when active, Cdc42 can control many aspects of cell migration through its diverse range of downstream effectors, including actin polymerisation, cell contractility, vesicle trafficking, adhesion turnover, invadopodia formation and cell polarity (Figure 1.9).

Cdc42 can contribute to acto:myosin contractility in addition to Rho/ROCK pathways through its effector MRCK. Similarly to ROCK, MRCK can phosphorylate the light chain regulatory subunit on non-muscle myosin to allow crosslinking to actin to generate contractile force. In addition to generating cell contractility, Cdc42 can contribute to the protrusive force required for cell motility by activating the WASP family NPF N-WASP to generate branched actin filaments, and the FH domain NPF Dia1 to extend linear filaments (Raftopoulou and Hall, 2004). In some cell types, activation of FH domain proteins by Cdc42 results in filopodia formation to aid cell migration (Nobes and Hall, 1995). In addition to promoting branched filament polymerisation, the activation of N-WASP by Cdc42 is also crucial for invadopodia (Yamaguchi et al., 2005). The F-BAR domain protein TOCA-1 has been shown to play a key role in N-WASP activation downstream of Cdc42 (Ho et al., 2004). This family of proteins are large scaffolding proteins that play a crucial role in the interface between membrane dynamics and actin reorganisation (Reviewed in (Aspenström, 2014)). Cdc42 has also been linked to adhesion turnover through the PAK family of kinases, however the mechanism linking Cdc42 to adhesion turnover is unknown. Cdc42 is also widely regarded as master regulator of cell polarity.

1.3.2 Cdc42 and polarity

1.3.2.1 Early insights from *Saccharomyces cerevisiae*

Studies using this model revealed the importance of Cdc42 in establishing cellular asymmetry otherwise known as 'polarity'. Building polarity in yeast is essential for many processes such as response to pheromones, cytokinesis, shmoo formation and differentiation (Sinha and Yang, 2008). The simplicity of this model allowed us to gain molecular insight into how Cdc42 builds such asymmetries (reviewed in (Woodham and Machesky, 2014)). Cdc42p drives bud growth in *S. cerevisiae* by localising to the small cortical area at the bud site. Recent models suggest that yeast amplify random, transient

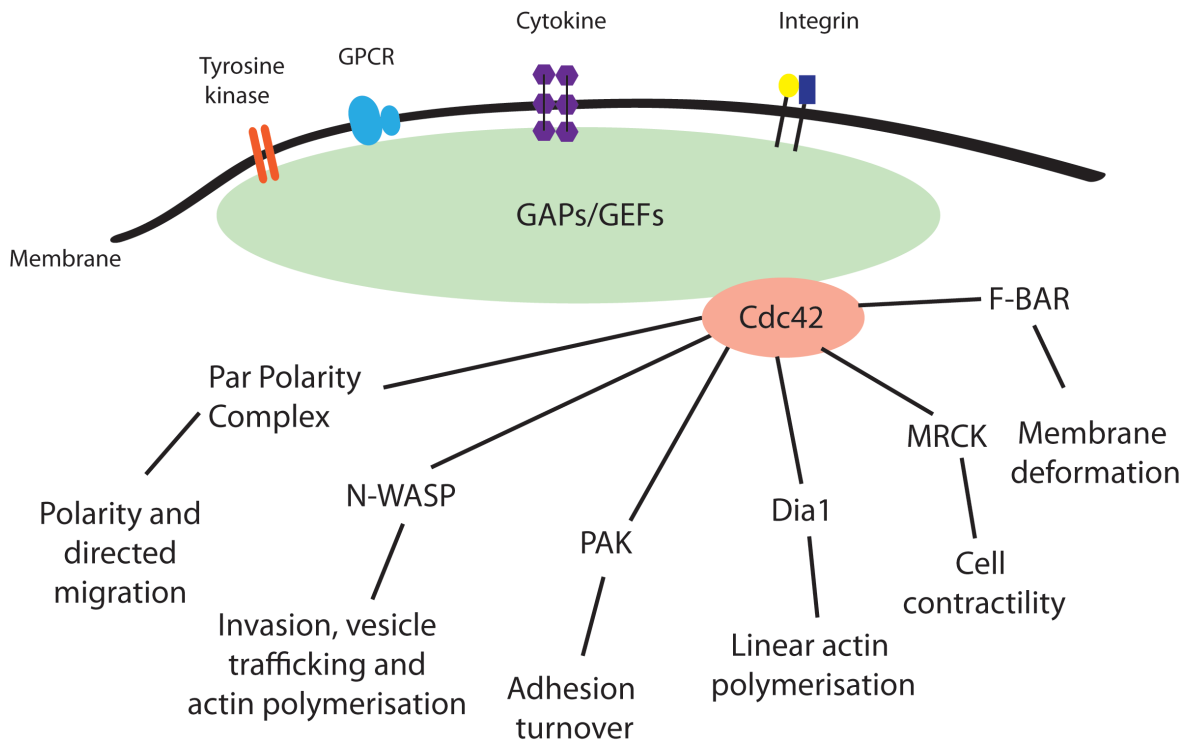


Figure 1.9 Cdc42 integrates multiple signalling inputs into diverse cellular effects

Cdc42 can be activated via a diverse array of signalling pathways initiated by many types of cell surface receptors such as tyrosine kinases, G-protein coupled receptors, cytokine receptors and integrins. Cdc42 activity is controlled through regulation of GAP and GEF activity. When active, Cdc42 can control many aspects of cell behaviour, acting through many effectors. Cdc42 is a master regulator of cell polarity, acting through the Par polarity complex. It can induce actin polymerisation through its effectors N-WASP and Dia1, cell contractility through MRCK and adhesion turnover through PAK. The F-BAR family of BAR domain proteins have also been reported to be Cdc42 effectors. Cdc42 controls the localisation of the Cdc42 effector interacting protein 4 (CIP4) and also binds the CIP4-like protein TOCA-1. Both of these proteins play important roles in the interface between cytoskeletal dynamics and membrane trafficking, such as during clathrin-mediated endocytosis.

breaks of symmetry to create asymmetry. The scaffold protein Bem1 has been identified as a key player in this process. Bem1 binds the Cdc42-GEF Cdc24 and the Cdc42 effector PAK. This complex can be captured by spontaneously arising Cdc42-GTP at the cortical site via PAK. This brings the Cdc42 GEF into close proximity to neighbouring Cdc42-GDP creating Cdc42-GTP, which in turn recruits more Bem 1 complex (Johnson et al., 2011). This positive feedback loop leads to a cluster of Cdc42-GTP at the bud site, which orientates actin cables and therefore directs vesicular transport to the site, reinforcing this as the site of bud emergence. In addition to these mechanisms, recent work suggests that asymmetries in the lipid composition of the cell membrane may aid the development of polarity. Using a GFP-Lat-C2 probe to visualise phosphatidylserine (PS) distribution in *S. cerevisiae*, Fairn et al. demonstrated that PS is concentrated in the plasma membrane of growing buds, and acts as a platform for the accumulation of Cdc42 at the bud neck. Mutants in PS biosynthesis were unable to localise Cdc42 to the bud neck (Fairn et al., 2011).

Since the discovery of the role of Cdc42 in yeast polarity, much work has been done using mammalian cells to try to uncover if this role in generating cellular asymmetry is conserved throughout evolution.

1.3.2.2 Cdc42 and mammalian polarity

The complexity of multicellular life brings another dimension to the concept of polarity. Cells must integrate a whole host of signals to divide, differentiate and migrate at the correct time and in a coordinated manner. Despite the complexity these cells encounter, there is evidence for a conserved molecular toolbox to interpret these signals into polarisation. As in yeast, Cdc42 is a master coordinator of polarisation in mammalian cells. However, its intricate regulation and its many effectors have made it difficult to elucidate the mechanisms through which Cdc42 exerts its effects on polarity. Cdc42 has maintained its major role in coordination of the cytoskeleton in mammalian cells, though the part it plays has become more complex.

Unlike in yeast, polarity in mammalian cells is mainly driven by external cues, such as cell-cell contact, soluble factors or release of physical constraints such as in a scratch wound (Etienne-Manneville, 2004). The molecular mechanism

through which Cdc42 initiates asymmetry in mammals was investigated in an elegant set of studies analysing astrocyte migration into a scratch wound. It was noted that after wounding, the actin and microtubule cytoskeleton aligned perpendicular to the wound, and the MTOC moved to face the direction of migration. This process was abrogated in the presence of a dominant negative Cdc42 (Etienne-Manneville and Hall, 2001). To achieve this, Cdc42 activates the PAR polarity complex, consisting of the scaffold proteins PAR-6 and Par-3 and atypical protein kinase (aPKC)(Etienne-Manneville et al., 2005). Cdc42 binds to PAR-6 inducing a conformational change that activates aPKC, leading to activation of GSK3-B and association of adenomatous polyposis coli (APC) with microtubule plus ends (Etienne-Manneville and Hall, 2003). Re-orientation of the MTOC and microtubule network supports persistent and directional migration.

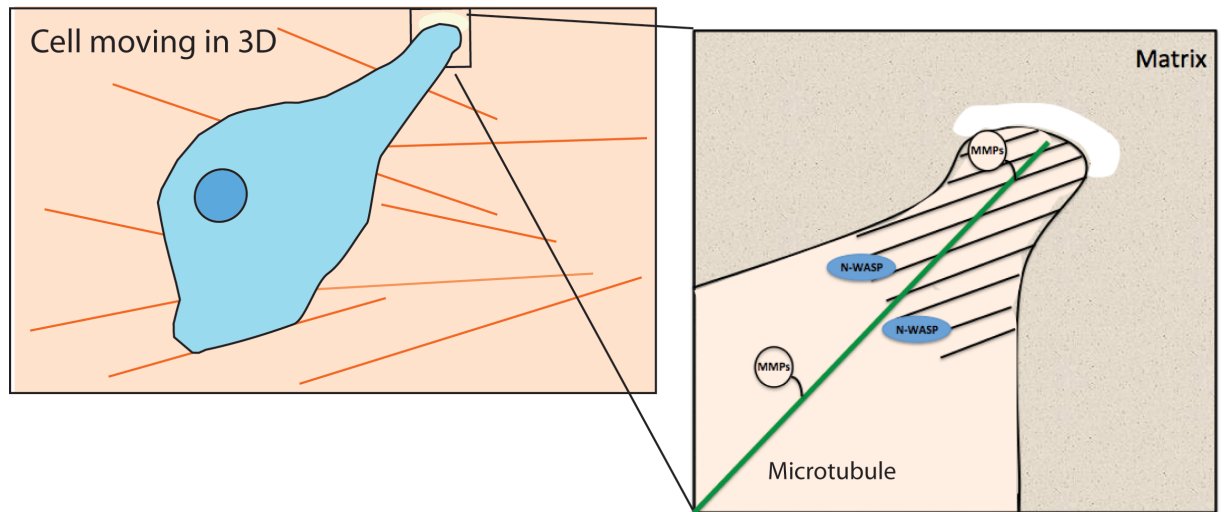
1.3.3 Cdc42 and mammalian cell division

Shortly after the discovery of Rho-GTPases, it was shown that Rac, Rho and Cdc42 could control cell-cycle progression. Injection of Rac1 and Cdc42 into quiescent fibroblasts stimulated G1 to S transition (Olson et al., 1995). Microinjection of dominant negative Rac and Cdc42 blocked serum induced DNA synthesis, giving the first indication that these GTPases were essential for cell growth. The downstream signalling events linking GTPases to division were further elucidated shortly afterwards, when it was shown that Cdc42 and Rac could induce cyclin D1 accumulation and subsequently phosphorylation of the 'pocket protein' retinoblastoma to induce transcription by E2F family transcription factors leading to G1 to S transition (Gjoerup et al., 1998). In addition, Cdc42 has also been proposed to localise directly at the spindle and on kinetochores of condensed chromosomes, regulating spindle assembly, and controlling the orientation of division (Chircop, 2014). Therefore, Cdc42 is not only a master regulator of the actin cytoskeleton, but also has control over diverse signalling pathways including those responsible for cell cycle transition. However, there is still much to be learned about Cdc42s role in the cell cycle and during cell division.

1.3.4 Cdc42 in invasion and cancer

Due to Cdc42's prominent role in cell migration, polarity and division, it is unsurprising that it has been suggested to be a putative oncoprotein. Cdc42 is not usually mutated in human cancer, but is overexpressed in many cancers including non-small cell lung cancer (Liu et al., 2009), melanoma (Tucci et al., 2007), breast cancer (Fritz et al., 1999) and testicular cancer (Fritz et al., 2002). The exact role that Cdc42 plays in cancer progression, or indeed at which stages it is most crucial is still unclear. Interestingly, it has been observed that mutant Cdc42 fibroblasts display elevated levels of glutamine, a crucial metabolite required to support proliferation and sustained manufacture of lipids, proteins and nucleic acids (Wang et al., 2010). It will be interesting in the future to further investigate Cdc42's role in cancer cell metabolism, as we have made great advances in understanding of this field in recent years.

Cdc42 has also been linked to cancer cell invasion and metastasis (Gao et al., 2013, Bouzahzah et al., 2001, Johnson et al., 2010). As described earlier, the spread of cancer is a multifaceted process, involving escape from the primary tumour and degradation of the surrounding matrix to reach blood or lymphatic vessels (Figure 1.5). This role may be in part due to Cdc42's role in the formation of invasive structures found on the base of the cell known as invadopodia, and that Cdc42 can help to traffic matrix degrading enzymes to the invasive protrusions of cells, helping them invade the surrounding matrix (Yamaguchi et al., 2005) (Sakurai-Yageta et al., 2008). Cdc42 can localise to tumour cell-matrix contacts where it activates the scaffold protein IQ-GAP which can interact with the exocyst complex to select vesicles containing Matrix metalloproteinases (MMP) for incorporation into the invading membrane compartment (Sakurai-Yageta et al., 2008). Release of MMPs leads to degradation of the surrounding matrix. The invading pseudopod can then advance through Arp2/3 mediated actin polymerisation via the Cdc42 effector N-WASP (Yamaguchi et al., 2005) (Figure 1.10). In addition, constitutively active forms of Cdc42 (Cdc42 Q61L and Cdc42 G12V), promote anchorage independent growth in immortalised fibroblasts (Fidyk et al., 2006) (Lin et al., 1997).

**Figure 1.10 Cdc42 and invasion**

Cdc42 aids tumour cell invasion by localising to tumour cell-matrix contacts where it activates the scaffold protein IQ-GAP. There it can interact with the exocyst complex to select vesicles containing matrix metalloproteinases (MMPs) for incorporation into the invading membrane compartment. MMPs cleave and degrade matrix components, creating a tunnel through which the cell can advance through using Arp2/3 mediated actin polymerisation via the Cdc42 effector N-WASP. Orange lines represent matrix, black represent actin filaments and green microtubules.

Recent work has provided some mechanistic insight into Cdc42's role in the transendothelial migration of breast cancer and prostate cancer cells, a key process during metastatic spreading (Reymond et al., 2012). Cdc42 knockdown cells were less able to intercalate between endothelial cells due to a decrease in B1 integrin expression. Transient depletion of Cdc42 decreased early colonisation of the lungs. Their data indicate an interesting and unique role for Cdc42 in the metastatic cascade.

In addition to Cdc42's role in cancer invasion, it has also been suggested that in some contexts, Cdc42 could act as a tumour suppressor through its roles in maintaining cell polarity and adhesions. This role of Cdc42 is particularly important in epithelial sheets, consisting of a monolayer of polarised epithelial cells surrounding a lumen. Cdc42 maintains polarity by arranging an asymmetric distribution of cytoskeletal components, vesicle trafficking and adhesion types, and by controlling the orientation of division. Loss of Cdc42 or Par6/aPKC leads to aberrant cysts with multiple lumens (Jaffe et al., 2008) (Durgan et al., 2011). We have yet to determine the activity and expression pattern of Cdc42 during the stages of cancer progression, or to fully understand its role in different tumour types and microenvironments. This knowledge will be key to develop any strategies to target Cdc42 activity in tumours. It is likely that any inhibition of Cdc42 activity to combat tumourigenesis might also impact on cell polarity, complicating this as a potential therapeutic agent. Inhibitors could however prove effective at low doses in combination with other therapies.

1.4 Melanoblasts and the melanocyte lineage

Melanocytes are the pigment producing cells in the skin. In humans most melanocytes reside in hair follicles and the epidermis of the skin, but in mice they mainly reside within the hair follicles. The main function of melanocytes is to produce melanin, which they pass to surrounding keratinocytes using dendritic protrusions in packages called melanosomes. This causes pigmentation of the skin in humans and the hair in mice. The melanocyte lineage originates from the neural crest, and their embryonic precursors are called melanoblasts. Unlike melanocytes, melanoblasts are plastic and highly migratory, moving large distances through the skin to reach their final destination in the epidermis from their site of origin at the neural tube. Studying the melanoblast lineage is of

interest for many reasons. Firstly we know very little about how these cells achieve this highly orchestrated journey during development, and we would like to understand the factors controlling this process. Secondly, melanoblasts provide an excellent model system for studying 3D cell migration, as there are methods available to perform high-resolution imaging. Lastly, there are parallels between these embryonic precursor cells and melanoma cells; therefore, understanding the migration of this lineage might also provide information on how melanocytes transform into melanoma and why they are so metastatic.

1.4.1 Melanoblast specification

Melanoblasts derive from the neural crest (NC) lineage, a transient population of pluripotent cells that delaminate from the neural tube between the overlying ectoderm and the somites, and migrate great distances through the developing vertebrate embryo before homing to their target destination. In addition to pigment cells, a diverse array of cell types derive from the neural crest, including bone, cartilage, adipose tissue, endocrine cells, neurons and glia. The specification of cells from the neural crest is a stepwise process, where pluripotent cells become specified to a certain lineage through expression of pivotal transcription factors and activation of signalling pathways. This induces certain neural crest populations to adopt a unique gene expression profile and morphology (Thomas and Erickson, 2008).

The process of melanoblast specification begins very early in their journey, as they emerge from the neural tube (Figure 1.11 adapted from (Silver et al., 2006)). As pigment cells are not essential for the viability of the organism, many mutants have been available to determine this developmental pathway. Melanoblasts specify from a glial/melanogenic bipotent precursor cell through the up- or down-regulation of a suite of transcription factors, controlled by signalling from the environment. These transcription factors include MITF, Pax3 and Sox10, and loss of these prevents development of the melanocyte lineage. Pax3 mutant mice have neural

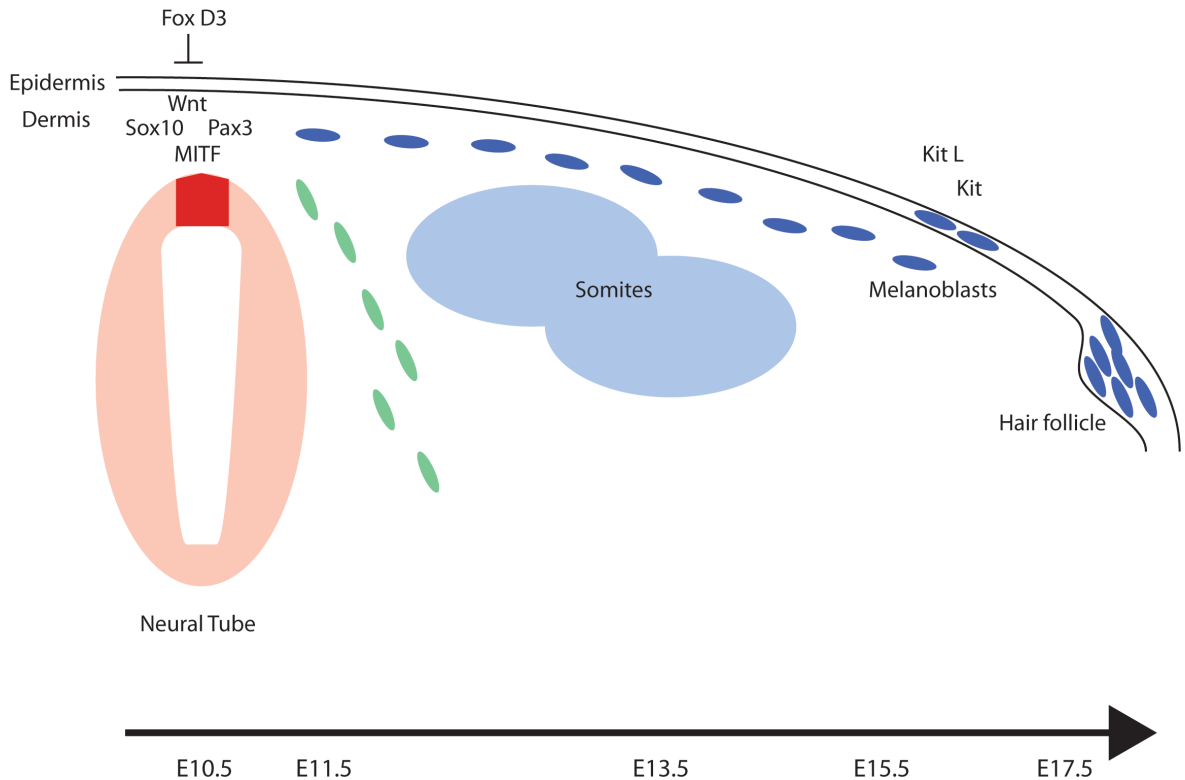


Figure 1.11 Melanoblast specification and migration during mouse embryonic development

Cells of the neural crest lineage emerge from the neural tube below the overlying ectoderm (red). Melanoblast specification begins as they emerge through the presence of Wnt signalling and the expression of transcription factors Sox10 and Pax3 and repression of the FoxD3 transcription factor. These in turn drive expression of MITF, which is the master transcription factor defining the melanocyte lineage by driving expression of melanocyte genes such as dopachrome tautomerase (DCT) and tyrosinase. During early development, melanoblasts (blue) take a dorsolateral path through the dermis, above the somites, initially moving through the dermis (E11.5-13.5). Melanoblasts then cross the basement membrane into the epidermis. By E15.5, the majority of melanoblasts reside in the epidermis of the skin, and some begin homing to hair follicles. Expression of the Kit receptor and signalling through Kit ligand (KitL) binding promote survival and proliferation of melanoblasts. By birth, melanocytes reside almost exclusively in the hair follicles in mice. Neural crest cells of the neuronal lineage take a ventral path through the developing embryo, populating the lower levels of the skin.

Adapted from Silver et al (2006)

tube defects and in other neural crest derivatives (Moase and Trasler, 1992), whereas Sox10 mutants can have megacolon due to a deficit of enteric NC cells (Tachibana et al., 2003). These transcription factors in turn drive expression of the transcription factor MITF. MITF is regarded as the master regulator of melanogenesis, and is crucial for the specification and survival of melanoblasts. It is expressed soon after emergence from the neural tube (Opdecamp et al., 1997, Nakayama et al., 1998, Lister et al., 1999, Kumasaka et al., 2004). In addition, 20 MITF mutants that lead to pigmentation defects have been described in mice (Steingrimsson et al., 2004), highlighting the importance of this transcription factor in regulating the function of this lineage. MITF regulates the transcription of tyrosinase and dopachrome tautomerase (DCT), key enzymes in the biosynthesis of melanin, by binding to the E-box regulatory site (Aksan and Goding, 1998). The Wnt signalling pathway also plays a key role in the specification of melanoblasts. Wnt3a is expressed in the dorsal neural tube, and MITF has been shown to be upregulated by Wnt3a in melanocytes (Takeda et al., 2000). Targeting of the Wnt pathway by knockout of B-catenin in NC cells abrogates melanocyte and sensory neuron development (Hari et al., 2002).

1.4.2 The melanoblast journey

Melanoblast specification begins early during embryonic development, as they emerge from the neural tube. This however is only the beginning of their journey, and we are still investigating the paths and modes that melanoblasts use to populate the embryo by birth. Different populations of the neural crest take different defined paths through the skin. Our understanding of neural crest pathways comes from a set of elegant experiments using the chick and quail embryos. Neural tubes can be dissected from chick embryos and transplanted, as chick and quail cells can be distinguished by the amount of heterochromatin in their nuclei (Teillet and Le Douarin, 1970). Similar experiments were also performed using chimeric albino and black-6 mice (Mayer, 1973). These experiments showed that melanoblasts take a dorsolateral path between the somites and the ectoderm, whereas neurogenic NC cells migrate ventrally along the neural tube. After gathering in the migration staging area at E10.5, melanoblasts in the developing mouse embryo must then proliferate and migrate to fill the embryo by birth (Figure 1.12). From E11.5 to 13.5, melanoblasts

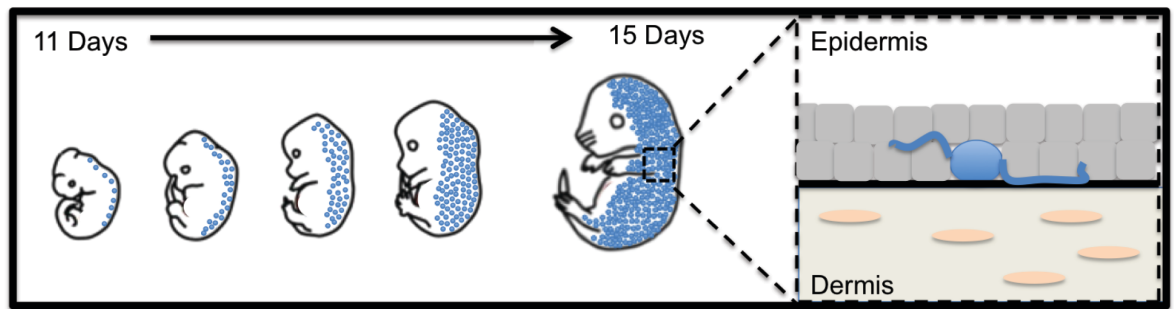


Figure 1.12 Melanoblast population of the developing embryo

During development, the melanoblast lineage must expand greatly in numbers to fill the embryo before birth. At E11.5 melanoblasts reside in the migration staging area either side of the neural tube. As the embryo develops, the melanoblast population migrates and proliferates, filling the developing embryo in a dorsoventral manner. By E15.5, melanoblasts mostly reside in the epidermis, squeezing between the neighbouring keratinocytes in order to move.

migrate in the dermis of the skin, with some beginning to transverse the developing basement membrane into the epidermis. At E15.5, the majority of melanoblasts are in the skin epidermis, some melanoblasts already residing within the developing hair follicle, which develops from placodes at sites of thickening of the epidermis. By birth, nearly all melanoblasts home to hair follicles (Figure 1.11). We are still trying to fully understand the factors that induce melanoblasts to move into hair follicles. Jordan et al. have suggested that KIT ligand could be involved in this process (Jordan and Jackson, 2000). The KIT tyrosine kinase receptor and its associated ligand are essential for the proliferation and survival of melanoblasts at later stages in their journey. They observed more melanoblasts in hair follicles after treatment of cultures of skin explants with KIT ligand. However, it is possible that this treatment simply sped up melanoblast migration into the hair follicle, as melanoblasts did not move towards KIT ligand coated beads, suggesting it might not act as a chemoattractant.

1.4.2.1 Melanoblast modes to colonise the skin

We are beginning to build a picture of how melanoblasts move individually through the skin, but it still remains unclear what controls the global coordination of their journey. It is clear however that melanoblasts must migrate and proliferate to complete their journey. Recent advances on the ex-vivo imaging of skin explants has helped us understand how these cells migrate, and have provided a nice model to understand the role of different actin regulators in 3D cell migration (Mort et al., 2014). As melanoblasts migrate through the epidermis, they extend multiple dynamic pseudopods between the surrounding keratinocytes (Figure 1.13). The extension of long pseudopods is dependent on Rac1 which is crucial for efficient melanoblast migration, loss of Rac1 in the melanoblast lineage leads to coat colour defects (Li et al., 2011). Myosin contractility allows pseudopod retraction and force generation to squeeze through the junctions between keratinocytes. We have also identified a role for the actin bundling protein fascin in the size and lifetime of melanoblast pseudopods; loss of fascin leads to coat colour defects in adult mice (Ma et al., 2013). Interestingly, it appears that melanoblasts do not rely on matrix

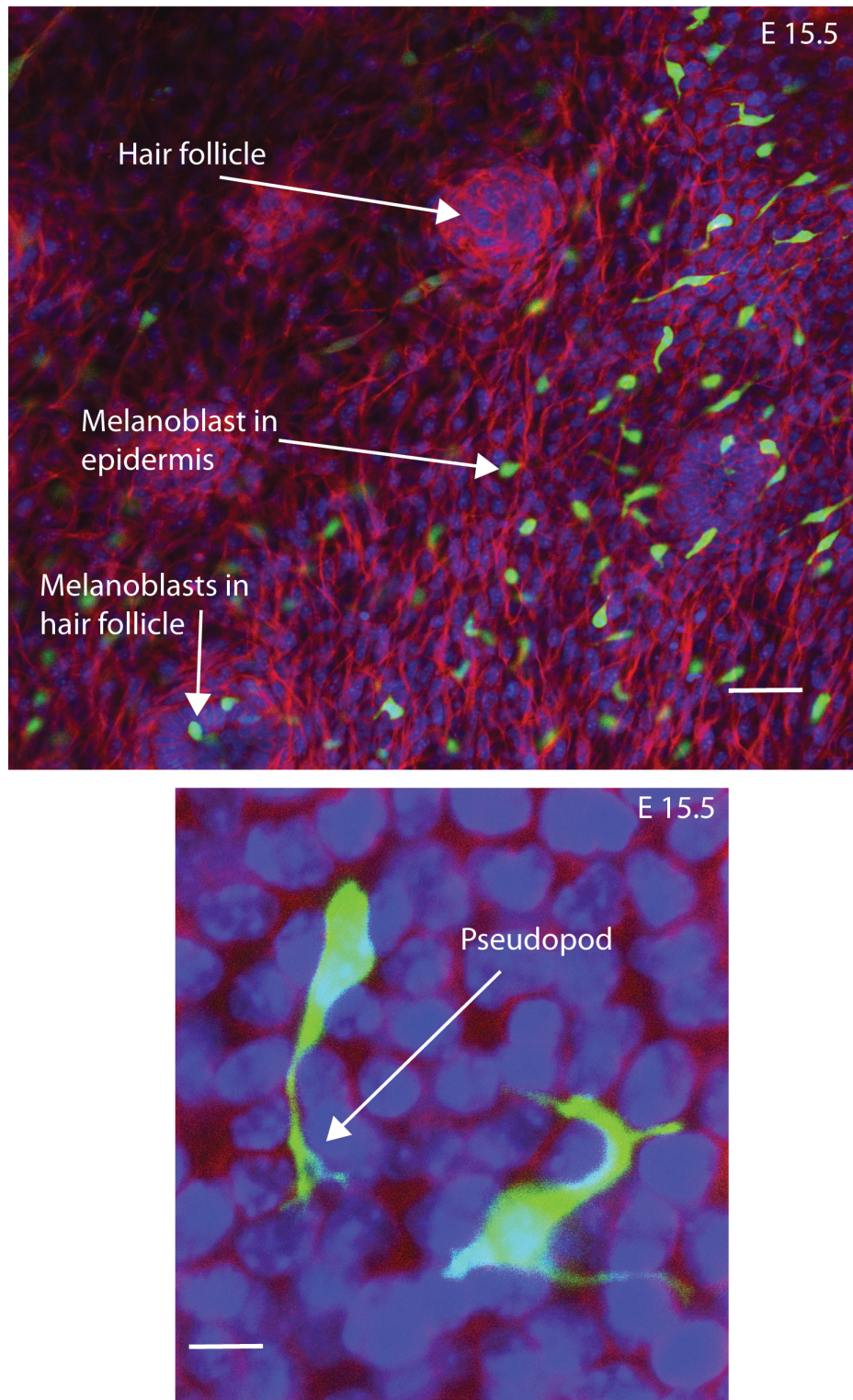
Nuclei Melanoblast Microtubules

Figure 1.13 Melanoblasts use pseudopods to migrate between keratinocytes
Staining skin from embryos at E15.5 expressing GFP in melanoblasts with tyrosinated tubulin (Red) and DAPI (Blue) shows that melanoblasts extend multiple pseudopods between the surrounding keratinocytes. Hair follicles can be seen as dense groups of keratinocytes, and at this time point melanoblasts have started to enter this structure. Scale 100 μm (top panel) 10 μm (bottom panel).

degradation to cross the basement membrane or to move between keratinocytes as deletion of N-WASP, a key factor in invadopodia formation did not lead to coat colour defects (Li et al., 2011).

In addition to their efficient migration, melanoblasts must also proliferate to fill the developing embryo. By combining mathematical modelling with experimental observation, Larue et al. have suggested that melanoblast-doubling time is around 16 hours, and that melanoblasts proliferate three times faster in the epidermis (Larue et al., 2013). Interestingly, the numbers of melanoblasts present at each time point are extremely consistent between embryos, suggesting tight regulation over this process. It remains unclear, however, whether melanoblast migration and proliferation, in conjunction with contact inhibition together suffice to fill the embryo. It is still under debate whether the melanoblast journey is also driven by some kind of attractant, or if melanoblasts are following paths carved out by the developing nervous system below. Mathematical models are useful tools to investigate which of these factors might be playing a role in this process. A recent mathematical model by Mort et al. has suggested that melanoblast migration occurs through undirected migration, and that proliferation alone can explain defects in pigmentation (Mort et al., 2016). However, the parameters and assumptions behind these models are still being debated.

1.4.3 Melanoblasts from Schwann cells: a second wave

In addition to this ‘traditional’ mode of melanoblast migration through the epidermis, recent work from Adameyko et al. has provided substantial *in vivo* evidence that Schwann cell precursors (SCPs) could provide a second ‘wave’ of melanoblasts later in development (Adameyko et al., 2009). SCPs are associated with the perinatal nerves and provide protection and trophic support. Unlike early-specified melanoblasts, these neuronal lineage cells take a ventral path through the embryo, innervating lower levels of the skin (Figure 1.11). SCPs are dependent on contact with the nerve for survival. If they remain associated with the nerve, they will develop into myelinating and non-myelinating glial cells. However, their work demonstrates that SCPs which move away from the signalling environment of the developing nerve with high levels of neuregulin 1 take on melanocytic properties in both chicks and mouse models (Figure 1.14).

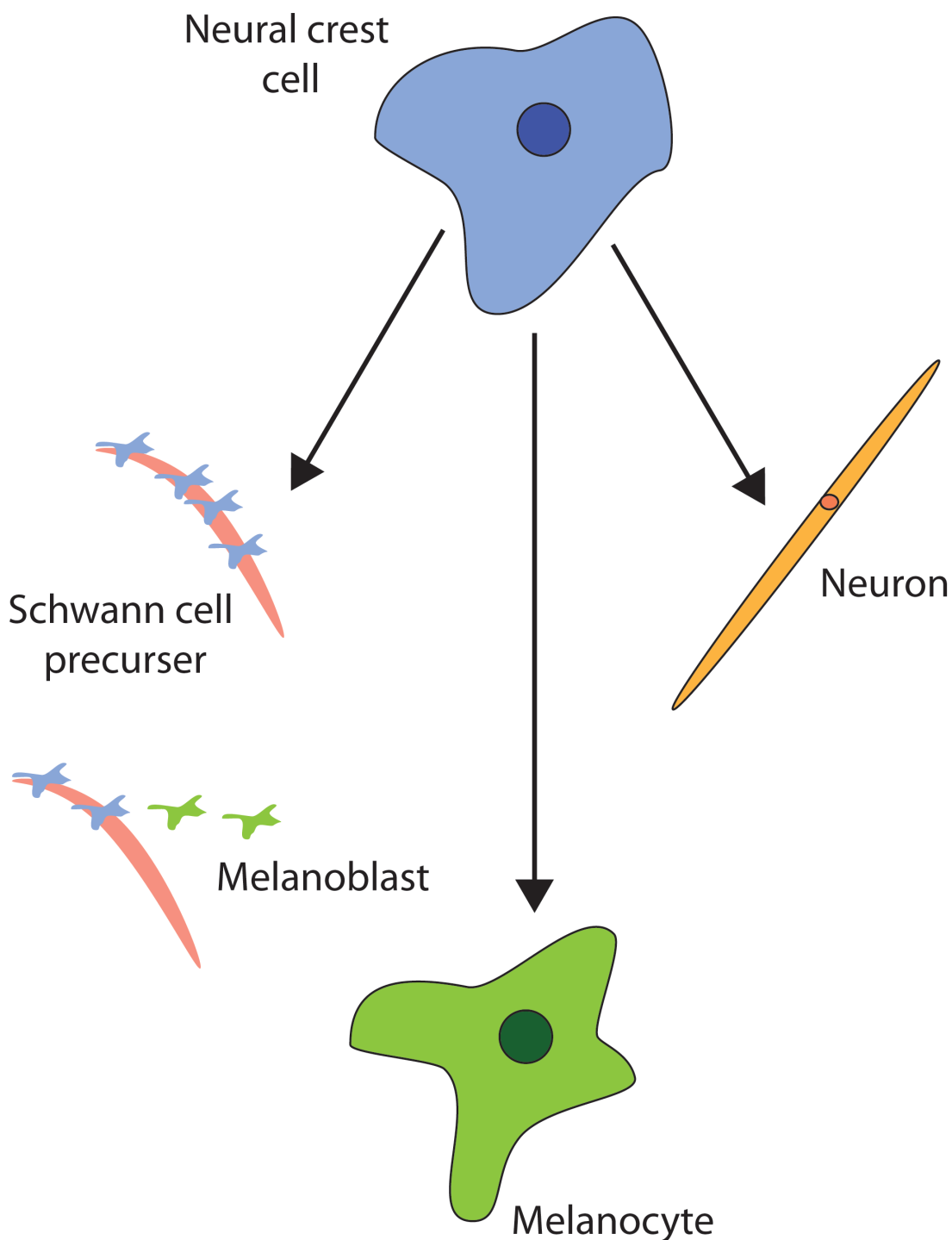


Figure 1.14 The peripheral nerve: a novel melanoblast source during development

It is widely believed that the majority of melanoblasts are specified from neural crest cells as they emerge from the neural tube, early in development. There is however now substantial *in vivo* evidence that this population of melanoblasts can be supplemented later on in development via differentiation of schwann cell precursors into melanoblasts. This occurs when schwann cell precursors move away from the signalling environment of the nerve, inducing gene expression changes towards the melanoblast lineage.

Adapted from Adameyko et al (2010).

It remains unclear, however, what proportion of melanoblasts derive from this pathway. Recent advances in imaging will allow further elucidation of the contribution of this pathway, and could change how we understand the melanoblast journey.

1.4.4 Melanoblasts to melanoma

1.4.4.1 Stages of melanoma progression

Melanoma, the most dangerous form of skin cancer, arises from the neoplastic transformation of melanocytes. Melanoma cells are plastic and aggressive, with a high propensity to metastasise. Melanoma most commonly develops from a benign nevus, a group of melanocytes that has undergone controlled division. A host of driver mutations have been associated with the development of melanoma, but the most common mutations occur in BRAF, a serine/threonine kinase that signals downstream of RTKs and Ras proteins. It is mutated in 30-70% of melanomas with mutation at V600E by far the most common (Klein et al., 2013). Mutations in BRAF, along with other mutations, drive progression from a benign to dysplastic nevus, which can then expand in the epidermis during the radial growth phase. Down-regulation of E-Cadherin and upregulation of N-cadherin are associated with downward growth through the basement membrane into the dermis, termed the vertical growth phase. At this stage, tumour cells acquire the ability to invade through the surrounding matrix and metastasise to secondary sites such as the lungs and brain via the bloodstream or lymphatic system (Figure 1.15).

1.4.4.2 Melanoma and embryonic signalling networks

The aggressive and motile nature of melanoma is in contrast to melanocytes, their cell of origin, which are terminally differentiated and largely static. However, as previously discussed, during development, the melanoblast lineage is extremely plastic and highly migratory. It is unsurprising then that a hypothesis was put forward, suggesting that melanoma is the result of aberrant re-activation of the embryonic signalling pathways that support the plastic differentiation and migration of the melanoblast lineage. Bailey et al. cleverly

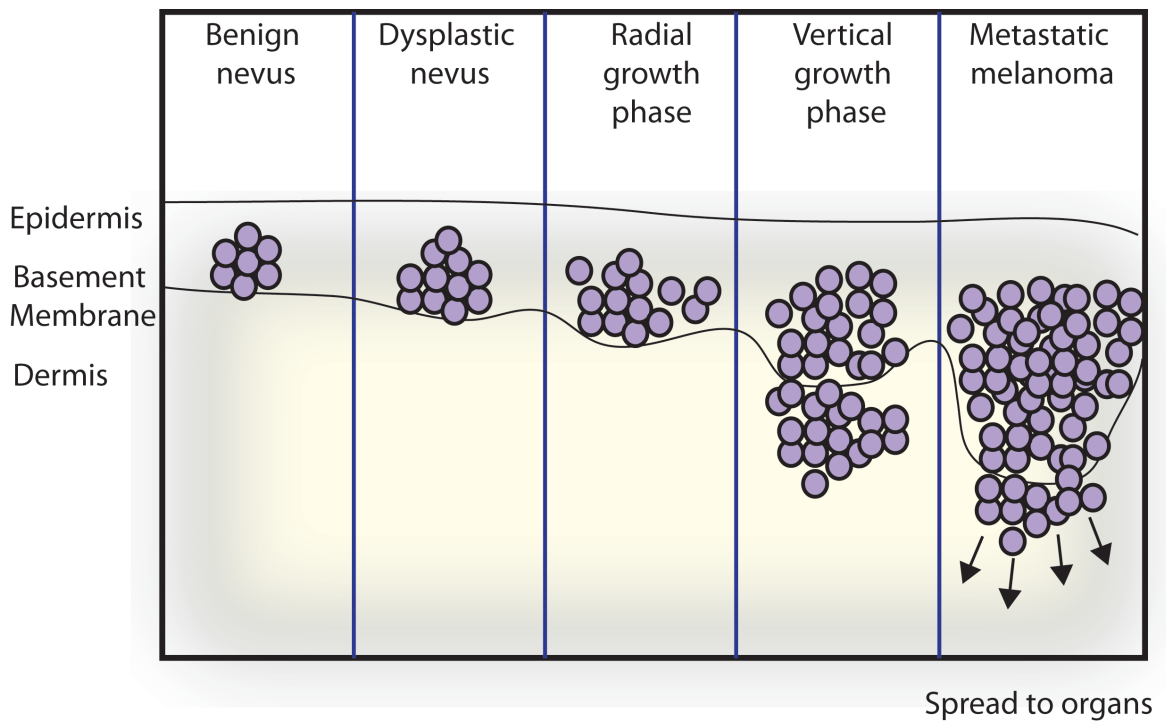


Figure 1.15 Melanoma Progression

Melanocytes in human skin can proliferate in a controlled manner into a group called a nevus. Commonly, mutations in BRAF can drive progression from a benign to a dysplastic nevus. Aberrant proliferation of this nevus, which is limited to the epidermis, is termed the 'radial growth phase'. In time, the lesion can progress to 'vertical growth phase' where transformed melanocytes invade through the basement membrane into the dermis. At this time, melanoma cells are extremely invasive, and they can invade towards the bloodstream and metastasise rapidly to secondary organs.

investigated this hypothesis by transplanting metastatic melanoma cells into the chick embryonic neural crest microenvironment. They saw that melanoma cells could respond to cues from the host tissue, adopting the correct migratory path through the skin, which was not the case for poorly invasive melanoma cells (Bailey et al., 2012). By carrying out genetic analysis on cell populations by laser-capture microdissection, they demonstrated that this ability was through the upregulation of genes associated with neural crest induction.

The transcription factor Pax3, which is pivotal in shaping the melanoblast lineage from the neural crest, is an interesting candidate to study in the context of melanoma. Studies have shown that Pax3 expression continues on after development of the melanocyte lineage (Gershon et al., 2005) and is expressed in melanoma (Plummer et al., 2008) where it can contribute to tumour cell survival (Scholl et al., 2001). We are still striving to understand what exact role Pax3 plays, but it is likely that its roles in maintaining stemness and promoting proliferation and migration could explain its function in melanoma progression (Medic and Ziman, 2009). Therefore, understanding the factors controlling melanoblast population of the embryonic skin may provide us with clues as to how melanoma cells spread through the body, giving us a new insight and markers for metastasis, with the aim of providing better therapeutic options for those with this disease.

2 Materials and Methods

2.1 Materials

2.1.1 Reagents and solutions

Table 1 Reagents and solutions

Reagent/Solution	Description	Source
Inhibitors		
CK869	Arp2/3 inhibitor	Tocris Bioscience
Nocodazole	Microtubule Polymerisation Inhibitor	Sigma
SMIFH2	Broad spectrum formin inhibitor	Sigma
Matrix		
Growth Factor Reduced Matrigel	Matrix	BD Bioscience
Fibronectin from Bovine Plasma	Matrix	Sigma
X-Gal Embryo Staining		
X-Gal		Promega
Gluteraldehyde		Sigma
Permeabilisation Solution	2 mM MgCl ₂ , 0.02% NP-40 and 0.01% sodium deoxycholate in PBS, pH 7.5	In house
X-Gal Buffer	2 mM MgCl ₂ , 0.02% NP-40, 2 mM K ₃ Fe(CN) ₆ and 2 mM K ₄ Fe(CN) ₆ containing 2 mg/ml X-Gal	In house
Immunohistochemistry		
Citrate Buffer		Dako
Hematoxylin		Beatson Histology Service
PBST		In house
Blocking buffer	Rabbit/Goat serum in PBS	Sigma
SDS-PAGE and Western Blotting		
RIPA Buffer	50 mM Tris-HCl, 150 mM NaCl, 1% NP-40 and 0.25% Nadeoxycholate	In house
NuPAGE Reducing Reagent 10X		Invitrogen
NuPAGE Bis-TRIS gels	4-12%, 10%, 12%	Invitrogen
Protein Ladder	PageRuler	Thermo Fisher Scientific
Nu PAGE Protein Sample buffer 4X		Invitrogen
Western Membranes	Amersham Protran 0.45 µm	GE healthcare

MOPS Running Buffer 20X		Life technologies
Transfer Buffer 10X		Beatson Central Services
TBST 10X	10mM Tris-HCl, pH 7.4, 150mM NaCl	Beatson Central Services
Protease Inhibitor Cocktail		Thermo Scientific
Phosphatase Inhibitor Cocktail		Thermo Scientific
Cloning and Molecular Biology		
DNA Loading Dye		In house
DNA Ladder	O'GeneRuler	Thermo Fisher Scientific
DNA Visualisation Dye	Midori Green	Geneflow
TAE	40mM Tris, 0.1% glacial acetic acid, 1 mM EDTA	Beatson Central Services
TE	10mM Tris-HCl, pH 8.0, 1mM EDTA	Beatson Central Services
PCR Mastermix		Takara
Kanamycin		Sigma
Ampicillin		Sigma
L-Broth		Beatson Central Services
Genotyping Buffer	100mM Tris HCl, 5 mM EDTA, 0.2%SDS, 200 mM NaCl at pH 8.5	In house (Max Nobis)
Cell Culture		
DMEM		Gibco
F-12 Nutrient Mixture		Gibco
Fetal Bovine Serum		Gibco
L-Glutamine		Gibco
Primocin		InvivoGen
PMA		Sigma
HBSS 10X		Gibco
Dissociation Buffer		Gibco
Trypsin		Gibco
PE	PBS 1 mM EDTA	Beatson Central Services
OHT		Sigma
DMSO		Fisher Chemicals
Doxycyclin		
Penicillin-Streptomycin		Gibco
PBS	170mM NaCl, 3.3mM KCl, 1.8 mM Na ₂ HPO ₄ , 10.6mM H ₂ PO ₄	Beatson Central Services
PBT	0.1% BSA+0.01% Tween 20 in PBS	In house
OptiMEM		Gibco
Collagenase Type I		Gibco
Collagenase Type IV		Gibco
Puromycin		Invivogen
Polybrene		Sigma
Propidium Iodide		Sigma
Ethanol		VWR chemicals
AllStars Neg control siRNA	20 nmol	Qiagen

Immunofluorescence		
PFA		Electron Microscopy Studies
Methanol		VWR Chemicals
Permablisation buffer	PBS 1% Triton	In house (triton sigma)
Blocking buffer	PBS 10% Goat serum	Sigma
Mounting Solution	Prolong Antifade	Thermo Fisher
BSA		Sigma
Formalin		In house
RNA Isolation and Sequencing		
RNA ScreenTape Sample Buffer		Agilent Technologies
RNA ScreenTape Ladder		
RNase-free water		Ambion

2.1.2 Antibodies and Dyes

Table 2 Antibodies and dyes

Antibody	Source	Usage
Mouse anti-Cdc42	BD Bioscience	WB 1:500
Goat anti-DCT TRP2	Santa Cruz	IHC 1:200 WB 1:500
Mouse anti-Rac1	Cytoskeleton	WB 1:500
Rabbit anti-RhoA	Cell Signalling	WB 1:1000
Rabbit anti-IQGAP1	Cell Signalling	WB 1:1000
Rabbit anti-PAK2	Cell Signalling	WB 1:1000
Rabbit Phospho-PAK1 (Ser199/204)/PAK2 (Ser192/197)	Cell Signalling	WB 1:1000
Rabbit anti-Phospho-Myosin Light Chain 2(Thr18/Ser19)	Cell Signalling	WB 1:1000
Rabbit anti-FAK	Cell Signalling	WB 1:1000
Rabbit anti Phospho-FAK	Cell Signalling	WB 1:1000
Mouse anti- YAP(1A12)	Cell Signalling	WB 1:1000
Rabbit anti-Phospho-YAP	Cell Signalling	WB 1:1000
Ki67 rabbit anti-Ki67	Neomarkers, SP6	IHC 2:200
BrdU mouse	DAKO	FACS 1:40
BrdU mouse	BD Bioscience	IHC
Rabbit N-WASP	Cell Signalling	WB 1:1000
Mouse T-MLC MRCL3/MRCL2/MYL9 (E-4)	Santa Cruz	WB 1:500
Rabbit anti-p34-Arc	Millipore	WB 1:500 IF 1:200
Mouse ERK	Cell Signalling	WB 1:500
Rabbit P-ERK	Upstate	WB 1:500
Rat Beta 1 integrin	Millipore	WB 1:500 IF 1:1000
Rabbit α 4 integrin	Cell Signalling	WB 1:1000

Rabbit α 6 integrin	Cell Signalling	WB 1:1000
Rabbit α V integrin	Cell Signalling	WB 1:1000
Rabbit B 3 integrin	Cell Signalling	WB 1:1000
Rabbit P-Paxillin	Cell Signalling	WB 1:1000 IF 1:200
Goat WAVE2 (H-110)	Santa Cruz	IF 1:50
YAP mouse	Santa Cruz	IF 1:100
Rabbit Ki67 (SP6)	Thermo Scientific	IHC 1:400
Mouse GAPDH	Ambion	WB 1:3000
Rabbit GAPDH	Cell Signalling	WB 1:3000
Mouse Alpha Tubulin	In house	WB 1:3000
Rabbit WASH	Atlas	IF 1:100
Rabbit EEA1	Cell Signalling	IF 1:200
Rabbit Rab7	Cell Signalling	IF 1:50
Rabbit Clathrin	Cell Signalling	IF 1:100
Mouse HRP secondary	Cell Signalling	WB 1:200
Rabbit 800	Thermo Scientific	WB 1:10000
Mouse 800	Thermo Scientific	WB 1:10000
Donkey anti- Rabbit 680	Life Technologies	WB 1:10000
Donkey anti- Mouse 680	Life Technologies	WB 1:10000
Donkey anti-goat 680	Invitrogen	WB 1:10000
Goat anti-Mouse 594	Life Technologies	IF 1:1000
Goat anti-Rabbit 488	Life Technologies	IF 1:1000
Goat anti-Mouse 488	Life Technologies	IF 1:1000
Donkey anti-Rabbit 594	Life Technologies	IF 1:1000 IHC 1:500
Donkey anti-Goat 488	Life Technologies	IF 1:1000 IHC 1:500
Donkey Anti-Mouse 594	Life Technologies	IHC 1:500
Goat anti-Rat 568	Life Technologies	IF 1:1000
Phalloidin 488	Life Technologies	IF 1:200
Phalloidin 589	Life Technologies	IF 1:200
Phalloidin 647	Life Technologies	IF 1:200
Rabbit anti-Goat biotinylated	Dako	IHC 1:250

2.1.3 Kits

Table 3 Kits

Kit	Source
Precision Red Advanced Protein Assay	Cytoskeleton
Rapid DNA ligation kit	Roche
RNeasy isolation kit	Qiagen
DNase Kit	Ambion
QIAshredder	Qiagen
RNase OUT	Invitrogen
Lipofectamine 2000	Invitrogen
Lullably	OZ Biosciences
Gel Extraction kit	Zymo Research
ECL substrate pico	Thermo Scientific

ECL Substrate fempto	Thermo Scientific
Melanin bleach kit	Polysciences Inc
ABC reagent	Vector Laboratories
Alkaline phosphate	Vector Laboratories
Active Rac pull-down kit	Cytoskeleton
PCR mastermix	Takara
pHrodo Green pH indicator	Thermofisher

2.1.4 DNA Constructs

Table 4 DNA constructs

Construct	Vector type	Source
Cdc42 shRNA clone 70288	GIPZ Lentiviral shRNAmir vector	GE Healthcare
Cdc42 shRNA 2 clone 488921	GIPZ Lentiviral shRNAmir vector	GE Healthcare
Non-Targeting	TRIPZ Lentiviral shRNAmir vector	GE Healthcare
Cdc42 shRNA clone 70288	TRIPZ Lentiviral shRNAmir vector	This study
Cdc42 shRNA 2 clone 488921	TRIPZ Lentiviral shRNAmir vector	This study
Cdc42-FLARE.dc	Transient expression vector	Dr. Klaus Hahn
dTurquoise	Transient expression vector	Dr. Klaus Hahn
GFP-paxillin	Transient expression vector	
RacV12	Transient expression vector	Prof. L Machesky
Rac-GFP	Transient expression vector	Prof. L Machesky
Cdc42-YFP	Transient expression vector	Prof. L Machesky
EGFP.N1	Transient expression vector	Prof. L Machesky
Venus	Transient expression vector	Max Nobis/Kurt Anderson

2.1.5 Oligos

Table 5 Oligos

Gene	Catalogue number	Sequence
PCR Primers		
RhoA JVH 11		AGCCAGCCTCTTGACCGATTTA
RhoA JVH 15		TGTGGGATACCGTTTGAGCAT
pTRIPZ sequencing primer		GGAAAGAATCAAGGAGG

2.1.6 RNA Sequences

Table 6 RNA sequences

	Clone ID	Sequence
Cdc42 (mouse) 70288	V2LMM-70288	TAGGAACTCAATCCATTTG
Cdc42 (mouse) 488921	Gene	AACTTAGCGGTCGTAGTCT

2.2 Methods

2.2.1 Mouse strains and genotyping

Table 7 Mouse strains and genotyping

Allele	Source	Details
Cdc42 flox	Cord Brakebusch	Previously described (Czuchra et al., 2005)
Tyrosinase CreB	Lionel Larue	Previously described (Delmas et al., 2003)
Lifect-mEGFP	In house	Previously described (Li et al., 2011)
LacZ/EGFP	Peter Jackson	Previously described (Novak et al., 2000)
DCT-LacZ	Peter Jackson	Previously described (Mackenzie et al., 1997)
Tyrosinase Cre-ERT2	Owen Samson	Previously described (Yajima et al., 2006)
Ink4a	Owen Samson	Previously described (Ackermann et al., 2005, Serrano et al., 1996)

2.2.1.1 Extracting mouse tail DNA and manual genotyping

Mice tails were lysed in 400 μ l genotyping buffer (Table 1) by incubation overnight at 800 rpm at 55 °C. The following day, 300 μ l of water was added and lysates were clarified by spinning for 15mins at 14000 rpm at 4 °C and the supernatant transferred to a new tube. Then 600 μ l of isopropanol was added and mixed. Tubes were spun down at 14000 rpm at 4 °C and the supernatant was removed carefully. The pellet was washed in 500 μ l of ethanol and spun again at 14000 rpm at room temperature. The ethanol was aspirated carefully and the pellet was left to air dry. The pellet was resuspended in 30 μ l of TE (Table 1). The PCR reaction was carried out using the BIO-RAD T100 Thermal Cycler. 1 μ l of the isolated tail DNA was used in the PCR reaction along with 0.5 μ l of each primer and 25 μ l of the PCR mastermix (Table 3) (cycle : 94°C 2 min, 94°C 30 sec, 55°C 30 sec, 72°C 30sec, 72°C 10 min, 4°C, 35cycles. The reaction mixture was made up to 50 μ l with water. Then 5 μ l of PCR product was run through a 0.8% agarose gel to obtain the genotyping information.

2.2.2 Cell culture

2.2.2.1 Source of cell lines

Mouse melanoma B16 cells were obtained from ATCC. Primary melanocytes and primary mouse-tail fibroblasts were isolated from stock mice as described below.

2.2.2.2 Cell line maintenance

All cell lines were grown at 37°C in 5% CO₂ typically in 10 cm cell culture dishes. Melanocytes were cultured in F-12 growth media containing 10% FCS, 200nM PMA and 100 µg/ml primocin. Mouse melanoma B16 cells and mouse tail fibroblasts were grown in DMEM containing 10% FCS, 2 mM glutamine and penicillin-streptomycin. To passage cells, media was aspirated from confluent plates and washed briefly in PE (melanocytes) or PBS then incubated for 5 minutes with 1X trypsin and resuspended in 5 ml of media. Melanocytes were typically passaged at 1 in 5 and B16 F10 cells and mouse-tail fibroblasts at 1 in 10. Media was changed every 3 to 4 days.

2.2.2.3 Storage and defrosting of cell lines

To be frozen down, cells were washed and trypsinised as described above. Cells were re-suspended in growth media and spun down at 1000rpm for 5 mins. Cells were re-suspended in freezing down media (50% growth media, 40% FCS, 10% DMSO) and aliquoted into 1 ml cryovials and wrapped in cotton wool for gentle freezing at -80°C and then long-term storage in liquid nitrogen tanks. To defrost, vials were thawed at 37°C then diluted into 10ml of fresh media. Media was changed the following day.

2.2.2.4 Isolation of primary melanocytes

Melanocytes were isolated from 1 day old Cdc42 f/f CreER CDKN2^{-/-} (#1 #7, #2.1 #2.2) according to methods already described (Li et al., 2011). Mouse pups were culled by concussion of the cranium followed by exsanguination. Each pup was briefly dipped in 70% Ethanol then skin dissected from the back of the pup and cut into small pieces in 1.5 ml of type I and IV collagense and incubated for 40 mins at 37°C. Skin pieces were then centrifuged at 1000 rpm for 5 mins then re-

suspended in 10 ml 1x HBSS. Skin was spun down again at 1000 rpm for 5 mins and re-suspended in 2 ml dissociation buffer (Table 1) and incubated for 20 mins at 37°C. Skin pieces were then passed through 18g needle 10 times then 20g needle 10 times to break pieces up then strained through a 70 µm filter into 10 ml of wash buffer. Cells were then centrifuged and the pellet re-suspended in 4 ml of F12 media and plated into two wells of a 6-well dish. After cells had settled for 4 days, contaminating fibroblasts and keratinocytes were removed by treatment with G418 (50 µg/ml) for 4 days per week and extensive washing for at least 4 mins with PE. Pure cultures were obtained one to two months after isolation. Cells were treated with DMSO or 1 µM OHT for 5 days prior to use in assays, with media with drugs refreshed once.

2.2.2.5 Transient transfection

Typically, 1×10^5 cells were seeded into 6-well plates the day preceding transfection. Each well was transfected according to manufacturers instructions. For each well, 4 µg of plasmid was mixed in 200 µl of Opti-MEM media in an eppendorf. In a separate eppendorf, 8 µl of lipofectamine 2000 reagent was mixed with 200µl Opti-MEM media. Both were left for 5mins then mixed together for 20 mins before adding onto cells.

2.2.2.6 Lentiviral infections

On day 1, 2×10^6 293T cells were plated in 10 cm dishes, one for each transfection. On day 2, they were transfected using the calcium phosphate method. Cells were transfected with 10 µg of lenti construct, 7.5 µg of pSPAX2 packaging plasmid, 4 µg of pVSVG packaging plasmid. DNA was diluted in 440 µl of water then 500 µl of 2x HBS was added and mixed. Then 60 µl of 2 M CaCl was added and mixed thoroughly. The mixture was incubated at 37°C for 30 mins then mixed and added to plate. The following day media was removed and replaced with DMEM with 20% FCS. Recipient cells were also plated in appropriate media to be sub-confluent the following day. On day 4, the medium was removed from 239T cells with a 10 ml syringe and filtered directly onto the recipient cells and 2.5 µl of polybrene was added on top. Fresh medium was added to the 293T cells. This process of transferring virus containing medium to the recipient cells was repeated on day 5. On day 6, virus containing medium

was removed and replaced with DMEM/10% FCS containing the appropriate selection antibiotic. Medium with selection antibiotic was also added to a plate of untransfected cells to act as a control.

2.2.2.7 siRNA transfections

Typically, 1×10^5 cells were treated in suspension 6-well plates. For each well, 10 μl of 20 μM oligo or 2.5 μl of each of a 20 μM 4-oligo flexi-tube pack were mixed with 200 μl of Opti-MEM media. In another eppendorf, 8 μl of lullaby transfection reagent was mixed with 200 μl of Opti-MEM. Both tubes were left for 5 mins then mixed for 20 mins before being added onto cell suspension. This procedure was repeated 48 h later to deliver the second shot of siRNA. After 48 h cells were then tested for knockdown of protein by SDS-PAGE and western blotting.

2.2.3 SDS-PAGE and western blotting

2.2.3.1 Cell lysate isolation

Cells in appropriate culture dish were removed from the incubator, media aspirated and washed three times in ice cold PBS. Plates were then placed on ice and the appropriate volume of RIPA buffer containing protease and phosphatase inhibitors (typically 100 μl in 6-well dish and 300 μl for 10 cm dish) added to dish for 3-5 mins. Dishes were then scraped on ice and lysate transferred into chilled eppendorfs and centrifuged at 13000 rpm for 10 mins. The supernatant was transferred to a new eppendorf and either used immediately for SDS-PAGE or frozen down at -20°C for later use.

2.2.3.2 Lysate protein quantification

The protein concentration was estimated by adding 20 μl of lysate to 1ml Precision Red reagent (Table 3). The absorbance was read on the spectrophotometer and the protein concentration was directly calculated from this absorbance. Typically, 15 μg of protein was used for SDS-PAGE.

2.2.3.3 SDS-PAGE

Samples for SDS-PAGE were prepared by adding the correct volume of cell lysate (up to 26 μl) to 4 μl of NuPAGE sample reducing agent and 10 μl of NuPAGE

sample buffer. Samples were made to 40 µl with water. Samples were boiled for 1 min at 100°C before being loaded into correct percentage (4-12%, 10% or 12%) pre-cast Bis-Tris 10-well gel along with 10 µl of PageRuler protein ladder. Gels were run in MOPS running buffer at 140 V for around 100 mins.

2.2.3.4 Western blotting

Proteins separated by SDS-PAGE were transferred onto a membrane sandwiched between two pieces of whatman paper at 160V for 60 mins in blotting buffer with an ice pack. Membranes were blocked for 45 mins at room temperature in 5% milk TBST then incubated with primary antibody in 5% BSA TBST overnight at 4°C. Membranes were then washed for 3x 10 mins in TBST before adding the secondary antibody in 5% BSA TBST for 1 h at room temperature.

2.2.3.5 Development and quantification of western blots

Membranes were incubated with secondary antibodies conjugated with infra-red dye picked up in the 700 nm and 800 nm channels. Membranes were then scanned using LI-COR Odyssey CLx scanner. Blots shown are representative blots performed multiple times. Band intensities were quantified using the Li-COR Image Studio lite software.

2.2.4 Immunofluorescent staining of cells and immunohistochemistry

2.2.4.1 Immunofluorescence

Cells to be fixed and stained were seeded on 13 mm fibronectin-coated coverslips in a 6-well dish the previous day. Media was aspirated from coverslips and then they were washed 3 times with PBS. They were then fixed in 4% PFA for 20 mins or in -20°C methanol for 4 mins if staining to image microtubules. Coverslips were then washed 3 times in PBS then incubated with permeabilisation buffer (Table 1) at room temperature for 3 mins, washed three times with PBS then incubated with blocking buffer (Table 1) for 1 h at room temperature. After washing three times in PBS, coverslips were then inverted on top of 30 µl of primary antibody diluted to the manufactures instructions in 1% goat serum on parafilm for 1 h in a humidified chamber. Coverslips were returned to 6-well plates and washed three times with PBS. Coverslips were then inverted on top of

30 μ l of the appropriate species and class specific secondary antibody, with phalloidin if desired, in 1% goat serum on parafilm again in a dark humidified chamber. They were then returned to a 6-well dish and washed three times in PBS before being mounted in mounting media on glass slides. Slides were left overnight in the dark for mounting media to set then stored in the fridge. Staining was images using an inverted Nikon A1R confocal microscope.

2.2.4.2 Immunohistochemistry

Tissue was dissected and fixed at least overnight in formalin. For adult skin sections, skin was shaved dissected from the belly and back and stretched dermis down onto whatman paper. Skin and paper was cut into strips with the direction of the hair to achieve full cross-sections of the hair follicle and placed into formalin. For embryos sections, whole embryos were dissected, fixed in formalin then trimmed, cut transversely and embedded head or back limbs down onto the wax block by histology services. For staining, sections were first deparaffinised and rehydrated by passing through xylene then through an ethanol gradient. After washing in TBST, antigen retrieval was achieved by placing rehydrated slides in 300 ml of citrate buffer and microwaving in a pre-heated pressure cooker for 13 mins. Slides were then left to cool on ice. For fluorescent immunohistochemistry of embryo sections, slides were blocked, washed, then incubated in the correct dilution of primary antibody overnight in a humidified chamber at 4°C. After washing, sections were incubated with fluorescently conjugated secondary antibodies for 1h at room temperature. After final washing, sections were covered with coverslips in mounting media and left to set at room temperature overnight before moving to 4°C for long term storage. For immunohistochemical staining of adult skin, slides were blocked in 10% rabbit serum, washed in TBST, then incubated in the correct dilution of primary for 2 h in a humidified chamber at room temperature. After washing in TBST, sections were incubated with Rabbit-anti-goat biotinylated secondary antibody for 1 h at room temperature. Signal amplification was achieved using the Vectastain ABC kit prepared in TBST, incubation for 30 mins. The staining was revealed with the red alkaline phosphatase substrate kit prepared in 5 ml 200 mM TRIS-HCL pH8.2 (Table 3). When staining was complete, sections were passed up an ethanol gradient and finally in xylene. Sections were counterstained with hematoxylin for 2 mins then covered with coverslips in

mounting media and left to set at room temperature overnight before moving to 4 °C for long term storage.

2.2.4.3 Fixing and staining embryo skin explants

After imaging, skins were removed from the microscope and the media was removed from the imaging set-up. The skin was then fixed in 4% PFA overnight. After fixation, the skin was washed and the skin was cut from the dish and inverted onto a slide. The nucleopore membrane was slid from the top and the skin was mounted underneath a large coverslip in vectashield mounting media with DAPI. The skin was imaged the following day on a Nikon A1R confocal microscope.

2.2.5 Cloning and molecular biology

2.2.5.1 Agarose gel electrophoresis

Agarose gels were made up to the correct percentage (between 0.8% and 1.5% depending on the DNA fragment size) by mixing the agarose with TAE buffer and heating in the microwave until dissolved. Midori green was added before setting the gel with comb in a gel tank. Gels were run at 140 V in TE buffer and then viewed in the transilluminator. DNA fragments were excised using gel purification kit (Table 3).

2.2.5.2 Restriction digests

Enzyme digests were planned using the New England Biolabs double digest finder. Digests contained 1X the appropriate amount of enzyme buffer typically 10 ug of DNA, 5-10 U of enzyme made up to 20 µl with water. Reactions were incubated overnight at 37°C.

2.2.5.3 Ligation

DNA ligations were achieved using the Roche Rapid DNA ligation kit according to the manufacturers instructions. Vector DNA and insert DNA were diluted in 1X DNA dilution buffer to a final volume of 10 µl. Then 10 µl of T4 DNA ligation buffer was added to the vile. Finally 1 µl of T4 DNA ligase was added. After mixing, the vile was incubated for 5 min at room temperature. 2 µl of this

reaction was then used in a transformation reaction and clones were selected and screened by sequencing.

2.2.5.4 Transformation of competent cells

Competent *E. coli* DH5 α were thawed on ice for 15 mins, the plasmid DNA was added to cells and incubated on ice for a further 15 mins. Cells were then heat-shocked at 40°C for 30 seconds then incubated on ice for a further 2 mins. Then 500 μ l of pre-heated L-Broth was added to the heat shocked cells and the cells were placed shaking in a 37°C incubator for 1 h before plating on pre-warmed LB agar plates containing the correct selection antibiotic and incubated overnight at 37°C.

2.2.6 Embryo study techniques

2.2.6.1 X-Gal staining of embryos

Timed embryos expressing B-Galactosidase under the control of the DCT promoter were harvested and stained as described previously (Loughna and Henderson, 2007, Ma et al., 2013). Embryos were dissected in PBS and immediately fixed in ice-cold 0.25% glutaraldehyde in PBS for 30 mins. Embryos were washed for 10 mins in ice-cold PBS, and placed in permeabilisation solution (Table 1) for 30 mins at room temperature and stained with X-gal buffer (Table 1) in PBS for 48 hrs at 4°C. Embryos were stored in 10% formalin after extensive washes with PBS. Embryo images for quantification were taken at the same magnifications with a Zeiss Stemi-2000 dissection microscope (EOS utility, Edmund Optics, NJ, USA).

2.2.6.2 Ex-vivo skin explant imaging

Experimental set up was adapted from (Mort et al., 2010) and (Li et al., 2011). Briefly, a freshly dissected E15.5 embryonic skin sample was sandwiched between a nuclepore membrane (Whatman) and a gas permeable Lumox membrane in a 24-well Greiner Lumox culture dish, so that the epidermal side of skin was in contact with Lumox membrane. To immobilize the sample, Matrigel (BD Bioscience) was used to cover the membrane and incubated at 37°C for 10 min. Culture medium (Phenol red free DMEM supplied with 10% FBS and 100

mg/ml primocin (InvivoGen)) was added. Time-lapse images were captured using an Olympus FV1000 or Nikon A1 confocal microscope in a 37°C chamber with 5% CO₂ for 4 hrs.

2.2.6.3 Melanoblast tracking in ex-vivo skin explants

Melanoblasts were tracked separately using the MTrackJ ImageJ plugin from time-lapse images taken every 5 minutes for 4 hrs. Speed measurements were taken from these tracks produced by the MTrackJ plugin. At least 100 melanoblasts from at least three different skin explants from different embryos were quantified. Mean values \pm SEM and statistical analysis were calculated and plotted using Graphpad Prism (Graphpad Software), and significance was determined using two-tailed unpaired t-tests.

2.2.6.4 Melanoblast proliferation studies

To assess the proliferation rate of melanoblasts, the mother was injected with BrdU either 2 hrs or 24 hrs before harvesting, dissecting and fixing of embryos. Once fixed, embryos were trimmed and cut transversely and embedded head or feet down into the paraffin block. These sections were then stained fluorescently by IHC to visualise DCT, BrdU and Ki67 expression within the skin as described above.

2.2.6.5 Dermal/Epidermal imaging of embryos

Timed embryos expressing B-Galactosidase under the control of the DCT promoter were stained with X-Gal as described above. After staining and fixation, embryos were trimmed, sectioned transversely and embedded head or tail down into wax blocks by the histology department. Sections were then counterstained with light eosin and the number of melanoblasts sitting above and below the basement membrane was quantified from at least three different sections from three different embryos from three different litters.

2.2.7 Cell biology techniques

2.2.7.1 Live cell imaging

To image melanocyte migration, cells were plated onto glass-bottom dishes coated with fibronectin. The dishes were prepared by incubation with 20 $\mu\text{g}/\text{ml}$ fibronectin in PBS for 2 hrs followed by extensive PBS washes. Cells were seeded onto dishes the day prior to imaging. Time-lapse movies were acquired using a Nikon TE2000 microscope in a 37°C chamber with 5% CO₂.

2.2.7.2 Quantifying adhesion dynamics

For adhesion dynamics quantification, melanocytes were transfected with GFP-Paxillin, replated on fibronectin and imaged 24 hrs later. Live-cell imaging was performed using a Zeiss 880 Laser Scanning Microscope with Airyscan at 37°C/5% CO₂ with a Plan-Apochromat 63x/1.4 oil DIC M27 objective. Cells were imaged for 30 min at 1 min intervals using the 488 nm laser. Movies were processed and exported using ZEN software (version 2.1 SP1 (black)). The x/y drift was corrected using the Image Stabilizer plugin (K. Li, "The image stabilizer plugin for ImageJ: http://www.cs.cmu.edu/~kangli/code/Image_Stabilizer.html, February, 2008) for Fiji/Image J (version 1.49o) prior to analysis.

Movies were submitted to the Focal Adhesion Analysis Server (FAAS) (Berginski and Gomez, 2013) for analysis of adhesion dynamics. The mean rate of adhesion assembly/disassembly was calculated for each cell (n = 15 cells per condition over 3 independent experiments).

2.2.7.3 Melanocyte growth assay

DMSO or OHT treated melanocytes as described were seeded into 6 well plates in triplicate. Cells were counted each day for 4 days using a haemocytometer. This was carried out 3 times.

2.2.7.4 FACS

For cell-cycle analysis, three sub-confluent plates treated for 5 days with either DMSO and OHT were incubated for 3hrs with 10 μM BrdU (BD bioscience). Plates were then washed in PBS, trypsinised and spun down at 1000 rpm for 5 mins.

Cells were then fixed in room temperature 70% Ethanol in PBS while vortexing and left at 4°C overnight. Tubes were brought to room temperature before pelleting and washing with PBS. Cells were pelleted and bleached using a melanin bleach kit (Table 3) according to the manufacturers instructions. Pelleted cells were re-suspended in 1ml of pre-treatment solution A from kit for 2 mins, washed with PBS then treated with treatment solution B from kit for 1 min. After extensive washes with PBS cells were then treated with 4N HCl for 15 mins then stained with mouse Anti-BrdU in PBT for 30 mins. Cells were then pelleted and washed then incubated with Alexa-488 conjugated goat anti-mouse secondary antibody in PBT for 30 mins. After washes, cells were stained with Propidium Iodide for 30 mins at room temperature then acquired on a BD FACS-Calibur flow cytometer.

2.2.7.5 Adhesion studies

To quantify adhesion size and number, melanocytes pre-treated with DMSO or OHT for 5 days were seeded onto coverslips coated with 20 µg/ml fibronectin the day prior to fixation. The following day, coverslips were fixed in 4% PFA and stained with p-paxillin and rhodamine phalloidin according to the immunofluorescence protocol described above. Adhesions were quantified using the 'analyse particle' function of the ImageJ software. Cells were selected one at a time using the imageJ selection tool on the p-paxillin stained channel. A standard threshold was applied to the cell, picking out individual adhesions. Next, the ImageJ binary 'watershed' filter was applied to the image to separate areas joined by only one or two pixels, helping to separate adjacent adhesions. The 'analyse particle' function was then applied to count the number of adhesions per cell and the area of each adhesion. The results generated from this analysis were compared with some test quantifications done by hand to ensure accuracy. Cells taken from three independent experiments, at least 46 cells per genotype

2.2.7.6 IncuCyte ZOOM invasion and proliferation assays

For invasion assays using the IncuCyte ZOOM, 1×10^5 B16 cells pre-treated for 5 days with 2 µg/ml doxycyclin were plated into 96-well forming a confluent layer the next day. A scratch wound was then made in this layer using the

WoundMaker tool to create 96-homogeneous scratches simultaneously. The well was then cleaned with PBS and dried before placing 50 μ l of matrigel diluted 1:2 on top of the layer. Once set for 45 mins at 37°C, media containing doxycycline was then added on top and the plate was taken to the IncuCyte ZOOM system. For proliferation assays using the IncuCyte ZOOM, 1×10^4 B16 cells pre-treated for 5 days with doxycycline were plated the previous day in media containing doxycycline. The following day, the plate was taken to the IncuCyte ZOOM system. Each well was imaged every 2 h and the data collected using the IncuCyte ZOOM software. Invasion data was analysed using the wound confluence option and cell proliferation data was analysed using the confluence option. Data was exported into Excel format and plotted using Prism software.

2.2.7.7 xCELLigence cell spreading assay

For this assay, 1×10^4 melanocytes were seeded on a gold microelectrode microtiter plate well plate previously coated with fibronectin. The plate was immediately fitted into an ACEA RTCA xCELLigence machine and the conductivity of the plate was read every 15 mins. The conductivity is proportional to the area of the microtiter plate well covered with cells. The assay was performed in triplicate wells over two independent experiments.

2.2.7.8 Spheroids

To form spheroids, 70 μ l of 1.5% agarose was set in each well of a 96 well plate. After setting for 10 mins, 1000 B16 melanoma cells pre-treated with 2 μ g/ml doxycycline were added in 100 μ l of media to each well. Media was refreshed after two days of growth. After 5 days of growth, the spheroid was transferred onto 50 μ l of set matrigel and the media removed. Then 50 μ l of matrigel was placed on top, forming a sandwich with the spheroid in the centre. 100 μ l of media containing doxycycline was then added onto of the set matrigel. Embedded spheroids were then left to invade and images taken every second day.

2.2.7.9 Active Rac pull-downs

Pull-downs to determine the levels of active Rac in melanocytes were achieved using the Rac Activation Assay Biochem Kit (Cytoskeleton) according to

manufacturers instructions. Three sub-confluent dishes of melanocytes pre-treated for 5 days with DMSO or OHT were removed from the incubator and washed in 10 ml of PBS. All PBS was removed from the plate and plates were transferred to the cold room. Immediately, 400 μ l of lysis buffer was added to one DMSO and one OHT plate and the plates were sequentially scraped, lysed and the lysate finally transferred into a chilled eppendorf. The lysates were immediately clarified by centrifugation at 13,000 g for 1 min. At this point, 20 μ l of lysate was taken to estimate the protein quantification using Precision Red Advanced Protein Assay Kit. The absorbance was multiplied by 5 to determine the protein concentration in mg/ml. Samples were then diluted to be of equal protein concentration using ice-cold lysis buffer. 20 μ l of these equivalent samples was taken to represent the input on SDS-PAGE. Equal volumes of lysates now at equivalent protein concentration were added to 10 μ g of GST-PBD beads and incubated at 4°C rotating for 1 h. The beads were then pelleted at 10,000 xg at 4°C for 1 min. Most of the supernatant was removed and the beads then re-suspended in 500 μ l of wash buffer. Beads were once again pelleted and the supernatant removed. Beads were then re-suspended in 20 μ l of laemmli sample buffer and boiled for 2 mins. The samples were then analysed by SDS-PAGE then western blot probing with mouse-anti-Rac primary antibody (Cytoskeleton).

2.2.7.10 FLIM

A dual-chain Rac1 biosensor (CFP/YFP) was used to determine levels of active Rac in melanocytes. This construct and the control turquoise vector were gifted as collaboration from Hahn group (Machacek et al., 2009, Goedhart et al., 2010). The probe and control vectors were transfected transiently into melanocytes using the lipofectamine 2000 kit as described earlier. The day after transfection, melanocytes were moved onto fibronectin-coated plates. The following day, lifetime readings were taken from the whole-cell using the Nikon FLIM/TIRF system Z6014. The system was calibrated using fluorescein and readings from each repeat were taken on the same MCP. Lifetimes were read from at least 15 cells per condition from three independent experiments.

2.2.7.11 Melanocyte Inhibitor Studies

Melanocytes pre-treated with DMSO or OHT for 5 days were seeded onto fibronectin-coated (20 µg/ml) coverslips in 6-well plates. The following day, cells were treated with either 5 µm or 10 µm SMIFH2 (Sigma) or 20 µm or 40 µm of CK-869 (Tocris Bioscience) for 3 hrs. Control cells were treated with the corresponding volume of DMSO. Cells were then fixed in 4% PFA and stained according to the protocol above. For nocodazole experiments, cells were treated for 1hr on ice with 5 µg/ml of drug or appropriate volume of DMSO. Cells were then moved to 37°C for a further h before fixation in -20°C Methanol and staining via protocol above. For re-settling experiments, the same procedure was described above, but instead of fixation cells were trypsinised and moved onto a fresh 6-well glass-bottom plate with appropriate concentration of drug or DMSO. Cells were left for 30 mins to attach then imaged for 10 hrs using a Nikon TE2000 microscope in a 37°C chamber with 5% CO₂. Plates containing cells re-settled in the presence of nocodazole were removed from the microscope and fixed in -20°C methanol to ensure microtubules were still disrupted.

2.2.8 RNA Sequencing

2.2.8.1 RNA Isolation

RNA was isolated using the RNeasy kit from Qiagen according to the manufacturers instructions. Working with 1-5x10⁶ adherent cells per 10 cm plate, plates were removed from the incubator and placed on ice. Media was removed and the plate was washed with 10 ml ice cold PBS. Cells were then harvested in 1 ml cold PBS by scraping into an eppendorf. Cells were pelleted at 250 rcf for 5 min at 4°C and then placed on ice. The supernatant was aspirated and the pellet snap-frozen. At room temperature, 350 µl buffer RLT was added to the cell pellet. The lysate was pipetted into a QIAshredder column in a 2 ml collection tube and spun at full speed for 2 min. One volume of 70% ethanol was added to the homogenised lysate. The lysate was transferred into an RNeasy spin column placed in 2 ml collection tube. The column was centrifuged for 30 sec at 8000 rcf, the flow-through discarded and 350 µl buffer RW1 was added to the RNeasy spin-column. The column was centrifuged for 30 sec at 8000 rcf and the flow-through discarded. The bound RNA was eluted with 50 µl RNase free water. The RNA was then DNase treated using the DNase kit from ambion. To each tube

of isolated RNA, 6 µl of 10X buffer, 2 µl DNase1, and 2 µl RNase out was added. Tubes were incubated for 30 min at 37°C then 20 µl of DNase inactivation reagent was added. The inactivation reagent was removed by centrifugation at 8000rcf for 30 sec. RNA concentration was measured on the nanodrop and stored at -80°C before sequencing.

2.2.8.2 RNA quality check

The quality of the RNA isolated was checked using the Agilent Technologies TapeStation instrument according to the manufacturers instructions. 5 µl of RNA sample buffer and 1 µl of the RNA Ladder was added to the first tube in a mini-tube strip (RNase free). 5 µl of RNA sample buffer and 1µl of the RNA sample were then loaded into the following tubes. Samples were mixed in a vortex at 2000 rpm for 1 min. Samples were spun down and then heated to 72°C for 3 mins then placed on ice for 2 mins. Samples were spun down once again and loaded into the Agilent 4200 TapeStation instrument.

2.2.8.3 RNA sequencing and analysis

The RNA library was prepared using the Library Prep kit (Illumina TruSeq RNA Sample prep kit v2) according to methods previously described (Fisher et al., 2011). Libraries were sequenced using the Illumina NextSeq500 platform using the sequencing Kit High Output v2 75 cycles (2x36cycle Paired End, single index). Quality checks on the raw RNASeq data files were done using fastqc (<http://www.bioinformatics.bbsrc.ac.uk/projects/fastqc>) and fastq screen (http://www.bioinformatics.babraham.ac.uk/projects/fastq_screen/). RNASeq reads were aligned to the GRCm38 (Church et al., 2011) version of the mouse genome using tophat2 version 2.0.10 (Kim et al., 2013) with Bowtie version 2.1.0 (Langmead and Salzberg, 2012). Expression levels were determined and statistically analysed by a combination of HTSeq version 0.5.4p3 (<http://wwwhuber.embl.de/users/anders/HTSeq/doc/overview.html>), the R 3.1.1 environment, utilizing packages from the Bioconductor data analysis suite and differential gene expression analysis based on a generalized linear model using the DESeq2 (Love et al., 2014). Significantly changed genes ($p_{adj}<0.05$) were submitted to DAVID for Gene Ontology (GO) analysis (Huang da et al., 2009). KEGG Pathway analysis was performed for genes demonstrating an increase (Up)

or decrease (Down) in RNA expression between KO and WT cell lines. Significant KEGG GO Terms were identified ($pValue < 0.05$, Supplementary spreadsheet 1). Hierarchical clustering of \log_2 fold changes in gene expression was performed on the basis of Euclidian Distance using complete linkage and visualised using MultiExperiment Viewer (MeV v4.8).

3 Investigating the Role of Cdc42 in Melanoblast Migration and Proliferation

3.1 Introduction and aims

Since their discovery over 20 years ago, the Rho family of GTPases have been studied intensively, largely through *in vitro* studies using constitutively active and dominant negative mutants. Understanding this family and uncovering their roles in the global coordination of the actin cytoskeleton have revolutionised the way we understand cell movement. We are growing increasingly familiar with the different downstream effectors of the classic Rho GTPases Rho, Rac and Cdc42 and the roles they play individually in a motile cell in 2D. We now face the challenge of extending this knowledge into 3D systems. To date, amenable systems such as *Drosophila melanogaster* and *Caenorhabditis elegans* have helped us with this challenge, confirming that the classic Rho GTPase Cdc42 is indeed a master regulator of the actin cytoskeleton *in vivo*, required for epithelial morphogenesis, polarity and spindle orientation during development (Genova et al., 2000, Gotta et al., 2001). Knockout mice are also becoming available, however due to the prominent role of Cdc42 during embryonic development, a constitutive whole body knockout is lethal before E7.5 (Chen et al., 2000). For this reason, a tissue-specific knockout approach is necessary to investigate Rho GTPases *in vivo*.

Melanoblasts, the embryonic precursors of melanocytes, are an attractive and effective model in which to study 3D cell migration. These cells migrate great distances during development, navigating through both the dermal and epidermal skin environments. Recent technological advances now permit high resolution imaging of embryo skin. We can now observe melanoblast movement through the epidermis closely, and by driving melanoblast-targeted deletion of actin regulators, we are building a picture of how the actin cytoskeleton is controlled during 3D migration.

The role of Rac1 in melanoblast migration has previously been investigated in the lab, revealing Rac1 as a pivotal player in the melanoblast journey (Li et al., 2011). Targeted deletion of Rac1 in the melanoblast lineage led to coat colour

defects in adult mice. Skin explant imaging revealed that Rac1 null melanoblasts could only extend short stubby protrusions, resulting in extremely poor migration through the skin. Rac1 was therefore identified to be essential in the extension of long pseudopods through its activation of the SCAR/WAVE and Arp2/3 pathway. In addition to Rac1's role in migration, it is also important in promoting G1 to S phase cell cycle transition. This study demonstrated how effective and informative the melanoblast model could be in the study of Rho GTPases, and we therefore wanted to utilise it to investigate the loss of the other classical GTPases Cdc42 and RhoA.

The aim of this chapter is primarily to explore the function of Cdc42 during melanoblast population of the developing embryo, but also touching on RhoA's part in the melanoblast journey. We wanted to understand if these other classical Rho GTPases played distinct or similar roles to Rac1 in 3D cell migration. To do this, we aimed to delete these proteins in the melanoblast lineage and monitor mice for coat colour defects. In addition, we wanted to gain a deeper understanding of the part played by these Rho GTPases by performing high-resolution imaging of melanoblast migration and detailed analysis of melanoblast proliferation and cytokinesis. This study would provide a rare insight into the role of this family in mammalian cell migration in 3D. In combination with our previous knowledge of Rac1 in this system, this knowledge would also allow us to build a model of how these classical GTPases cooperate during 3D cell migration, while at the same time defining any unique contributions of individual GTPases.

3.2 Results

3.2.1 Loss of Cdc42 in the melanocyte lineage leads to coat colour defects, suggesting migration and proliferation defects

To investigate the role of Cdc42 in the melanoblast journey, a strategy was designed to achieve targeted deletion of a portion of the Cdc42 gene in the melanoblast lineage. To do this, mice carrying a Cdc42 transgene with two internal loxP sites (Czuchra et al., 2005) were bred with mice carrying CreB recombinase under control of the tyrosinase promoter. Tyrosinase is an enzyme which is important for melanin biosynthesis, and expression from its promoter begins around E10.5 in the melanoblast lineage (Delmas et al., 2003). CreB expression in melanoblasts leads to recombination between the loxP sites, and subsequent loss of the floxed Cdc42 allele (Figure 3.1A). Cdc42 f/f Tyr::CreB embryos were born at the expected Mendelian ratio, but pups were smaller and shaky due to some tyrosinase expression by neuronal tissues (not shown).

All Cdc42 f/f Tyr::CreB mice (n=20) displayed a white patch running down the ventral midline, ranging from half the area of the belly region to almost the whole area in size (Figure 3.1B). As well as the white belly region small white patches could often be seen along the dorsal midline of mice (indicated by yellow arrows). Pigmented areas contained frequent white hairs, and the paws and tails were hypopigmented. The back legs of Cdc42 f/f Tyr::CreB mice were often 'frog like', resulting in back leg paralysis on some occasions.

We wondered whether the hair follicles in hypopigmented areas of adult skin were devoid of melanocytes. To investigate this, dorsal and ventral sections of adult skin were histologically processed and stained with anti-Dopachrome tautomerase (DCT) antibody to reveal melanocyte location (Figure 3.2). Like tyrosinase, DCT is also involved in melanin biogenesis and is expressed by melanoblasts in the developing embryo at E10.5. Using this marker, melanocytes can be seen in both dorsal and ventral skin sections of control skin (Ctr). Hair follicles on the back of Cdc42 f/f Tyr::CreB embryos contain melanocytes, demonstrating that some Cdc42 null melanoblasts are able to home to hair follicles. However, hair follicles in areas

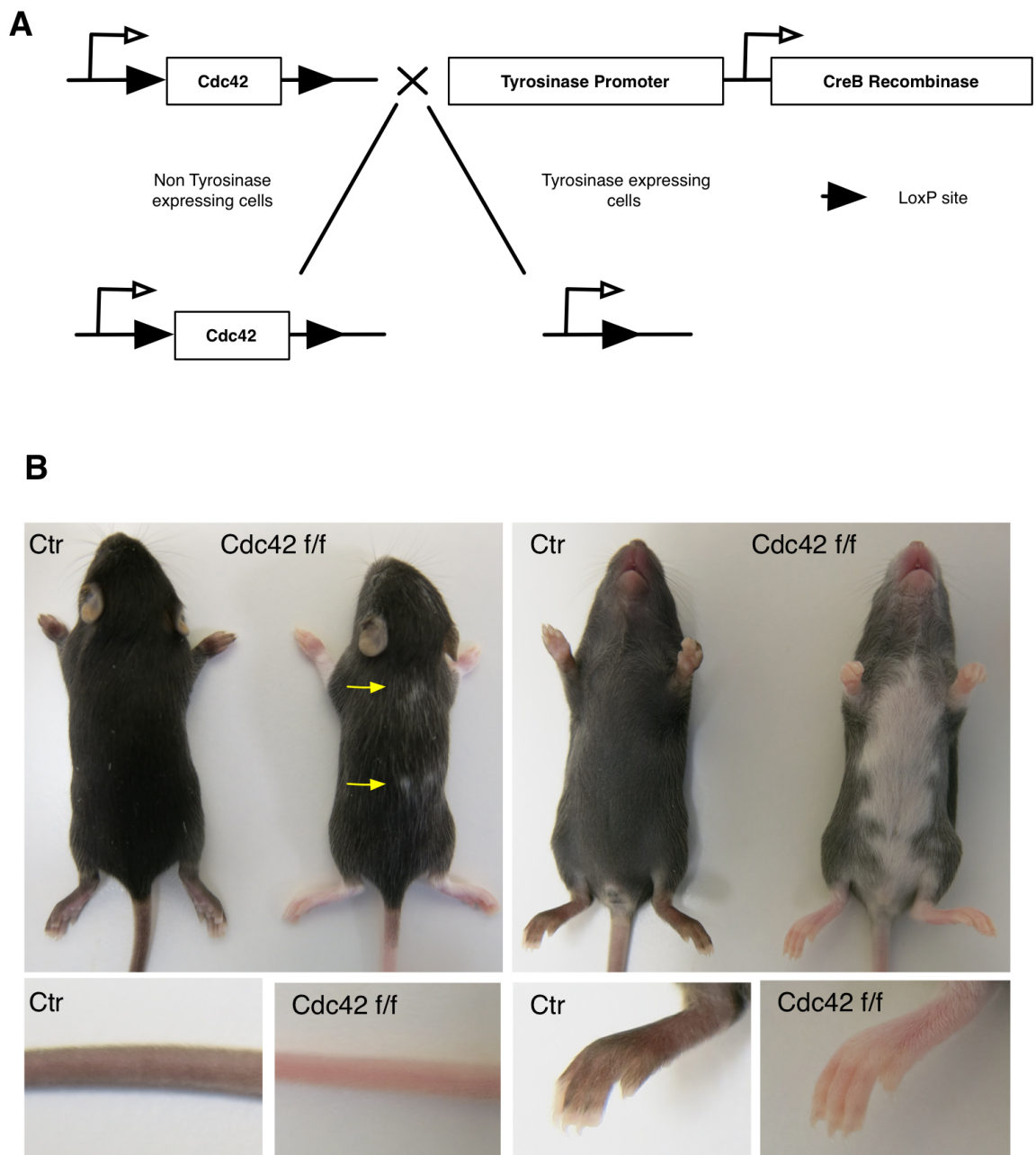


Figure 3.1 Loss of Cdc42 in the melanoblast lineage leads to coat colour defects in adult mice

In all images, Ctr=Control (Cdc42 wt/wt), Cdc42 f/f= Cdc42 f/f Tyr::CreB **(A)** Schematic of the gene targeting strategy leading to Cdc42 f/f Tyr::CreB mice. Cre recombinase is under the control of the tyrosinase promoter, leading to targeted deletion of Cdc42 in the melanocyte lineage. **(B)** Images showing coat, tail and limb colour of wild-type (Ctr) mice and Cdc42 f/f Tyr::CreB (Cdc42 f/f) mice at P22. Yellow arrows indicate dorsal white patches. Images represent n=20 mice.

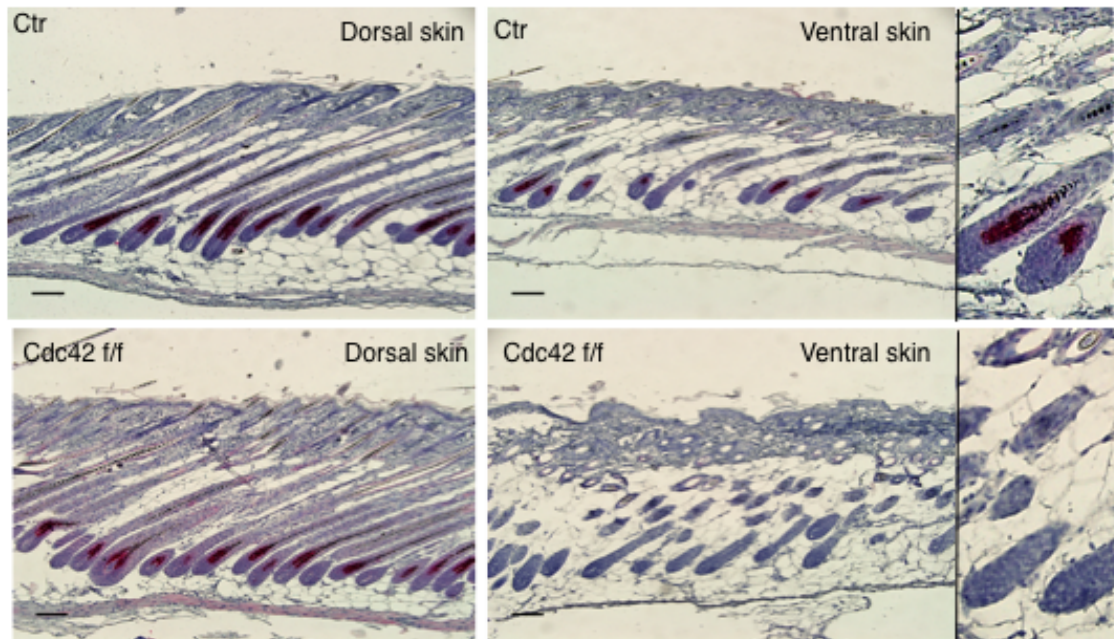


Figure 3.2 Melanocytes are not present in the hair follicles of hypopigmented areas

Sections from dorsal and ventral control (Ctr) and *Cdc42 f/f* *Tyr::CreB* (*Cdc42f/f*) pup skin stained with anti-DCT (melanocyte marker) and developed with alkaline phosphatase (red), counterstained with haematoxylin. Scale 100 μ m. Insets show hair follicles.

devoid of pigment on the ventral side of Cdc42 f/f Tyr::CreB embryos do not contain melanocytes. Therefore, the pigment defects seen in Cdc42 f/f Tyr::CreB embryos are due to a lack of melanocytes in areas distal to the neural tube, where these cells begin their journey.

3.2.2 Loss of RhoA in the melanoblast lineage does not lead to coat colour defects

Having previously described a role for Rac1 in the melanoblast journey (Li et al., 2011), and having observed that Cdc42 was also important, we were curious to investigate the role RhoA plays, as it is also a key regulator of the actin cytoskeleton. RhoA most notably plays a role in stress fibre formation and in acto:myosin contractility, amongst many other functions important for cell migration (Raftopoulou and Hall, 2004).

RhoA was removed from the melanoblast lineage using the same strategy as for deletion of Cdc42 (Figure 3.1A). RhoA f/f Tyr::CreB mice were born at the expected Mendelian ratio and appeared to be healthy and indistinguishable from control littermates (Figure 3.3A). The fur, paws and tail of RhoA f/f Tyr::CreB mice were normally pigmented, and this was still the case after aging mice to 6 months (data not shown). To confirm successful floxing of the RhoA gene in our mouse model, we carried out a genotyping PCR on mouse-tail DNA. This showed that the RhoA allele was indeed floxed (Figure 3.3B). This suggests that RhoA alone is not necessary for melanoblasts to populate the developing embryo, but it does not rule out the possibility that other Rho family GTPases, including RhoB and RhoC might compensate for the loss of RhoA.

3.2.3 Cdc42-null melanoblasts fail to fully populate the developing mouse embryo before birth

To further understand the pigment defects observed after removing Cdc42 from the melanoblast lineage, the melanoblast journey was visually tracked in control and Cdc42 f/f Tyr::CreB embryos at different embryonic stages by breeding these mice with DCT::LacZ reporter mice (Figure 3.4). This reporter gene leads

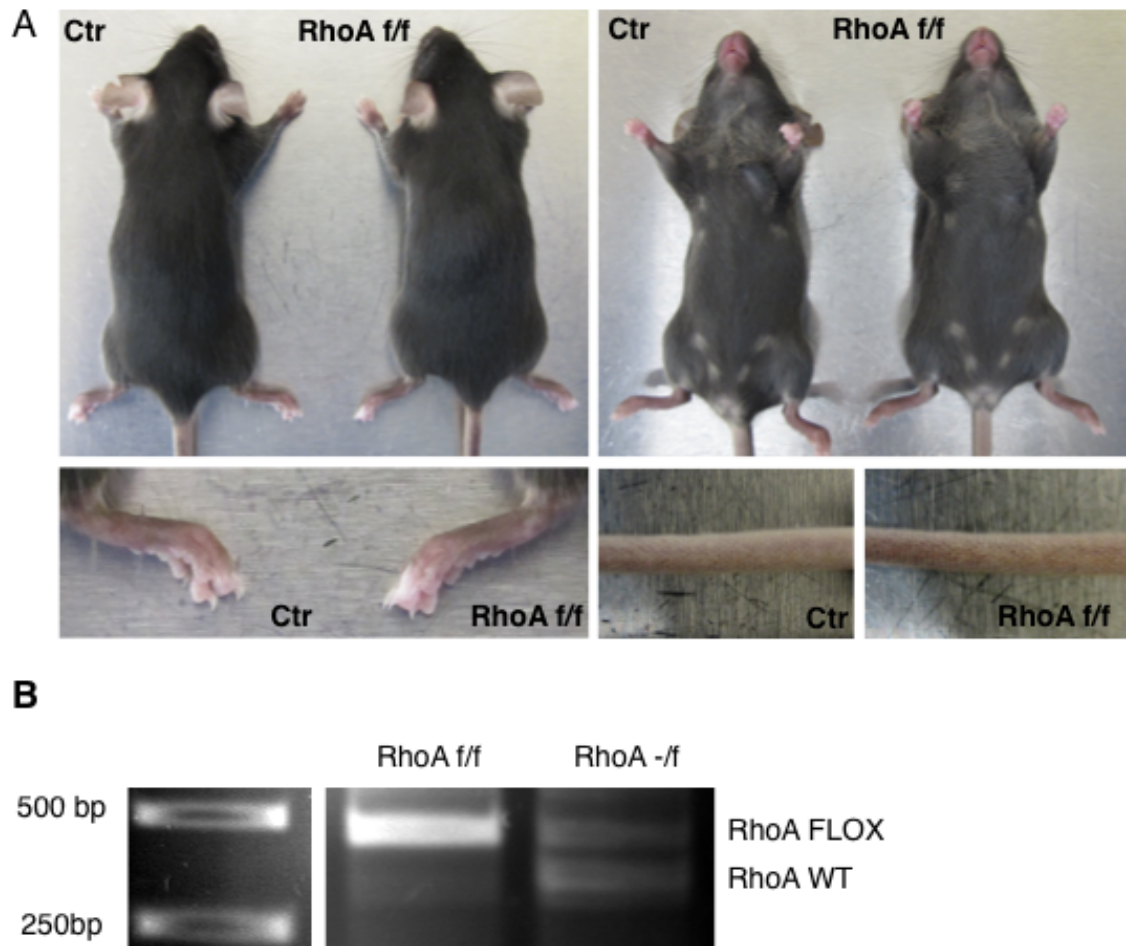


Figure 3.3 Deletion of RhoA from the melanoblast lineage does not result in any coat colour defects

(A) Images showing coat-colour of wild-type (Ctr) mice and RhoA f/f Tyr::CreB (RhoA f/f) mice at 6 weeks. (B) DNA gel showing PCR from wild-type RhoA locus (RhoA WT) and floxed RhoA locus (RhoA FLOX).

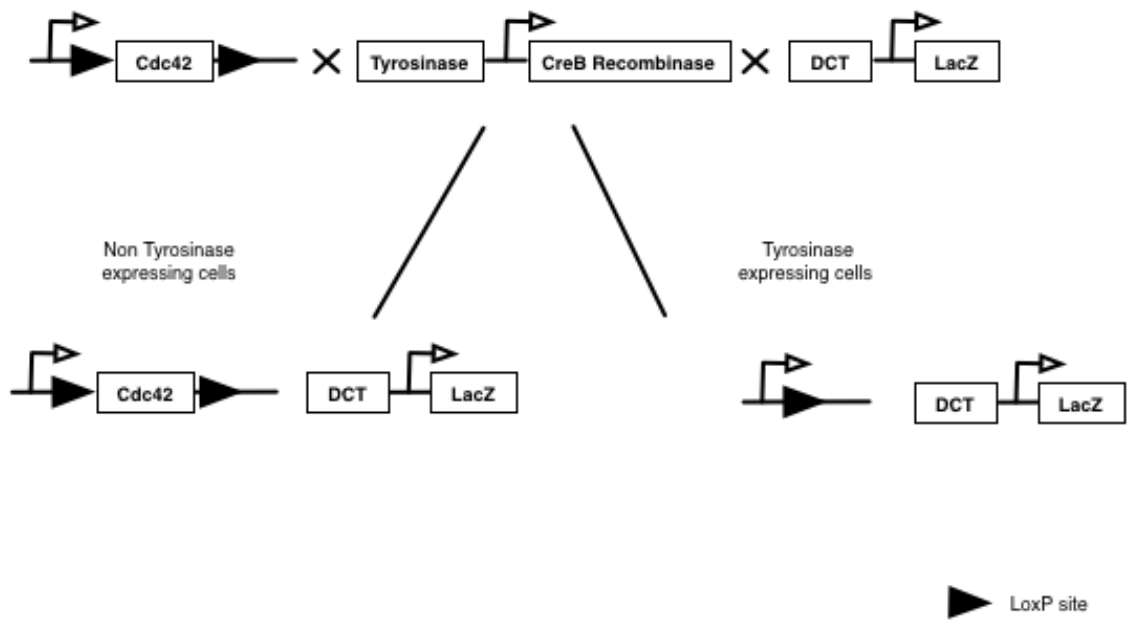


Figure 3.4 Gene strategy to achieve melanoblast-specific expression of β-galactosidase to track the melanoblast journey

The DCT::LacZ transgene was introduced onto the Cdc42^{ff} Tyr::CreB model to achieve targeted expression of β-galactosidase in the melanoblast lineage alongside loss of Cdc42

to expression of the enzyme β -galactosidase in cells expressing DCT (cells of the melanocyte lineage). When embryos are fixed and stained with X-Gal, melanoblasts specifically metabolise this compound into a blue substrate. After staining embryos with X-Gal, the dorsolateral positioning and number of melanoblasts can be imaged and quantified.

The first embryonic snapshot investigated was E11.5. At this early time-point in development, melanoblasts have emerged from the neural tube and are residing in two populations either side in the migration staging area (Figure 3.5A). The number of melanoblasts present between the two dashed lines placed between the limbs was quantified to investigate whether Cdc42 controlled melanoblast number at this stage in the journey. No difference in melanoblast number was observed between control (Ctr) embryos, and embryos with one ($f/+$) or both (f/f) copies of Cdc42 disrupted (Figure 3.5B).

At E13.5, melanoblasts in control embryos have expanded around the developing embryo, reaching half way around the dorsal-ventral axis (Figure 3.6A). This expansion is delayed in Cdc42 f/f Tyr::*CreB* embryos, with the melanoblast front only having partially progressed around the embryo (dashed line indicates front). Melanoblast progression was quantified by placing a box between the limbs which was segregated into 6 smaller areas, box 1 being the furthest dorsally (Figure 3.6B and C). Quantification shows there is a deficit of melanoblasts in all boxes of Cdc42 f/f Tyr::*CreB* (Figure 3.6D). Box 1 sits behind the leading wave of melanoblasts at an area of average melanoblast density, suggesting that there are fewer melanoblasts overall in knockout embryos. There are also significantly fewer melanoblasts in boxes 2-5, suggesting knockout melanoblasts are delayed in progression around the embryo at this time-point compared to control embryos.

At this time-point, melanoblasts in Cdc42 f/f Tyr::*CreB* embryos have also progressed less far down the developing limb (Figure 3.7A). Melanoblasts in control embryos have progressed half way down the developing limb, whereas melanoblasts in Cdc42 f/f Tyr::*CreB* embryos have only progressed to the top of the limb. This was quantified by placing a box over the developing limb and separating it into four smaller areas, with box 1 sitting at the top of the limb

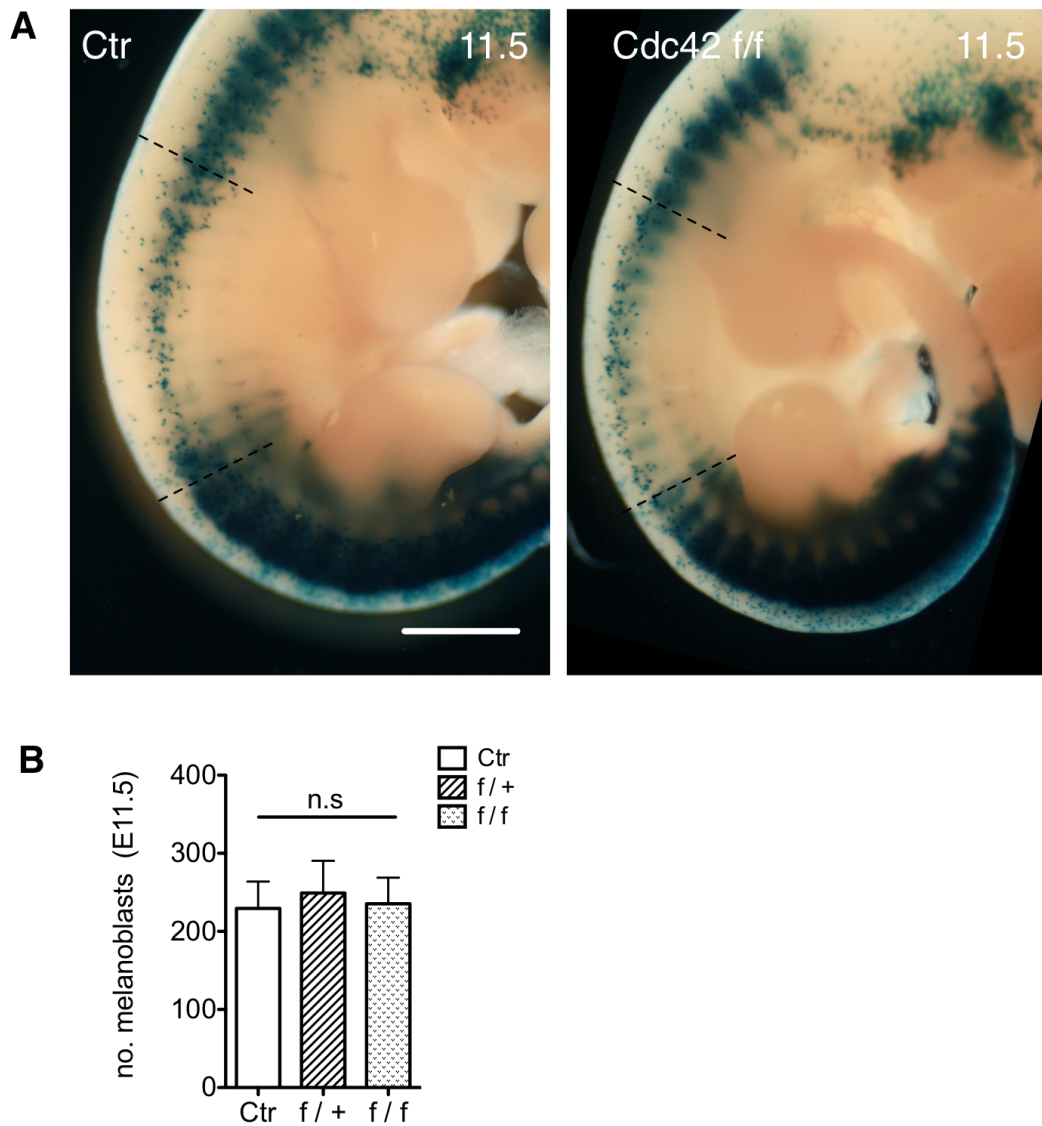


Figure 3.5 Loss of Cdc42 does not affect melanoblast number at E11.5

(A) β -Galactosidase stained DCT::LacZ Control (Ctr) and Cdc42 f/f Tyr::CreB (Cdc42 f/f) embryos at E11.5. Area between dashed lines in (A) represents area quantified. Scale 1 mm. (B) Number of melanoblasts within area quantified in E11.5 embryos. Scale 1mm Quantification from at least four different embryos taken from three separate litters. Graph shows SEM, Kruskal-Wallis one-way ANOVA test and Mann-Whitney test performed, n.s=not significant. Kruskal-Wallis denoted on graph.

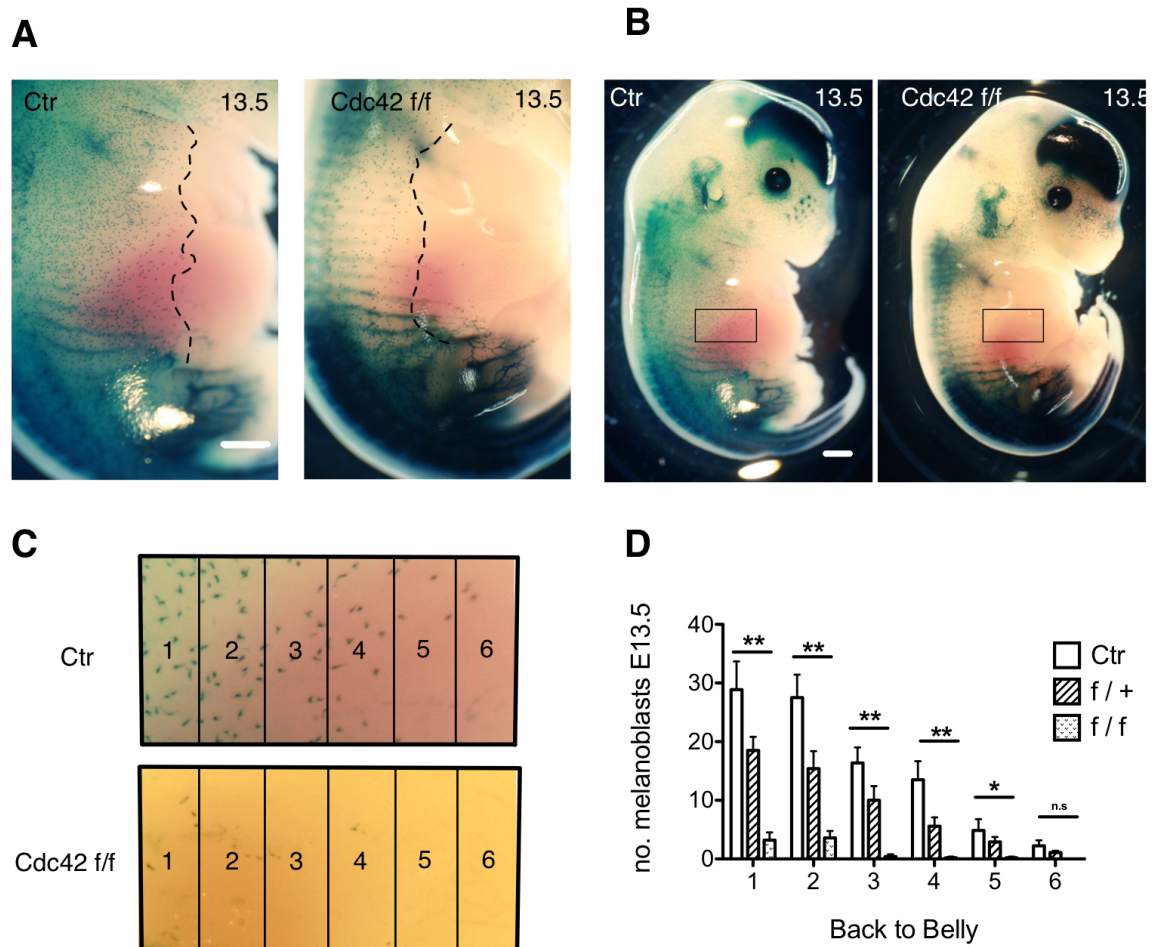


Figure 3.6 Cdc42 controls the number and position of melanoblasts around the belly at E13.5

(A) β -Galactosidase stained DCT::LacZ Control (Ctr) and Cdc42 f/f Tyr::CreB (Cdc42 f/f) embryos at E13.5. Furthest extent of the melanoblast journey traced with dashed line. Scale 1mm. (B) Lower magnification images of embryos showing area quantified (box). Scale 1 mm. (C) Representative cropped sections of stained embryos showing six boxes used for quantification. (D) Number of melanoblasts spanning from box 1 (most dorsal) to box 6 (most ventral) at E13.5. Results are expressed as mean + SEM. Quantification from at least four different embryos taken from three separate litters. Kruskal-Wallis one-way ANOVA test and Mann-Whitney test performed, * $p < 0.05$, ** $p < 0.01$ n.s, not significant. Kruskal-Wallis denoted on graph.

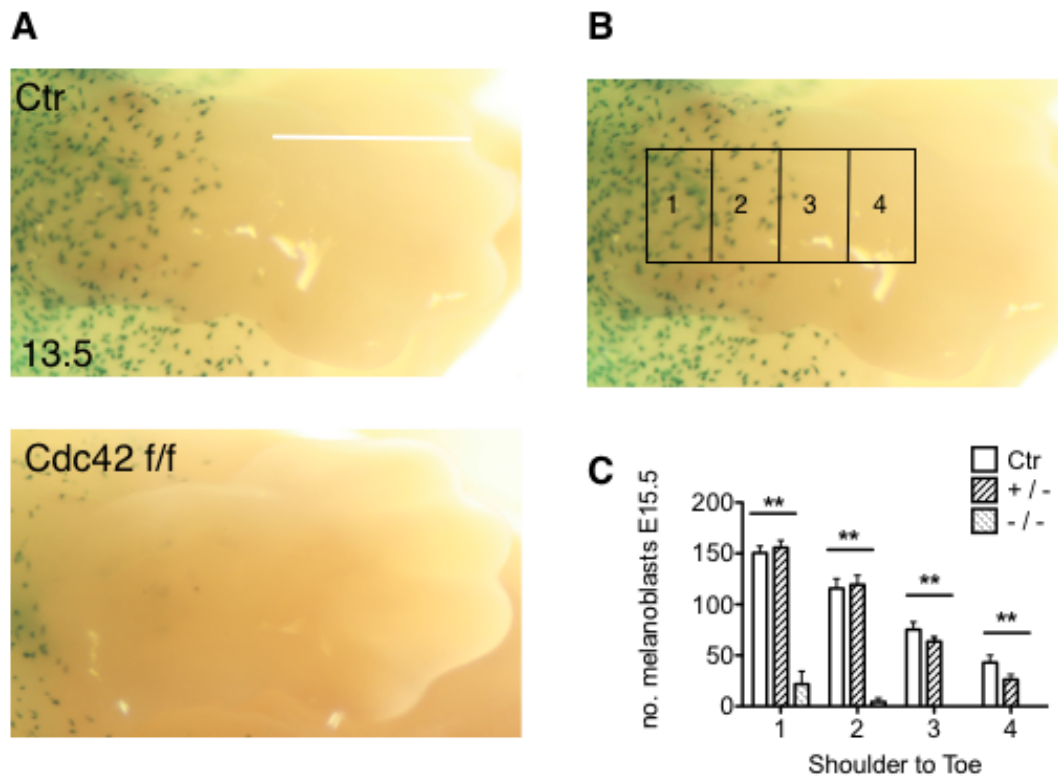


Figure 3.7 Cdc42 controls the number and position of melanoblasts down the developing limb at E13.5

(A) Forelimb of β -Galactosidase stained DCT::LacZ Control (Ctr) and Cdc42 f/f Tyr::Cre (Cdc42 f/f) embryos at E13.5. Scale 500 μ m. **(B)** Forelimb of E13.5 β -Galactosidase stained embryo, showing the grid used for quantification. **(C)** Quantification of melanoblast number and positioning down the developing limb of E13.5 embryos. Quantification from at least four different embryos taken from three separate litters, error bars show SEM. Kruskal-Wallis one-way ANOVA test and Mann-Whitney test performed, * $p < 0.05$, ** $p < 0.01$. Kruskal-Wallis denoted on graph.

(Figure 3.7B). Similarly to quantification around the belly, this revealed that there are fewer melanoblasts in each box, showing that melanoblasts in Cdc42 f/f Tyr::CreB embryos have not progressed as far down the developing limb (Figure 3.7C).

Finally, we investigated melanoblast positioning at E15.5. At this later time-point, melanoblasts in control embryos have spread around the entire embryo and down to the paws of the developing limbs, and are beginning to group into hair follicles (Figure 3.8A and B). Melanoblasts in Cdc42f/f Tyr::CreB embryos are still delayed in their journey, having reached part way around the belly and half way down the developing limb (Figure 3.8A). Cells have begun to group into hair follicles towards the back of Cdc42 f/f Tyr::CreB embryos, but less efficiently than in control embryos (Figure 3.8A and B). These high magnification images also reveal that Cdc42 null melanoblasts appear larger than control melanoblasts, with longer thinner protrusions (Figure 3.8B). Melanoblast number and positioning were again quantified by placing boxes over embryos, as previously shown with E13.5. Similarly, fewer melanoblasts can be seen in box 1 of Cdc42 f/f Tyr::CreB embryos, suggesting knockout embryos still contain fewer overall melanoblasts than control embryos. There are also significantly fewer melanoblasts in boxes 2-6 of Cdc42 f/f Tyr::CreB embryos, demonstrating that melanoblasts have progressed less far around the developing embryo (Figure 3.8C).

Quantification of melanoblast positioning down the developing limb at this time point also shows that knockout melanoblasts are also slower to make the journey. Melanoblasts in control embryos are now at the paw of developing limbs, in contrast to Cdc42 f/f Tyr::CreB where the migrating front is only half way down the developing limb (Figure 3.9A). In a similar way to E13.5, melanoblast progression was quantified by placing a box over the developing limb to quantify melanoblast number (Figure 3.9B). Fewer Cdc42 null melanoblasts were observed in each box down the limb than in control embryos, confirming the delay in the melanoblast journey in the absence of Cdc42 (Figure 3.9C).

These data shows that Cdc42 does not play a part in determining the number of melanoblasts at E11.5, assuming complete loss of Cdc42 has occurred at this

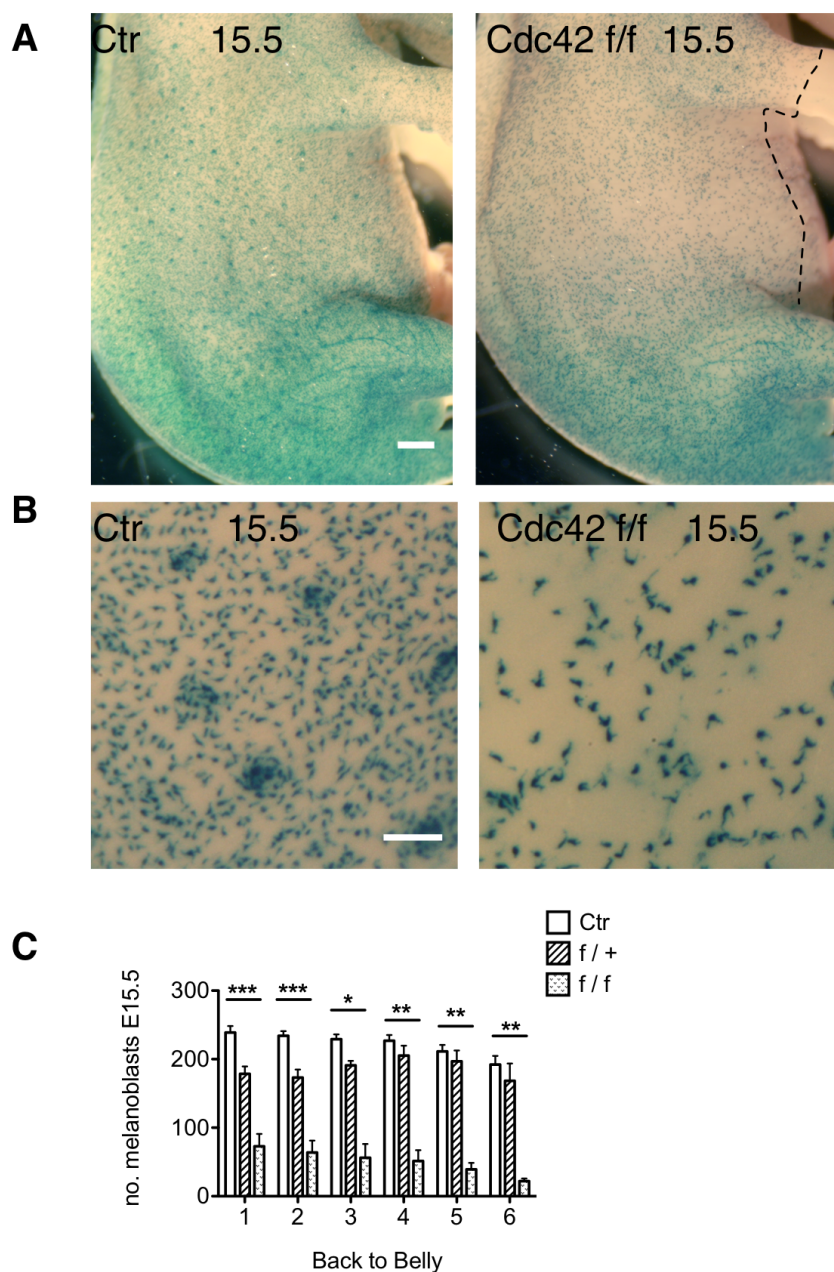


Figure 3.8 Cdc42 controls the number and position of melanoblasts around the belly at E15.5

(A) β -Galactosidase stained DCT Lac::Z Control (Ctr) and Cdc42 f/f Tyr::CreB (Cdc42 f/f) embryos at E15.5. Scale 1 mm. (B) Higher magnification image from E15.5. Scale 200 μ m (C) Number of melanoblasts spanning from box 1 (most dorsal) to box 6 (most ventral) at E15.5. Results are expressed as mean \pm SEM Quantification from at least four different embryos taken from three separate litters. Kruskal-Wallis one-way ANOVA test and Mann-Whitney test performed, * p <0.05, ** p <0.01, *** p <0.001. Kruskal-Wallis denoted on graph.

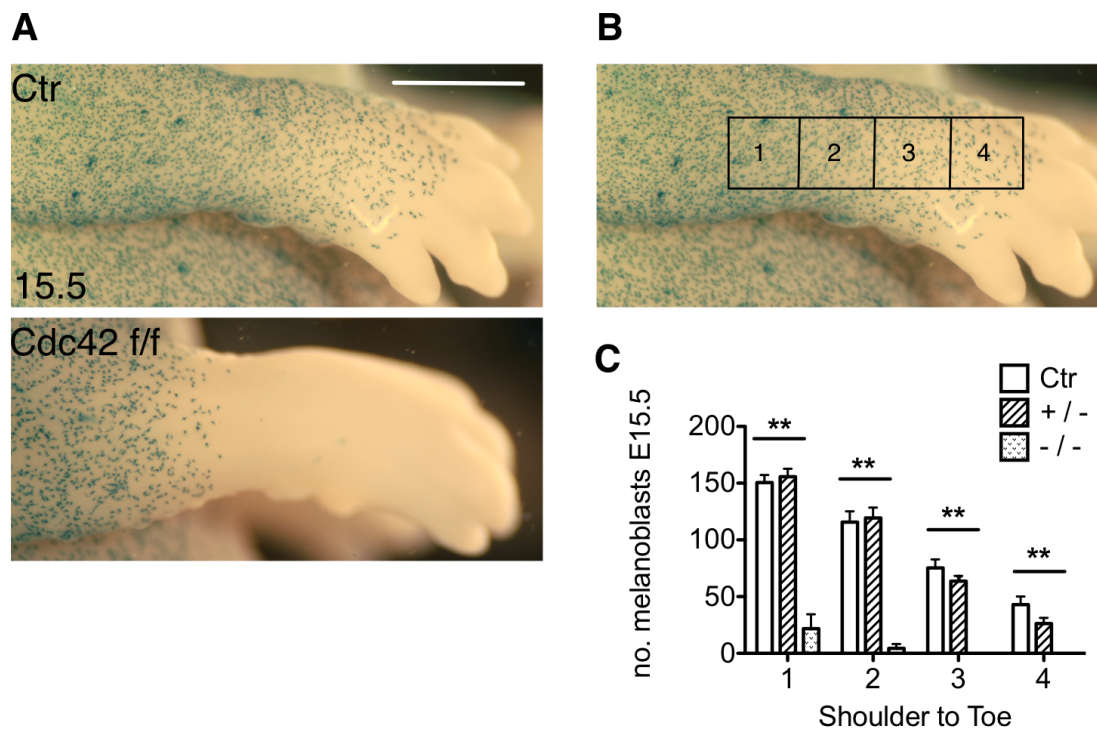


Figure 3.9 Cdc42 controls the number and position of melanoblasts down the developing limb at E15.5

(A) Forelimb of β -Galactosidase stained Control (Ctr) and Cdc42 f/f Tyr::Cre (Cdc42 f/f) embryos at E15.5. Scale 1 mm. (B) Forelimb of E15.5 β -Galactosidase stained embryo showing grid used in quantification. (C) Quantification of melanoblast number and positioning in E15.5 embryos from at least four different embryos taken from three separate litters. Kruskal-Wallis one-way ANOVA test and Mann-Whitney test performed. Error bars show + SEM. ** $p < 0.01$. Kruskal-Wallis denoted on graph.

early stage in CRE expression (Adameyko et al., 2009). However, Cdc42 is required for the proliferation and possibly the migration of melanoblasts after this time-point. Fewer melanoblasts can be seen in Cdc42 f/f Tyr::CreB embryos at E13.5 and E15.5, and these cells have progressed less far around the developing embryo and down the limb than in control embryos. We assume this delay in their journey prevents melanoblasts reaching areas distant to the neural tube before birth, resulting in the belly, paws and tail being hypo-pigmented.

3.2.4 Cdc42 controls melanoblast cell-cycle progression and cytokinesis

As Cdc42 f/f Tyr::CreB embryos had fewer melanoblasts after E11.5, we wanted to further investigate the role of Cdc42 in melanoblast proliferation. To determine the number of melanoblasts in the cell-cycle, embryos were embedded and sectioned transversely and co-stained fluorescently with anti-DCT and anti-Ki67 antibodies (Figure 3.10A). Ki67 is an endogenous protein present during all phases of the cell cycle (G1, S, G2 and mitosis). Overall, the percentage of Ki67 positive (Figure 3.10A, yellow arrows) and negative (white arrows) melanoblasts was similar in control and Cdc42 f/f Tyr::CreB embryos (283/302 cells in control embryos and 166/184 cells in Cdc42f/f embryos from four embryos, $p=0.32$) (Figure 3.10A). This indicates that Cdc42 is not required for entry into the cell-cycle in melanoblasts at this stage.

Since cell-cycle entry was not affected in Cdc42 null cells, we explored the possibility of cell-cycle delay. The number of melanoblasts in S phase was determined by injecting the pregnant mother with the thymidine analogue BrdU 2 hrs or 24 hrs prior to harvesting of embryos. Embryos from these mothers were sectioned and co-stained with anti-BrdU and anti-DCT antibodies, revealing cells that were proliferating (yellow arrows) and those that were not (white arrows) (Figure 3.10B). After 2 hrs, an average of 21% of Cdc42 null melanoblasts per embryo (71/343 cells in total) were in S phase compared with 34% in control embryos (136/420 cells) (n.s, $p=0.0607$). However at 24 hrs post BrdU injection, 29% (79/259) were in S phase in Cdc42 null embryos compared with 51% in control embryos (119/239 cells in total) (* $p=0.014$), indicating that loss of Cdc42 slows cell cycle progression in melanoblasts *in vivo* (Figure 3.10B and C).

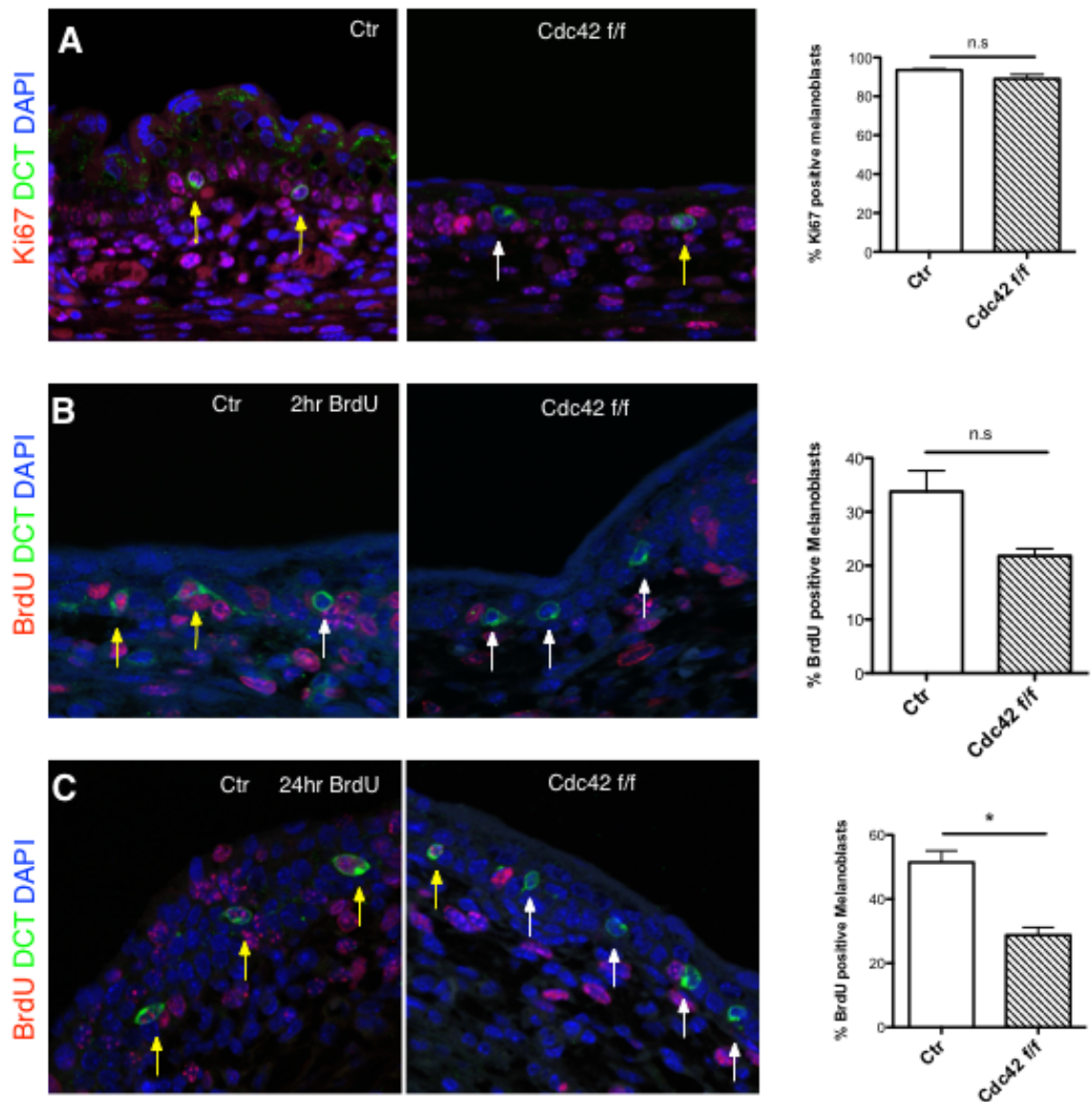


Figure 3.10 Cdc42 null melanoblasts are in the cell cycle, but fewer are in S-phase

(A-C) Representative images of transverse sections of control (left panels) and Cdc42 f/f Tyr::CreB (right panels) E15.5 embryos stained with DAPI (blue) to mark nuclei, the melanoblast marker DCT (green) and: (A) Ki67 (red) staining to mark cells within the cell-cycle, plus quantification of the percentage of Ki67 positive melanoblasts in control (Ctr) and Cdc42 f/f embryos. (B) BrdU (red) staining on embryo sections from mothers injected with BrdU 2 hrs or 24 hrs (C) before embryos were harvested, plus quantification of the percentage of BrdU positive melanoblasts in control (Ctr) and Cdc42 f/f embryos. Yellow arrows highlight DCT-positive cells expressing Ki67 or labelled with BrdU. White arrows show only DCT-positive cells. At least 184 cells from three embryos per genotype were quantified. Graph shows mean +SEM, * $p < 0.05$, n.s, not significant, t-test with Welch's correction.

Using videos from skin explant imaging (technique described in section 3.2.6), we also investigated the time melanoblasts took to divide in the absence of Cdc42. Division time was calculated as the time taken for melanoblasts to round up through to separation of daughter cells. Control melanoblasts begin division by rounding up (first frame), followed by cleavage furrow formation (shown in green) and then efficient separation into two daughter cells (shown in red) (Figure 3.11A). In contrast, Cdc42 null melanoblasts struggle to round up completely, leaving the remains of pseudopods extended. The cleavage furrow is formed, but cells struggle to undergo cytokinesis (Figure 3.11A). In Cdc42 knockout embryos melanoblasts take twice as long to progress through division (Figure 3.11B). This extended division time is specifically due to the extra time these cells take to undergo cytokinesis (Figure 3.11B and C) (Supplementary video 1).

Altogether, these data demonstrate that Cdc42 plays an important role in melanoblast division. It is required for efficient transition from G1 into S Phase, stimulating melanoblast proliferation to fill the developing embryo. Cdc42 also controls melanoblast cytokinesis, as Cdc42 null melanoblasts struggle to complete this process efficiently.

3.2.5 Cdc42 is not required for melanoblasts to cross the basement membrane into the epidermis

As embryos develop, their skin thickens and matures, forming a dermis and an epidermis, which are separated by a basement membrane. Melanoblasts initially reside and migrate through the dermis of the skin, but by birth melanoblasts reside largely in hair follicles within the epidermis. We are still in the process of understanding this transition. It is still unclear what drives the melanoblasts to cross the basement membrane, but we know that this process is not invasive (Li et al., 2011). To investigate whether Cdc42 null melanoblasts are capable of completing this process, control and Cdc42 f/f Tyr::CreB embryos were harvested, stained with X-Gal then embedded and sectioned transversely to investigate melanoblast positioning within the skin layers at E13.5 and E15.5. At E13.5, around 25% of melanoblasts reside in the dermis and around 75% in the

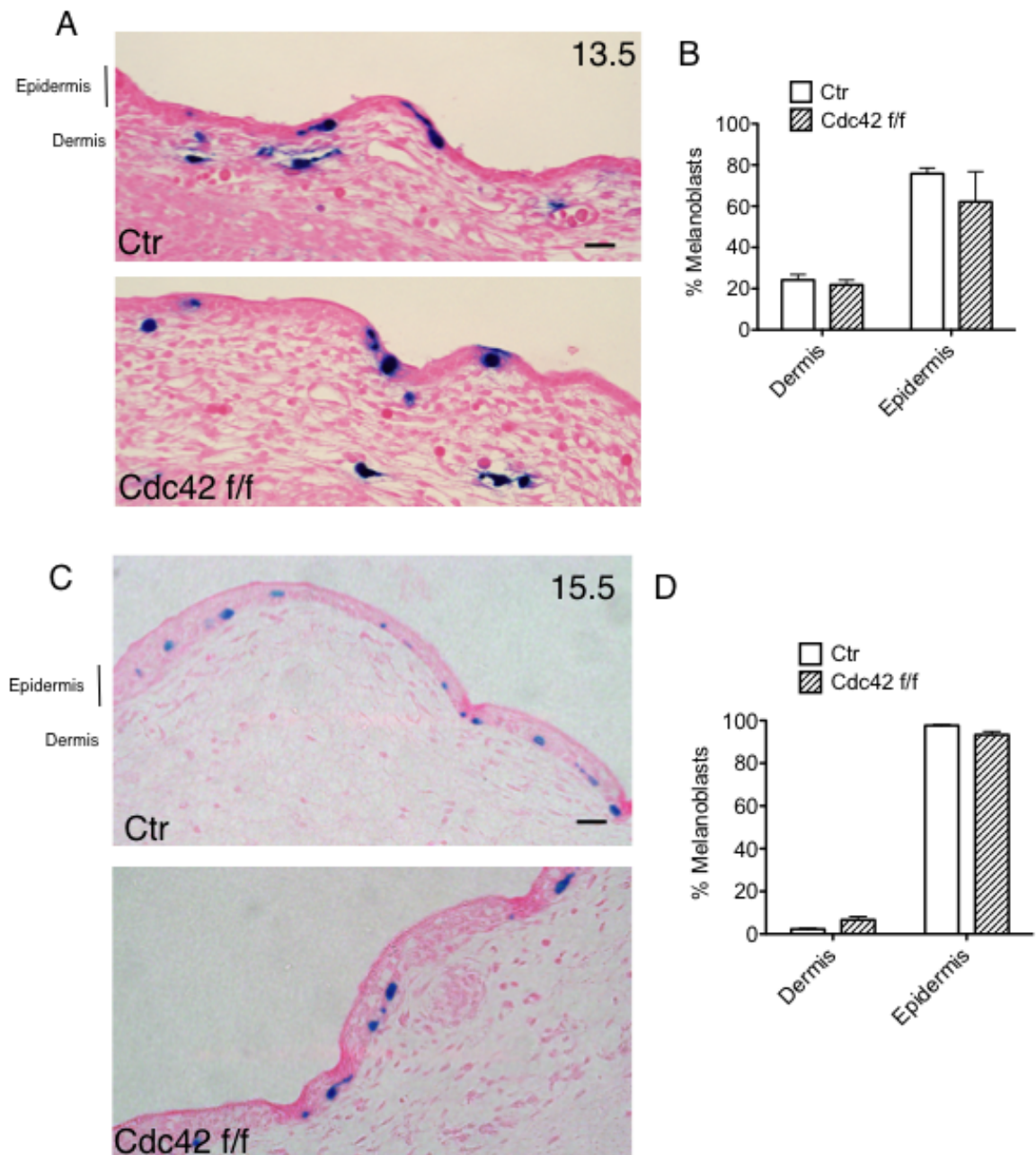


Figure 3.12 Cdc42 knockout melanoblasts are able to cross from the dermis into the epidermis during development.

(A) Transverse sections of embedded β -Galactosidase stained DCT::LacZ Control (Ctr) and Cdc42 f/f Tyr::Cre (Cdc42 f/f) embryos at E13.5 counterstained with eosin. (B) Quantification of melanoblasts in dermis and epidermis from (A) from at least five different embryos for each genotype, at least 85 cells per embryo. Error bars show SEM. Scale bar 10 μ m. (C) Transverse sections of embedded β -Galactosidase stained Control (Ctr) and Cdc42 f/f Tyr::Cre (Cdc42 f/f) embryos at E15.5 counterstained with eosin. Scale 20 μ m. (D) Quantification of melanoblasts in dermis and epidermis from (C) from at least four different embryos for each genotype, at least 140 cells per embryo.

epidermis in both control and Cdc42 f/f Tyr::CreB embryos (Figure 3.12A and B). By E15.5, the epidermis has thickened and the melanoblasts reside mostly in the epidermis, sitting on the basement membrane. The epidermis also begins to invaginate into hair follicles, with some melanoblasts already resident inside. At this time-point, only 5% of melanoblasts are left in the dermis, with around 95% having moved into the epidermis (Figure 3.12C and D). Therefore, Cdc42 expression is not necessary for melanoblasts to transition from the dermis to the epidermis.

3.2.6 Loss of Cdc42 uncouples actin dynamics and pseudopod extension from migration

3.2.6.1 Cdc42 null melanoblasts have altered pseudopod dynamics and migration defects

X-Gal staining revealed that the melanoblast journey is delayed in Cdc42 f/f Tyr::CreB embryos, which suggested that Cdc42 may be important for melanoblast migration as well as division. In order to image melanoblast migration through embryo skin, the Cdc42 f/f Tyr::CreB mouse was bred with transgenic mice containing the Z/EG reporter gene (Novak et al., 2000). This reporter consists of GFP downstream of a lox-stop-lox sequence. Upon CreB expression, this stop sequence is removed and expression of GFP is driven in the melanoblast lineage (Figure 3.13A).

Skin from Tyr::CreB Z/EG^{+/-} control mice and Cdc42 f/f Tyr::CreB Z/EG^{+/-} mice was imaged using *ex vivo* skin explant imaging, a method refined by Mort et al. to achieve high resolution imaging of melanoblasts moving through mouse embryonic skin (Mort et al., 2014). Skin from embryos at E15.5 was dissected and placed epidermis side down onto a 24-well membrane-bottom dish, with a nuclepore membrane placed on top. The set-up was overlaid with Matrigel and then phenol-free growth media (Figure 3.13B). Imaging of these skin explants revealed that Cdc42 null melanoblasts had an elongated morphology, which we refer to as ‘bipolar’, as well as extending long pseudopods that had a ‘beads on a string’ morphology (Figure 3.14A). Knockout melanoblasts also appeared to be larger, and fewer melanoblasts were present overall than in control skins. Fixation of the skin explants and staining with DAPI revealed that the pseudopods of Cdc42 null melanoblasts extended between

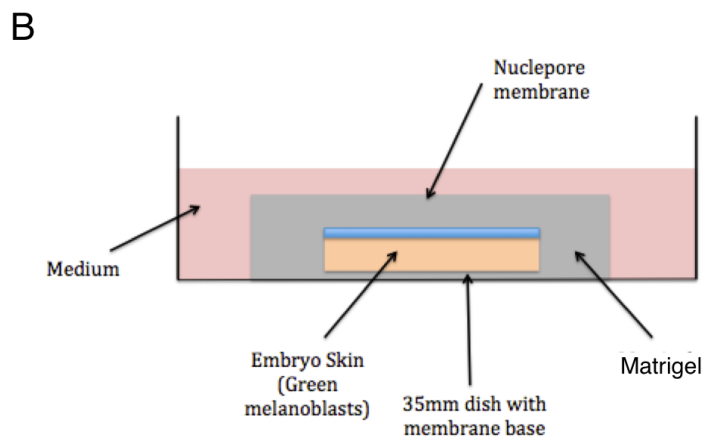
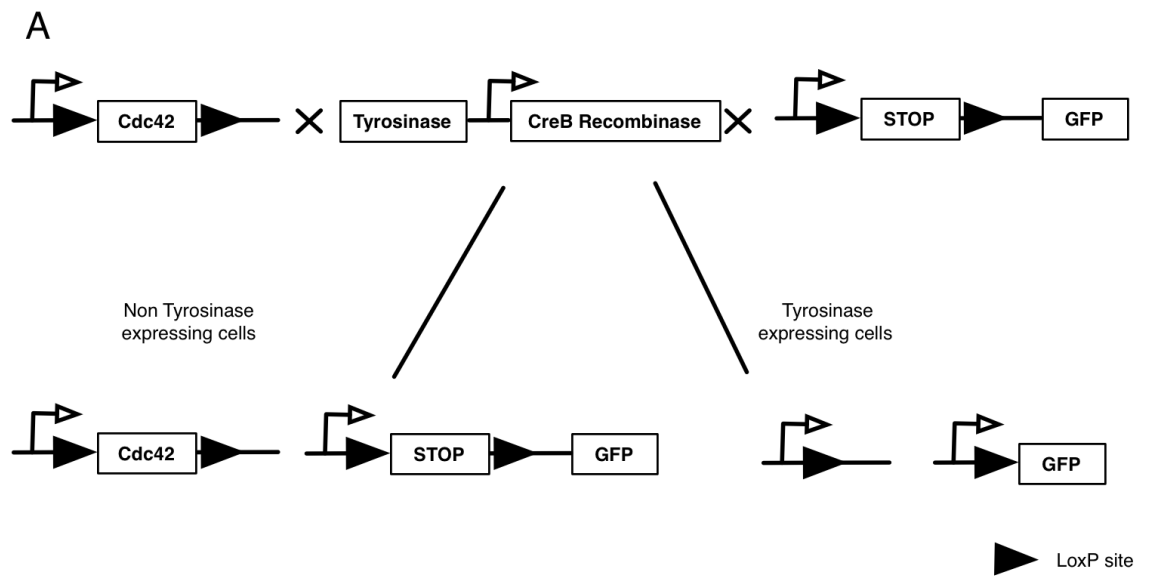


Figure 3.13 Gene strategy to achieve melanoblast specific expression GFP to image live melanoblast migration through skin

(A) The Z/EG transgene was introduced onto the *Cdc42^{f/f} Tyr::CreB* model to achieve targeted expression of GFP in the melanoblast lineage alongside loss of *Cdc42*. Tyrosinase expression leads to recombination and removal of the STOP sequence preceding the GFP gene. This leads to removal of *Cdc42* alongside GFP expression. *Cdc42* WT *Tyr::CreB* Z/EG mice were used for controls in these experiments. **(B)** Set up to perform skin explant imaging. The dissected skin was sandwiched between a membrane dish and a nucleopore membrane and overlaid with matrigel then media prior to imaging.

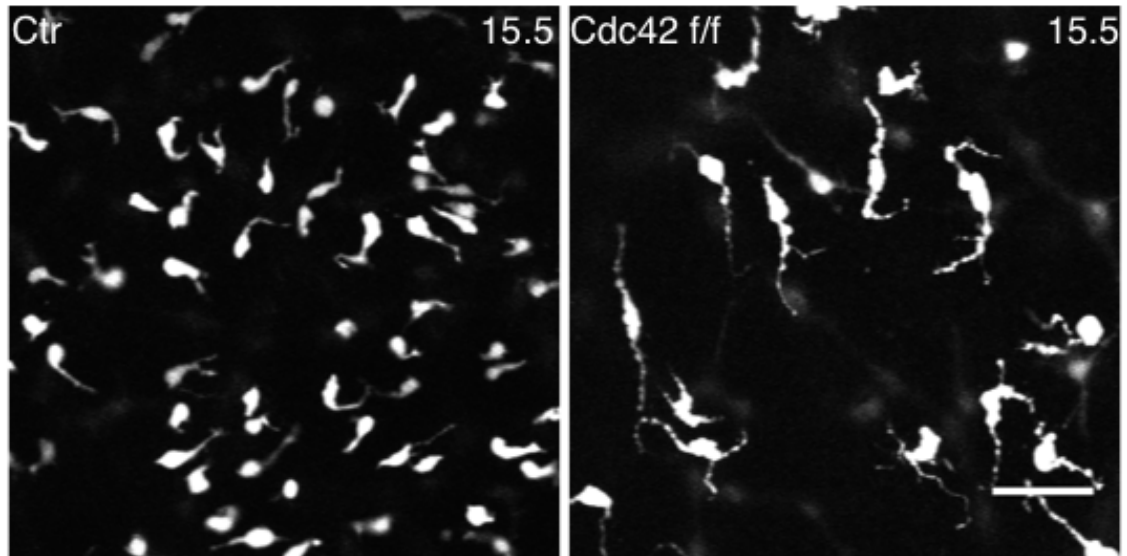
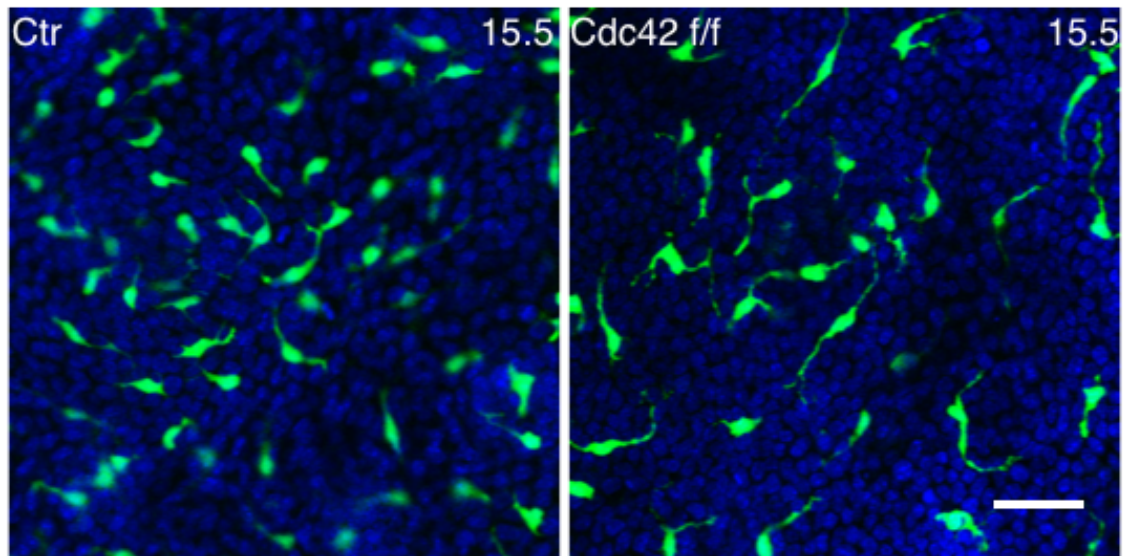
A**B**

Figure 3.14 Cdc42 null melanoblasts have a striking elongated and bleb-like morphology as they move through the skin

(A) Stills from explant imaging of Control Tyr::CreB Z/EG^{+/-} skins (Ctr) or Cdc42f/f Tyr::CreB Z/EG^{+/-} skins at E15.5. 50 μ m scale. **(B)** Confocal imaging of fixed skins stained with DAPI (Blue). Scale 30 μ m.

many surrounding keratinocytes (Figure 3.14B). Time-lapse imaging of melanoblast migration showed that wild-type melanoblasts extend multiple, dynamic pseudopods to help them navigate efficiently between surrounding keratinocytes (Figure 3.15 yellow arrow). In contrast, melanoblasts from *Cdc42 f/f Tyr::CreB Z/EG^{+/-}* skins extend long, static pseudopods which the cell struggles to retract (yellow arrow). They also take on a bi-polar shape, with a preference to producing two pseudopods (orange arrows). Knockout pseudopods appear to be segregated into 'beads on a string' in a bleb-like morphology (red arrow) (Figure 3.15) (Supplementary video 2).

It was also clear from this imaging that knockout melanocytes were larger, with a statically significant increase of around 40% in area (Figure 3.16A). In addition, *Cdc42* null cells frequently displayed two pseudopods, with 56% adopting what we termed a 'bipolar' phenotype (Figure 3.16B). Melanoblasts in control skins do not display this bias towards two pseudopods, with 10% displaying four or more pseudopods. The 'bipolar' morphology of knockout cells led to a significant increase in the length to width ratio (Figure 3.16C), and was accompanied by an increase in pseudopod length (Figure 3.16D). Elongated knockout pseudopods were extremely long-lived, with 10% lasting the entirety of the 4-hour time-lapse video, as they do not seem to retract efficiently. In contrast, pseudopods created by wild-type melanoblasts were transient, with the majority (84%) only lasting between 5 and 80 minutes (Figure 3.16E).

Melanoblasts from *Tyr::CreB Z/EG^{+/-}* control skins and *Cdc42 f/f Tyr::CreB Z/EG^{+/-}* skins were tracked from a 4 hour time-lapse video using an ImageJ plugin to gain information about their migration speed and persistence (Figure 3.17A and B). Due to the extended nature of knockout melanoblasts and their ability to form pseudopods, one might expect these cells to move well through the skin, however this is not the case. On average, control melanoblasts move twice as fast ($0.42 \mu\text{m}/\text{min}$) as *Cdc42* null melanoblasts ($0.2 \mu\text{m}/\text{min}$) (dashed lines Figure 3.17A). Overall, melanoblasts from control skins moved further than knockout melanoblasts. As control skins are densely packed with melanoblasts,

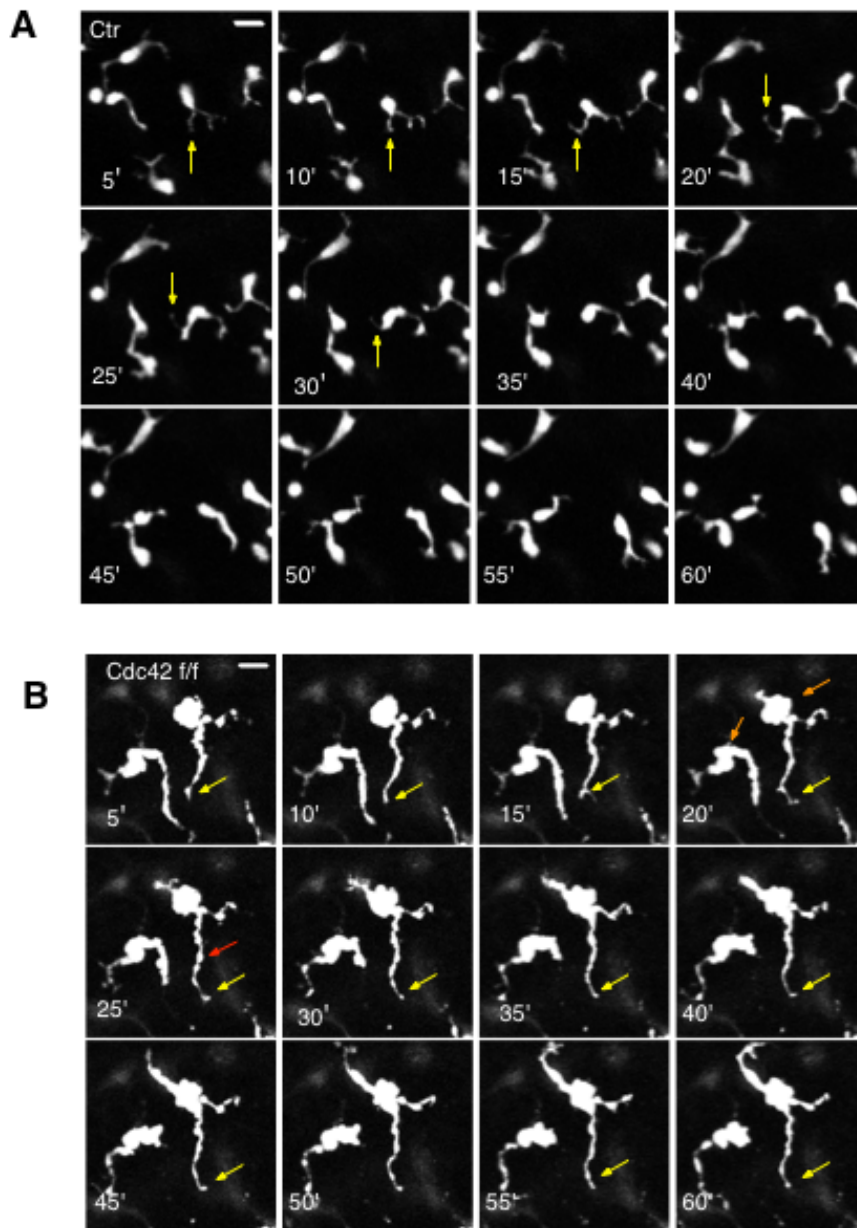


Figure 3.15 Cdc42 null melanoblasts display less-dynamic pseudopods and have a ‘bi-polar’ morphology

Stills from imaging of melanoblasts in (A) Control (Ctr) and (B) *Cdc42 f/f Tyr::CreB Z/EG^{+/-}* (*Cdc42 f/f*) skin explants. Yellow arrows highlight pseudopod dynamics. Red arrow highlights bead-like structures. Orange arrows show cells with ‘bi-polar’ phenotype. Scale 10 μm

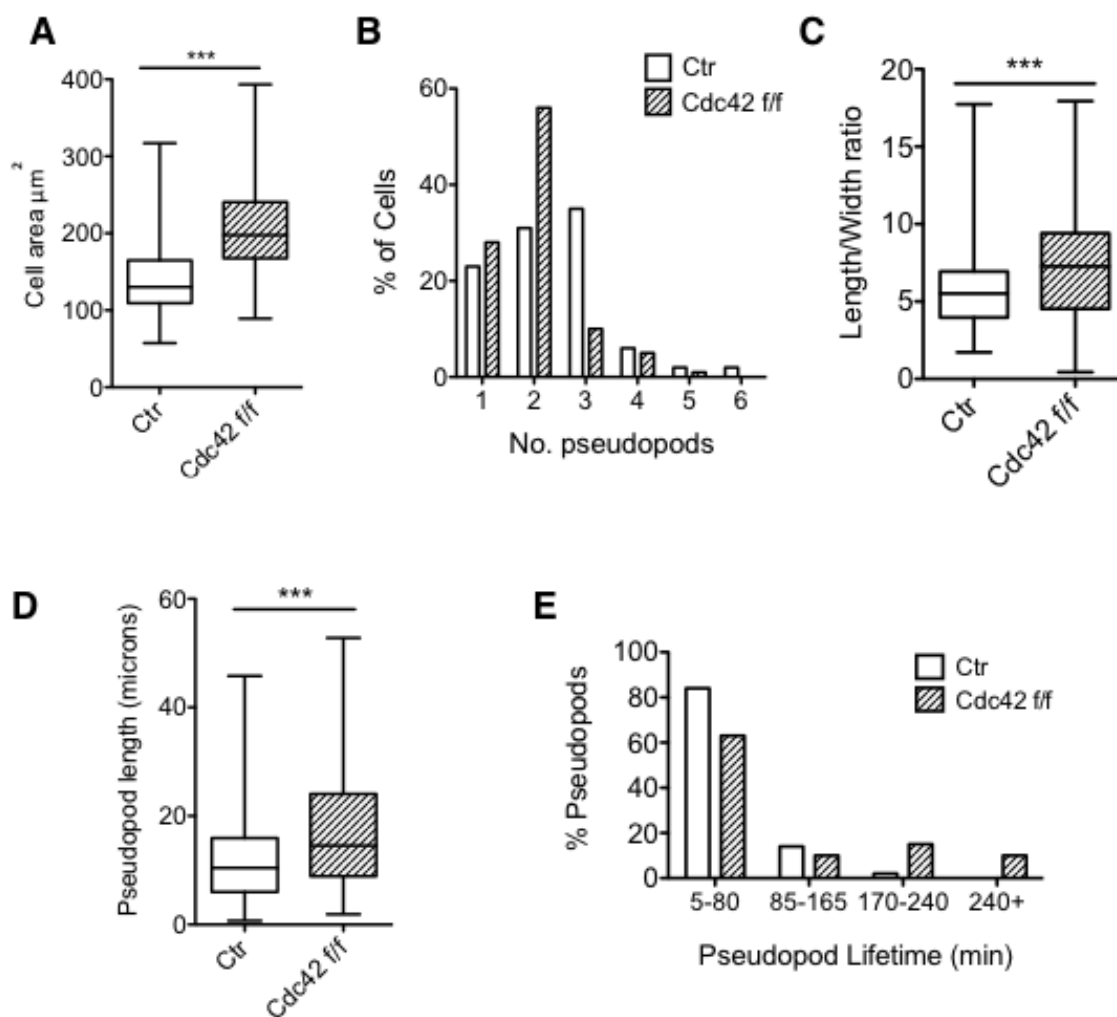


Figure 3.16 Cdc42 null melanoblasts have an altered morphology and defects in pseudopod dynamics

Graphs represent measurements taken from Control (Ctr) and Cdc42 f/f Tyr::CreB Z/EG^{+/-} skin explants from 5-6 embryos from four different litters. Data are from 125 cells per genotype, from 301 control pseudopods and 239 Cdc42 f/f pseudopods.

(A) Cell area (B) Number of pseudopods per melanoblast (C) Length to width ratio (D) Pseudopod length (E) Distribution plot of pseudopod lifetimes. Box plots show mean and minimum and maximum values, ***p<0.001 t-test.

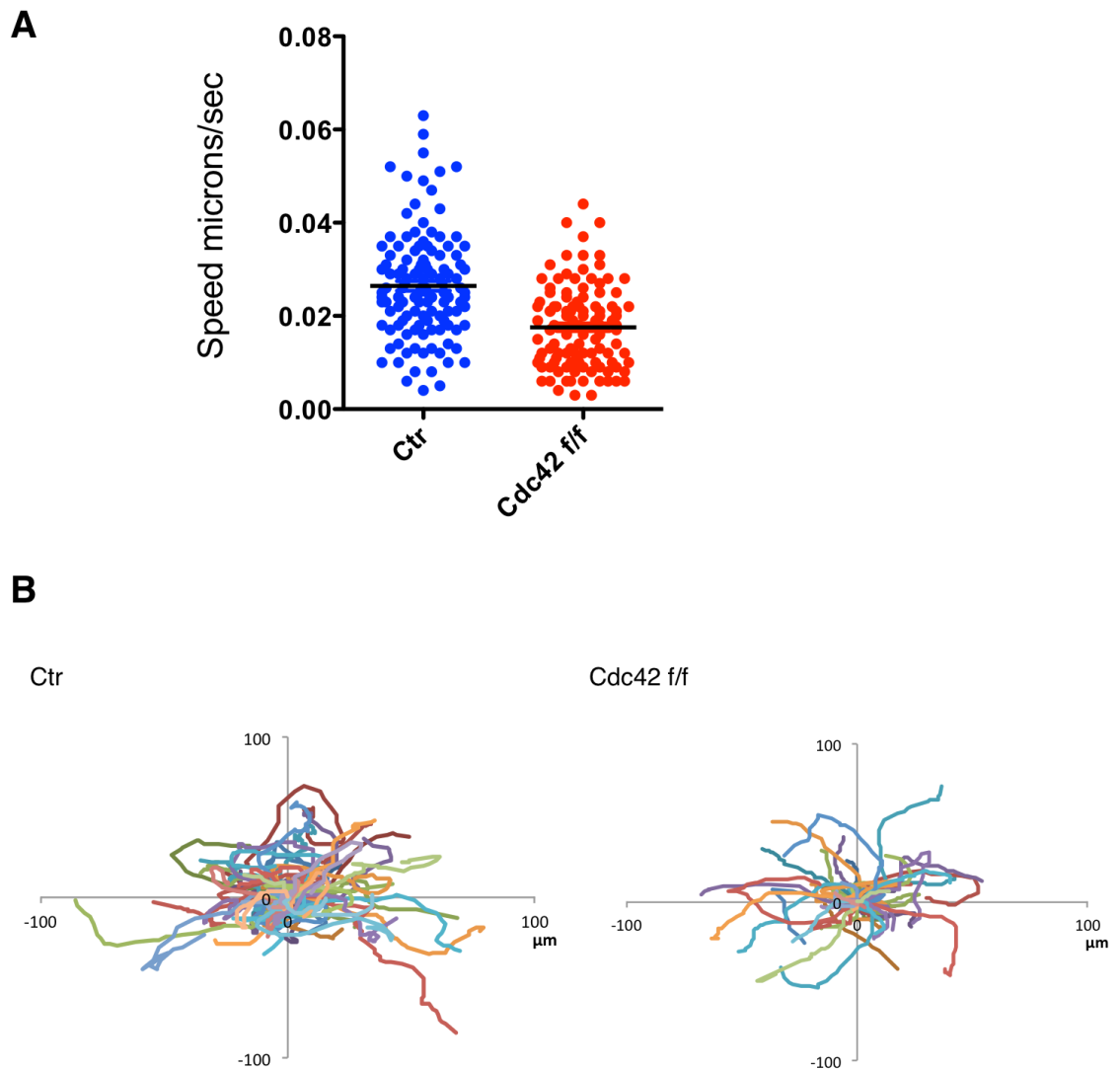


Figure 3.17 Loss of Cdc42 in melanoblasts leads to less efficient migration

(A) Average speed ($\mu\text{m}/\text{min}$) of melanoblasts gained from tracking individual melanoblasts for 4 hours moving through skin explants. Measurements from 115 cells per genotype from five different skins. (B) Spider plots showing migration paths of melanoblasts from Tyr::CreB Z/EG^{+/-} Control (Ctr) and Cdc42 f/f (Cdc42 f/f) skins over 4 hours of imaging.

they move in circular paths, because when they encounter each other they change direction, most likely due to contact inhibition. Knockout melanoblasts fell into two subsets, most not moving far (tracks around the graph origin), and those able to move (around 20/100 cells tracked). This subset moved persistently as they had fewer neighbouring melanoblasts to block their migration, unlike in control skins which are densely packed with melanoblasts (Figure 3.17B).

Therefore, Cdc42 plays an important role in regulating the overall size and shape of melanoblasts. It is essential in regulating melanoblast pseudopod dynamics to facilitate migration. Null melanoblasts are unable to retract their elongated pseudopods and use this force to translocate between the surrounding keratinocytes. Therefore, these cells struggle to migrate as efficiently through the skin as wild-type melanoblasts. We believe that these defects, together with the reduced number of melanoblasts in Cdc42 f/f Tyr::CreB embryos leads to the pigment defects seen in adult mice.

3.2.6.2 Cdc42 null melanoblasts are unable to translate actin bursts into efficient migration

We wondered whether defects in actin dynamics might explain the inability of Cdc42 knockout cells to translocate in the epidermis. To investigate whether actin polymerisation was occurring normally in these cells, Cdc42 f/f Tyr::CreB mice were bred with mice expressing a lox-stop-lox lifeact transgene (Schachtner et al., 2012). Lifeact is expressed in the presence of CreB. It is a chemically modified peptide that binds to filamentous actin, allowing visualisation of actin polymerisation *in vivo* (Riedl et al., 2008) (Figure 3.18).

Skin explant imaging from these embryos revealed that regular actin bursts could be seen at the tips of both control and knockout pseudopods (Figure 3.19A). However, there was a small but significant difference in the time between actin bursts, increasing from an average of 8.9 min between bursts in control cells to 11.5 min in the absence of Cdc42 (Figure 3.19B). Therefore, actin bursts occur in knockout conditions at a relatively normal frequency, but this protrusive force is apparently not translated into coordinated pseudopod extension and translocation. Scatter plots illustrating pseudopod lifetime and

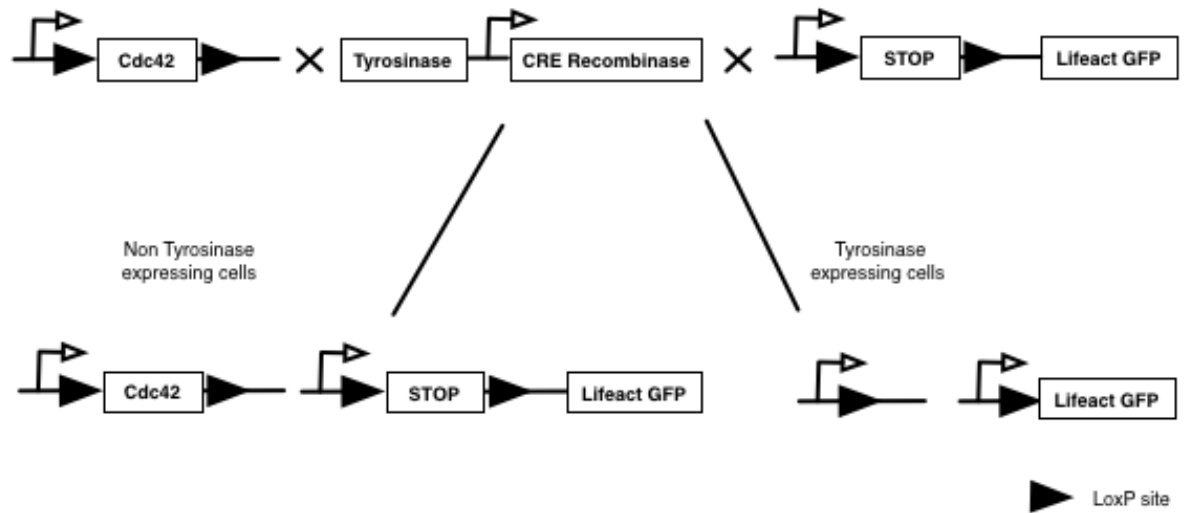


Figure 3.18 Gene strategy to achieve melanoblast-specific expression of Lifact-GFP to image live actin dynamics

The Lifact-GFP transgene was introduced onto the *Cdc42^{f/f} Tyr::CreB* model to achieve targeted expression of Lifact-GFP in the melanoblast lineage alongside loss of Cdc42. Tyrosinase expression leads to recombination and removal of the STOP sequence preceding the Lifact-GFP gene. This leads to removal of Cdc42 alongside Lifact-GFP expression. *Cdc42* WT *Tyr::CreB* Z/EG^{+/-} mice were used as controls in these experiments.

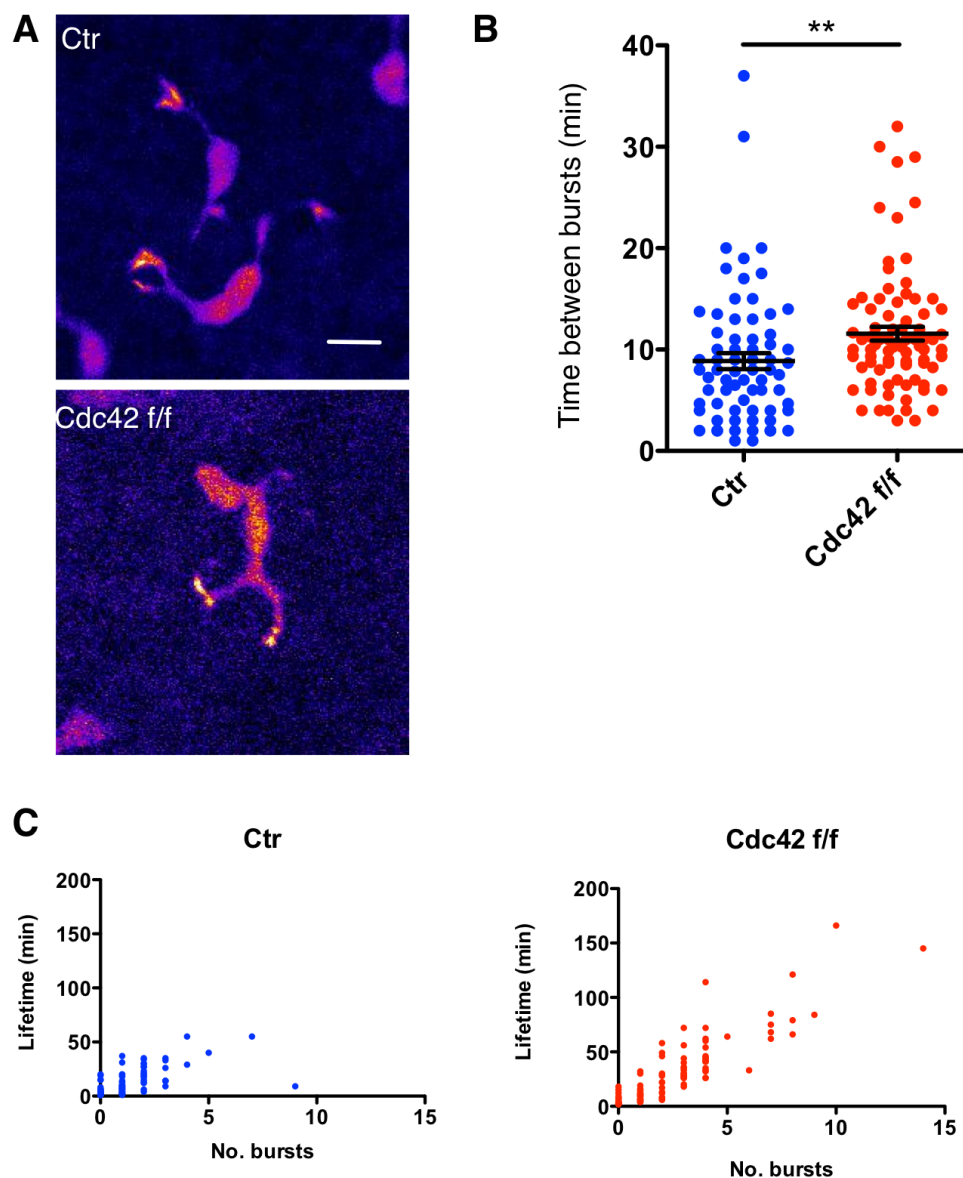


Figure 3.19 Actin bursts can be seen at the tips of knockout pseudopods

(A) Representative images of melanoblast F-actin dynamics in Control GFP-Lifeact f/f Tyr::Cre (Ctr) skin explants and GFP-Lifeact f/f Cdc42 f/f Tyr::CreB (Cdc42 f/f) skin explants. Scale 10 μ m.

(B) Quantification of the time between actin bursts within a pseudopod **(C)** Scatter plots showing individual pseudopod lifetime against number of actin bursts observed during its lifetime.

Quantification of 100 pseudopods per genotype from at least four different embryos from three different litters. Dot plot shows mean \pm SEM. ** $p < 0.01$ t-test

number of actin bursts shows a different distribution of protrusions in each condition. The majority of pseudopods made by control melanoblasts are short lived, displaying a few actin bursts (Figure 3.19C). Unexpectedly, knockout pseudopods last longer, producing many actin bursts without resulting in migration (Supplementary video 3). Therefore, Cdc42 appears to play a crucial role in the coordination of actin polymerisation into efficient cell translocation. Despite displaying a relatively normal rate of actin bursts, knockout melanoblasts appear unable to couple this to efficient migration.

3.2.7 Loss of Cdc42 and Rac1 from the melanoblast lineage leads to death at birth and a reduction in melanoblast number

Having identified a prominent role for Cdc42 and Rac1 in the melanoblast journey, we wanted to investigate the effect of a double Rac1 and Cdc42 deletion in the melanoblast lineage. To do this, mice carrying a floxed copy of Rac1 were bred with Cdc42 f/f Tyr::CreB mice, leading to double knockout of Cdc42 and Rac1 in the melanoblast lineage (Figure 3.20). Loss of one copy of Cdc42 or Rac1 alongside deletion of one or both copies of the other had no effect on pup survival. Loss of both copies of both Rac1 and Cdc42 lead to death at birth, although these pups appeared to have developed normally (Figure 3.21A). To investigate melanoblast positioning in double knockout embryos, they were harvested at E15.5, embedded and sectioned and stained with anti-DCT antibody (Figure 3.21B). Imaging of these stained sections showed that double knockout embryos appear to contain no melanoblasts at any position around the circumference of the embryo in the dermis or epidermis (Figure 3.21C). Although preliminary, these data indicate that without Rac1 and Cdc42, the melanoblasts lineage does not develop, or there are very few melanoblasts due to a severe proliferation defect.

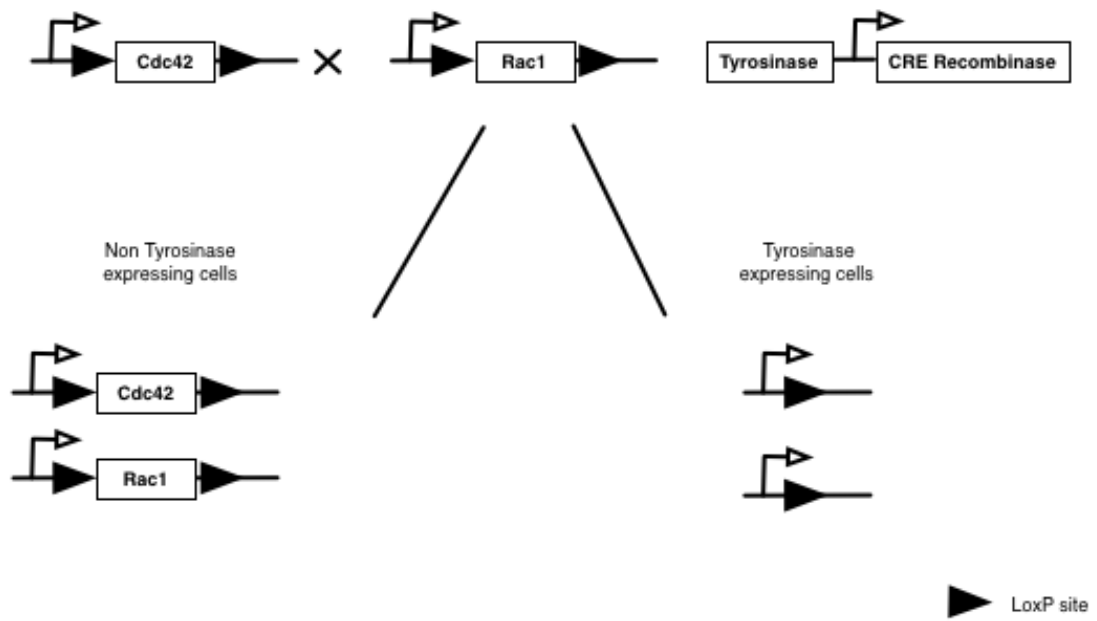


Figure 3.20 Gene strategy to achieve melanoblast targeted double knockout of both *Rac1* and *Cdc42*

Schematic of the gene targeting strategy leading to *Cdc42* *f/f* *Rac1* *f/f* *Tyr::CreB* mice. Cre recombinase is under the control of the tyrosinase promoter, leading to targeted deletion of *Cdc42* and *Rac1* in the melanocyte lineage.

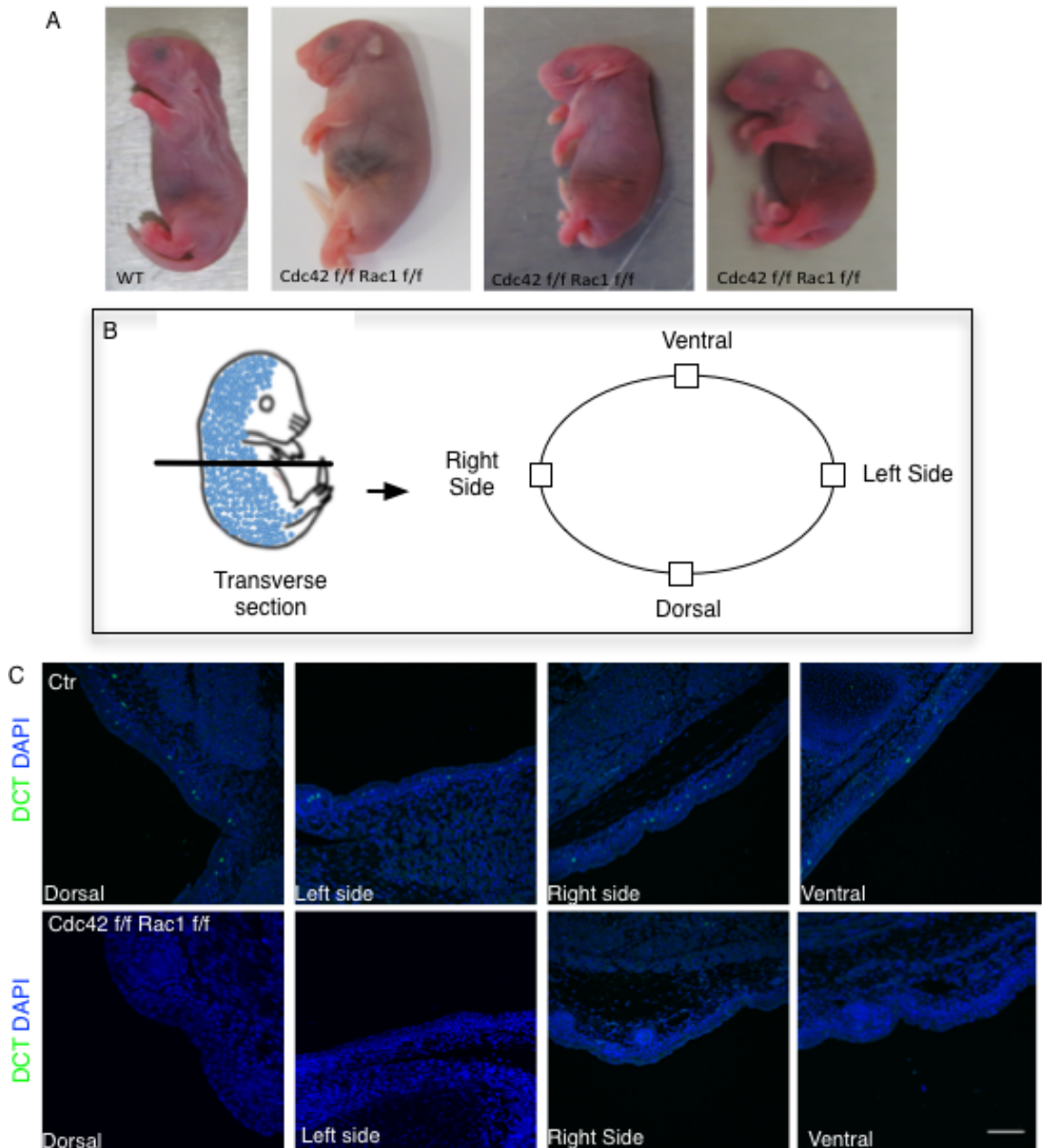


Figure 3.21 Loss of both Cdc42 and Rac1 in the melanoblast lineage leads to death at birth and many fewer melanoblasts at E15.5

(A) Images of wild-type (WT) and *Cdc42 f/f Rac1 f/f Tyr::CreB* (*Cdc42 f/f Rac1 f/f*) pups which were found dead at birth. (B) Schematic of approach used to investigate melanoblast positioning in *Cdc42 f/f Rac1 f/f Tyr::CreB* embryos. A transverse section was taken and images around the dermis/epidermis were imaged as seen below (C). (C) Transverse sections of control (Ctr) and *Cdc42 f/f Rac1 f/f Tyr::CreB* (*Cdc42 f/f Rac1 f/f*) embryos stained with DCT (green) (melanocyte marker) and DAPI (blue) (nuclear marker). Scale 100 μm .

3.3 Discussion

3.3.1 Cdc42 is necessary for melanoblast population of the developing embryo before birth

The role of Cdc42 in cell migration in 2D systems *in vitro* has been well studied, and we understand Cdc42 as a master regulator of the actin cytoskeleton in this context. However, we do not yet fully appreciate how these functions translate into 3D migration *in vivo*, and the role of Cdc42 during development is not well understood. Targeted deletion of Cdc42 in the melanoblast lineage during development led to striking coat colour defects in adult mice, suggesting Cdc42 was controlling melanoblast proliferation and/or migration (Figure 3.1). These coat colour defects mirrored those seen in Rac1 f/f Tyr::CreB mice (Li et al., 2011). Interestingly, Cdc42 is not required for melanoblasts to enter developing hair follicles although we still do not fully understand the factors controlling this process (Figure 3.2).

Visually tracking the melanoblast journey at different embryonic stages by X-Gal staining revealed that Cdc42 controls melanoblast number at later stages in development, but does not control the initial number of melanoblasts that gather in the migration staging area at E11.5 (Figure 3.5). Tyrosinase expression, and therefore Cdc42 deletion occurs at E10.5, suggesting that loss of Cdc42 at this time point does not affect melanoblast number. This observation confirms those made by Fuchs et al. that Cdc42 is dispensable for the migration of early neural crest cells (Fuchs et al., 2009). Cdc42 expression was however essential for melanoblast proliferation and positioning at E13.5 and E15.5 (Figure 3.6-3.9). Cdc42 f/f Tyr::CreB embryos at these time points displayed a paucity of melanoblasts and delay in melanoblast progression away from the neural tube towards the belly. It is, however, difficult to separate the relative contribution of melanoblast migration versus proliferation in successful population of the embryo. It is clear that the melanoblast population must expand rapidly from the 'founder' population of melanoblasts that are specified from the neural tube, so proliferation defects alone can lead to coat colour defects. However, melanoblasts must also migrate away from each other to spread throughout the embryo. Recent evidence demonstrating that the melanoblast population may also be 'topped up' by differentiation from Schwann cell precursors later on in

development complicates our currently accepted model. These findings may require a rethink of mathematical models of melanoblast population of the developing embryo, building upon and refining those models already suggested (Mort et al., 2016) (Larue et al., 2013). We could therefore conclude that Cdc42 controls melanoblast number and positioning after E13.5, but could not yet determine its role in migration.

3.3.2 Cdc42 controls melanoblast proliferation by promoting S phase entry and aiding cytokinesis

Injection of BrdU into pregnant mice revealed a 22% drop in the number of melanoblasts in S phase in Cdc42 f/f Tyr::CreB embryos compared to control embryos after 24 hrs (Figure 3.10). This defect in G1 to S transition was also observed in Rac1 null melanoblasts (Li et al., 2011), which confirms *in vitro* work that demonstrated that microinjection of dominant negative Rac and Cdc42 blocked serum induced DNA synthesis (Olson et al., 1995). It is likely that both Cdc42 and Rac1 control G1 progression in melanoblasts by controlling the activation of cyclins D and E (Chou et al., 2003, Gjoerup et al., 1998). In addition to controlling S phase entry, Rho GTPases are also associated with various stages of mitosis including cytokinesis. This is not surprising, due to the drastic changes in cell architecture that occur during mitosis. To divide, cells must alter their adhesion placement and cortical rigidity to round up during mitotic onset. Cdc42-GTP levels peak at metaphase in Hela mitotic extracts, whereas Rac-GTP levels are relatively constant (Oceguera-Yanez et al., 2005).

In skin explants, we frequently saw that Cdc42 null melanoblasts were unable to fully round up when entering mitosis, sometimes leaving their long thin protrusions extended (Figure 3.11A). This may be due to a defect in adhesion disassembly in these pseudopods in the absence of Cdc42, leaving them stuck outside the cell body. This adhesion defect could be occurring in combination with actin:myosin contractility defects, preventing the cells from retracting the extended pseudopod. It appears that these melanoblasts are able to initiate cleavage furrow formation in a timely manner, but on average take three times longer to undergo cytokinesis than control melanoblasts (Figure 3.11C). We also observed an increase in cytokinesis time in Rac1 null melanoblasts, but the defect was not as striking (Li et al., 2011). Efficient cytokinesis and membrane

scission after chromosome segregation are dependent on the formation of a contractile ring, which consists of parallel filaments of actin and non-muscle myosin II. Its assembly and myosin motor are driven by phosphorylation of MLC at position T18 S19. It has been demonstrated that tight regulation of Cdc42 activation is necessary for proper equatorial actin assembly and to control RhoA localisation to the ring to initiate contractility (Zhu et al., 2011). The combination of cell cycle and cytokinesis defects imparted by the loss of Cdc42 presents a compound problem for melanoblasts, explaining the drop in melanoblast number in Cdc42 f/f Tyr::CreB embryos.

3.3.3 Loss of Cdc42 uncouples actin dynamics and pseudopod extension from migration

The coat colour defects and melanoblast proliferation and positioning issues highlighted by X-Gal staining of Cdc42 f/f Tyr::CreB embryos were reminiscent of Rac1 f/f Tyr::CreB embryos. This raised the question if loss of Cdc42 was mimicking Rac1 loss, suggesting that these two GTPases were carrying out similar functions in these cells. However, *ex vivo* imaging revealed that loss of Cdc42 led to a drastically different morphology to Rac1 loss. In contrast to the rounded nature of Rac1 null melanoblasts, which moved with short stubby protrusions (Li et al., 2011), Cdc42 null melanoblasts are larger and more elongated than control cells (Figure 3.14A and B). The number, length and lifetime of knockout pseudopods are strikingly different to controls, with Cdc42 null cells being biased to forming two pseudopods, taking on what we termed a ‘bipolar’ phenotype. Many pseudopods were extremely long-lived and they were longer in length than control pseudopods (Figure 3.16 D and E). These weedy, bleb-like pseudopods could not provide the drive and support necessary to sustain cell translocation between keratinocytes, as null melanoblasts moved much more slowly through the skin (Figure 3.17). Despite their division defects, these cells were not bi-nucleate, but may have issues with nuclear movement.

Taking into account these defects, we were very surprised to find that melanoblasts could polymerise actin at a relatively normal rate. Both control and Cdc42 null pseudopods produced an actin burst at their tip every 10 min on average (Figure 3.19B). However, it was clear that knockout pseudopods struggled to harness the protrusive force of the actin burst into efficient

migration. The dynamic nature of control melanoblasts is underpinned by their ability to channel actin bursts into nascent pseudopods, retracting older ones. Although Cdc42 null melanoblasts display regular actin bursts, they also extend longer lived pseudopods, without branching or retracting them (Figure 3.19C). From these data, we hypothesise that Rac1 is responsible for producing actin bursts in the absence of Cdc42. As we have previously found no role for N-WASP or PAK alone in melanoblast migration, we assume a minor role for Cdc42 in these bursts (Li et al., 2011). However, Cdc42 appears to be necessary for coordinating actin polymerisation by Rac1 and cell contractility into coordinated and persistent migration.

3.3.4 Loss of RhoA in the melanoblast lineage does not lead to coat colour defects

Despite the prominent role of Rac1 and Cdc42 in the melanoblast lineage, targeted deletion of RhoA did not lead to coat colour defects (Figure 3.3). From this phenotypic observation, we can infer that there is no drastic difference in melanoblast number, as this would most likely lead to grey hairs or white patches in adult mice. We cannot however rule out that there may be some minor defects in proliferation, or that these cells migrate in an alternative way. We hypothesise that loss of RhoA is compensated by other members of the Rho sub-family of Rho GTPases, such as Rho B or C. Through this mechanism melanoblasts could retain their ability to contract and move normally through the epidermis.

3.3.5 Rac1 and Cdc42 double knockout melanoblasts fail to populate the developing embryo

Having observed unique roles for the classic Rho GTPases Rac1 and Cdc42 in melanoblast migration *in vivo*, we were curious to investigate what effect losing both of these proteins might have on melanoblast migration. Pilot experiments have revealed some very interesting and striking observations. It appears that either very few or no melanoblasts are present in double knockout embryos at any location dorso-ventrally (Figure 3.21). Because these pups died at birth, it was not possible to study the coat colour of these mice. This lethality may be due to expression of CreB in other neural crest lineages, such as the neuronal

lineage, as it is unlikely that mice would not survive due to the absence of melanocytes.

3.4 Summary

The work presented in this chapter has provided a rare insight into the role of the classical Rho GTPases Cdc42 and RhoA in 3D cell migration *in vivo*. By comparing these findings with previous work from the lab, we have demonstrated that Cdc42 and Rac1 play unique roles in controlling melanoblast migration, but RhoA alone does not appear to have a prominent role. Whereas Rac1 provides the protrusive force behind migration by inducing actin polymerisation at the tips of pseudopods, Cdc42 is responsible for the coordination of pseudopod extension, branching and retraction. In addition, Cdc42 induces G1 to S cell-cycle transition in melanoblasts, similarly to Rac1. However, Cdc42 appears to play an even more vital role than Rac1 during cytokinesis, where it is essential in controlling contractile ring formation and completing membrane scission to allow separation of daughter cells. Loss of both Cdc42 and Rac1 in the melanoblast lineage appears to abrogate or abolish the melanoblast population. However, these are only preliminary findings, and further investigation would be needed to discover if the melanoblast lineage is determined from the neural crest at all, and if so what migration or proliferation defects these cells might encounter at earlier stages, or indeed if they are dying due to apoptosis

4 Investigating the Role of Cdc42 in Melanocyte Migration and Proliferation

4.1 Introduction and aims

Our investigation into the role of Cdc42 in cell migration *in vivo* using the melanoblast model uncovered an essential role for this GTPase in driving their migration and division. High resolution imaging of knockout melanoblasts migrating through developing embryo skin revealed their strikingly elongated cell morphology, and their inability to dynamically extend and retract pseudopods. This rendered them unable to migrate efficiently through the skin. Remarkably though, relatively normal actin polymerisation occurred in the tips of these pseudopods, however the force generated by these bursts was not harnessed into migration, although it was not clear why this was the case. Interestingly, this work suggested that Cdc42 was playing a different role to Rac in the migration of these cells, apparently coordinating actin polymerisation with pseudopod extension and retraction. We were keen to investigate further the molecular details and signalling behind this role.

To investigate these more closely, our aim was to isolate an inducible Cdc42 knockout melanocyte cell line from one-day-old pups. By culturing and studying these cells *in vitro* we first wanted to discover if deletion of Cdc42 caused the same sort of defects to those seen in melanoblasts. Using these cells as a model, we wanted to investigate the expression and localisation of classic Cdc42 effectors and actin related proteins to more fully understand the striking morphology and migration defects of melanoblasts *in vivo*. We also aimed to study the impact of Cdc42 loss on their progression through the cell-cycle and cytokinesis.

4.2 Results

4.2.1 Knock-down of Cdc42 in cultured melanocytes leads to migration and proliferation defects

We began these studies using the M4 primary immortalised melanocyte cell line (Rac1 f/f Tyr::Cre-ERT2; CDKN2^{-/-}) previously isolated and described (Li et al., 2011). Taking an siRNA approach, Cdc42 was successfully depleted in these cells by two independent oligos (Figure 4.1A). Knockdown of Cdc42 by both oligos, but particularly Si2, resulted in an elongated bipolar morphology. Like Cdc42 null melanoblasts, their pseudopods were long and weedy. This was in contrast to control melanocytes, which produce large fan-like lamellipods (Figure 4.1B). This knockout morphology was very reminiscent of Cdc42 knockout melanoblasts (Figure 3.14 and 3.15). In addition, knockdown also induced a proliferation defect, with Si2 affecting proliferation most severely (Figure 4.1C). Tracking the movement of non-treated melanocytes or those treated with scramble (SC) or anti-Cdc42 oligos revealed a striking migration defect in Cdc42 knockdown conditions (Figure 4.2). These migration and proliferation defects were also similar to the defects seen in Cdc42 null melanoblasts, making cultured melanocytes a useful model to study *in vitro* to more fully understand Cdc42's role in this lineage.

4.2.2 Isolation of an inducible Cdc42 knockout primary melanocyte cell line

Having confirmed that primary melanocytes are an interesting and valid model to understand the role of Cdc42 in the melanoblast journey, we set out to isolate a primary melanocyte line in which Cdc42 deletion was inducible by addition of tamoxifen. To achieve this, mice carrying Cdc42 containing a floxed portion of the gene were bred with mice carrying Cre recombinase under control of the estrogen receptor promoter. Inducible deletion of the tumour suppressor CDKN2 was also incorporated to help immortalise cells isolated from this model. Upon addition of tamoxifen, Cre recombinase is expressed and Cdc42 and CDKN2 are lost (Figure 4.3).

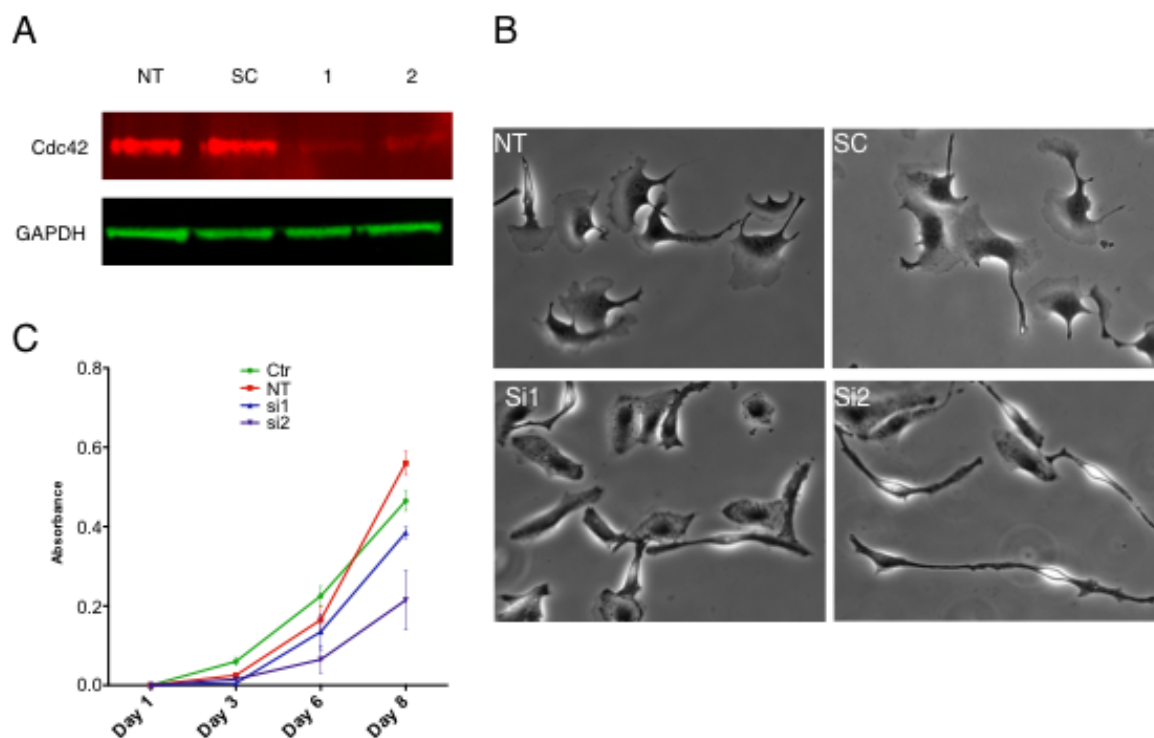


Figure 4.1 Knockdown of Cdc42 by siRNA leads to an elongated cell morphology and slows proliferation

Knockdown experiments were performed on M4 (*Rac1 f/f Tyr Cre-ERT2; CDKN2^{-/-}*) primary melanocytes. Conditions include non treated (NT) and scramble (SC) controls. Cdc42 was knocked down using two separate oligos referred to as Si1 and Si2. **(A)** Western blotting on control and knockdown primary melanocyte lysate probed with anti-Cdc42 and anti-GAPDH antibodies. **(B)** Images showing the morphology of control and knockdown melanocytes. **(C)** Proliferation curve of control and knockdown melanocytes over 8 days, absorbance taken every 2 days. Plot is an average of three repeats, error bars show SEM.

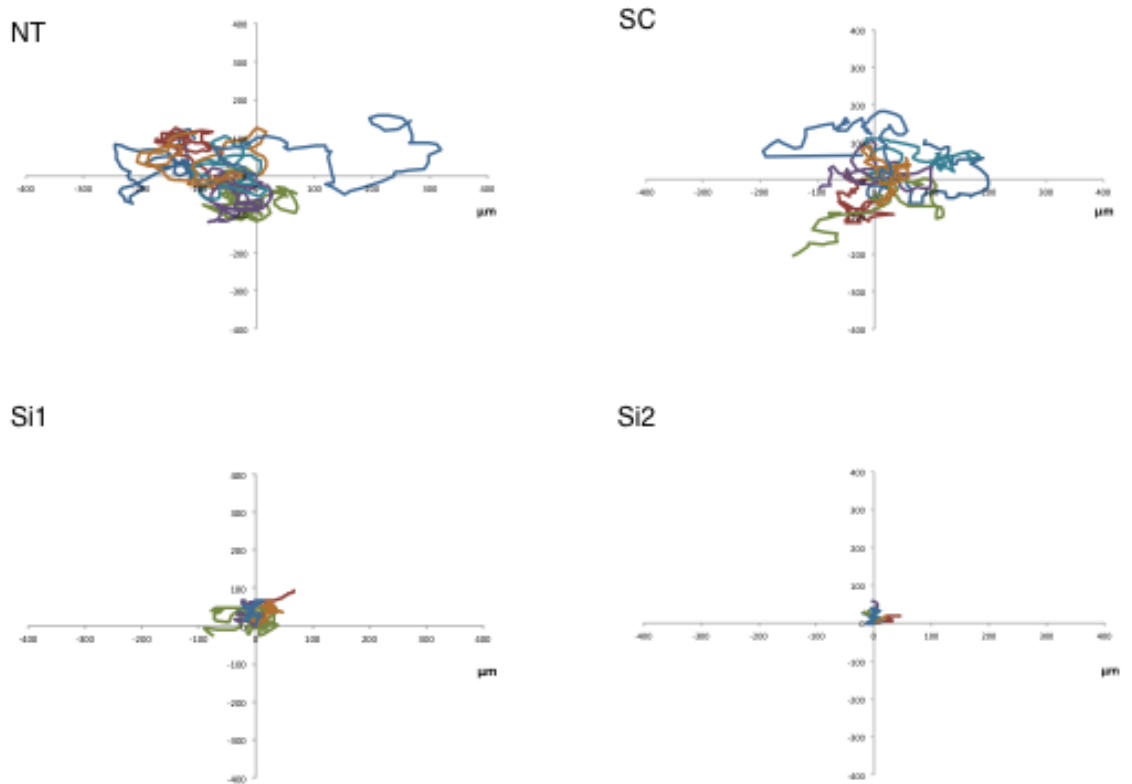


Figure 4.2 Cdc42 knockdown melanocytes have a severe migration defect

Spider migration plots showing tracks of M4 (*Rac1 f/f Cre-ERT2; CDKN2^{-/-}*) primary melanocytes. Conditions include non treated (NT) and scramble (SC) controls. *Cdc42* was knocked down using two separate oligos referred to as Si1 and Si2. Plots show tracks from 7 cells.

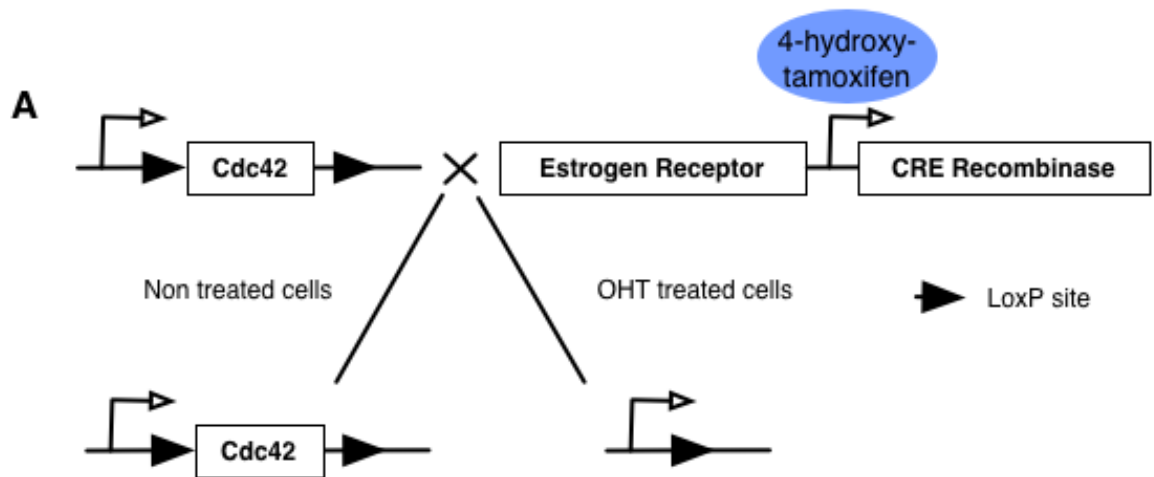


Figure 4.3 Generation of an inducible Cdc42 knockdown melanocyte cell-line

(A) Melanocytes were isolated from the skin of one-day-old Cdc42 *f/f* Cre-ERT2; CDKN2^{-/-} pups. Expression of Cre in this case was placed under the control of the estrogen receptor; allowing knockout to be induced by addition of the potent tamoxifen metabolite 4-hydroxytamoxifen (OHT). Loss of the tumour suppressor CDKN2 was included in this model to promote growth of the isolated lines in culture

Melanocytes were isolated from the skin of 1-day-old pups. Initially, cultures are a mixed population of melanocytes and fibroblasts. Pure melanocyte cultures were obtained after 2 months of selection. The purity of cultures was verified by staining for the melanocyte transcription factor MITF (Figure 4.4A). The two melanocyte lines EW1 and EW7 were incubated with 1 μ M OHT or an equivalent volume of DMSO for 5 days, and loss of Cdc42 protein was confirmed by western blot (Figure 4.4B). As Cdc42 protein is depleted from the primary melanocyte line EW7, cells become increasingly elongated in comparison to the DMSO treated cells (Figure 4.4C and D). Therefore, both knockdown of Cdc42 using siRNA in melanocytes and knockout of Cdc42 in melanoblasts using a genetic, inducible model induces an extended morphology. In a strikingly similar manner to that seen *in vivo*, loss of Cdc42 leads to an elongated cell morphology due to long, weedy pseudopods, which render the cells unable to move efficiently. This suggests a conserved role for Cdc42 in melanocytes and melanoblasts.

4.2.3 Primary melanocytes require Cdc42 for efficient pseudopod extension and ruffling

DMSO and OHT treated primary melanocytes from lines EW1 and EW7 (Cdc42 *f/f* Cre-ERT2; CDKN2^{-/-}) were plated on fibronectin to investigate their ability to engage and migrate on matrix. DMSO treated melanocytes from both lines formed large lamellipodia, leading to a small length to width ratio. This is in contrast to Cdc42 knockout cells of both lines, which, similarly to Cdc42 knockdown melanocytes, stretched out over the matrix forming extended thin protrusions in opposite directions leading to a 10 fold increase in their length to width ratio from 2 to 20 (Figure 4.5A and B). The long thin protrusions of knockout melanocytes are often static, with the majority lasting over 600 minutes in both lines EW1 and EW7 (Figure 4.5C). Once extended, these protrusions are stuck in place, and the cells seem unable to coordinate adhesion formation and release with protrusion formation. As seen in melanoblasts *in vivo*, the majority of protrusions extended by DMSO treated melanocytes are very dynamic, lasting under 100 minutes (Figure 4.5C). These cells migrate efficiently over the matrix using large fan-like lamellipods at an average speed of 0.4 μ m/min. The static

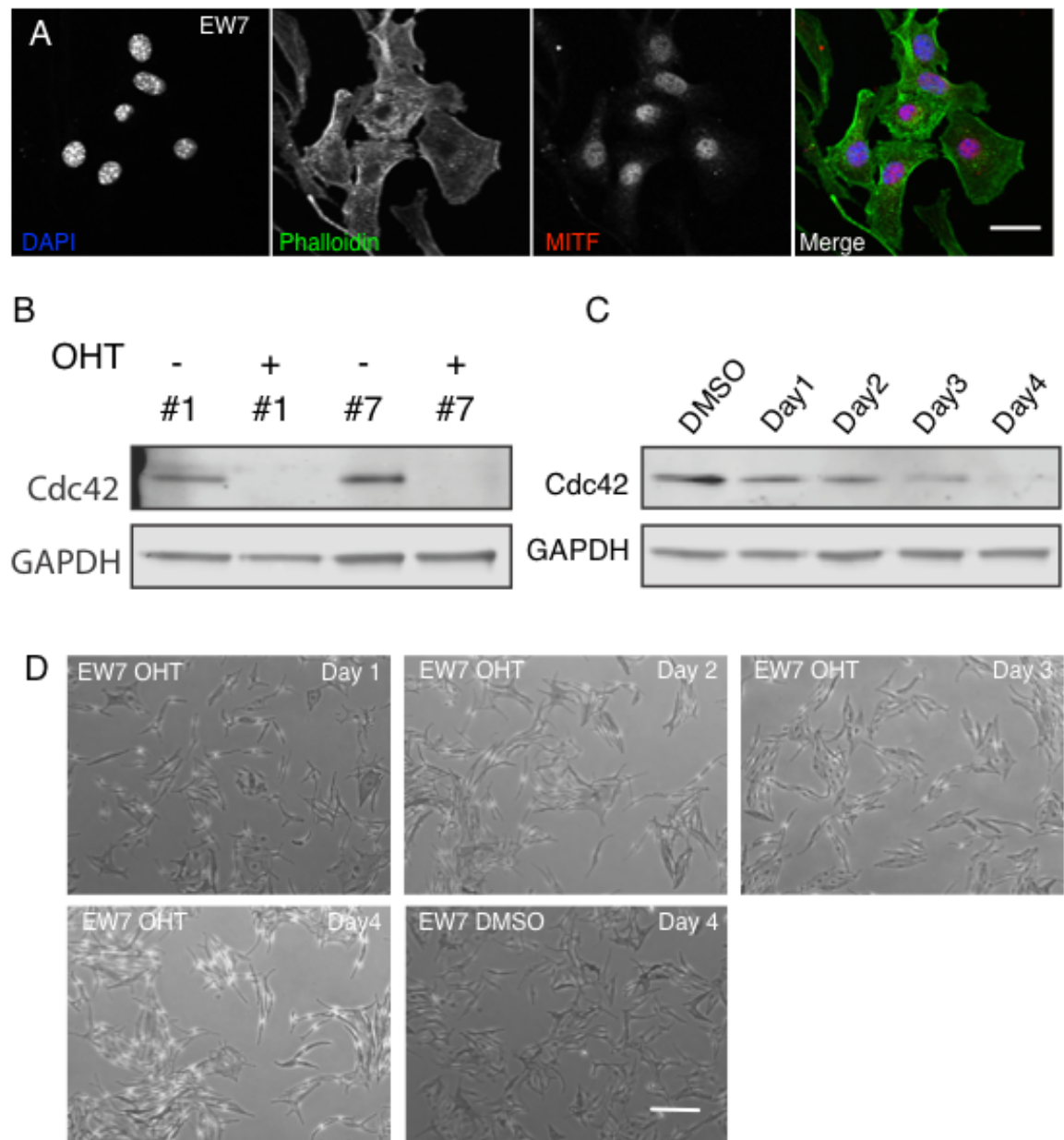


Figure 4.4 Cdc42 is lost at the protein level after 5 days of OHT treatment

(A) Primary melanocyte line EW7 (*Cdc42* f/f Cre-ERT2; *CDKN2*^{-/-}) fixed and stained with DAPI to stain nuclei (Blue), phalloidin to stain F-actin (green) and the melanocyte transcription factor MITF (red). Scale 20 μ m (B) Western blot from two primary melanocyte cell lines (EW1 and EW7) with and without treatment, probed with anti-Cdc42 and anti-GAPDH antibodies. (C) Western blot on EW7 lysate over days 1-4 of OHT treatment probed for Cdc42 and GAPDH. (D) Images of EW7 primary melanocytes after treatment with OHT over 4 days and control DMSO cells on day 4. Scale 100 μ m.

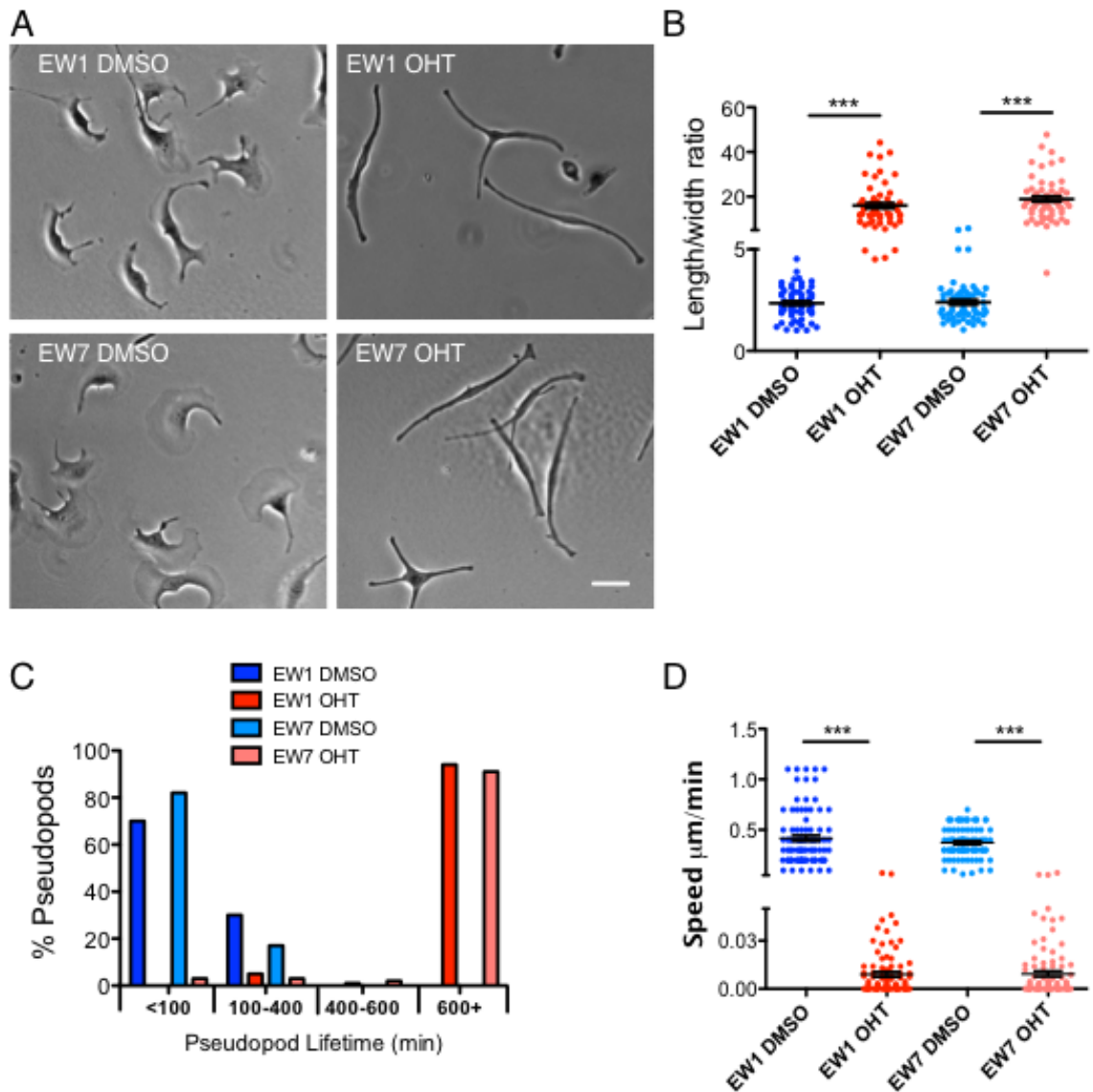


Figure 4.5 Cdc42 knockout melanocytes fail to make lamellipods and have pseudopod and migration defects

(A) Stills from time-lapse imaging of primary EW7 *Cdc42*^{f/f} Cre-ERT2; *CDKN2*^{-/-} melanocytes treated with DMSO or OHT, migrating on fibronectin. Scale 30 μM . (B) Length to width measurements of DMSO treated and OHT treated primary melanocyte lines EW1 and EW7 (59 cells quantified per condition). (C) Pseudopod lifetimes (57 pseudopods quantified per condition). (D) Melanocyte migration speed from time-lapse imaging of cells on fibronectin (90 cells quantified per condition). Graphs (B and D) show mean \pm SEM, *** $p < 0.001$ t-test.

nature of knockout pseudopods appears to prevent them from migrating efficiently; these cells barely move over the matrix, and a large proportion are completely static over the 10 hour time-lapse (Figure 4.5D) (Supplementary video 4). Similarly to Cdc42 knockdown melanocytes, the morphology of these inducible knockout melanocytes is very similar to that of Cdc42 null melanoblasts (Figure 3.14 and 3.15). We therefore hypothesise that Cdc42 is playing a very similar role in both lineages. Our data suggests that Cdc42 is necessary for the coordination of pseudopod dynamics and possibly adhesion assembly and disassembly to achieve efficient cell migration.

4.2.3.1 Cdc42 is required to coordinate lamellipod formation despite elevated levels of active Rac1 in knockout cells

We wanted to look more closely at the mechanisms driving protrusions in the primary melanocyte lineage. Control melanocytes migrate efficiently over matrix by extending lamellipods, based on the branched actin network (Figure 4.5). Interestingly, loss of Cdc42 prevents formation of these structures and these cells instead are limited to the extension of pseudopods, often in opposite directions. To understand this difference in protrusion formation, we looked closely at the actin regulators responsible for protrusion generation.

We used antibodies to localise WAVE2 and p34, two subunits within the Scar/WAVE complex and Arp2/3 complex respectively. The Scar/WAVE complex and Arp2/3 play a prominent role in the induction and formation of the branched actin network that forms the structure and protrusive force behind lamellipod formation. Control (DMSO treated) melanocytes display large lamellipodia, and both p34 and WAVE are strongly recruited at the leading edge of these structures (Figure 4.6A). Both WAVE2 and p34 can be seen at the tips of knockout pseudopods, but their localisation appears weak and patchy (Figure 4.6B), suggesting that Cdc42 is required for the correct placement of these factors. In the absence of Cdc42, these players are limited to the tips of pseudopods, and seem unable to localise strongly to broad areas of the membrane to form large ruffling structures, which are imperative for efficient migration. This agrees

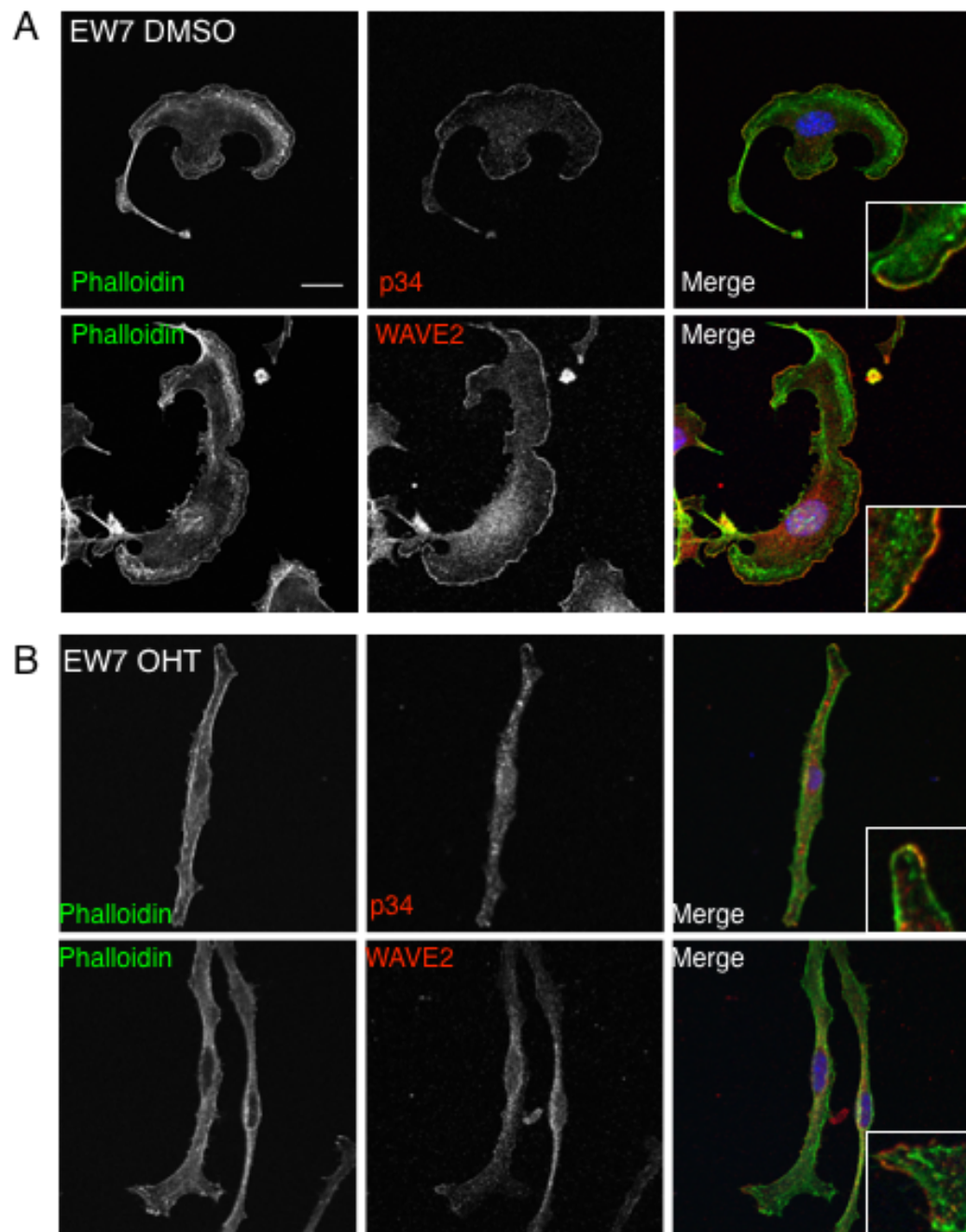


Figure 4.6 Actin branching machinery is poorly localised in knockout melanocytes

Immunofluorescence imaging of EW7 *Cdc42*^{f/f} Cre-ERT2; *CDKN2*^{-/-} melanocytes: **(A)** DMSO treated then fixed and stained with phalloidin to stain F-actin (green) and p34 or WAVE2 (red). Scale 15 μ m. **(B)** OHT treated then fixed and stained with phalloidin (green) and p34 or WAVE2 (red). Scale 15 μ m.

with our skin explant data in, showing that actin bursts still occurred in the narrow pseudopods formed in null melanoblasts, but this was not as productive for motility as in the wild-type.

A possible explanation for lack of lamellipodia in Cdc42 null melanoblasts could be due to defects in activation of Rac1, which is most commonly associated with the formation of lamellipodia (Insall and Machesky, 2009). We therefore measured the levels of active Rac1 in melanocytes using FLIM imaging of a Rac1FLARE dual-chain biosensor, in which activated Rac1-CFP binds to PAK (fragment)-YFP leading to a decrease in lifetime of the donor CFP fluorophore (Machacek et al., 2009, Goedhart et al., 2010). Lifetime heat maps of melanocytes expressing the control dTurquoise (donor alone) vector or the Rac1FLARE.dc vector shows that the donor fluorophore has a lower lifetime in the biosensor cells than the control, showing that FRET is occurring (Figure 4.7A). When the lifetimes of the CFP donor fluorophore are expressed as a percentage of the lifetime of the donor alone, we see this is higher in Cdc42 knockout cells indicating that these cells have more active Rac1 than control cells (Figure 4.7B).

To complement this data, active Rac1 levels were also quantified using a pull-down method. This involved incubation of lysate from DMSO and OHT treated cells with GST-PAK beads. The specificity of these beads was verified using lysate from DMSO and OHT treated M4 Rac1 f/f Tyr::Cre-ERT2; CDKN2^{-/-} primary melanocyte line (Figure 4.7C). Roughly equal levels of Rac1-GTP were found in DMSO and OHT treated EW7 primary melanocytes. Combined ratios of input to active levels of 2.7 in DMSO and 2.8 in OHT were observed, suggesting no significant difference in the levels of Rac1 in the absence of Cdc42 using this method (more replicates necessary to perform statistics). It is likely however that this approach is substantially less sensitive than the FLIM approach, and may not report modest changes on active Rac levels.

Therefore, in the absence of Cdc42, cells show reduced pseudopod dynamics, only forming small lamellipods at the tips of their pseudopods due weaker recruitment of branched actin nucleation machinery. We found normal to high levels of active Rac1 (the predominant GTPase required to orchestrate

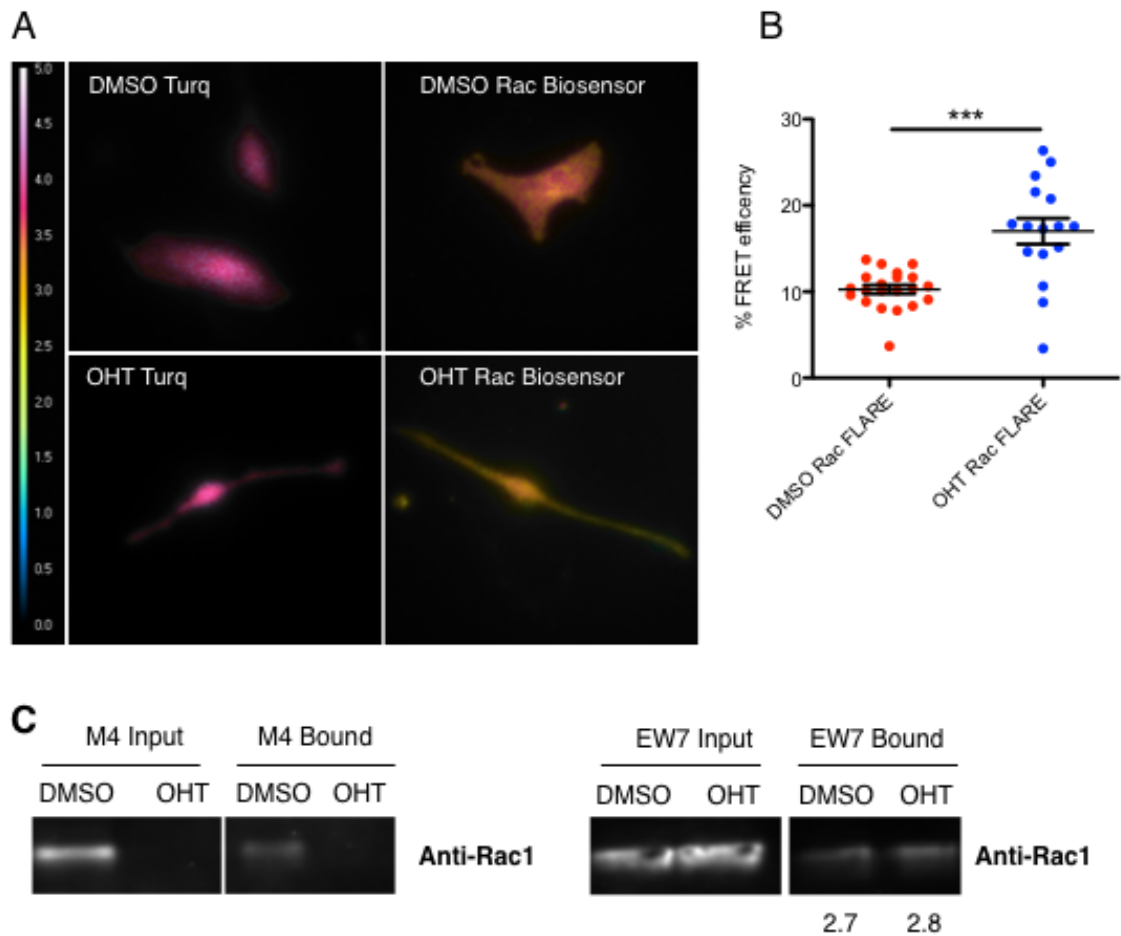


Figure 4.7 Levels of active Rac1 are modestly enhanced in the absence of Cdc42

(A) Heat maps showing lifetimes of control fluorophore (dTurquoise) and fluorophore in Rac1FLARE.dc biosensor in DMSO and OHT treated EW7 *Cdc42 f/f Cre-ERT2; CDKN2^{-/-}* melanocytes. (B) FRET efficiency of fluorophores in DMSO and OHT treated melanocytes, calculated as a percentage of the control lifetime. (C) Pull-down for active Rac1 in DMSO and OHT treated M4 (*Rac1 f/f Tyr::Cre-ERT2; CDKN2^{-/-}*) primary melanocytes and EW7 (*Cdc42 f/f Cre-ERT2; CDKN2^{-/-}*) primary melanocytes, showing input and bound fractions blotted for Rac1. Graph shows mean \pm SEM, *** $p < 0.001$ Mann-Whitney test

lamellipod formation), in knockout melanocytes. This may explain why Cdc42 null melanoblasts displayed a relatively normal rate of actin bursts in skin explants. However, Cdc42 knockout cells are unable to harness and direct these bursts of actin polymerisation to produce pseudopods dynamic enough to support migration.

4.2.3.2 Re-expression of Cdc42-YFP in melanocytes rescues cell morphology

We wanted to confirm whether rescuing levels of Cdc42 in knockout primary melanocytes would revert their extended morphology and lead to normal pseudopod generation. Using expression of YFP as a control, both DMSO and OHT treated melanocytes were transfected with YFP tagged Cdc42 (Figure 4.8A). Expression of Cdc42-YFP in DMSO treated melanocytes did not alter the length to width ratio of cells relative to the YFP control. However, expression of Cdc42-YFP in OHT treated cells rescued the elevated length to width ratio of 30 seen in YFP transfected down to an average of 4 (Figure 4.8B). Therefore, rescuing levels of Cdc42 in knockout melanocytes back to wild-type levels restores normal cell morphology.

4.2.4 Expression levels of Cdc42 effectors and other actin regulators is unchanged in knockout cells

To further investigate the molecular mechanisms behind the striking phenotype of Cdc42 knockout melanocytes, the protein levels of Cdc42 effectors and other actin regulators were assessed using western blotting (Figure 4.9). The lineage of these cells was confirmed by western blotting against the melanocyte marker DCT. We noted that there was no significant changes in the levels of the other Rho GTPases family members Rac1, Rac2 or Rac3 or RhoA, however this does not reflect the activation levels of these species. The Cdc42 associated actin nucleation promoting factor N-WASP is also unchanged at the protein level, similarly to p34, a subunit of the actin branching complex Arp2/3. Interestingly, there was no change in the total or phosphorylated levels of the PAK family of kinases, which are well-characterised down-stream effectors of Cdc42. Blotting for total levels of myosin light chain (MLC) showed that the primary melanocyte line EW1 expresses more MLC than EW7, furthermore a

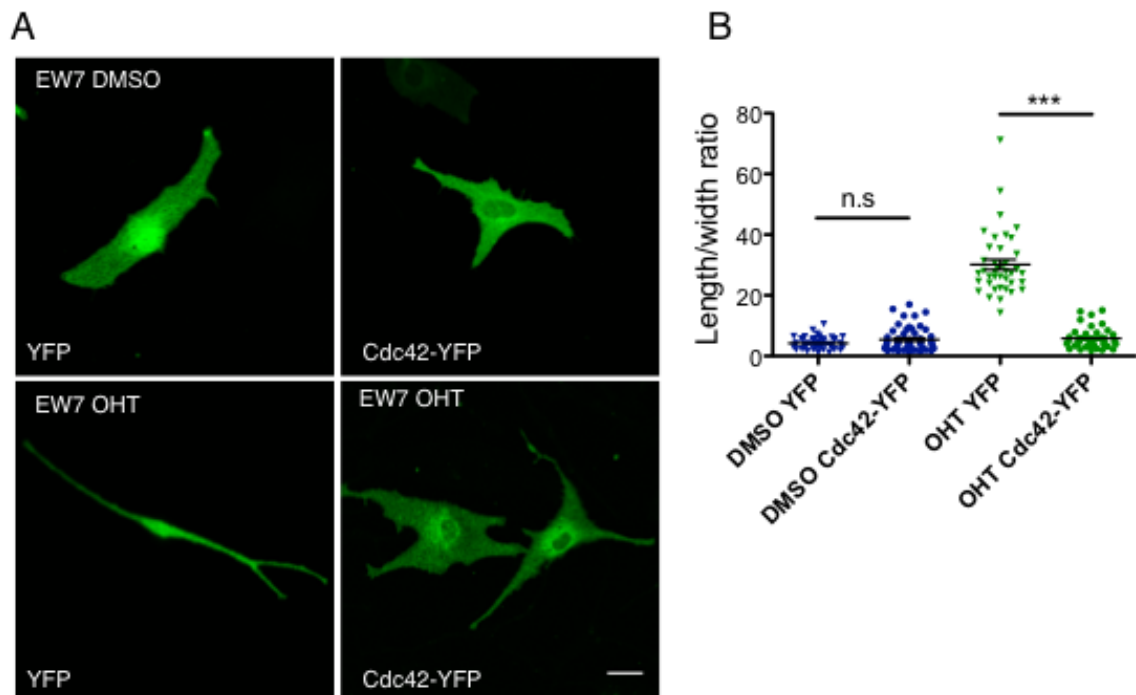


Figure 4.8 Transient expression of Cdc42-YFP in Cdc42 knockout cells rescues cell morphology changes

(A) Images of DMSO and OHT treated EW7 melanocytes on fibronectin transfected transiently with YFP or Cdc42-YFP. Scale 20 μm . **(B)** Quantification of length/width ratio of transfected melanocytes. Graphs show mean \pm SEM, *** $p < 0.001$ t-test, n.s.= not significant

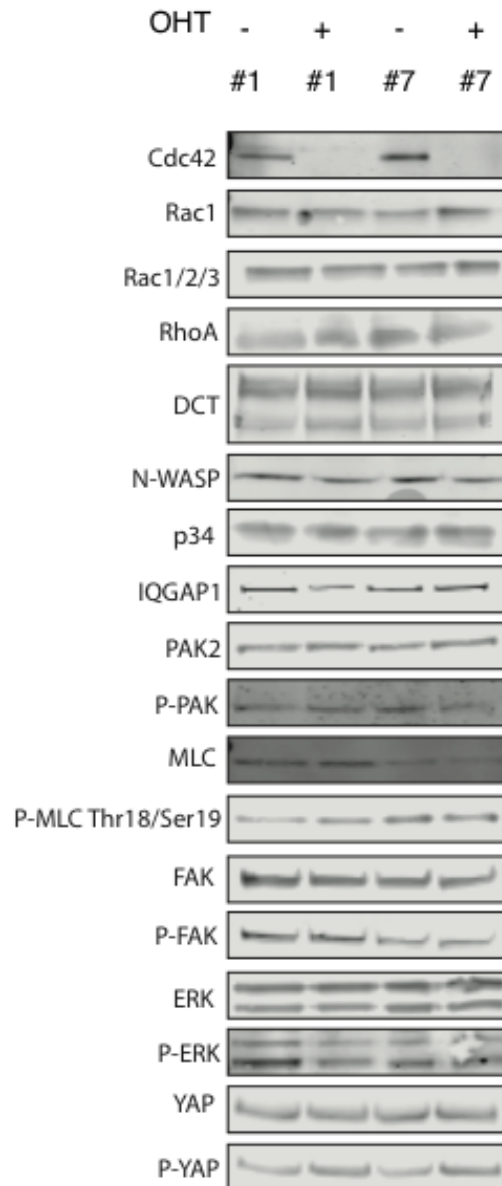


Figure 4.9 Protein levels of Cdc42 regulators and actin related proteins were not altered in the absence of Cdc42

Cell lysates from *Cdc42* *f/f* Cre-ERT2; *CDKN2*^{-/-} primary melanocyte cell lines (EW1 and EW7) treated with DMSO or OHT were separated by SDS-PAGE, transferred to PVDF membranes and probed with antibodies as indicated. Blots were repeated at least three times and loading always verified to alpha tubulin or GAPDH. Conclusions were made taking into account these three repeats and the loading of each blot.

much higher proportion of this MLC is phosphorylated in EW7 cells. However, phosphorylated levels of MLC remains unchanged in OHT treated cells relative to DMSO treated cells. This is investigated further later in this chapter. In addition, levels of FAK, P-FAK, ERK and P-ERK remain unchanged in knockout cells. Intriguingly, the only significant and consistent change at the protein level in knockout cells was the level of P-YAP. This observation is further explored later in this chapter. We conclude that the morphology of knockout cells can not be explained by a down regulation at the protein level of the Cdc42 effectors explored or of other actin related proteins. It is possible that the spatio-temporal control or localisation of some of these proteins at a global level leads to the observed phenotype.

4.2.5 Cdc42 controls the localisation of P-MLC in primary melanocytes

Imaging of Cdc42 knockout melanocytes and melanoblasts revealed that they were inefficient at retracting their pseudopods (Figure 3.15B, 3.16 and Figure 4.5). Cell contractility occurs through interaction between actin filaments and myosin motors, and their interaction is controlled through phosphorylation of the myosin regulatory light chain (MLC). It has been reported that Cdc42 can control phosphorylation of MLC through its downstream effector MRCK. Active Cdc42 can activate MRCK, which in turn can phosphorylate the myosin light chain, leading to opening up of the myosin protein structure and binding onto nearby actin filament. This cross binding of myosins to the actin cytoskeleton allows contractile force generation as the myosin heads walk along filaments (Figure 4.10A). This led us to hypothesise that this phenotype may be caused by a reduction in this regulatory phosphorylation.

However, as shown earlier in this chapter (Figure 4.9), phosphorylation levels of the MLC were unchanged in DMSO and OHT treated cells. The graph in Figure 4.10B expresses this data as a ratio as an average from three blots, showing that the levels of P-MLC between DMSO and OHT treated EW7 and EW1 melanocytes is unaltered. This lead us to question whether in fact it was the localisation of MLC phosphorylation that was altered in these cells. To investigate this,

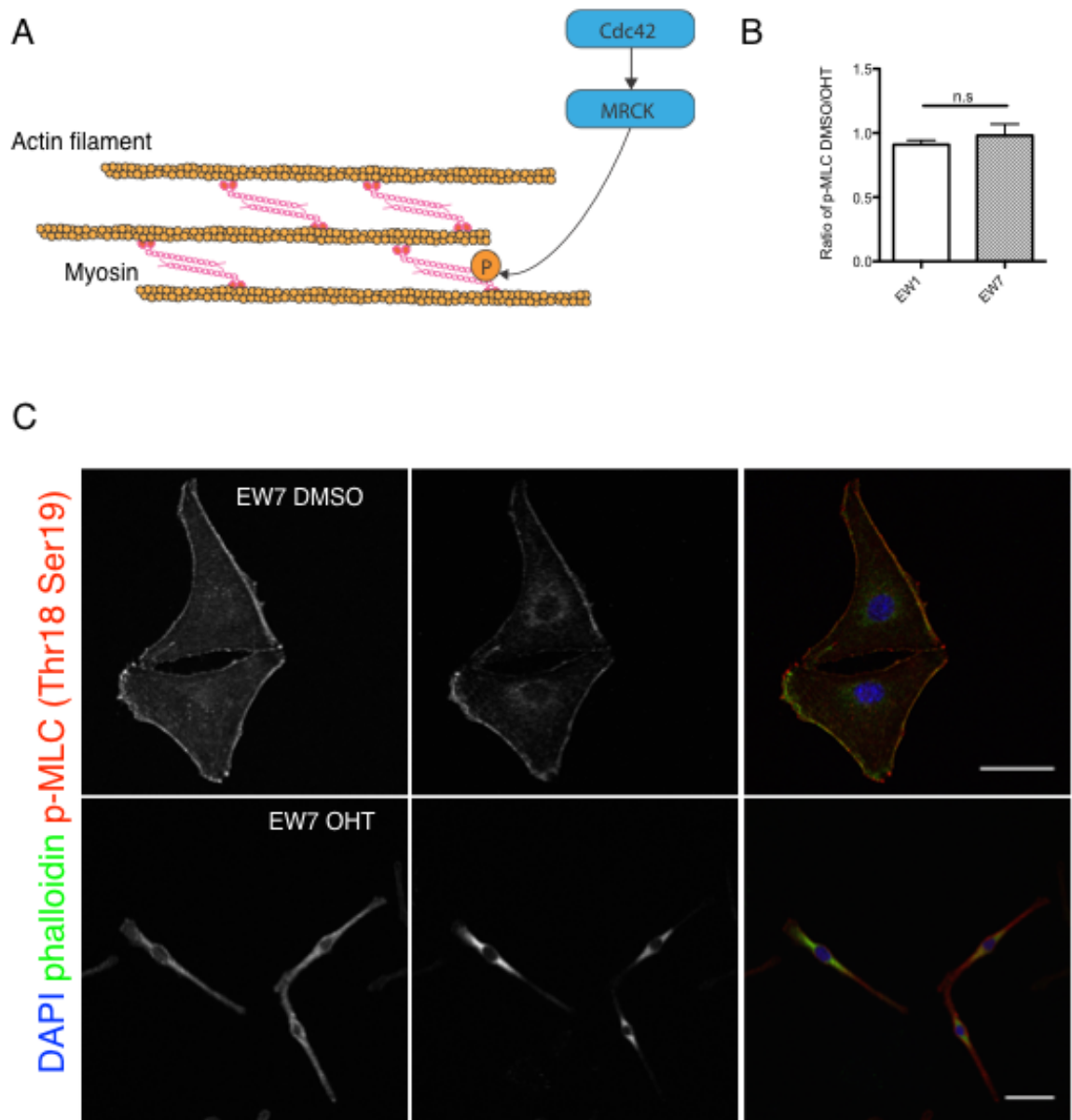


Figure 4.10 Knockout melanocytes have the same levels of phosphorylated-MLC but is differently localised

(A) Schematic demonstrating that Cdc42 can control phosphorylation of the regulatory myosin light chain through its effector MRCK. (B) Graph showing the p-MLC ratio between DMSO/OHT treated melanocytes from three independent western blots from lysates of EW1 and EW7 Cdc42 f/f Cre-ERT2; CDKN2^{-/-} primary melanocyte probed for P-MLC Thr18/Ser 19. (C) Immunofluorescence staining of EW7 primary melanocytes treated with DMSO or OHT stained for DAPI (nucleus) (blue) phalloidin (F-actin) (red) and P-MLC Thr18/Ser19 (green). Scale 20 μ m.

immunofluorescence staining was performed to visualise the localisation of MLC phosphorylation at position threonine 18 or serine 19 (Figure 4.10C). Staining in DMSO control cells revealed that myosin phosphorylation occurs around the cell cortex, co-localising with actin staining. However, staining in OHT treated cells revealed a very different localisation, with phosphorylation mainly occurring around the cell nucleus. We therefore believe that Cdc42 is required by the cell to phosphorylate the MLC in the correct location in the cell. The lack of P-MLC in knockout pseudopods may partly explain why these cells are unable to retract these extensions, rendering them unable to migrate efficiently.

4.2.6 Cdc42 controls the activation and nuclear accumulation of YAP, but not its response to serum starvation

As highlighted earlier, YAP phosphorylation was increased in Cdc42 knockout cells (Figure 4.11A). YAP and TAZ are newly emerging transcriptional regulators that play exciting roles in development, tissue homeostasis and cancer (Low et al., 2014). Due to recently reported links between Cdc42 and YAP during kidney development (Reginensi et al., 2013), we decided to further investigate the relationship between YAP and Cdc42 in primary melanocytes. According to the literature, an increase in the phosphorylated population of YAP would mean more inactive, cytoplasmic YAP. To explore this, we quantified the nuclear/cytoplasmic ratio of YAP in fixed DMSO and OHT treated primary melanocytes on fibronectin by immunofluorescence (Figure 4.11B). This quantification suggested that there is in fact more YAP in the cytoplasm of OHT cells compared to DMSO treated cells (Figure 4.11C).

We were intrigued by this finding, and we wondered whether this inactivation of YAP in the absence of Cdc42 led to the migration and morphology defects of these cells. However, knocking down YAP in EW7 primary melanocytes did not result in a Cdc42 null-like phenotype, showing that less transcription from YAP related targets are not alone responsible for the knockout morphology (Figure 4.12A and B). We were also intrigued whether Cdc42 played a role in YAP signalling in response to serum addition. In DMSO treated cells, addition of serum after serum starvation results in a decrease in YAP phosphorylation,

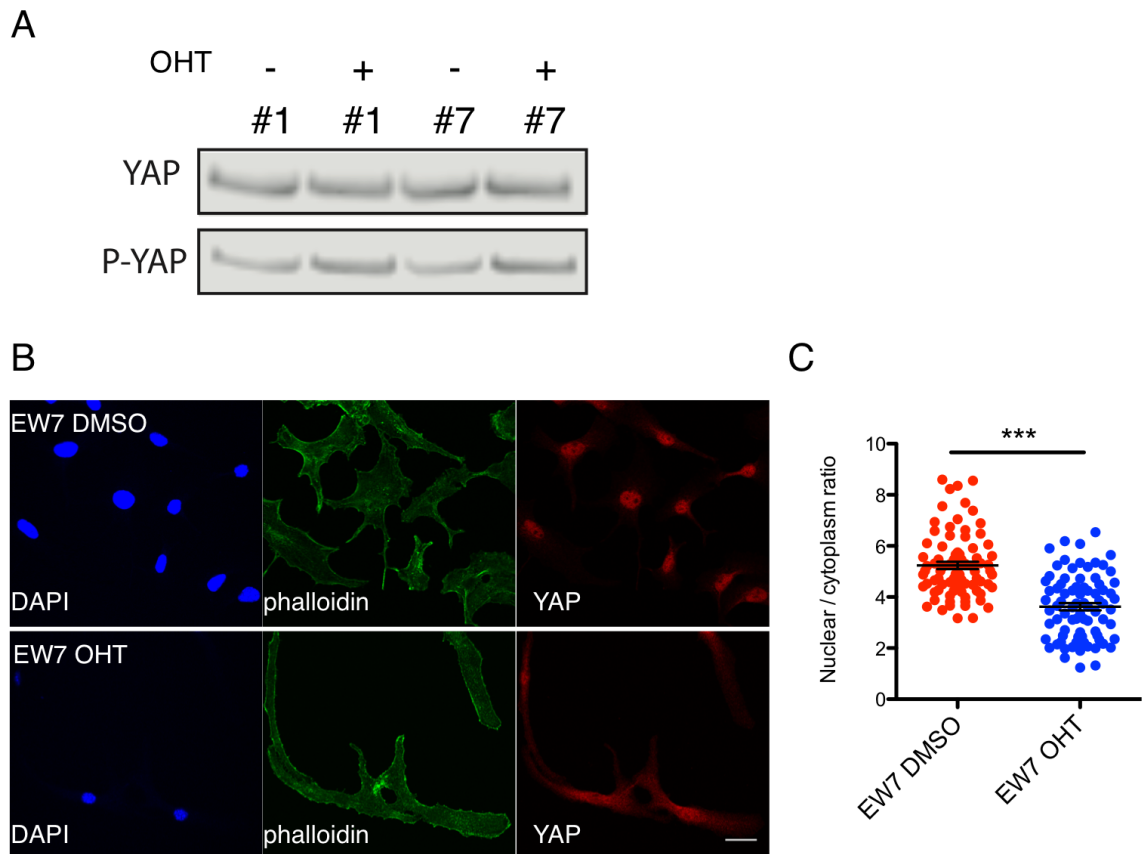


Figure 4.11 YAP phosphorylation is increased in the absence of Cdc42 leading to a decrease in nuclear YAP

(A) Western blotting on lysates from EW1 and EW7 Cdc42 *f/f* Cre-ERT2; CDKN2^{-/-} primary melanocyte cell lines treated with DMSO or OHT probed for YAP and P-YAP. **(B)**

Immunofluorescence staining of EW7 primary melanocytes treated with DMSO or OHT on fibronectin, fixed and stained for DAPI (nucleus) (blue) phalloidin (F-actin) (green) and YAP (red).

Scale 20 μ m. **(C)** Quantification of the nuclear-to-cytoplasmic ratio of YAP in DMSO or OHT treated EW7 melanocytes. Measurements taken from 80 cells from each condition from 3 separate experiments Graph shows mean \pm SEM, *** p <0.001 t-test.

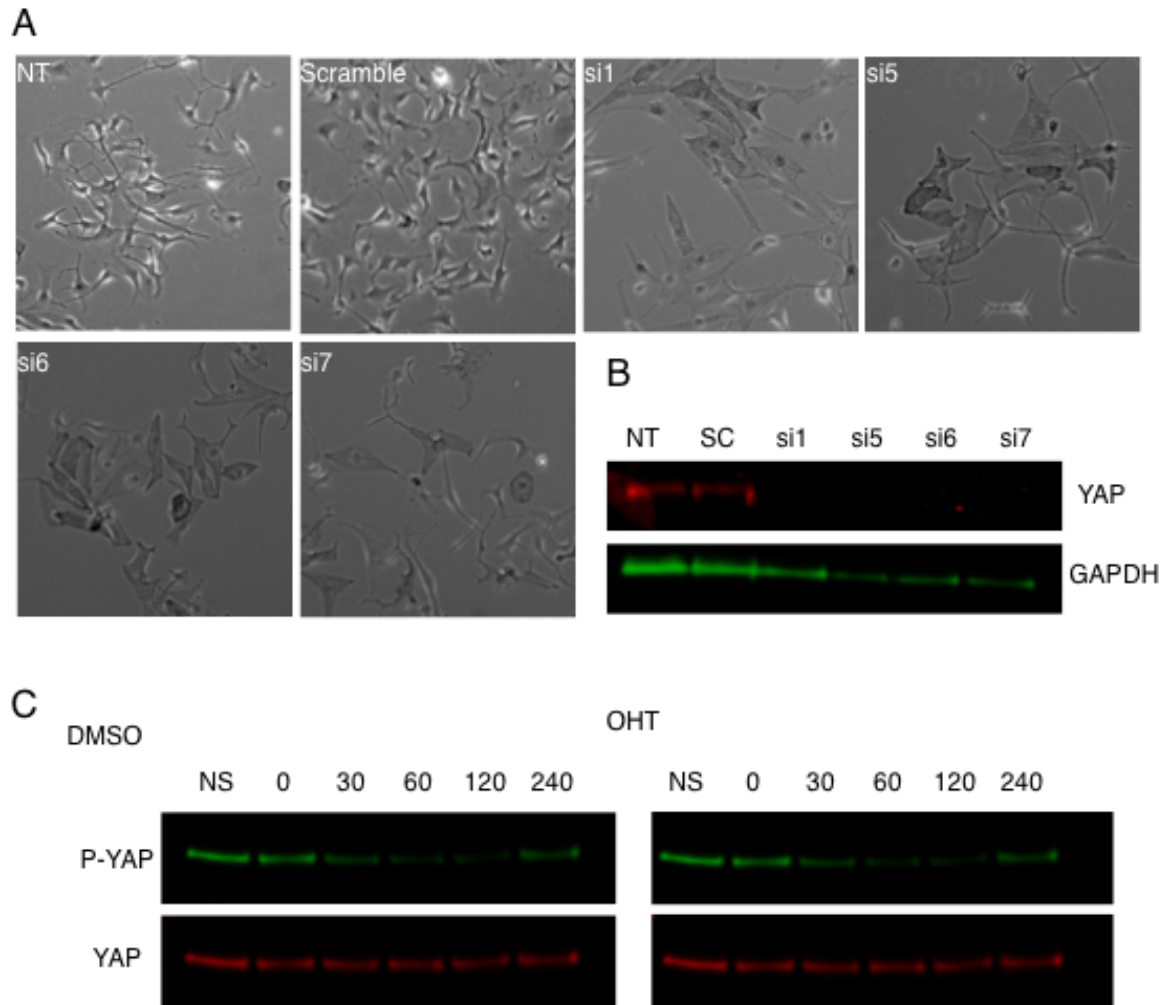


Figure 4.12 Knockdown of YAP in melanocytes does not mimic loss of Cdc42

(A) Images of EW7 *Cdc42*^{ff} *Cre-ERT2*; *CDKN2*^{-/-} primary melanocytes non-treated (NT) or treated with scramble siRNA (Scramble) or YAP siRNA (si1,5,6 and7). (B) Western blot on lysates from cells treated in (A). (C) Western blotting on DMSO or OHT treated EW7 melanocyte lysate for levels of YAP and P-YAP in response to serum starvation. Cells were serum starved overnight (0) then serum was added back and lysates taken 30, 60, 120 and 240 min after re-addition. Control lysate shows levels prior to starvation (NS). Blots representative of three independent experiments.

meaning signalling from these factors leads to YAP activation and nuclear translocation (Figure 4.12C). However, loss of Cdc42 did not impair this signalling, showing it is not a major player in this pathway (Figure 4.12C). We conclude that levels of phosphorylated-YAP are elevated in the absence of Cdc42, and that this leads to confinement of YAP in the cytoplasm. However, YAP signalling alone does not seem to underpin the morphology of these cells, although it may contribute in some way along with other factors.

4.2.7 Knockout protrusions are not solely dependent on microtubules, formins or Arp2/3 to form

Following on from our investigation into the actin dynamics at the tips of knockout pseudopods, we wanted to gain a deeper understanding of how these were generated. We wanted to see if in the absence of Rac driven lamellipod formation, whether pseudopods were based on other drivers such as the microtubule network or formins.

Given the relative stability of knockout pseudopods, we thought it possible that the microtubule cytoskeleton was driving and supporting them. To investigate this, DMSO and OHT treated primary melanocytes were treated with the microtubule destabilising agent nocodazole. Immunofluorescent staining using the tyrosinated tubulin antibody revealed that the microtubule network was indeed abolished (Figure 4.13A). Interestingly, OHT treated cells were still elongated after drug treatment, and their long, thin protrusions were still present. This told us that microtubules alone are not supporting these aberrant pseudopods. We then wondered if these protrusions could form in the absence of microtubules, and whether they were in fact driving their formation. To answer this we imaged these nocodazole treated control and knockout primary melanocytes re-settling in the presence of nocodazole (Figure 4.13B and C). Intriguingly, when knockout melanocytes are challenged to settle in the absence of the microtubule network, they no longer extend two long protrusions in either direction, instead they form multiple spider-like extensions in a similar manner to control cells in the same conditions. We therefore conclude that knockout

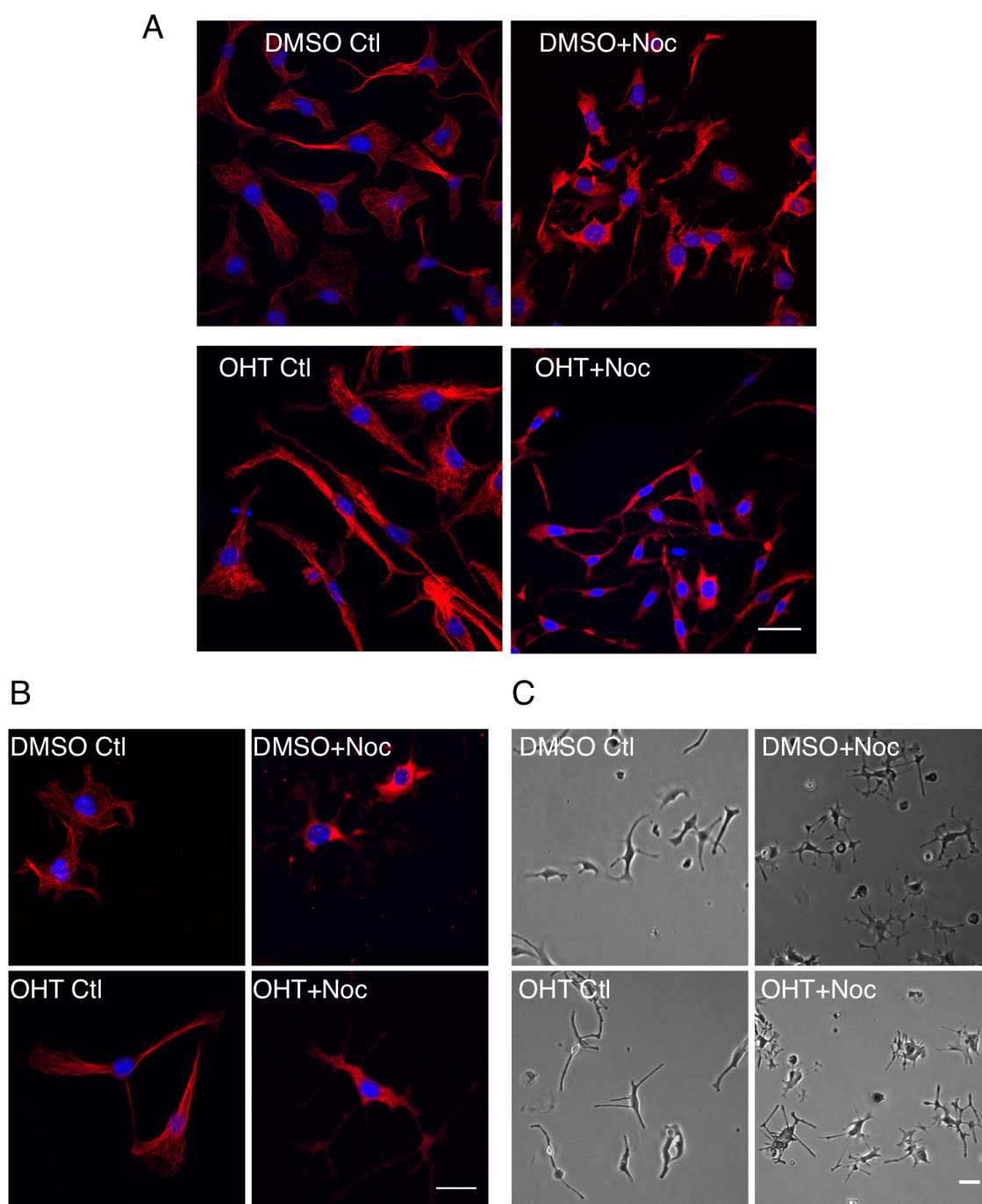


Figure 4.13 Microtubules are not essential to support the long thin protrusions made by knockout melanocytes, but they contribute to their bipolar nature

(A) Immunofluorescence staining of DMSO or OHT treated EW7 *Cdc42* *f/f* *Cre-ERT2*; *CDKN2*^{-/-} primary melanocytes on fibronectin after 2 hours treatment with 5 μ g/ml nocodazole. Stained to show the microtubule cytoskeleton using tyrosinated tubulin (red) and the nucleus using DAPI (blue). 30 μ m scale. **(B)** Immunofluorescence staining of EW7 melanocytes pre-treated with 5 μ g/ml nocodazole then trypsinised and re-settled in the presence of 5 μ g/ml nocodazole. Stained for tyrosinated tubulin (red) and DAPI (blue). 20 μ m scale **(C)** TL images on melanocytes described in (B) prior to fixation and staining. Scale 30 μ m.

pseudopods are not dependent on the microtubule network for support or to drive their growth. It does seem however that in the absence of Cdc42 that the microtubule cytoskeleton may be responsible for the bi-polar aspect of their morphology.

To extend these findings, we performed similar experiments using the broad formin inhibitor SMIFH2 and the Arp2/3 inhibitor CK-869 to investigate whether actin polymerisation via formins or the Arp2/3 was responsible for the Cdc42 knockout phenotype. Treatment with either drug on settled OHT treated melanocytes did not appear to drastically alter cell morphology (Figure 4.14A and 4.15A), however, as expected treatment with 20 μ M CK-869 prevented control melanocytes from ruffling (Figure 4.15A). Knockout melanocytes pre-treated with these drugs also successfully managed to settle in the presence of these inhibitors (Figure 2.14B and 2.15B). It seems therefore that in the absence of Cdc42, cells are not reliant on formins or pathways leading to activation of the Arp2/3 complex to extend their characteristic static protrusions, forming the knockout morphology that we see when these cells are spread.

4.2.8 Cdc42 promotes G1 to S transition and is necessary for efficient cytokinesis in melanocytes

Cultured primary melanocyte lines also provided a tool to further investigate the proliferation defects observed in Cdc42 null melanoblasts *in vivo*. OHT treated melanocytes were markedly slower to proliferate on plastic in culture, with cultures barely increasing in number over a four day period after treatment (Figure 4.16A). Cell-cycle analysis was performed on DMSO and OHT treated EW7 melanocytes by incubating adherent cells with BrdU for 3 hours, followed by flow-cytometry analysis using an anti-BrdU antibody to highlight cells in S-phase and propidium iodide to stain the chromatin of all cells (Figure 4.16B). The cell-cycle distribution of Cdc42 knockout melanocytes showed significantly less cells in S phase, falling to just 5% compared to 18% in DMSO populations. More cells were seen in G1 increasing from around 80% in DMSO conditions to 93% knockout populations. This demonstrates that cells are gathering in G1 and not progressing

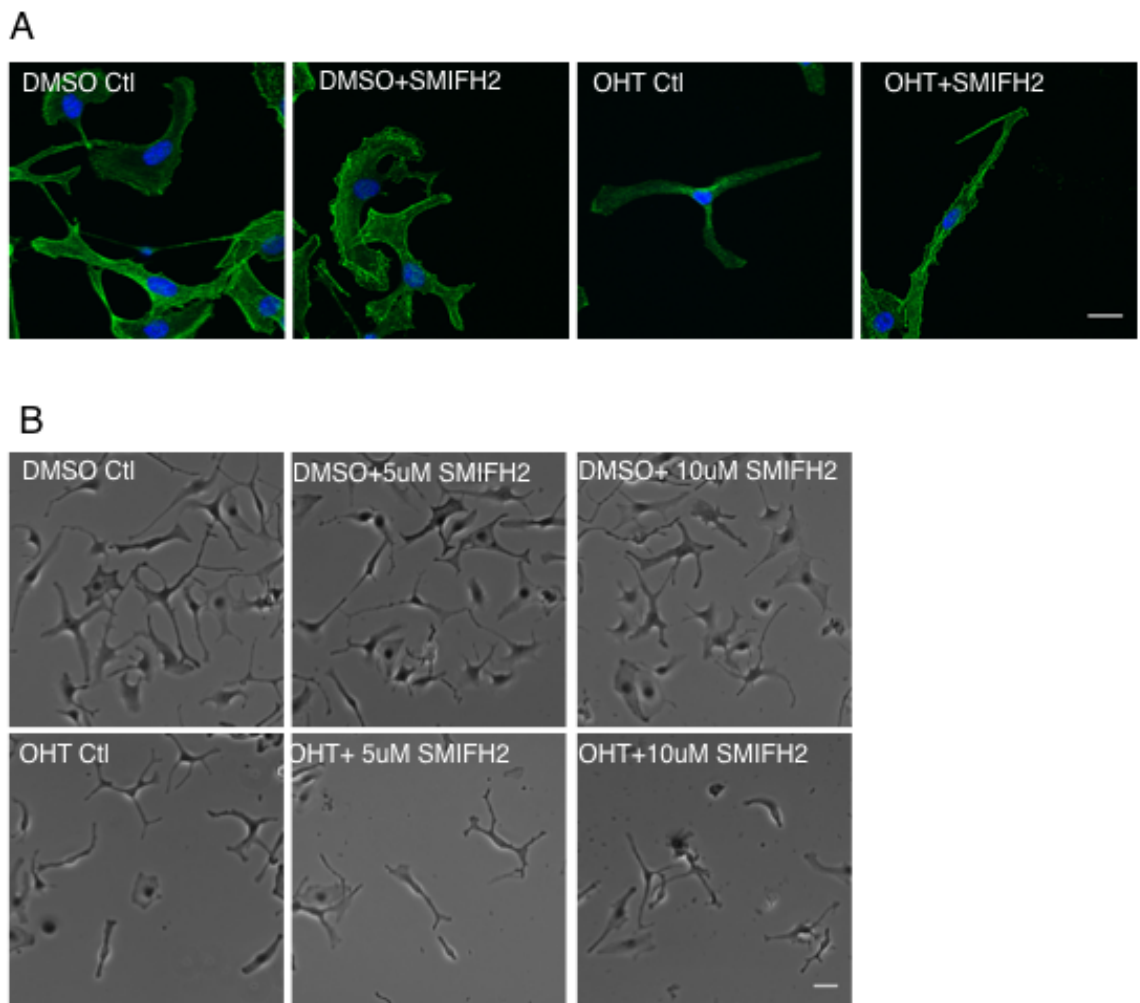


Figure 4.14 Cdc42 knockout melanocytes do not rely on formins to form protrusions or spread.

(A) Immunofluorescence staining of DMSO or OHT treated EW7 Cdc42 *f/f* Cre-ERT2; CDKN2^{-/-} primary melanocytes on fibronectin after 3 hours treatment with 5µM of the formin inhibitor SMIFH2, stained with phalloidin (green). 30 µm scale. **(B)** Time lapse images of EW7 melanocytes pre-treated with 5 µM SMIFH2 then trypsinised and re-settled in the presence of 5 µM SMIFH2 stained with phalloidin. Scale 30 µm.

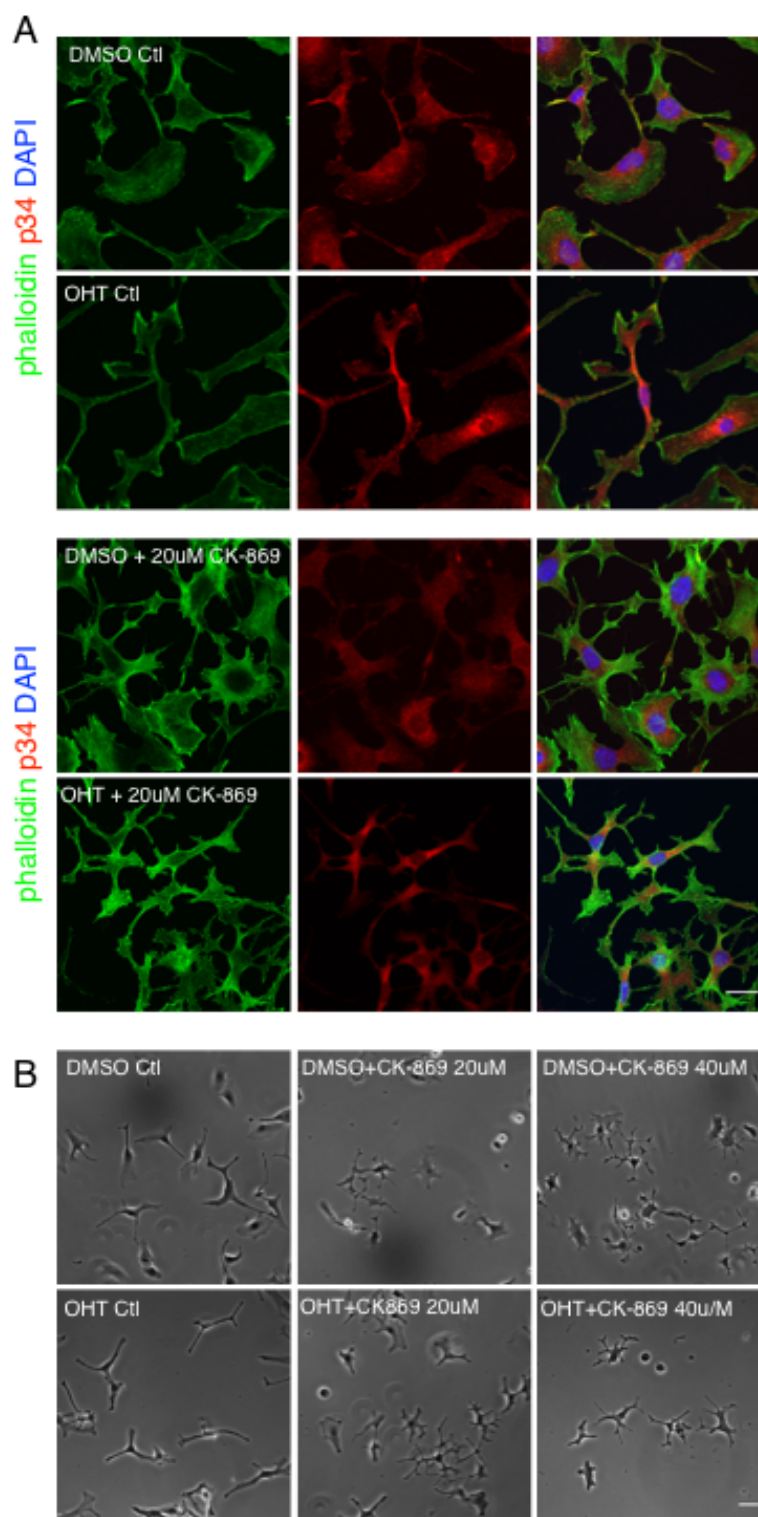


Figure 4.15 Knockout melanocytes can still spread in the presence of Arp2/3 inhibitor and cells are less bi-polar

(A) Immunofluorescence staining of DMSO or OHT treated EW7 *Cdc42 f/f Cre-ERT2; CDKN2^{-/-}* primary melanocytes on fibronectin after 3 hrs treatment with DMSO (Ctl) or 20µM of the Arp2/3 inhibitor CK-869, stained with phalloidin (green) and p34 (red). 20 µm scale. **(B)** TL images of EW7 melanocytes pre-treated with 20 µM or 40 µM CK-869 then trypsinised and re-settled in the presence of 20 µM or 40 µM CK-869. 30 µm scale.

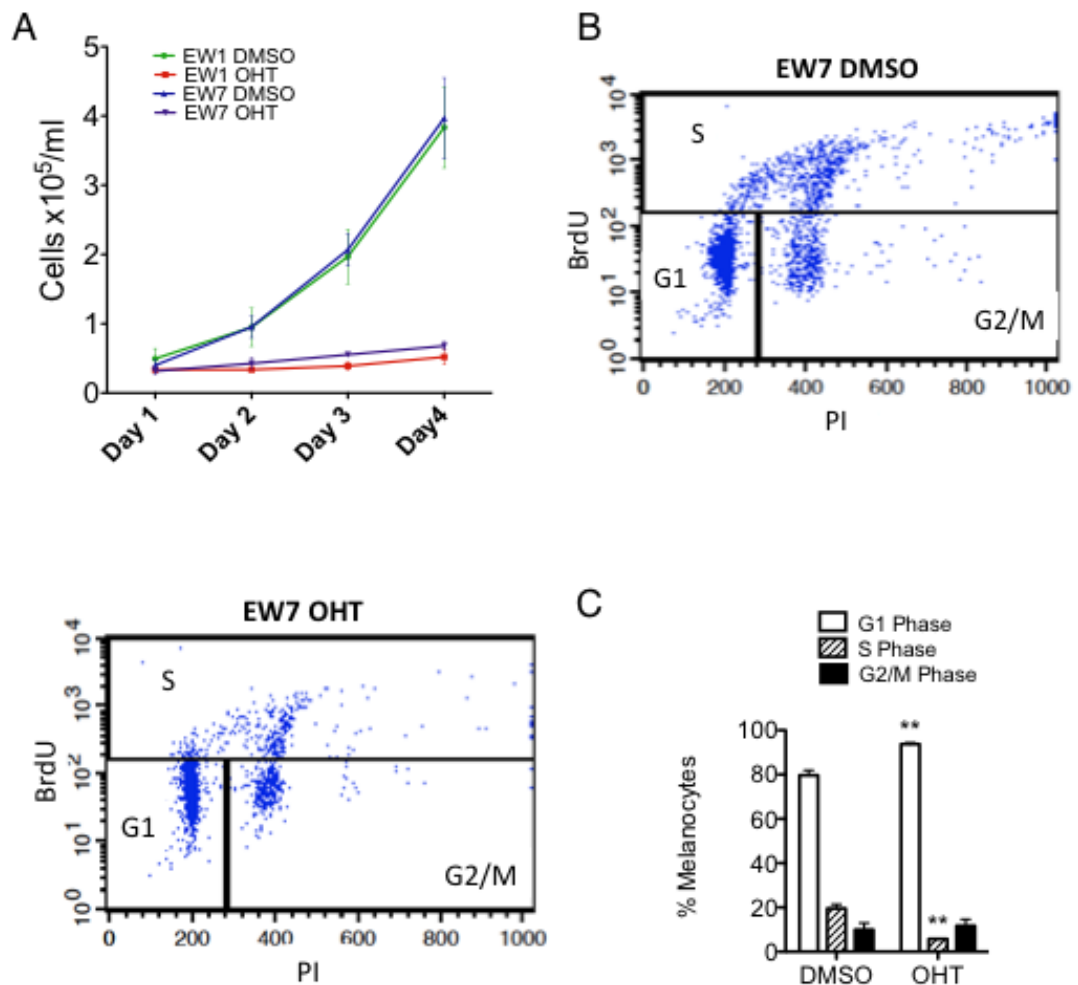


Figure 4.16 Cdc42 is required for cell-cycle transition from G1 to S-phase

(A) Melanocyte proliferation assay of control (DMSO treated) and Cdc42 knockout (OHT treated) cell lines (EW1 and EW7). Error bars show SEM from three independent experiments in triplicate. (B) Representative plot from flow-cytometry analysis of Cdc42 *f/f* Cre-ERT2; CDKN2^{-/-} melanocytes pre-treated with DMSO or OHT and pulse labeled with BrdU for 3 hrs and stained with PI. (C) Percentage of melanocytes in cell-cycle phases from three independent experiments (B). Error bars show SEM **p= 0.0039 (G1 phase) **p= 0.0017(S phase). *p<0.05, **p<0.01 t-test. Scale 10 μ m

efficiently into S phase (Figure 4.16C). This confirms our findings *in vivo* that loss of Cdc42 results in a smaller population of cells entering S phase. This work using cultured primary cells adds to this finding, and support a role of Cdc42 in G1 progression.

Cdc42 appears to play a similarly important role in cytokinesis *in vitro* as seen *in vivo*. Analysis of time-lapse imaging of melanocyte division from rounding up to cytokinesis showed that melanocytes from both EW1 and EW7 lines took over twice as long to complete the division cycle (Figure 4.17A and B). As seen during Cdc42 null melanoblast division, this extended time can be attributed to a defect in cytokinesis (highlighted between green and red frames). Knockout melanocytes failed to separate efficiently from each other, suggesting that Cdc42 plays a key role in cytokinesis (Supplementary video 5). Taken with our *in vivo* findings that Cdc42 controls the number of cells entering S phase, and that is required for normal cytokinesis in melanoblasts, this data show that Cdc42 is in fact promoting transition of cells from G1 into S-phase. It also confirms that Cdc42 is not only required for cytokinesis in 3D, but cultured melanocytes dividing on a 2D substrate also require Cdc42 to efficiently carry out cytokinesis.

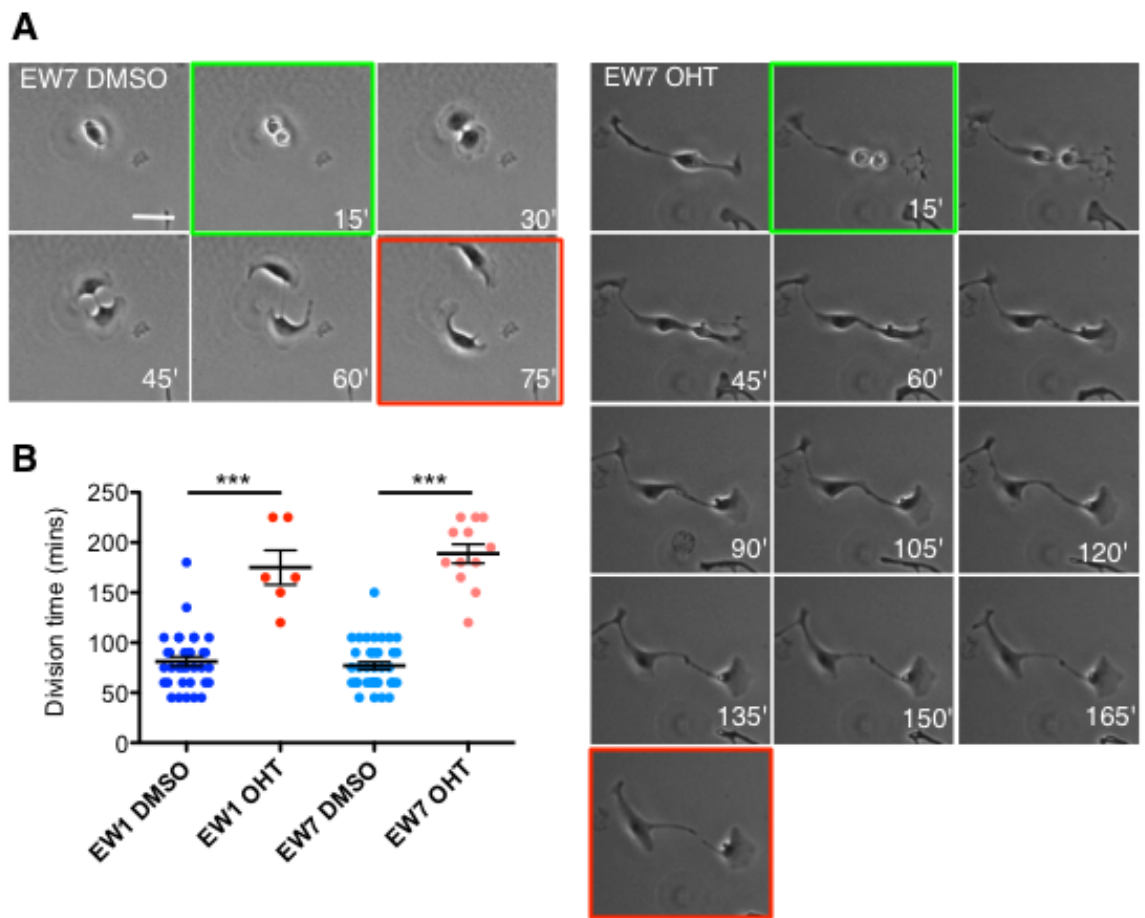


Figure 4.17 Cdc42 knockout melanocytes have an extended division time and cytokinesis defect

(A) Time-lapse imaging of division of DMSO or OHT treated *Cdc42 f/f Cre-ERT2; CDKN2^{-/-}* primary melanocyte cells (EW7) on fibronectin from rounding up, cleavage formation (green) to separation of daughter cells (red). Images captured every 15 mins, Scale 10 μ m. (B) Total division time from rounding up to complete separation of daughter cells (red) of primary melanocyte lines EW1 and EW7. Graph shows mean \pm SEM, *** $p < 0.001$ t-test.

4.3 Discussion

4.3.1 Cdc42 is essential for normal pseudopod dynamics and migration in melanocytes, as in their melanoblast precursors

Knockdown or inducible knockout of Cdc42 in three primary melanocyte lines consistently resulted in an elongated morphology, preventing the formation of lamellipodia, which were frequently seen in control melanocytes (Figure 4.1B and 4.5A). Instead, knockout melanocytes could often only extend two long, thin protrusions in opposite directions, bearing a striking similarity to Cdc42 null melanoblasts. Imaging of the inducible Cdc42 knockout lines EW1 and EW7 showed that their pseudopods were extremely long-lived, in fact these cells were often static, confined to the location where they initially spread (Figure 4.5C and D). The bipolar nature of these cells, together with their defects in pseudopod dynamics and inability to migrate mirrored almost exactly our observations in Cdc42 knockout melanoblasts. In fact, loss of Cdc42 *in vitro* caused a more severe phenotype than *in vivo*. Cdc42 null melanoblasts *in vivo* are at least able to migrate some distance, and extend some short-lived protrusions (Figure 3.16), whereas knockout melanocytes are almost static even on fibronectin matrix (Figure 4.5). This difference could be due to the extra structural support from surrounding cells *in vivo*, and it would be interesting to see if knockout melanocytes were more motile in a co-culture of keratinocytes. These observations confirmed that these melanocytes were a valid and interesting *in vitro* model to further investigate the role of Cdc42 in the migration of the melanocyte lineage.

4.3.2 Cdc42 coordinates the regulators of branched actin networks, but not the activation of Rac1

It was clear from the morphology of Cdc42 knockout melanocytes that loss of Cdc42 in some way prevented the formation of lamellipodia (Figure 4.5A). Traditionally, the Rho GTPase Rac1 is more commonly associated with formation of these branched actin structures, as it can activate the Arp2/3 complex through activation of the NPF SCAR/WAVE, inducing extension of existing F-actin filaments at a 70° angle (Figure 1.1)(Insall and Machesky, 2009). We confirmed that there was strong recruitment of both the Arp2/3 and SCAR/WAVE

complexes at the leading edge of lamellipodia in control melanocytes (Figure 4.6A). However, only weak, patchy recruitment could be seen at the tips of Cdc42 knockout cells, presumably contributing to the formation of the small ruffles at the tips of these cells (Figure 4.5B). This is also in agreement with our observation that actin bursts can be seen at the tips of Cdc42 null melanoblasts (Figure 3.19).

Remarkably, this lack of branched actin networks in the absence of Cdc42 is not due to a reduction of active Rac, as shown using a FLIM reporter of Rac activity and by pull-downs for active Rac with PAK-CRIB beads. Indeed, results from FLIM assays suggest more active Rac is present in knockout cells (Figure 4.7). Our current knowledge of the interaction and feedback/feed forward loops between Rac1 and Cdc42 are limited, but this observation is in contrast to that of Nishimura et al. who suggest that Cdc42 is responsible for Rac activation through the Rac GEFs STEF/Tiam1 (Nishimura et al., 2005). It is likely that the activation of Rac by Cdc42 and vice versa is cell type and context dependent. In this system, we hypothesise that Cdc42 is responsible for the correct localisation of Rac within the cell. Without Cdc42, Rac can be activated, possibly to higher levels than that of control cells possibly due to its aberrant localisation and GEF proximity. However, without Cdc42 to provide positional cues, knockout melanocytes have a restricted ability to form branched actin networks, and can't open up into lamellipodia to facilitate efficient migration. Cdc42 also appears to provide cues for the robust recruitment of Arp2/3 and SCAR/WAVE to the membrane, which may also contribute to the lack of lamellipodia in knockout cells.

4.3.3 Cdc42 controls cell contractility by directing the location of myosin light chain phosphorylation

Loss of Cdc42 in both melanoblast and melanocyte systems caused elongated and long lived pseudopods, presumably due to the cells inability to retract them. We were therefore interested in investigating the actin-myosin cytoskeleton in these cells. Force for movement can be generated through coordination of the elongation and retraction of actin-myosin meshes. The assembly of actin-myosin fibres can be controlled through multiple mechanisms, one of which is phosphorylation of the myosin regulatory light chain.

Due to their static nature and inability to achieve pseudopod retraction, we were surprised not to see a reduction in the phosphorylated levels of MLC in Cdc42 knockout melanocytes (Figure 4.10B). We therefore hypothesised that the contribution of the Cdc42/MRCK pathway to phosphorylation at this position could be compensated for through other pathways (such as the RhoA/ROCK) in the absence of Cdc42. Such convergence between Cdc42/MRCK and Rho/ROCK signalling has been described to enable switching between rounded and elongating cell migration (Wilkinson et al., 2005). We did observe however, that Cdc42 is essential for MLC to be phosphorylated in the correct location within the cell. This was intriguing as small changes in the spatial location of MLC phosphorylation are key in modifying actin-myosin dynamics, and can lead to changes in adhesion, morphology and motility (Unbekandt and Olson, 2014). Loss of Cdc42 resulted in a drastic accumulation of p-MLC around the cell nucleus, and we hypothesise that the lack of MLC phosphorylation along the length of their pseudopods is the reason why they are unable to retract them (Figure 4.10C). It seems therefore that Cdc42 controls the spatial cues for correct MLC phosphorylation. This observation is in line with Cdc42's role as a master regulator of cell polarity, leading the spatial organisation of various components. We suggest that this mislocalisation of myosin phosphorylation in the absence of Cdc42 partly underpins the elongated morphology and migration defects of melanoblasts and melanocytes, most likely in combination with other factors that still remained unclear.

4.3.4 Cdc42 controls YAP nuclear accumulation but abrogation of YAP signalling does not affect melanocyte morphology

In an attempt to identify the molecular players behind the Cdc42 knockout phenotype, we blotted for a broad array of Cdc42 effectors or actin binding proteins. We largely saw no difference at the protein levels of the classical Cdc42 effectors N-WASP, IQGAP1, PAK2 or ERK, actin related proteins p34 and FAK or the other classic Rho GTPases Rac1 or RhoA (Figure 4.9). This suggested that the knockout phenotype was most likely not due any obvious downregulation at the protein level of any single effector, but this approach does not take into account the activation state or localisation of these effectors.

Recent studies have implicated YAP, a transcriptional co-activator downstream of the hippo kinase pathway as a new Cdc42 effector. In a study of kidney development, Reginensi et al demonstrated that a tissue specific inactivation of Cdc42 caused a severe defect in nephrogenesis, which was strikingly similar to loss of YAP in this tissue (Reginensi et al., 2013). YAP and TAZ have recently been the focus of a great number of studies, and appear to regulate cell proliferation, differentiation and homeostasis (Varelas, 2014, Elbediwy et al., 2016). Due to their emerging roles in cancer, tissue regeneration stem cell biology, the race is on to fully understand how these hippo pathway effectors control these processes (Hiemer et al., 2014, Zanconato et al., 2016).

The activity of YAP/TAZ is regulated through phosphorylation, primarily by LATS kinase. This phosphorylation allows binding of 14-3-3 proteins, which harbour YAP/TAZ in the cytoplasm, preventing transcription of their target genes (Piccolo et al., 2014). We were interested in investigating the activation levels of YAP in our Cdc42 knockout melanocytes, particularly due to the reported role of YAP/TAZ in matrix adhesion, mechanotransduction and polarity. We hypothesised that these transcriptional co-activators may be downstream effectors of Cdc42 and therefore misregulated in knockout, leading to ineffective communication between cells and the underlying matrix. This could explain the morphology of our knockout cells. We did indeed see a consistent and substantial increase in the phosphorylation of YAP in Cdc42 knockout cells, suggesting a down regulation of YAP target genes (Figure 4.11A). Furthermore, we observed that this translated into a higher proportion of cytoplasmic YAP in knockout melanocytes (Figure 4.11B and C). However, this alteration in YAP/TAZ signalling does not appear to directly underpin the phenotype of our cells, as blocking YAP signalling by knockdown of YAP did not lead to an elongated cell morphology (Figure 4.12A and B).

4.3.5 Knockout protrusions are not dependent on microtubules, Arp2/3 or formins to extend

By observing control and knockout melanocytes spreading, we saw that their morphology resulted from the slow but steady extension of thin and long protrusions. To more fully understand the Cdc42 knockout phenotype, we used various inhibitors in order to disrupt cytoskeletal arrangements. We hoped this

would identify which cytoskeletal components or binding proteins were involved in the extension of knockout pseudopods.

Our data suggest that knockout protrusions do not rely on the microtubule cytoskeleton for support, and microtubule polymerisation does not drive their extension (Figure 4.13A and B). However, when knockout melanocytes spread after disruption of the microtubule cytoskeleton by nocodazole treatment, they no longer take on a bi-polar morphology. This might suggest that microtubules are providing the bi-polar framework during spreading in the absence of Cdc42, and with that driving the vesicle network down these two tracks. Due to Cdc42's role in organisation of the MTOC and microtubule network to drive cell polarity and support persistent migration, this could be a likely scenario (Etienne-Manneville and Hall, 2001) (Etienne-Manneville and Hall, 2003, Etienne-Manneville et al., 2005).

We hypothesised that the extended morphology of Cdc42 null melanocytes could be explained by switching from the activation of branched actin filaments to linear ones. The obvious candidates in this case would be formin homology domain proteins such as the diaphanous related proteins (Figure 1.1). However, we observed that knockout melanocytes spreading in the presence of the broad spectrum formin inhibitor SMIFH2 have no trouble in extending their long thin protrusions at the concentrations used (Figure 4.14). This was also the case when they were spread in the presence of the Arp2/3 inhibitor CK-869, suggesting that neither formins nor the Arp2/3 complex play a major role in the extension of these pseudopods in the absence of Cdc42 (Figure 4.15).

4.3.6 Cdc42 promotes G1 to S transition and controls cytokinesis in melanocytes

Similarly to Cdc42 null melanoblasts, loss of Cdc42 in primary melanocyte lines *in vitro* also led to a proliferation defect (Figure 4.16A). We investigated this defect more closely in melanocytes lines using flow-cytometry to separate the melanocyte population into the different cell-cycle phases after incubation with BrdU. This analysis confirmed our observation *in vivo* that fewer knockout melanoblasts are in S phase (Figure 4.16 B and C). We observed that instead of progressing into S phase, knockout cells accumulate in G1, suggesting that Cdc42

is important for this progression. Therefore, Cdc42 appears to play a similar role in promoting G1 to S transition *in vivo* and *in vitro*, confirming previous observations linking Cdc42 to cell-cycle progression (Olson et al., 1995). Interestingly, we also observed cytokinesis defects in cultured primary melanoblasts. As seen during melanoblast division *in vivo*, Cdc42 knockout melanocytes are unable to round up at mitotic onset (Figure 4.17). This defect is even more striking *in vitro*, as in the majority of cases knockout cells remain almost entirely attached and spread throughout division. The severity of this defect *in vitro* may be due to the lack of support by surrounding cells. As *in vivo* total division time is doubled, again largely due to the extended time the cell takes to complete cytokinesis in the absence of Cdc42. The requirement for Cdc42 during division in both 2D and 3D environments appears to be unique, as this was not the case for Rac1 (Li et al., 2011). Despite playing a role in the separation of daughter cells *in vivo*, no obvious delay was observed in Rac1 depleted melanocytes *in vitro*. This observation is in agreement with the current hypothesis that Rac1 activity must be repressed at the equator for efficient cytokinesis. Overexpression of a constitutively active form of Rac1 causes multinucleation or failed cytokinesis in HeLa cells (Bastos et al., 2012). Therefore, our observations of melanoblast and melanocyte division in 2D and 3D have highlighted similar but distinct roles for these GTPases during this process. Both Cdc42 and Rac1 are important in promoting G1 to S transition both *in vivo* and *in vitro*, but it remains unclear if they achieve this through the same pathway. Cdc42 maintains its integral role during cytokinesis *in vitro*, which is mostly likely due to its role in regulating formation of the contractile ring (Zhu et al., 2011). On the other hand, Rac1 activity must be repressed during cytokinesis, and loss of Rac1 does not impact cytokinesis *in vitro* (Bastos et al., 2012, Li et al., 2011).

4.4 Summary

Using cultured primary melanocyte cell lines with a capacity for inducible knockout of Cdc42, we have demonstrated that Cdc42 is also essential for normal pseudopod dynamics and efficient migration in this *in vitro* model. Using this system, we demonstrated that Cdc42 is essential for the recruitment of branched actin regulators to the leading membrane, but not for Rac activation. We hypothesise that Cdc42 is responsible for the correct positioning of active

Rac to the membrane to produce branched actin networks. In addition, we observed that Cdc42 directs phosphorylation of the myosin light chain to the correct localisation in the cell to control cell contraction. We also demonstrated a conserved role for Cdc42 in G1 to S transition and cytokinesis in 2D and 3D systems.

5 Cdc42, Melanocyte Gene Expression and Coordination of Adhesion Dynamics

5.1 Introduction and aims

Studying the effect of Cdc42 deletion on melanoblast and melanocyte migration and proliferation demonstrated a major role for Cdc42 in the global and spatial coordination of actin related proteins into efficient pseudopod extension, cell translocation and cytokinesis. Interestingly, our work suggests unique roles for Cdc42 and Rac1 in migration, with Rac primarily involved in inducing actin polymerisation to drive pseudopod extension. In contrast, Cdc42 null cells can produce pseudopods that display relatively normal actin dynamics, with elevated levels of active Rac. We therefore believe that Cdc42 has a more global role in coordinating the actin polymerisation stimulated by Rac into coordinated cell migration, however the link between these still remains unclear. Taking a global approach to discover the implication of Cdc42 deletion on melanocyte signalling networks may give us clues into the defects behind the morphology of Cdc42 knockout cells.

To achieve this, we selected an RNA sequencing approach due to our recent success with this technique in Rac1 knockout melanocyte cells lines. This technique begins with isolation of RNA from cells. RNA is then reverse transcribed into a cDNA library which is then mathematically processed to identify genes significantly up or down-regulated between conditions. We aimed to isolate RNA of sufficient quality from control and Cdc42 knockout melanocytes, perform library preparation and sequencing followed by pathway analysis to identify genes up or down-regulated in the absence of Cdc42. We could use this information to build a picture of changes in global cell gene expression in the absence of Cdc42, providing a deeper understanding of which networks Cdc42 controls to facilitate cell migration.

5.2 Results

5.2.1 RNA sequencing of Cdc42 knockout melanocytes reveals global changes in diverse signalling networks

In order to map changes in gene expression profiles when Cdc42 is lost in the melanocyte lineage, RNA sequencing analysis was performed on two primary melanocyte cell lines with capacity for inducible Cdc42 knockout. RNA was isolated from melanocyte lines EW2.1 and EW2.2, which are of the same genotype as melanocyte lines EW1 and EW7 (Cdc42 f/f Cre-ERT2; CDKN2^{-/-}). Lines EW1 and EW7 were not used in this study as RNA isolated from these lines was not of sufficient quality to proceed with sequencing. However, Cdc42 deletion was confirmed in EW2.1 and EW2.2 (Figure 5.1A), which adopt the same elongated morphology as seen in EW1 and EW7 lines. RNA was isolated in two separate experiments from these primary melanocyte lines previously incubated with DMSO or OHT for 5 days. Principle component analysis (PCA) of EW2.1 and EW2.2 (WT and KO) showed that these two biological replicates were consistent (Figure 5.1B).

From this analysis, seven genes were discovered to be significantly altered in expression between DMSO and OHT conditions in both cell lines (Figure 5.1C). The most significant of these was prostaglandin D2 synthase (Ptgds), which was found to be up-regulated 5-fold in Cdc42 knockout lines. This is an enzyme expressed mostly in the brain that catalyses the conversion of prostaglandin H2 to prostaglandin D2, which acts as a neuromodulator and trophic factor. The ADAMTS like 4 gene (a disintegrin and metalloproteinase with thrombospondin motifs) (Adamtsl4) encodes a protein with seven thrombospondin type 1 repeats was also seen to be up-regulated 3-fold. These domains are found in proteins with many different functions, such as modulation of cellular adhesion. Interestingly, expression of the adhesion receptor integrin α 4 was also significantly down-regulated, demonstrating a 3-fold down-regulation in Cdc42 knockout cells.

Transcripts from both DMSO conditions and OHT conditions were then pooled, and genes that demonstrated significant ($p_{adj} < 0.05$) down-regulation (290 genes) and up-regulation (343 genes) were submitted to DAVID for Gene

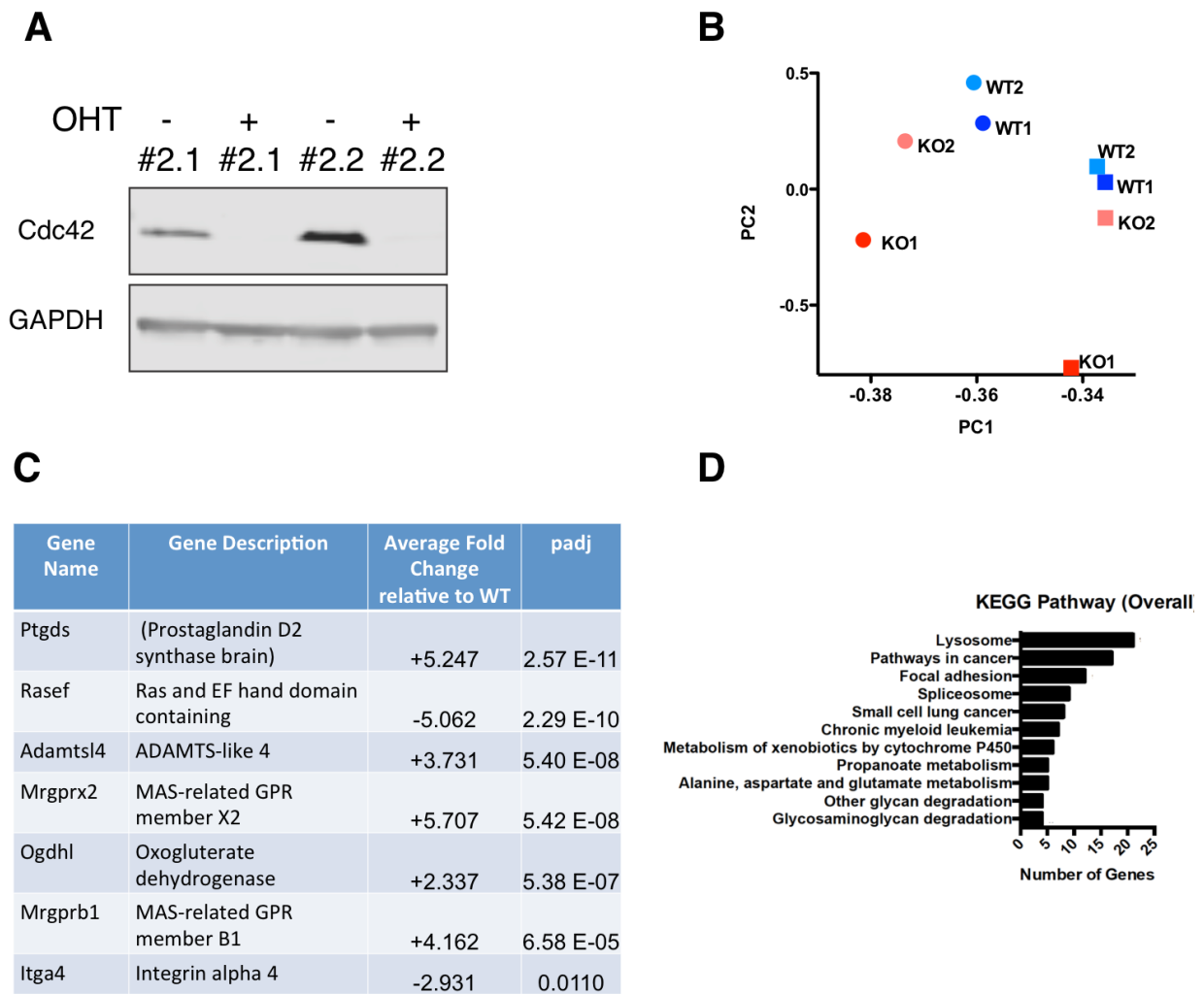


Figure 5.1 RNA sequencing of Cdc42 knockout melanocytes implicates Cdc42 in the expression of diverse signalling components

(A) Western blot of DMSO or OHT treated EW2.1 and EW2.2 Cdc42 f/f; Cre-ERT2; CDKN2^{-/-} primary melanocyte cell line lysates probed for Cdc42 and GAPDH. (B) Principal component analysis (PCA) plot of the RNA sequencing data showing the trends exhibited by the expression profiles of Cdc42 KO in EW2.1 (red) and EW2.2 (pink) and wild-type EW2.1 (dark blue) and EW2.2 (light blue). (C) Table summarising the genes found to be significantly up or down-regulated in the absence of Cdc42, that were consistent without grouping cell lines. (D) Significant expression changes between KO and WT cell lines ($p_{adj} < 0.05$) were submitted to DAVID Gene Ontology analysis. Significantly enriched KEGG Pathways ($pValue < 0.05$) for genes demonstrating a change in expression.

Ontology analysis to identify pathways that were altered in the absence of Cdc42 (Gene lists can be found in Supplementary Spreadsheet 1). Lysosomal signalling networks came out as most significant from this analysis, indicating that the largest group of genes significantly altered in Cdc42 knockout melanocytes fall into this category (Figure 5.1D). Genes involved in 'Pathways in cancer' and in 'Focal Adhesion' KEGG pathways were the next two significant groups (Figure 5.1D). Our analysis explores the role of Cdc42 at a global level in the melanocyte lineage and demonstrates that Cdc42 is affecting a wide array of signalling pathways.

5.2.1.1 Genes involved in lysosomal signalling are significantly up-regulated in Cdc42 knockout melanocytes

When genes that demonstrated significant up-regulation ($p_{adj} < 0.05$, 343 genes in total) were submitted to DAVID for Gene Ontology analysis, the lysosomal KEGG pathway was again the most significant pathway from this analysis (Figure 5.2A). Interestingly, multiple subunits of the V-ATPase enzyme are up-regulated in knockout cells (ATP6voc, ATP6ap1, ATP6voc-ps2, ATP6v0a1, ATP6v0b and ATP6vod2) (Figure 5.2B). These genes encode multiple components of the vacuolar ATPase, which acidifies organelles. The acidification of organelles is necessary for many processes, including protein sorting, receptor-mediated endocytosis, and the generation of the synaptic vesicle proton gradient. It seems likely that the up-regulation of this complex could indicate defects in organelle acidification in knockout cells. Changes caused by this up-regulation could in some way add to the unusual morphology of these cells.

5.2.1.2 Signalling to global adhesion networks is down-regulated in Cdc42 knockout melanocytes

We then focused on the 290 genes that were significantly ($p_{adj} < 0.05$) down-regulated in OHT treated cell-lines compared to DMSO treated cell-lines. These genes were submitted to DAVID for Gene Ontology analysis to find if they grouped into global signalling networks. The top two KEGG pathways from this analysis were 'Pathways in cancer' and 'Focal adhesion' (Figure 5.3A). We then looked closely at the genes involved in these pathways that had been picked out from our data set (Figure 5.3B). They included integrin $\alpha 4$ (Itga4),

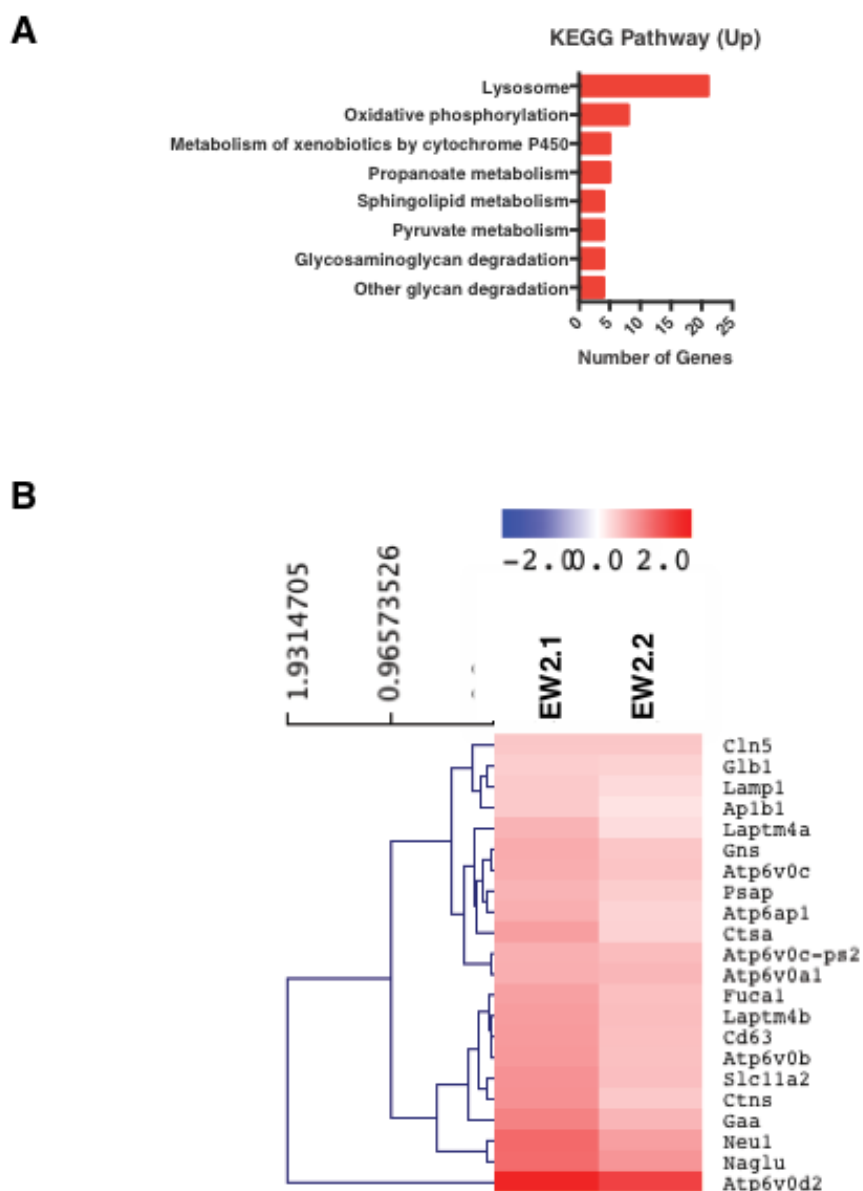


Figure 5.2 Genes involved in lysosomal networks are up-regulated in the absence of Cdc42
Data from RNA sequencing analysis from DMSO or OHT treated EW2.1 and EW2.2 Cdc42 *fl/fl*; Cre-ERT2; CDKN2^{-/-} primary melanocyte cell lines. **(A)** Significantly changed genes between KO and WT cell lines ($p_{adj} < 0.05$) were submitted to DAVID for Gene Ontology analysis. Significantly enriched KEGG Pathways ($p_{Value} < 0.05$) were identified for genes demonstrating an increase (Up) in expression. **(B)** Hierarchical clustering analysis of KEGG GO: 'Lysosome' genes identified as significantly changed in the dataset. Heat bar indicates the mean \log_2 fold change in gene expression between KO and WT cell lines EW2.1 and 2.2

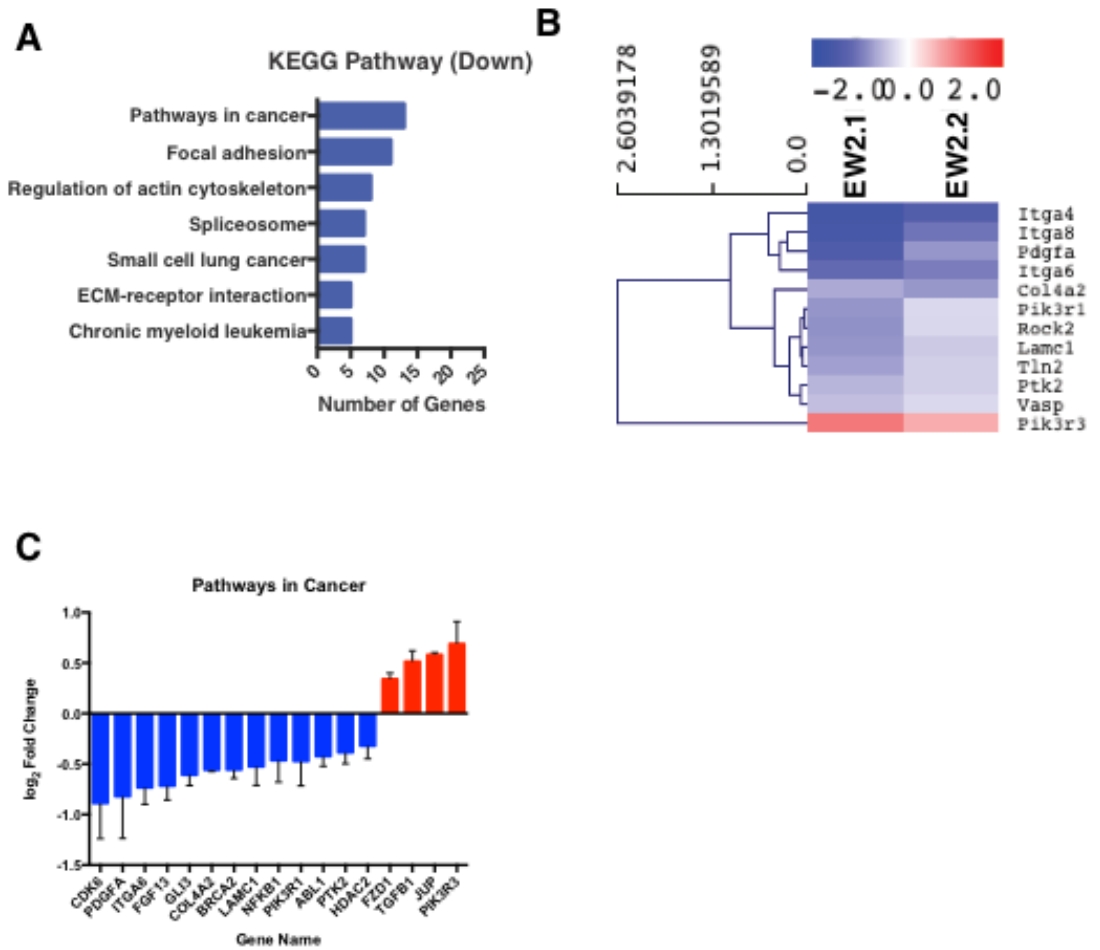


Figure 5.3 Genes involved in pathways in cancer and focal adhesion signalling are down-regulated in the absence of Cdc42

Data from RNA sequencing analysis from DMSO or OHT treated EW2.1 and EW2.2 Cdc42 *f/f* Cre-ERT2; CDKN2^{-/-} primary melanocyte cell lines. **(A)** Significant expression decreases between KO and WT cell lines ($p_{adj} < 0.05$) were submitted to DAVID Gene Ontology analysis. Significantly enriched KEGG Pathways ($p_{value} < 0.05$) for genes demonstrating a decrease (Down) in expression. **(B)** Hierarchical clustering analysis of KEGG GO: 'Focal adhesion' genes identified as significantly changed in the dataset. Heat bar indicates the mean log₂ fold change in gene expression between KO and WT cell lines EW2.1 and EW2.2. **(C)** Graph showing the relative log₂ fold change of the genes associated with the KEGG GO 'Pathways in cancer' data set.

Integrin $\alpha 8$ (Itga8), integrin $\alpha 6$ (Itga6), Rock2, FAK (Ptk2), and Vasp. All of the genes in this pathway were down-regulated in both EW2.1 and EW2.2 cell lines, with the exception of Phosphoinositide-3-Kinase regulatory subunit 3 (Gamma), which was up-regulated. Although most of these genes were significantly down-regulated in both cell lines, fold changes were consistently lower in EW2.1 than EW2.2. The 'Pathways in cancer' KEGG pathway showed down regulation of Cdk6 (cyclin dependant kinase 6), Pdgfa (Platelet-derived growth factor subunit A), Breast cancer associated gene 2 (Brca2), ABL1 (Abelson murine leukemia viral oncogene homolog 1) and Tgfb1 (transforming growth factor beta 1), all down between -0.5 to -1.2 \log_2 fold-change (Figure 5.3C).

Western blotting was used to investigate whether the down regulation of these focal adhesion signalling pathway genes would lead to a decrease at the protein level (Figure 5.4 A-J). Integrin $\alpha 4$ was significantly decreased at the protein level, reduced by over half. Interestingly, integrin $\beta 3$ was also reduced, although this gene was up regulated at the RNA level (Supplementary table 1). This may suggest that integrin $\beta 3$ is downregulated at the protein rather than the RNA level. Other adhesion related proteins such as Rock2, Talin and integrin $\alpha 6$ showed a trend towards lower protein levels, but these changes were not significant.

This striking change in the levels of integrin $\alpha 4$ prompted us to look at integrin $\beta 1$, the subunit with which it is often partnered. RNA transcript levels were modestly but not significantly decreased according to our data set (Supplementary table 1). There was no observable difference in the levels of integrin $\beta 1$ in either cell line tested (Figure 5.5A). However, looking at the localisation of integrin $\beta 1$ using immunofluorescence staining shows that Cdc42 null cells have fewer $\beta 1$ integrin mediated adhesions (Figure 5.5B). Integrin $\beta 1$ can be seen in adhesions beneath the lamellipod in DMSO treated cells. In OHT treated cells, integrin $\beta 1$ still localises to adhesions but there are many fewer foci and they appear to be smaller. We also confirmed that there is no change in integrin αV at the protein level as seen in our RNA sequencing data (Figure 5.5A).

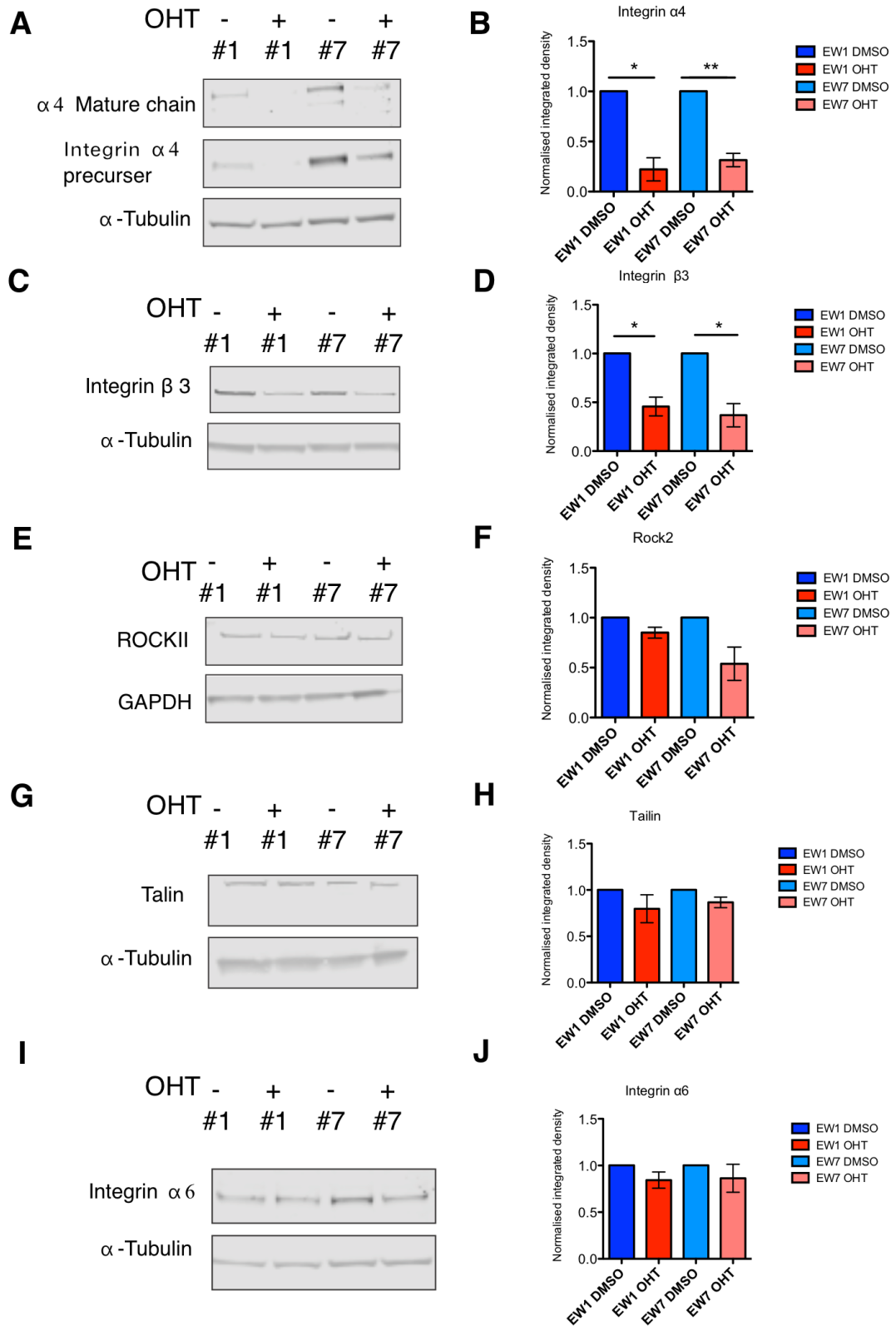


Figure 5.4 Protein levels of integrins α4 and β6 are decreased in Cdc42 knockout melanocytes

(A, C, E, G, I) Western blot of EW1 and EW7 melanocyte cell line lysates probed as indicated to show protein levels of adhesion related genes. (B, D, F, H, J) Normalised integrated density of western blot bands from three independent experiments as indicated. Graphs show mean ± SEM *p<0.05, **p<0.01 t-test

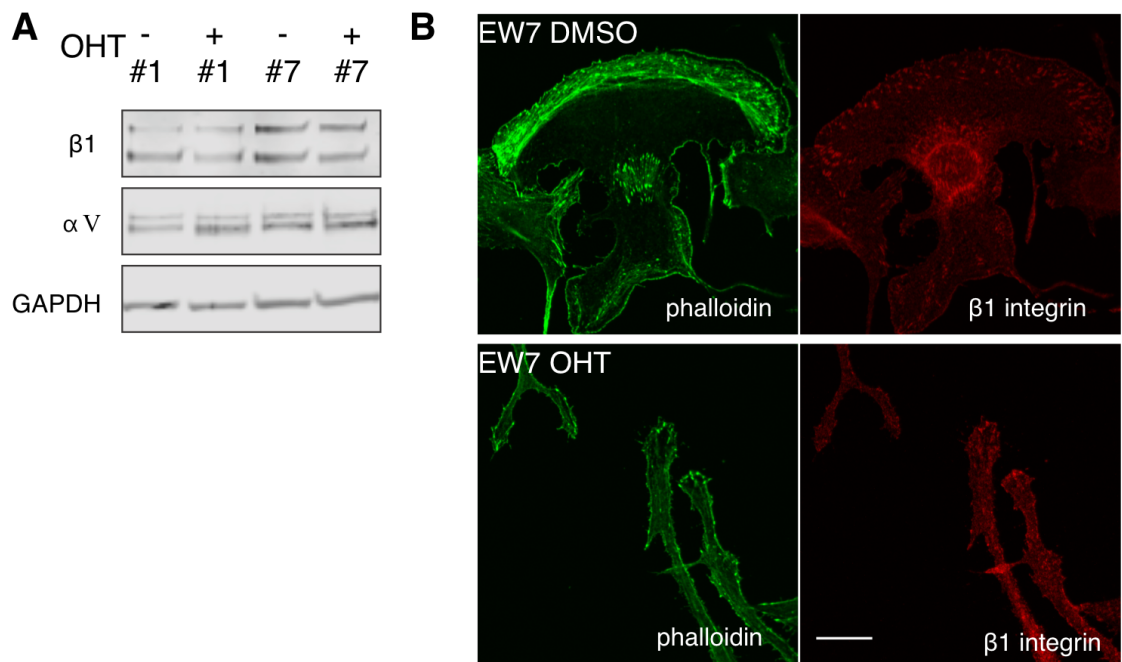


Figure 5.5 Integrin $\beta 1$ levels are unchanged in Cdc42 knockout melanocytes but less is recruited to adhesions

(A) Western blot of EW1 and EW7 melanocyte cell line lysates probed with anti- integrin $\beta 1$, αV and GAPDH antibodies. (B) DMSO or OHT treated EW7 melanocytes (*Cdc42 f/f; Cre-ERT2; CDKN2^{-/-}*) melanocytes fixed and stained with phalloidin (F-actin) (green) and integrin $\beta 1$ integrin (red).

We looked at the expression levels of other classical Rho GTPases in DMSO and OHT treated cells to discover if the loss of Cdc42 induced the expression of another GTPase to compensate (Figure 5.6). This appeared not to be the case. Cdc42 transcripts are still detected in the knockout cells as only one exon has been deleted from this gene, meaning it is transcribed but not translated. Rac1 expression also appears to be high in the melanocyte lineage, but levels are unaltered in the absence of Cdc42. Other members such as RhoB, C, G, J and Q are expressed in melanocytes, but again are unchanged in OHT conditions. Redundancy between these members may explain why RhoA is not necessary for normal melanoblast migration.

We conclude therefore that Cdc42 is involved in controlling the expression of a diverse range of signalling pathways. Interestingly, RNA sequencing analysis revealed that a suite of genes involved in focal adhesion signalling are down regulated in Cdc42 knockout melanocytes. Notably, integrin $\alpha 4$ and integrin $\beta 3$ were substantially reduced at the protein level in these cells, and other adhesion related genes were also modestly reduced at the protein level. However, loss of Cdc42 does not appear to induce the expression of any other GTPase family member in order to compensate for its loss.

5.2.2 Cdc42 controls melanocyte adhesion number, size and lifetime

Our data showing that Cdc42 knockout melanocytes have defects in migration and pseudopod dynamics, together with the down-regulation of adhesion signalling networks prompted us to ask whether adhesion dynamics were affected in these cells. To explore this, DMSO and OHT treated primary melanocytes were plated on fibronectin then fixed and stained for phosphorylated paxillin (p-paxillin), an adhesion adaptor protein that is recruited early in adhesion formation (Figure 5.7A). DMSO treated control melanocytes display a thick band of large adhesions underneath the lamellipod. This is in contrast to OHT treated melanocytes which have fewer, smaller adhesions at the tips of their protrusions. Quantification from this staining shows that OHT treated cells have significantly fewer adhesions per cell with an

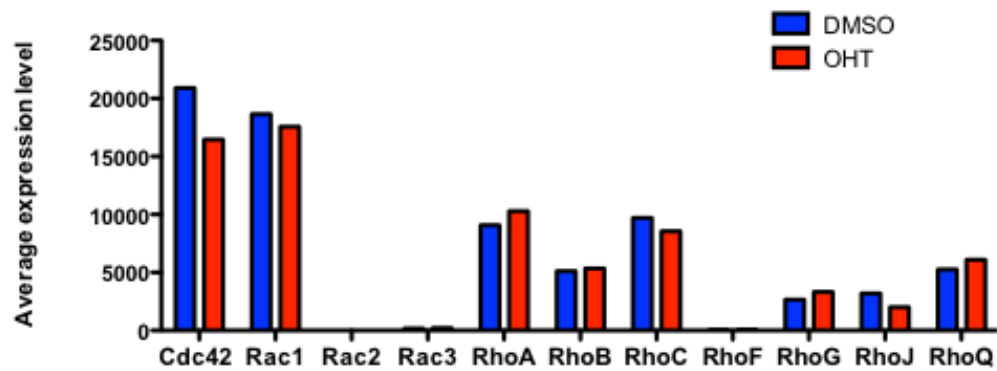


Figure 5.6 RNA levels of other classic Rho GTPases are unchanged in Cdc42 knockout melanocytes

Data from RNA sequencing analysis from DMSO or OHT treated EW2.1 and EW2.2 Cdc42 *f/f*; Cre-ERT2; CDKN2^{-/-} primary melanocyte cell lines. Graph showing the average expression level (RNA counts) of the classic Rho GTPase members

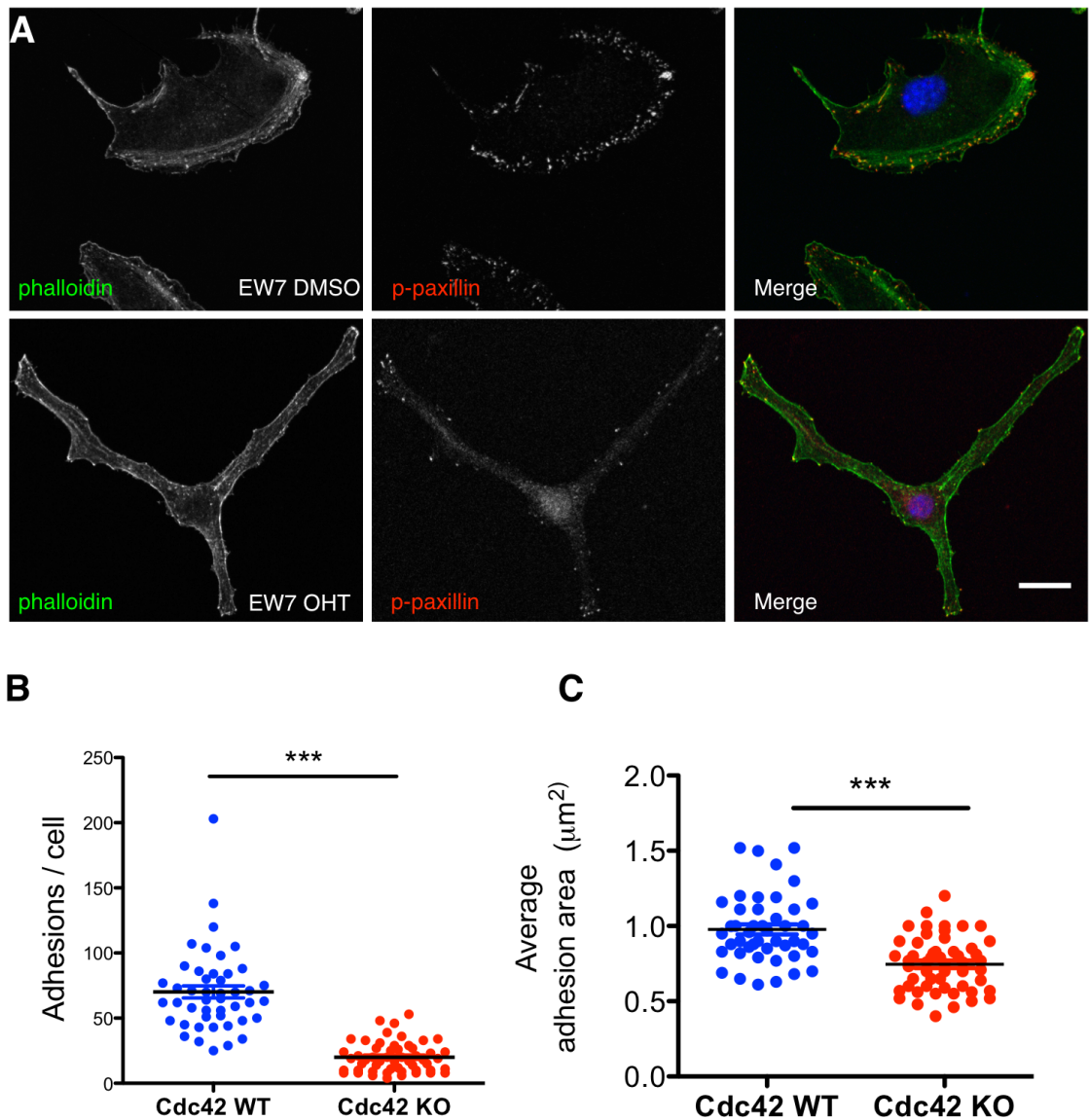


Figure 5.7 Cdc42 knockout melanocytes form less, smaller adhesions

(A) EW7 Cdc42 f/f; Cre-ERT2; CDKN2^{-/-} melanocytes treated with DMSO (control) or OHT (Cdc42 knockout) fixed and stained with F-actin phalloidin (green) and phospho-paxillin (red). Scale 15 μm . (B) Number of adhesions per cell and (C) Average adhesion area from at least 46 cells per genotype, quantified from phospho-paxillin staining, graphs show mean, ***p<0.001 t-test.

average of 20 compared to 70 in control cells (Figure 5.7B). Their adhesions are also significantly smaller, with an average area of $0.75 \mu\text{m}^2$ compared to $1 \mu\text{m}^2$ in control cells (Figure 5.7C).

Using live cell imaging, we also demonstrated that adhesion dynamics are also altered in knockout cells (Figure 5.8A). In control cells expressing paxillin-GFP, adhesions formed dynamically under the newly formed lamellipod. This can be seen clearly in the 'merge' panel, where each frame has been rendered in a different colour. Adhesions in knockout cells were relatively static over the 16 minute time-course, with much less adhesion assembly and disassembly occurring in their pseudopod extensions. Measurement of the rate of adhesion assembly and disassembly rates revealed that both of these processes occurred more slowly in the absence of Cdc42 (Figure 5.8B and C).

These data show that Cdc42 plays a role in the assembly, maturation, and disassembly of adhesions in the melanocyte lineage. Taken together with RNA sequencing data that shows a down regulation of focal adhesion signalling in knockout cells, we hypothesise that Cdc42 is a key regulator in the expression and control of adhesion related proteins. We hypothesise that in the absence of Cdc42, cells are unable to support membrane extensions due to this defect, and it is likely that this impedes the migration of these cells over matrix *in vitro* and in melanoblast migration *In vivo*.

5.2.3 Defects in adhesion and filopodia formation delay the spreading of Cdc42 knockout cells

We were curious whether the adhesion defects observed in cells at steady state would also affect their ability to spread after initial attachment to the ECM. We predicted that studying the spreading process may also help us understand the unusual morphology of Cdc42 knockout cells adopted during spreading. To investigate this, DMSO and OHT treated cells were fixed and stained with phalloidin at 15, 30, 60 and 120 minutes after seeding to visualise and quantify their ability to spread (Figure 5.9A). Cdc42 knockout melanocytes had a smaller area than control melanocytes at each time point, indicating that Cdc42 is important for these cells to spread (Figure 5.9B). Interestingly, knockout cells

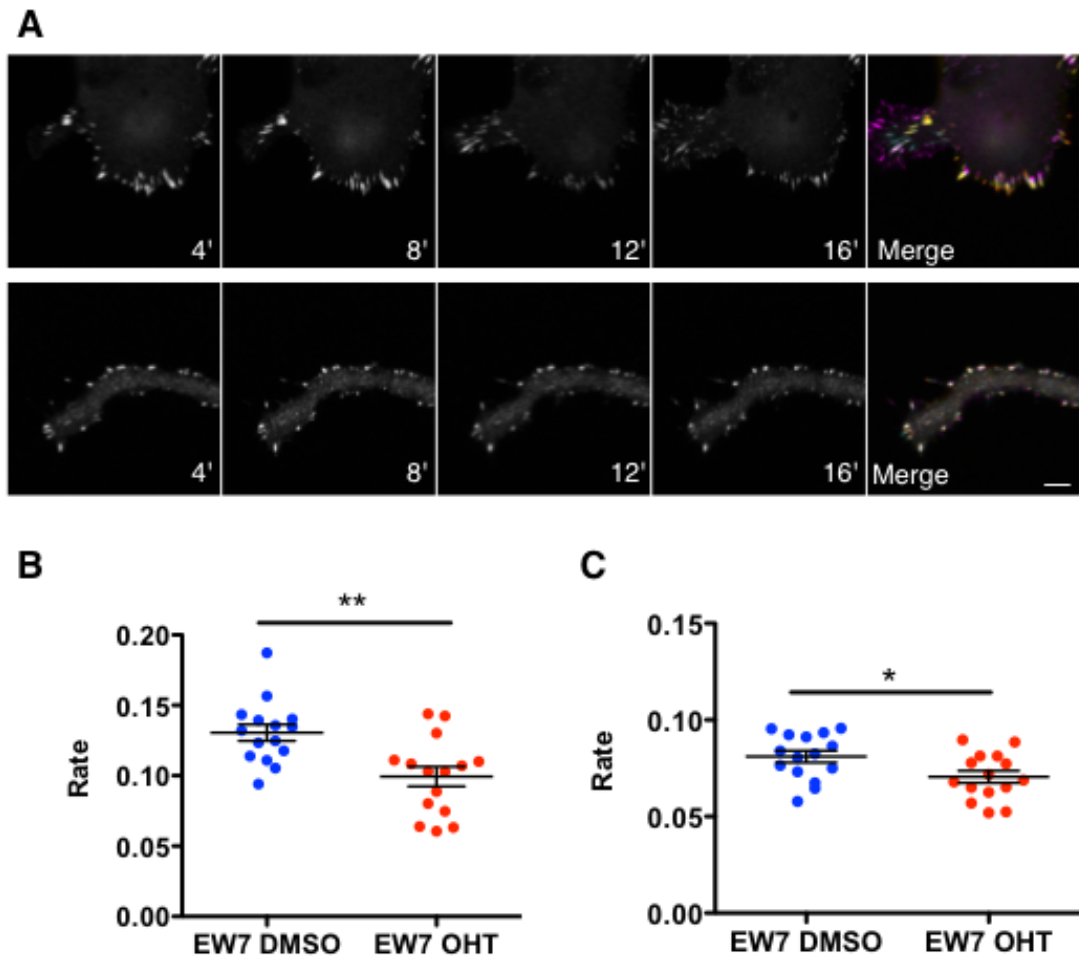


Figure 5.8 Cdc42 knockout melanocytes are slower to assemble and disassemble adhesions
(A) Live confocal imaging sequence of EW7 *Cdc42* *f/f*; Cre-ERT2; *CDKN2*^{-/-} melanocytes transiently transfected with paxillin-GFP, imaged every 4 mins. Merge with each frame in a unique colour. Scale 5 μ m. **(B)** Quantification of the rate of assembly and disassembly **(C)** of adhesions from melanocytes transiently expressing paxillin-GFP over 30 minutes. Movies were submitted to the Focal Adhesion Analysis Server (FAAS) for analysis of adhesion dynamics. The mean rate of adhesion assembly/disassembly was calculated for each cell ($n = 15$ cells per condition over 3 independent experiments). Graphs show mean \pm SEM ** $p < 0.01$, *** $p < 0.001$ t-test with Welch's correction

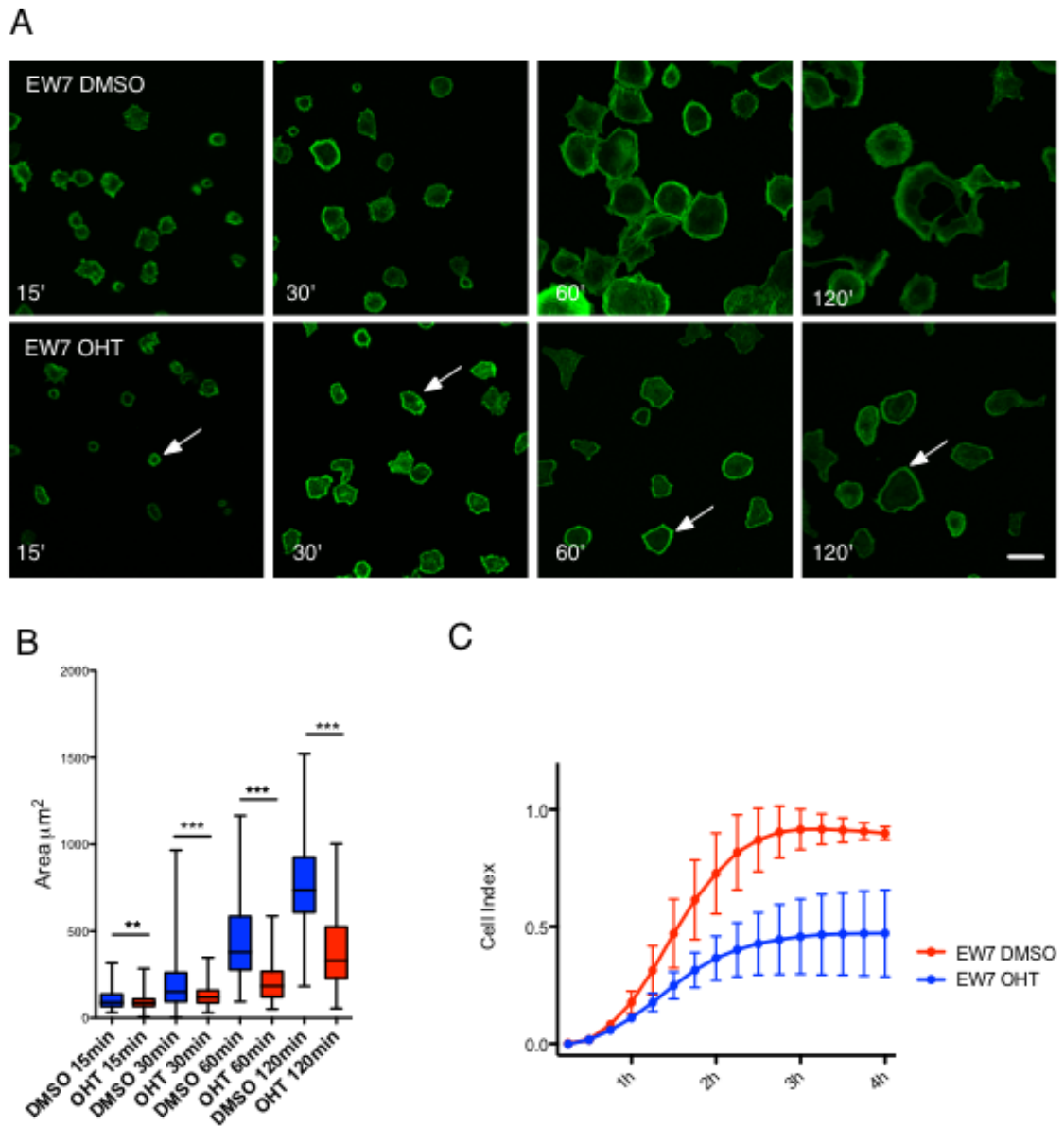


Figure 5.9 Cdc42 knockout melanocytes take longer to spread and have thick cortical actin
(A) Spreading assay where DMSO or OHT treated EW7 *Cdc42* *f/f*; *Cre-ERT2*; *CDKN2*^{-/-} melanocytes were plated onto fibronectin coated coverslips and fixed 15, 30, 60 or 120 minutes after seeding. Staining shows F-actin (phalloidin) (green). White arrows highlight cortical actin. Scale 30 μm . **(B)** Area of melanocytes (μm^2) spreading at indicated times, measurements from at least 123 cells per genotype per condition. Plot shows mean plus minimum and maximum values. **(C)** Line graph showing cell index reading from XCELLignence software (indicates cell attachment) over 4 hours after seeding. Graph shows average readings taken every 15mins from 3 wells from two independent experiments \pm SEM ** $p < 0.01$, *** $p < 0.001$ t-test

also have strong cortical actin at each time point, which may restrain these cells and prevent them from spreading as quickly. This spreading defect was also apparent when using the xCELLigence system. When cells are adhered to the microtitre plates used in this assay, it increases the conductivity of the system, which can be converted into a cell index. OHT treated cells have a similar index in initial stages of the assay, and lines are difficult to separate due to the error in this method. As the assay progresses, it becomes clear that OHT treated cells are slower to settle and spread than DMSO treated cells (Figure 5.9C).

The adhesion dynamics of the cells in this assay at 60 and 120 minutes were investigated using staining for phosphorylated-paxillin, a multi-domain scaffold protein which is recruited early to adhesions (Figure 5.10A). This demonstrated that knockout cells are not able to form as many adhesions as they spread as control cells. Control cells have an average of 24 adhesions at 60 minutes, increasing to around 37 at 120 minutes. Knockout cells only display an average of 16 adhesions at 60 minutes, and this increased marginally to an average of 20 at 120 minutes (Figure 5.10B). In addition, knockout cells also appear to have problems in producing and extending filopodia during spreading (Figure 5.11A). As discussed earlier, filopodia can act as probes to the external environment, and can provide a scaffold to support the advancing lamellipod (Section 1.1.3.3). At 60 minutes, fewer filopodia are seen per cell in knockout cells in comparison to control. However, by 120 minutes, knockout cells begin producing filopodia, with an average of around 7 filopodia being made per cell (Figure 5.11B). The filopodia produced by knockout cells are significantly shorter at both 60 and 120 minutes of spreading. Control filopods are an average of 2.3 μm long, reaching a maximum of 7.9 μm , but knockout filopods are on average 1.2 μm , reaching a maximum of 4 μm (Figure 5.11C).

We conclude therefore that Cdc42 is necessary for the efficient spreading of melanocytes. Knockout melanocytes are slower to spread, and our data suggest that this defect may be due to the role of Cdc42 in adhesion and filopod formation. Knockout melanocytes make fewer adhesions at both 60 and 120 minutes of spreading. They are also slower to produce filopods, and they are shorter which is important, as these structures may be important in helping cells spread.

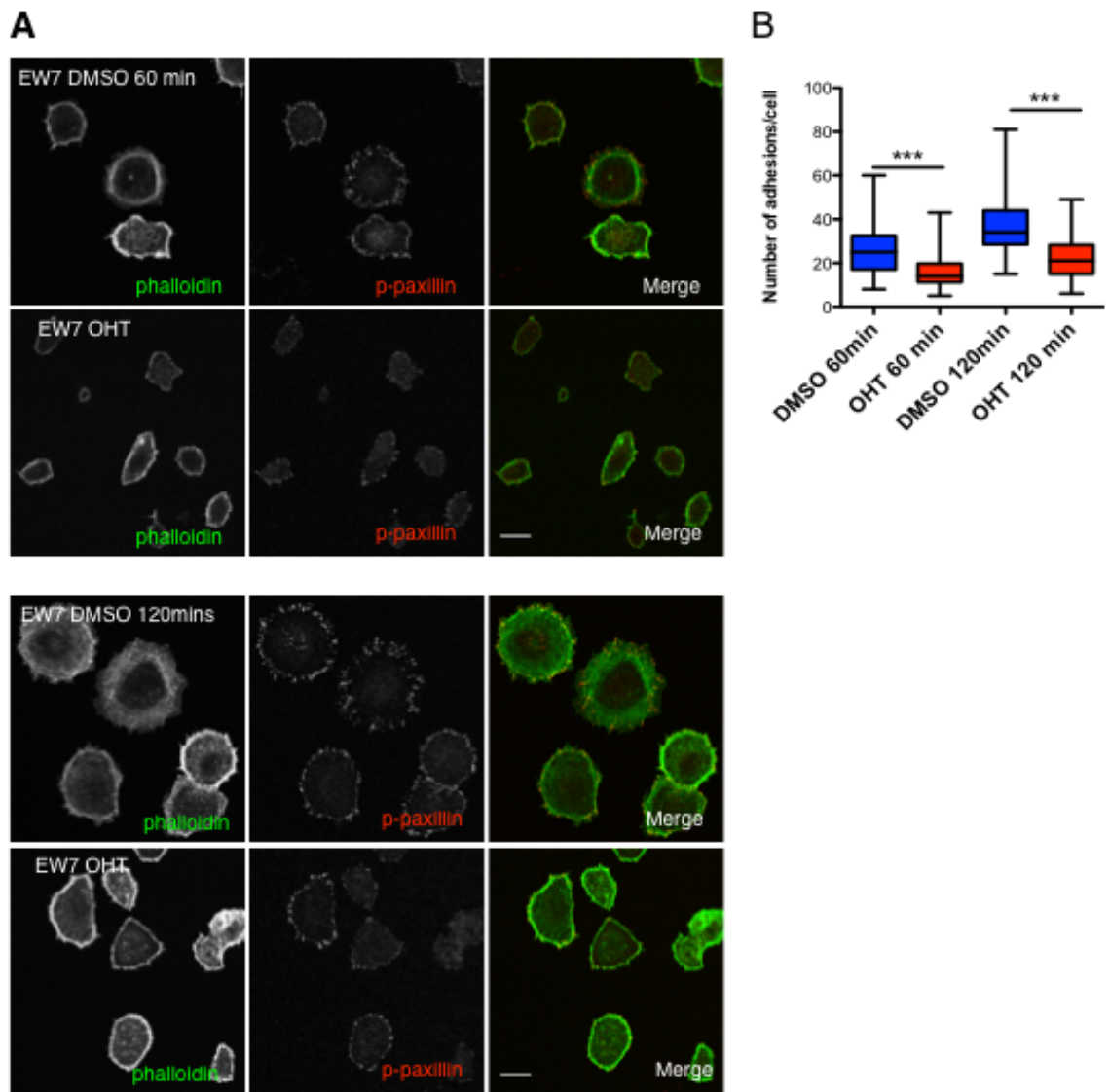


Figure 5.10 Cdc42 knockout melanocytes form less adhesions when spreading

(A) DMSO or OHT treated EW7 *Cdc42 f/f; Cre-ERT2; CDKN2^{-/-}* melanocytes seeded onto fibronectin coated coverslips and fixed after 60 or 120 minutes and stained for F-actin (phalloidin) and phospho-paxillin (red). **(B)** Quantification of the number of adhesions after 60 and 120 minutes from images in (A). 75 cells per genotype per condition were quantified from three independent experiments. Box plots show mean plus minimum and maximum values. *** $p < 0.001$ t-test. Scale 15 μm .

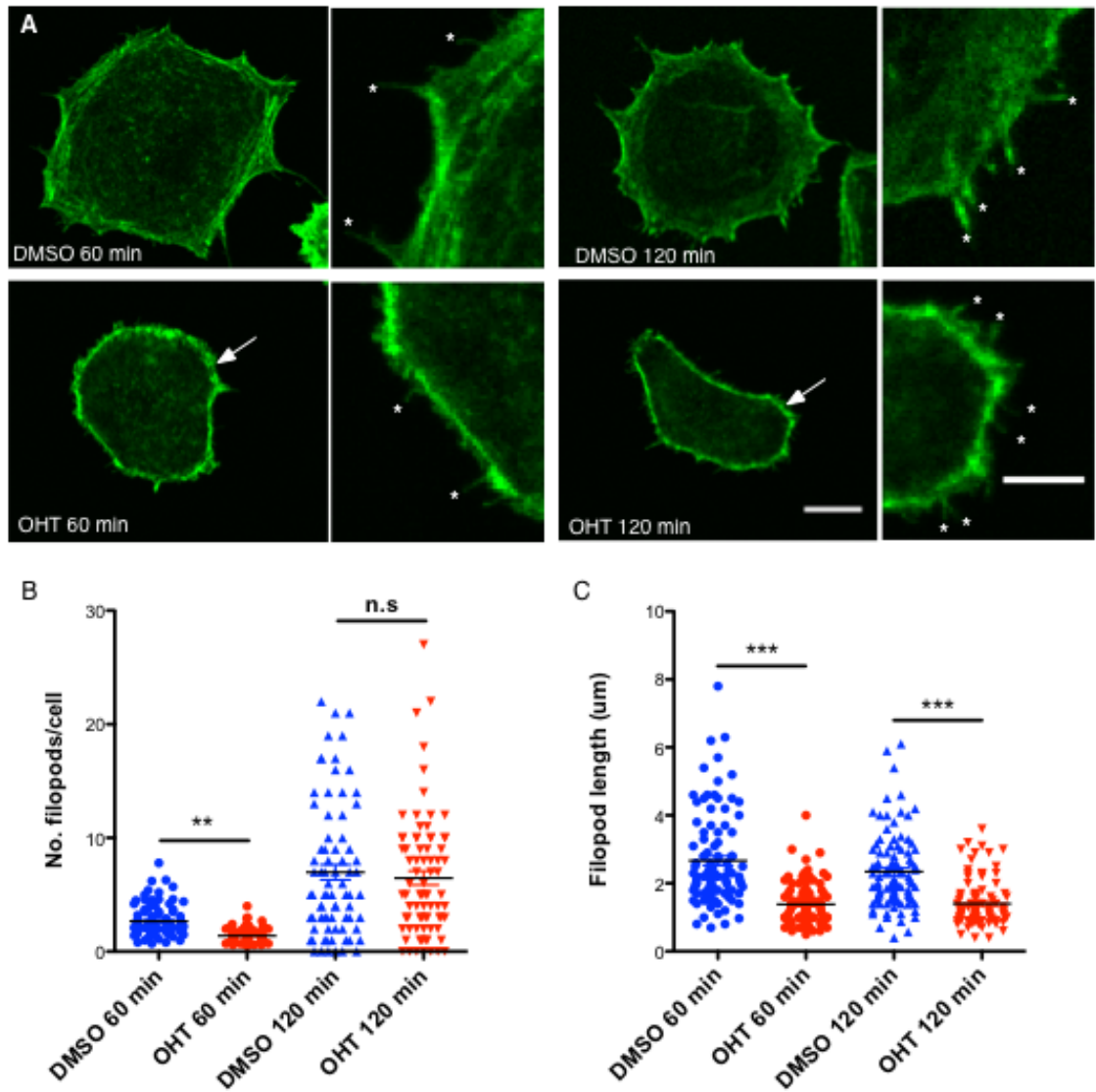


Figure 5.11 Loss of Cdc42 leads to fewer and shorter filopodia during spreading

(A) DMSO or OHT treated EW7 Cdc42 f/f; Cre-ERT2; CDKN2^{-/-} melanocytes seeded onto fibronectin coated coverslips and fixed after 60 or 120 minutes and stained for F-actin (phalloidin). White asterisks indicate structures counted as filopod like structures (FLS). (B) Average number of FLS per cell at 60 or 120 min after spreading, quantified from 77 different cells from three independent experiments. (C) Length of FLS 60 or 120 min after spreading. Measurements from at least 77 filopodia from at least 20 different cells from three independent experiments. Graphs show mean \pm SEM, n.s= not significant, **p<0.01, ***p<0.001 t-test.

5.3 Discussion

5.3.1 Loss of Cdc42 alters the expression of diverse signalling pathways including up-regulation of lysosomal proteins

We began our attempts to isolate RNA from control and Cdc42 knockout EW1 and EW7 primary melanocytes, as these were the lines that we had carried out our investigations with to this point. However, after multiple attempts, RNA of sufficient quality could not be isolated from OHT treated EW7 melanocytes. We believe the severity of the knockdown phenotype in these cells resulted in degradation of their RNA over time. We therefore began isolating RNA from other primary melanocyte lines isolated in the same way, but from a different litter of pups. Deletion of Cdc42 was successful in these lines (Figure 5.1A) and they displayed the same phenotype as lines EW1 and EW7. RNA isolated from these lines was of the highest quality (see appendix) and we decided to proceed to library preparation and analysis.

We were surprised to discover that lysosomal networks were the most significantly altered from KEGG pathway analysis using the DAVID software. This means that there were most matches between the list of genes altered after Cdc42 deletion within the lysosomal gene set defined by DAVID Gene Ontology analysis (Figure 5.1D). Lysosomes are the last organelle in the endocytic pathway containing many enzymes that digest macromolecules and make their components available to the cell. Lysosomal enzymes require a low pH for maximal activity, which is achieved through a proton-pumping V-type ATPase, which pumps protons into the lysosomal lumen (Mindell, 2012). Interestingly, we observed that multiple subunits of the V-ATPase enzyme are up-regulated in knockout cells (Figure 5.2B). In addition to mediating the acidification of lysosomes for lysosome mediated degradation, they also have a role in sorting cargo in the endosomal and secretory pathways (Marshansky and Futai, 2008), proton-coupled transport of ions and solutes and acidification of the pericellular space (Rath et al., 2014). It is not surprising therefore that changes in the function of the V-ATPase complex are linked to diverse diseases, including lysosomal storage disorders, neurodegeneration, myopathy, bone diseases and cancer (Hinton et al., 2009). If up-regulation of this complex in Cdc42 knockout melanocytes leads to aberrant acidification of vesicles, it could have a broad

and drastic effect on the endocytic pathway. This could lead to perturbation of vesicle trafficking systems, would could explain the mis-localisation of proteins in Cdc42 knockout cells and the poor recruitment of actin nucleators to the leading edge. In this way, changes in the expression of lysosomal genes, and those involved in the metabolism of signalling intermediates could in part underpin the morphology of these cells.

5.3.2 Cdc42 controls the expression of genes involved in focal adhesion pathways

Submission of genes down-regulated in the absence of Cdc42 to Gene Ontology analysis revealed that a substantial number were involved in focal adhesion signalling and regulation of the actin cytoskeleton (Figure 5.3A). Of these genes, integrin $\alpha 4$ displayed the highest fold change, and had the most significant adjusted p value. This down-regulation in expression led to a large drop in integrin $\alpha 4$ protein levels (Figure 5.4A). Interestingly, this integrin is expressed in cells of the neural crest lineage, as well as leukocytes and developing skeletal muscle (Shimizu et al., 1999). It most commonly dimerises with integrin $\beta 1$, binding to cell surface adhesion molecules such as VCAM-1, MAdCAM-1 and ECM components including fibronectin, binding to LDV sequences (Humphries et al., 2006). An increase in expression of integrin $\alpha 4$ has been correlated with melanoma progression from the radial to vertical growth phase, during the switch to invasive growth (Schadendorf et al., 1993, Albelda et al., 1990). It has also been shown to be crucial in assisting melanoma metastasis via the lymphatic system, with high expression of integrin $\alpha 4$ in melanoma cells increasing lung metastasis by 50% (Rebhun et al., 2010). This association with integrin $\alpha 4$ expression and migration in melanocyte lineage cells suggests that down regulation of this particular integrin may in part be responsible for the migration defects seen in Cdc42 knockout cells. In addition, the scaffold protein paxillin has been shown to associate tightly with the tail of integrin $\alpha 4$, with this interaction required for promotion of cell migration (Han et al., 2001). Due to its multiple protein binding domains, recruitment of paxillin to nascent adhesion sites is crucial to build and mature these sites into fully functional adhesions. It is interesting to speculate that the down regulation of integrin $\alpha 4$ in Cdc42 knockout melanocytes could prevent adhesion formation and maturation. We were surprised that the protein level of its most common partner, integrin $\beta 1$

was not altered in Cdc42 knockout melanocytes, however less was seen to be recruited to adhesion sites (Figure 5.5), showing some sort of adhesion recruitment defect in these cells despite consistent protein levels.

We also saw a significant decrease in integrin B3 protein in knockout cells (Figure 5.4). This was intriguing because the RNA levels were not significantly altered. We hypothesise that this could be due to aberrant degradation of this integrin in the absence of Cdc42. It is possible that defects during integrin recycling could shuttle this integrin for degradation. This fits in with our observation that the lysosomal networks of Cdc42 knockout cells are disrupted (Figure 5.2). Integrin B3 levels have also been linked to melanoma invasiveness; expression is repressed during melanoma progression by microRNAs, which accompanies reduced invasive potential (Muller and Bosserhoff, 2008).

5.3.3 Cdc42 controls adhesion formation and dynamics to support migration and spreading

Interestingly, down-regulation of focal adhesion signalling pathways in Cdc42 knockout melanocytes correlated with reduced adhesion number and area (Figure 5.7). By expressing paxillin-GFP in control melanocytes, we observed rapid extension of lamellipodia, which were dynamically supported by underlying adhesions which formed, grew and disassembled in a coordinated manner as the cell translocated (Figure 5.8). This observation is consistent with the standard migration cycle model, in which leading edge protrusion and matrix adhesion are tightly coupled both spatially and temporally (Gupton and Waterman-Storer, 2006, Giannone et al., 2004). The cycle begins with the extension of thin portions membrane driven by actin polymerisation, which are rapidly supported by tiny nascent adhesions containing integrins. A small proportion of these grow in size as a multi-molecular complex assembles on the cytoplasmic side of the membrane, linking these sites to the actin cytoskeleton. This linkage can act as a 'clutch' by immobilisation the cytoskeleton at this site, increasing the force exerted by extending filament, preventing the retrograde flow of actin (Gardel et al., 2010). Adhesion sites in migrating melanocytes therefore act as bi-directional platforms, transducing signals between the cell and the environment to induce cytoskeletal rearrangements to facilitate migration. However, we do

not fully understand the mechanisms that link adhesion and the actin cytoskeleton.

Our studies suggest that Cdc42 plays a major role in coordinating the molecules involved in this bi-directional conversation. We see that knockout cells form far fewer adhesions, dotted around the cell periphery but mainly concentrated at the tips of pseudopods (Figure 5.7). In addition, adhesions are less dynamic and take longer to assemble and disassemble (Figure 5.8). We hypothesise that Cdc42 coordinates either the recruitment or activation of proteins involved in the linkage of adhesion to the actin cytoskeleton. Recently, work by Swaminathan et al. have shown that FAK is crucial to this linkage of adhesions to actin polymerisation through its interaction with the Arp2/3 complex (Swaminathan et al., 2016). They showed that this interaction is essential for transient nascent adhesion stabilisation and advancement of the cell edge. It is interesting to speculate the Cdc42 can in some way control such interactions between focal adhesion proteins and the actin cytoskeleton, linking actin polymerisation at the leading edge to adhesion formation. In this way, Cdc42 could play a part in controlling the proposed 'molecular clutch', immobilising the actin cytoskeleton to allow generation of protrusive force at the cell membrane.

It is possible that Cdc42 facilitates this linkage to the actin cytoskeleton by controlling adhesion maturation through recruitment of adhesion proteins to the site of nascent adhesions. Therefore in the absence of Cdc42, failure to recruit the full complement of proteins could sever the link to the actin cytoskeleton. In addition, we understand that adhesions act as important sites for mechanosensing of matrix stiffness, which can in turn control cell polarity and migration (Prager-Khoutorsky et al., 2011, Hytonen and Wehrle-Haller, 2016). As Cdc42 knockout melanocytes possess fewer, smaller adhesions, they may be unable to effectively transmit signals such as stiffness or cellular tension back to the cell. It is likely that this break in outside-in signalling could lead to defects in the dynamic regulation of the cytoskeleton, disrupting the smooth migration cycle observed in control melanocytes.

This hypothesis fits nicely with our observations of Cdc42 knockout melanoblasts migrating *in vivo*, where we saw that actin polymerisation is unaffected, but

cells can't harness this force into migration. It appears that Cdc42 not only acts to promote the expression of adhesion related genes, but it is also essential in the coordination of adhesion with the actin cytoskeleton. Therefore melanoblasts *in vivo* are unable to form enough robust adhesions to tether extending pseudopods to the basement membrane below to communicate effectively with the matrix and to generate protrusive force to allow the cell to propel itself forward.

In addition to adhesion defects observed during cell migration, it is also clear that Cdc42 is an important regulator of adhesion dynamics and actin cytoskeleton arrangements during cell spreading (Figure 5.9 and 5.10). In general, when cells encounter matrix proteins in a 2D environment, they respond by adhering then spreading out into a flattened morphology. This complex process is mediated by integrins, which transmit signals about the underlying matrix to the actin cytoskeleton. This process appears to involve the activation of diverse signalling pathways, including tyrosine kinases, protein kinase C, arachidonic acid metabolism and calcium signalling (Chun and Jacobson, 1992, Chun and Jacobson, 1993, Pelletier et al., 1992, Vuori and Ruoslahti, 1993). However the contribution of these signalling pathways is not well understood.

Our data suggest that Cdc42 plays a key role in the coordination of adhesion formation and the actin cytoskeleton during spreading. Knockout melanocytes took longer to spread in the 2 hours after plating, and a thick actin cortex could be seen at all time-points (Figure 5.9A and B). In contrast to this, the cytoskeleton of control cells is highly dynamic during spreading, and after 2 hours they display lamellipodia and stress fibres. The cytoskeletal rearrangements seen in control cells are most likely facilitated by the many, mature adhesions that form underneath the cell. Similarly to our observations during migration of these cells, the inability of Cdc42 knockout cells to form and mature adhesions during spreading likely contributes to their slowness to spread.

Observations implicating Cdc42 in cell spreading are in agreement with Price et al., who showed that expression of a dominant negative form of Cdc42 profoundly inhibited spreading (Price et al., 1998). However, from their observations, they hypothesise that the primary role for Cdc42 during spreading

is to induce formation of filopodia and to activate Rac to induce lamellipodial spreading over the scaffold of filopodia. Our data partly agree with this model, as filopodia are shorter without Cdc42, but filopod number is largely unaltered in the absence of Cdc42 (Figure 5.11). This is a surprising discovery, as Cdc42 has always been primarily associated with the formation of these structures (Nobes and Hall, 1995). We therefore suggest that in addition to modulating the extension of filopods during spreading, that Cdc42 also coordinates adhesion formation and cytoskeletal rearrangements to achieve efficient cell spreading.

5.4 Summary

In this chapter, we used an RNA sequencing approach to investigate gene expression changes after deletion of Cdc42. This approach allowed us to take an unbiased, global view of Cdc42's role in the cell, providing insight that could not be gained from a single candidate approach. We observed an up-regulation of genes associated with the lysosomal network in Cdc42 knockout melanocytes, particularly components associated with the acidification of vesicles, which may disrupt endosomal recycling or trafficking. In addition, loss of Cdc42 leads to a down-regulation of focal adhesion signalling, which is accompanied by fewer smaller adhesions and a delay in spreading. We hypothesise that Cdc42 is a key player in linking adhesion formation and maturation to the actin cytoskeleton to coordinate and facilitate efficient cell migration by inducing the expression of focal adhesion genes, and providing the spatiotemporal signals to activate and recruit proteins to adhesion sites.

6 Investigating the role of Cdc42 in Melanoma Migration and Invasion

6.1 Introduction and aims

The data presented in previous chapters has described a major role for Cdc42 in the migration and proliferation of both melanoblasts and melanocytes. These findings prompted us to explore the role of Cdc42 in the migration and invasion of melanoma cells. As discussed in the introduction, the melanoblast lineage and melanoma share common molecular signatures, and it is thought the plastic and invasive nature of melanoma stems from reactivation of developmental signalling pathways of the neural crest. Currently, very little is known about the role that Cdc42 plays in melanoma progression and metastasis. We hypothesised that depletion of Cdc42 from mouse B16F10 melanoma cells might impede their migration and growth as seen in other cells of the melanocyte lineage (Data shown in previous chapters). We hoped that depletion of Cdc42 might also prevent the invasion of these cells into matrix, slowing the spread of these particularly aggressive cells.

We aimed to begin our investigation by producing a stable B16F10 melanoma cell line in which the deletion of Cdc42 could be induced. To do this, we first purchased a set of lentiviral shRNA constructs containing non-targeting or anti-mouse Cdc42 shRNA oligos (GIPZ from Dharmacon). Each oligo was then cloned into an inducible vector system (TRIPZ from Dharmacon), which tags the oligo onto turboRFP as a control to visualise oligo expression. Stable integration of this construct into B16F10 melanoma cells allowed inducible expression of shRNA oligos, and knockdown of Cdc42. We aimed to use this system to investigate the effect of Cdc42 knockdown of melanoma cell morphology and migration in 2D and invasion into *in vitro* invasion assays.

6.2 Results

6.2.1 Knockdown of Cdc42 in B16F10 melanoma cells does not effect cell morphology, migration or proliferation

Cdc42 was successfully knocked-down in B16F10 melanoma cells by inducible expression using two anti-Cdc42 oligos, 70288 and 488921 (Figure 6.1A). Oligo 488921 (sh2) provided the most effect knockdown, reducing Cdc42 levels by 70%. Expression of oligo 70288 resulted in a knockdown of 60% (Figure 6.1B) (values an average from three independent experiments). Having seen the major role Cdc42 played in the migration and proliferation of melanoblasts and melanocytes, we were intrigued whether knockdown of Cdc42 in this melanoma line would lead to an elongated morphology, altered pseudopod dynamics and proliferation defects. Interestingly, knockdown cells had a relatively normal morphology. F-actin was visualised by staining with phalloidin, which revealed that knockdown cells formed normal looking stress fibres and lamellipods (Figure 6.2A white arrows). Proliferation studies using the IncuCyte ZOOM system showed that cells expressing oligos against Cdc42 proliferate at the same rate as cells expressing a non-targeting (NT) oligo (Figure 6.2B).

The migration of Cdc42 knockdown B16F10 cells was first analysed using a random migration assay. Cells tracked in all conditions moved at around 0.8 $\mu\text{m}/\text{min}$ (Figure 6.2C), indicating that Cdc42 knockdown does not impair migration. The ability of these cells to close a wound was also investigated using the IncuCyte ZOOM system in a 96-well plate format. It is clear from the final images taken from these experiments by the system that knockdown cells had no problem closing the wound (Figure 6.3A) (initial wound shown by mask). This is confirmed by the quantification of the wound confluence in each condition over the experiment time course, which shows that cells close the wound at the same rate (Figure 6.3B). We can therefore conclude that knockdown of Cdc42 by 60-70% in B16F10 melanoma cells does not affect cell morphology, proliferation or migration. It is likely that residual Cdc42 protein left from the incomplete knockdown is enough to maintain these functions. In addition, as these cells are cancerous and not primary lines, it is possible that these cells have acquired additional mutations that help drive these processes in the absence of Cdc42.

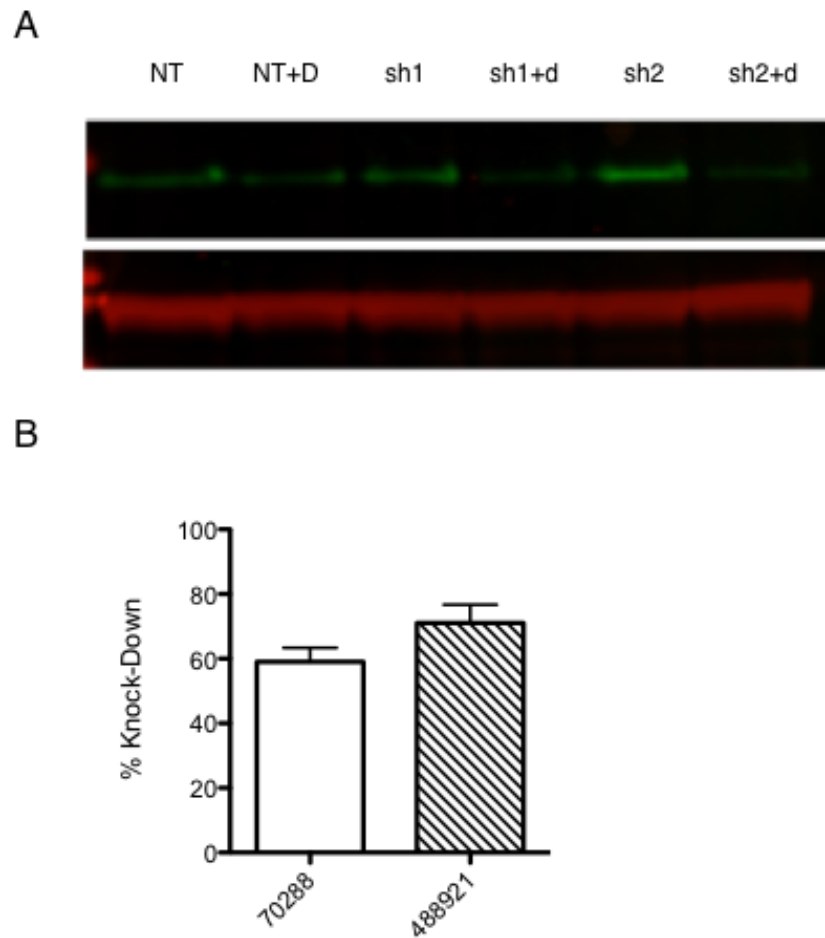


Figure 6.1 Cdc42 is successfully knockout-down in B16F10 melanoma shRNA cell lines
(A) Western on lysates taken from cells containing non-targeting shRNA vector (NT) or vectors containing shRNA against CDC42 (sh1 or sh2) with (+d) and without addition of doxycycline to induce shRNA expression from the vector. **(B)** Quantification of % knock-down of Cdc42 by sh1 (70288) and sh2 (488921). Quantification from 3 independent blots, graphs show mean \pm SEM.

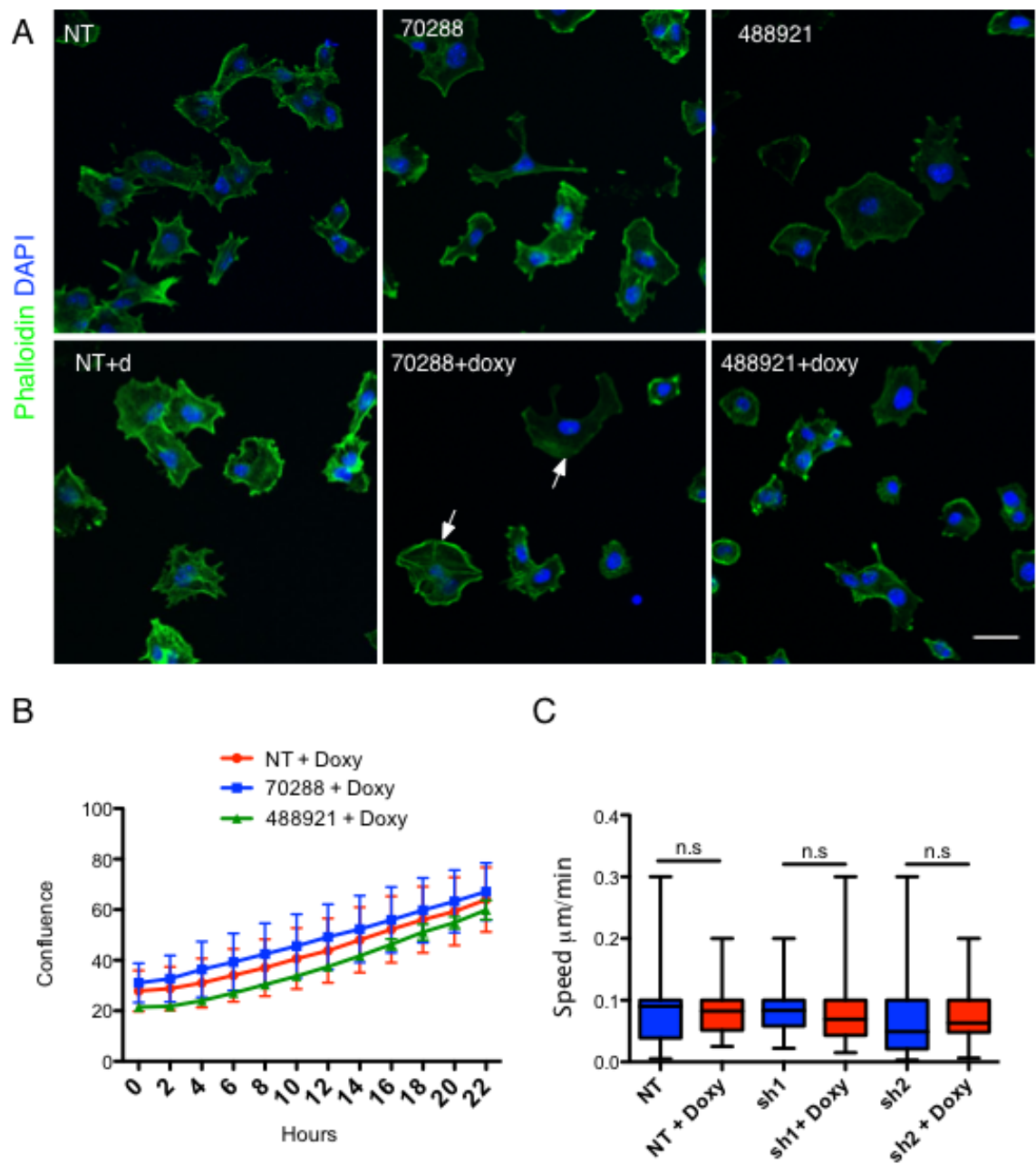


Figure 6.2 Knock-Down of Cdc42 does not change B16F10 melanoma cell morphology, proliferation or migration

(A) B16F0 melanoma cells containing non-targeting shRNA vector (NT) or vectors containing shRNA against CDC42 (70288 or 488921) with (+d) and without addition of doxycycline to induce shRNA expression. Cells plated on collagen, fixed and stained with phalloidin and DAPI. Scale 30 μm . **(B)** Proliferation assay of cells expressing non-targeting shRNA (NT) or CDC42 shRNA (70288 or 488921). Proliferation measured as cell confluence on IncuCyte ZOOM system, values plotted from readings every two hours are an average of multiple wells from three independent experiments. Graph shows mean \pm SEM. **(C)** Average speed of B16F10 melanoma cells on collagen.

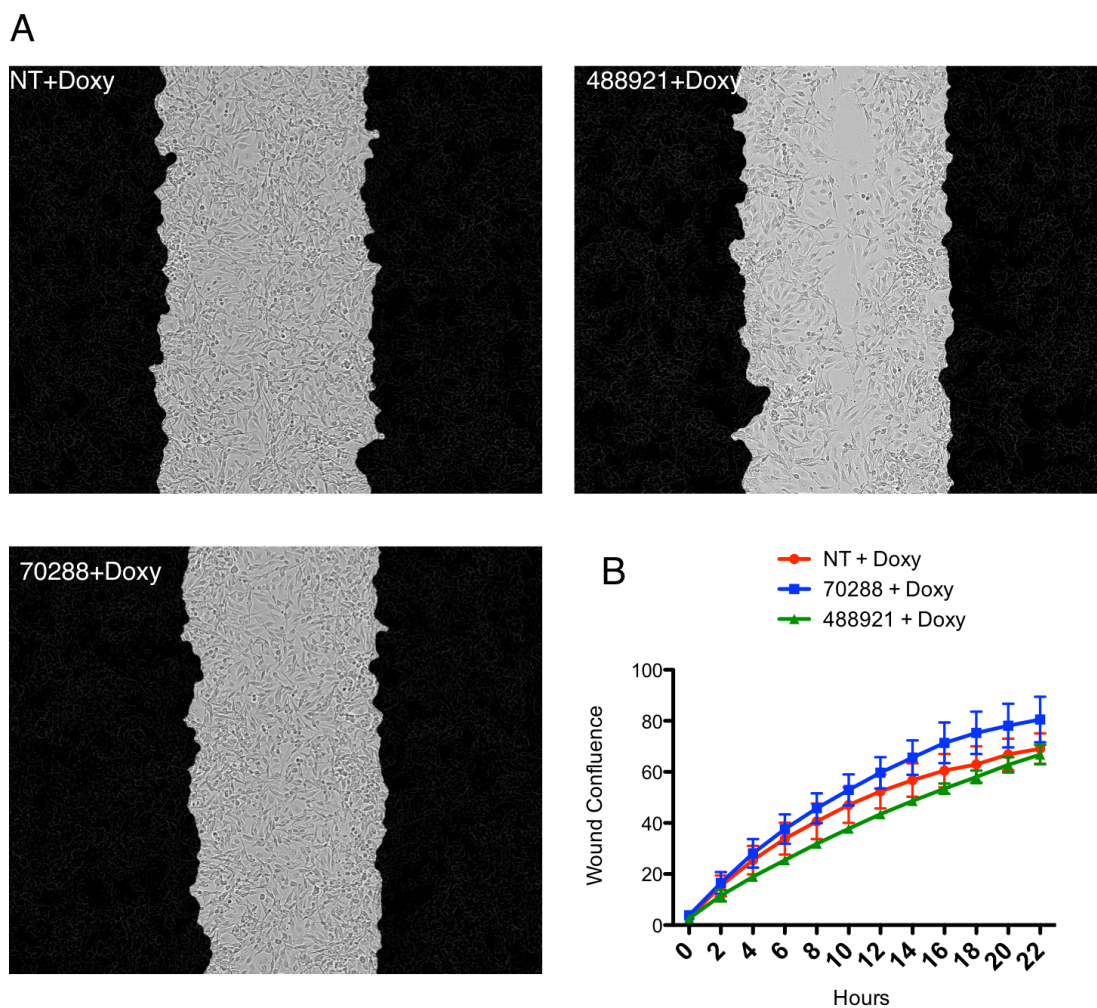


Figure 6.3 Knock-down of Cdc42 does not impair the ability of B16F10 melanoma cells to close a wound

(A) Images from IncuCyte ZOOM system showing cells expressing non-targeting shRNA (NT) or CDC42 shRNA (70288 or 488921) closing a wound. Image is a merge of a mask showing initial wound edge from first time-point and a clear image from the final time-point. **(B)** Graph showing wound confluence, readings taken every 2 hours using the IncuCyte ZOOM system. Readings are an average of multiple wells from three independent experiments. Graph shows mean \pm SEM.

6.2.2 Cdc42 knockdown slows the invasion on B16F10 melanoma cells

Given the invasive nature of this cell line, we decided to explore whether Cdc42 knockdown impaired their ability to invade into commonly used *in vitro* invasion assays. These cells did not display a proliferation defect, which makes them a good model to ask this question, as if cells divided more slowly this could have an impact on their invasive ability. We first investigated their ability to close a scratch wound overlaid with Matrigel using IncuCyte ZOOM system. It is clear from the last image from this experiment (taken 22 hours after wounding) that cells expressing either anti-Cdc42 oligo 70288 and 488921 have not moved as far into the wound as cells expressing a non-targeting (NT) oligo (Figure 6.4A)(wound showed by mask). This was confirmed in a high-throughput manner by the IncuCyte ZOOM software by tracking the wound confluence over the course of the assay. After 22 hours of invasion into the wound, cell expressing the non-targeting oligo showed nearly 80% cell confluence in the wound. In contrast, cells expressing the anti-Cdc42 oligo 70288 only displayed 50% wound confluence, and those expressing oligo 488921 only 38% (Figure 6.4B). The apparent difference in the invasive abilities of these two knockdown lines can follow nicely the difference in levels of Cdc42 knockdown, with oligo 488921 achieving an extra 10% knock-down than 70288 (Figure 6.1A and B).

To confirm if this defect could be observed in additional invasion assays, we asked whether Cdc42 was important for the invasion of B16F10 spheroids into matrigel. Spheroids were grown for 5 days with or without doxycycline then embedded into matrigel, overlaid with media and left to invade for 7 days. Spheroids at the end of this process can be seen in Figure 6.5A. Spheroids without doxycycline have invaded into the surrounding matrigel (Figure 6.5A left panel). Cells expressing the non-targeting oligo in the presence of doxycycline invade well into the surrounding matrigel. The invasion of spheroids expressing anti-Cdc42 oligos is poor (Figure 6.5A right panel). Successful expression of oligos can be confirmed as they are tagged with the red fluorescent protein turboRFP, which can be visualised seen under the red camera. We therefore conclude that knockdown of Cdc42 impairs the ability of B16F10 melanoma cells to degrade and invade the surrounding matrix, despite not effecting their migration and division in a 2D environment.

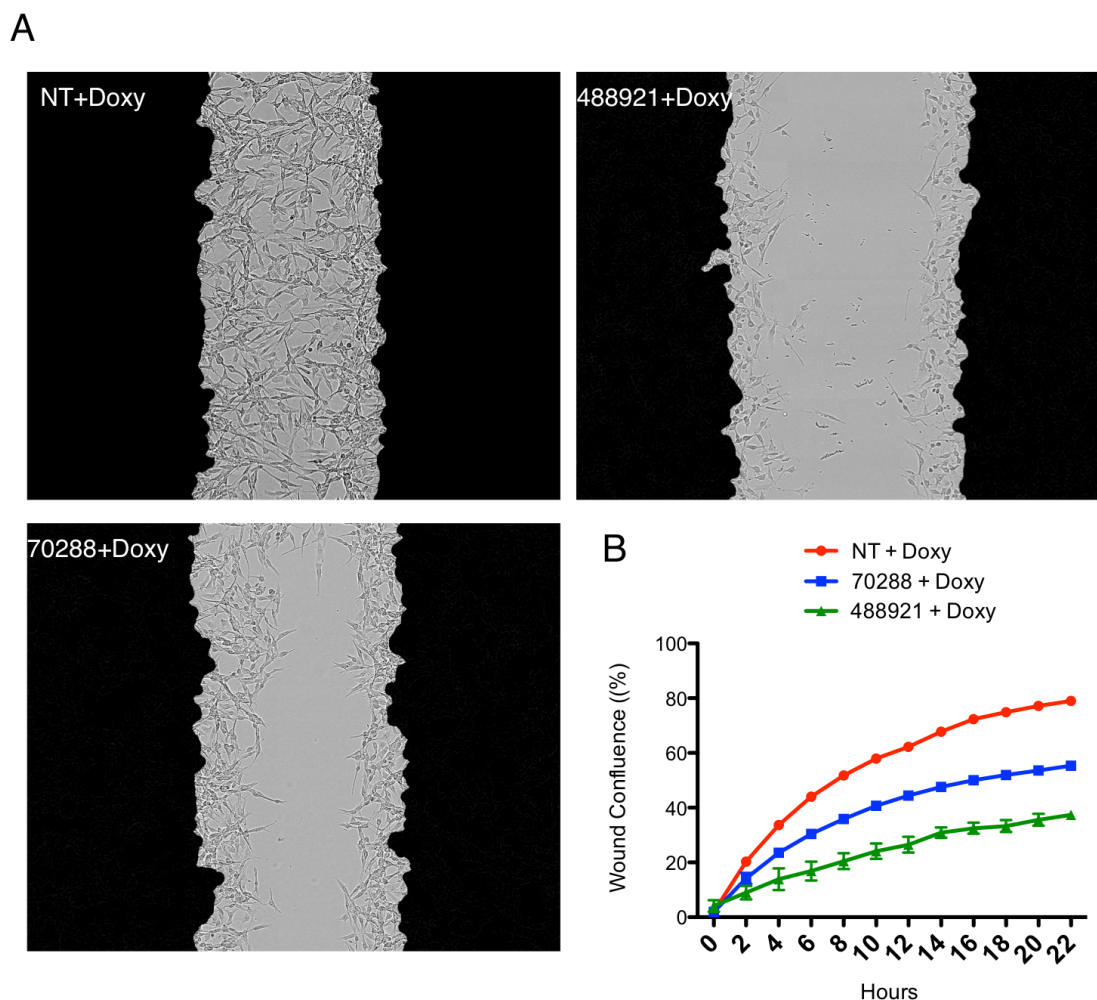


Figure 6.4 Knock-down of Cdc42 impairs the ability of B16F10 melanoma to invade into matrigel

(A) Images from IncuCyte ZOOM system showing cells expressing non-targeting shRNA (NT) or CDC42 shRNA (70288 or 488921) closing a wound overlaid with matrigel. Image is a merge of a mask showing initial wound edge from first time-point and a clear image from the final time-point.

(B) Graph showing wound confluence, readings taken every 2 hours using the IncuCyte ZOOM system. Readings are an average of multiple wells from three independent experiments. Graph shows mean \pm SEM.

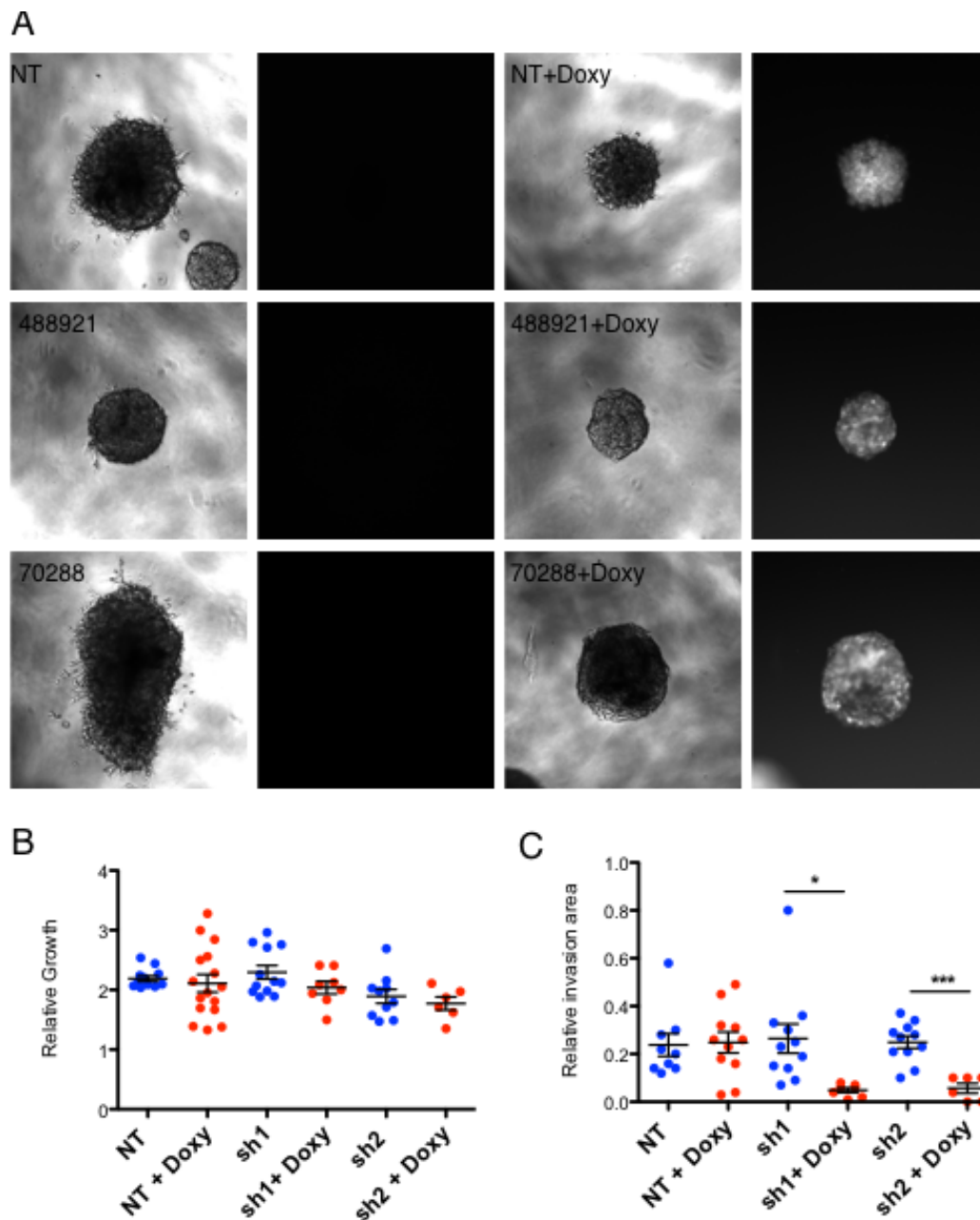


Figure 6.5 Expression of Cdc42 shRNA impairs B16F10 melanoma cell invasion into Matrigel

(A) Images of spheroids containing non-targeting shRNA vector (NT) or vectors containing shRNA against CDC42 (70288 or 488921) with (+d) and without addition of doxycycline to induce shRNA expression. Images taken under light (right) or with the red laser (left) to demonstrate turboRED expression. (B) Growth of spheroids over 7 days embedded in Matrigel. (C) Relative invasion of spheroids into Matrigel over 7 days. Graphs show mean \pm SEM, * p <0.05, ** p <0.01 t-test.

6.3 Discussion

6.3.1 B16F10 Melanoma migration and proliferation are not affected by Cdc42 knockdown

Inducible expression of anti-Cdc42 shRNA oligos reduced Cdc42 protein levels by 60-70%, with oligo 488921 consistently achieving a better knockdown than oligo 70288 (Figure 6.1). It appears that this partial reduction in Cdc42 levels does not impart any morphological changes in B16F10 melanoma cells, and their actin cytoskeleton appears to be organised normally (Figure 6.2A). Remarkably, knockdown cells are still able to form lamellipods, unlike Cdc42 knockout melanoblasts or melanocytes. We don't see these cells adopting an extended morphology, and they are able to proliferate and migrate normally unlike Cdc42 deletion in melanoblasts and melanocytes (Figure 6.2B and C and 6.3). It is possible that residual levels of Cdc42 in melanoma cells are enough to maintain regulation of the actin cytoskeleton in these cells. Given the aggressive nature of these cells, it is likely that these cells have acquired additional mutations, possibly in multiple different pathways such as those controlling cell division and survival. These additional changes may also compensate for any defects caused by a reduction in Cdc42 levels.

6.3.2 Cdc42 aids melanoma cell invasion

As Cdc42 knockdown did not appear to cause any problems for B16F10 melanoma cells, we thought it was unlikely to impair their invasion. When we explored the ability of Cdc42 knockdown cells to invade into matrigel during a high-throughput wound closure assay, we observed that Cdc42 knockdown cells were in fact slower to close the wound (Figure 6.4A and B). This defect was also apparent when the ability of B16F10 spheroids to invade into matrigel was assessed. After 5 days of invasion, cells expressing shRNA oligos were barely able to spread into the surrounding matrix. This defect was striking, and suggests Cdc42 plays a key role in the invasive motility of these cells. These observations are consistent with previous work that showed Cdc42 localisation to tumour cell-matrix contacts, where it activates the scaffold protein IQ-GAP to select vesicles containing Matrix metalloproteinases (MMP) for incorporation into the invading membrane compartment via interaction the exocyst complex (Sakurai-Yageta et al., 2008). We hypothesise that Cdc42 deletion prevents this coupling and

therefore less MMPs are released, impeding the cell's progress. It would be interesting to investigate the amount of MMP release at sites of cell-matrix contact to conform this hypothesis. Previous work has also identified Cdc42 as a key player in invadopodia formation. Invadopodia, formed by cancer cells, are actin-rich membrane protrusions with matrix degradation activity. Using an RNA interference approach, Yamaguchi et al. showed that N-WASP, Arp2/3 and their upstream regulators Nck1, Cdc42 and WIP are necessary for invadopodium formation downstream of EGF signalling (Yamaguchi et al., 2005). It is possible therefore that Cdc42 depletion reduces invadopodia formation in these melanoma cells, reducing their ability to degrade the matrix.

6.4 Summary

This preliminary work has revealed a key role for Cdc42 in B16F10 melanoma cell invasion. Our studies have shown that knockdown of Cdc42 in this cell line does not effect cell morphology, migration or proliferation, in contrast to melanoblasts or melanocytes. However, Cdc42 knockdown impairs the ability of B16F10 melanoma cells to invade into matrix from scratch wounds or out from spheroids. Given this fairly striking defect, it would be interesting to investigate the ability of these cell lines to invade *in vivo*. This could be achieved through injection into mammary fat pads or through tail vein injections to explore whether Cdc42 maintains this key role in invasion *in vivo*.

7 Conclusions and Future Directions

7.1 Conclusions

7.1.1 Cdc42 and Rac1 have important and distinct roles during the melanoblast journey, but RhoA is not required

During this project, we aimed to deepen our understanding of the role of the Rho GTPase Cdc42 in 3D migration by utilising the melanoblast model system. With this knowledge, and together with our previous studies in this system, we hoped to extend our currently limited understanding of how the Rho GTPase family members and other actin regulating proteins are coordinated globally during cell migration *in vivo*. Through targeted deletion of Cdc42 in the melanoblast lineage, we revealed a crucial role for Cdc42 during the melanoblast journey. Similarly to Rac1 null melanoblasts, Cdc42 null melanoblasts were unable to complete population of the developing embryo before birth leading to coat colour defects at birth. However, skin explant imaging revealed that, unlike Rac1 knockout melanoblasts which were largely rounded (Figure 7.1C), Cdc42 null melanoblasts were elongated and displayed large, bulky pseudopods (Figure 7.1B). Despite being able to extend pseudopods, Cdc42 knockout melanoblasts migrated slowly and inefficiently through the embryo epidermis and were unable to retract their pseudopods efficiently. Surprisingly however, we showed that these pseudopods have active actin dynamics, displaying frequent actin bursts at pseudopod tips.

We have previously established that Rac1 primarily promotes melanoblast migration by driving pseudopod extension through SCAR/WAVE and Arp2/3 signalling (Li et al., 2011). Rac1 null melanoblasts are therefore rounded and move slowly through the epidermis using short stubby protrusions (Figure 7.1). Our *in vivo* data showed a unique role for Cdc42 during 3D migration. We showed that Cdc42 null melanoblasts are able to polymerise actin at pseudopods tips, but appear unable to link the protrusive force generated into coordinated and persistent cell movement. We also showed that RhoA does not play a crucial role in melanoblast migration, as loss of RhoA in the melanoblast lineage did not lead

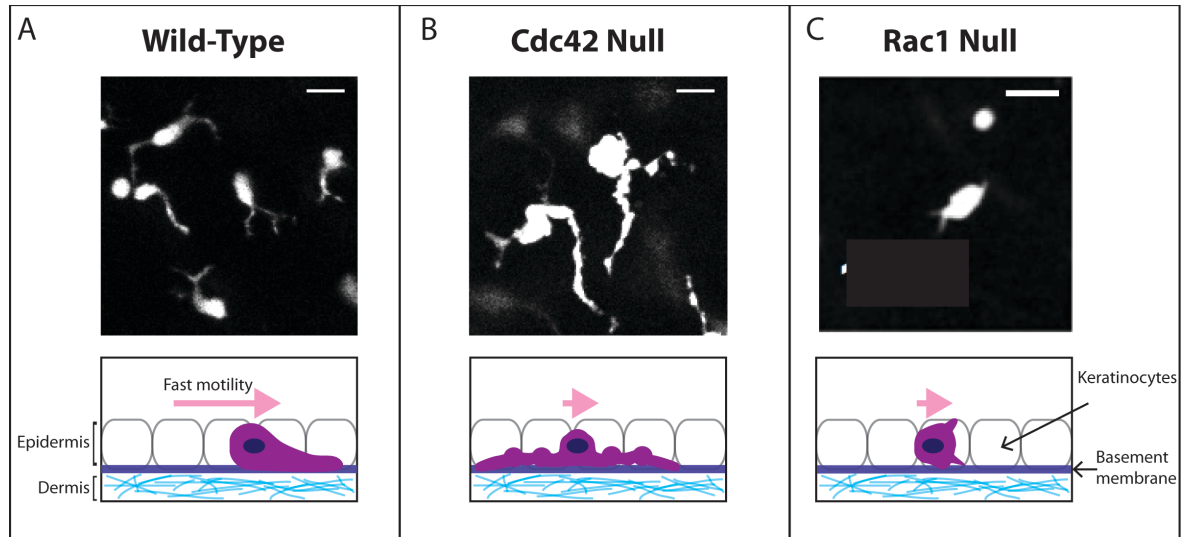


Figure 7.1 Rac1 null and Cdc42 null melanoblasts have different morphologies but both migrate more slowly than wild-type melanoblasts

Wild-type melanoblasts are highly motile and extend multiple, dynamic pseudopods between the surrounding keratinocytes (A). Loss of Cdc42 leads to an increase in cell area and elongated, bulky pseudopods which are extremely long-lived (B). Conversely, Rac1 null melanoblasts are rounded and migrate slowly through the skin using short stubby pseudopods (C).

to coat colour defects. In addition, preliminary results indicate that melanocytes must express Rac1 and Cdc42 for successful melanoblast specification and expansion during development, as melanoblast double knockout of these family members resulted in embryos devoid of melanoblasts.

7.1.2 Cdc42 coordinates the spatial positioning of key actin regulators to facilitate migration

Our next aim was to explore the molecular impact of Cdc42 loss on the melanocyte lineage, in order to understand and explain the morphology of Cdc42 null melanoblasts using an *in vitro* model. To do this, we isolated cultures of primary melanocytes from 1-day-old pups in which Cdc42 deletion could be induced. Using this system, we showed that the branched actin regulators N-Wasp and Arp2/3 were poorly localised in Cdc42 knockout melanocytes, preventing them from forming the large fan-like lamellipods that wild-type melanocytes use to migrate. Surprisingly however, we showed that the lack of branched actin networks in knockout cells was not due to reduced levels of active Rac1. We therefore hypothesise that Cdc42 does not control Rac1 activation in these cells, but is important for the correct placement of Rac1 at the membrane to induce branched actin networks. Immunofluorescence staining on these cells also revealed that Cdc42 coordinates the spatial positioning of myosin light chain phosphorylation, explaining the inability of Cdc42 null cells to retract their pseudopods.

7.1.3 Cdc42 promotes G1 to S cell cycle transition and cytokinesis

Through X-Gal staining of embryos expressing β -galactosidase in the melanoblast lineage, we saw that Cdc42 *f/f* Tyr::*CreB*^{+/-} embryos had a paucity of melanoblasts, similarly to Rac1 *f/f* Tyr::*CreB*^{+/-} embryos (Li et al., 2011). Live imaging of melanoblast division in skin explants revealed a crucial role for Cdc42 in melanoblast cytokinesis. Cdc42 null melanoblasts were unable to fully round up efficiently during mitotic onset, and took three times longer to complete cytokinesis than wild-type melanoblasts. Our data indicate that Cdc42 is particularly crucial for the final stages of membrane separation, unlike Rac1, which appears most crucial in regulating cleavage furrow formation (Li et al., 2011). In addition, Cdc42 also plays a key role in division in 2D. Cdc42 knockout

melanocytes also took over twice as long to divide than wild-type melanocytes whereas Rac1 null melanocytes did not display division defects *in vitro*. In line with previous work, we also showed that Cdc42 promoted G1 to S transition. Together, our findings show that by driving melanoblast cell-cycle progression and cytokinesis, Cdc42 is crucial for stimulating melanoblast expansion as well as migration during development.

7.1.4 Cdc42 coordinates adhesion dynamics and actin polymerisation to drive migration

Using a global RNA sequencing approach, we investigated the gene expression changes after deletion of Cdc42. Interestingly, our data showed a significant increase in the expression of genes within lysosomal pathways, most notably, loss of Cdc42 led to an up-regulation of six subunits of the V-ATPase enzyme responsible for the acidification of vesicles. This RNA sequencing approach also revealed a down-regulation of adhesion associated genes in the absence of Cdc42. We showed that Cdc42 null melanocytes had decreased levels of integrin $\alpha 4$ and $\beta 3$, but levels of integrin $\beta 1$ were unaltered. We showed that this down-regulation of adhesion related genes correlated with slower adhesion dynamics in Cdc42 null melanocytes. In addition, we also showed that knockout cells displayed fewer adhesions that were smaller in size. Our data indicate a role for Cdc42 in linking adhesions to actin dynamics. To this end, fewer adhesions were formed underneath spreading Cdc42 null melanocytes, and null melanocytes were slower to spread overall, displaying a thick band of cortical actin underneath the membrane. We hypothesise that Cdc42 coordinates the inside-out and outside-in signalling at adhesion sites, and in the absence of Cdc42 adhesion formation is reduced, along with adhesion maturation and dynamics. This defect within adhesions impacts the organisation of the actin cytoskeleton and renders the cell unable to migrate efficiently.

By combining the data gained from our *in vitro* melanocyte system with our observations of melanoblast migration *in vivo*, a new and exciting picture is beginning to emerge of Cdc42's role in the coordination of cell migration. We believe that unlike Rac1, which has a very specific role in signalling to branched actin network generation, Cdc42 functions to coordinate multiple systems including actin polymerisation, adhesion dynamics and contractility during cell

migration. In this way, it appears that Cdc42 has a clearly distinct role to Rac1 during migration. Our hypothesis, summarised in Figure 7.2, is that melanoblast pseudopod extension is primarily driven by Rac1 via SCAR/WAVE and Arp2/3 pathways. Cdc42 is key in linking this protrusive force into migration through controlling adhesion turnover and maturation through mechanisms still unknown, but possibly through linkage of adhesions to the actin cytoskeleton. Cdc42 is also crucial for the spatial organisation of cell components including actin-binding proteins and phosphorylation of myosin light chain to produce dynamic adhesions through coordination of extension and retraction of pseudopods to achieve efficient movement.

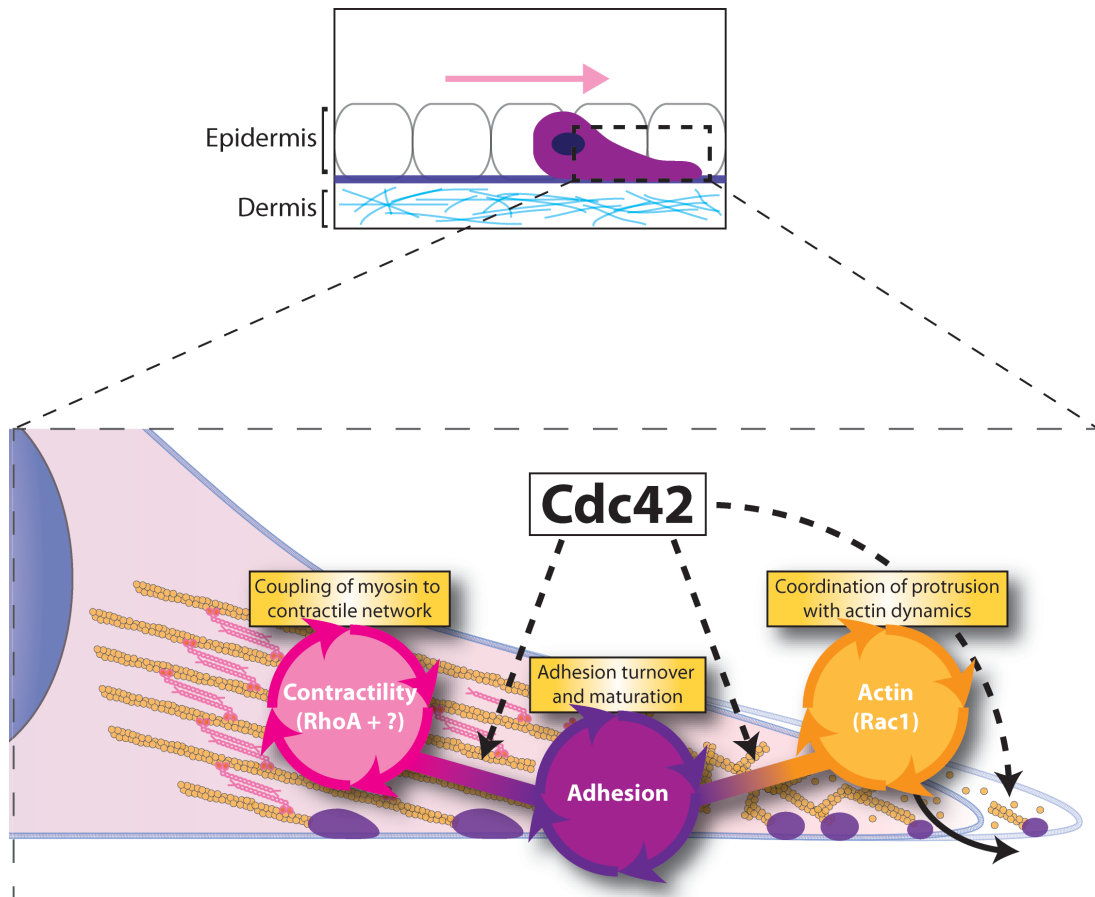
7.1.5 Cdc42 aids melanoma invasion

Given the prominent role of Cdc42 in the migration and proliferation of both melanoblasts and melanocytes, we also aimed to investigate whether loss of Cdc42 could slow the spread of melanoma cells. Somewhat surprisingly, knockdown of Cdc42 in B16F10 melanoma cells did not impact their ability to migrate or proliferate, presumably due to the residual levels of Cdc42 remaining in these cells. When analysed in invasion assays however, it was clear that Cdc42 does drive melanoma cell invasion. Our data showed that knockdown of Cdc42 reduced melanoma cell invasion into scratch wound assays and out from spheroids. It still remains unclear, however, exactly how Cdc42 aids melanoma invasion in these assays, or whether the same observations would be made in *in vivo* studies.

7.2 Future Directions

7.2.1 How do melanoblasts achieve orchestrated population of the developing embryo?

This project, along with previous work in the lab and other recent studies have utilised modern imaging approaches to understand the melanoblast journey. We are only beginning to understand how these dynamic and highly motile cells complete their journey through the developing embryo. In particular, the imaging techniques used in this study could be extended to investigate many



Melanoblast translocation in developing skin

Figure 7.2 Rho GTPases act in a coordinated manner to achieve coordinated cell migration
 In our current model, we believe that Rac1 is primarily responsible for stimulating actin polymerisation at pseudopod tips to drive pseudopod extension. Cdc42 then links the actin network with adhesions, controlling adhesion turnover and maturation, translating protrusive force into cell translocation. It is likely that RhoA couples myosin to actin to generate a contractile network, but Cdc42 controls the spatial organisation of myosin phosphorylation. As RhoA alone is not required for melanoblast population of the developing embryo, we believe that its role can be compensated for by RhoA isoforms that are highly expressed in melanoblasts.

elements of the melanoblast journey, such as their movement from dermis to epidermis, the role of gradients and contact inhibition during their migration, and their movement into hair follicles. Also, there are many other interesting actin regulating proteins that could be studied in addition to those already described in the melanoblast system. Knockout of interesting candidates in the same system allows us to build a detailed picture of how these proteins contribute to 3D cell migration, giving us a more valuable insight into how they might play different roles during 3D migration than previously understood from *in vitro* 2D studies. Our preliminary investigation concerning double knockout of both Rac1 and Cdc42 in the melanoblast lineage suggests that, together, Rac1 and Cdc42 are crucial for either melanoblast determination, their survival or expansion during development. Ideally, these findings could be confirmed and extended through X-Gal staining and explant imaging of double knockout embryos. In addition, double knockout cells could be studied *in vitro* to investigate the interplay between Rac1 and Cdc42 during migration.

7.2.2 Is the lysosomal network affected in Cdc42 knockout melanocytes?

Our data from global RNA sequencing of Cdc42 knockout melanocytes showed a significant up-regulation of genes involved in lysosomal networks. Given the substantial number of genes that changed in expression in this network, many questions remain as to the effect this might have on cell migration. Currently, understanding the lysosome is particularly exciting as substantial interest is gathering in its potential role as a novel target for cancer therapies (Piao and Amaravadi, 2016). We have begun some preliminary investigations to discover whether the vesicle network is intact in Cdc42 null melanocytes by staining for various vesicular markers (Figure 7.3). We stained for WASH (WASP and SCAR homologue), the Arp2/3 activating protein that is localised at the surface of endosomes where it induces the formation of branched actin networks. Surprisingly, this revealed an intact endosomal network spread throughout the cell. Similarly, staining for EEA1 (early endosomal antigen 1), a marker of early endosomes and Rab7, a marker found on late endosomes, in knockout melanocytes revealed no abnormalities. Staining for clathrin to investigate sites of clathrin mediated endocytosis suggested increased levels in the peri-nuclear region, possibly underneath the Golgi.

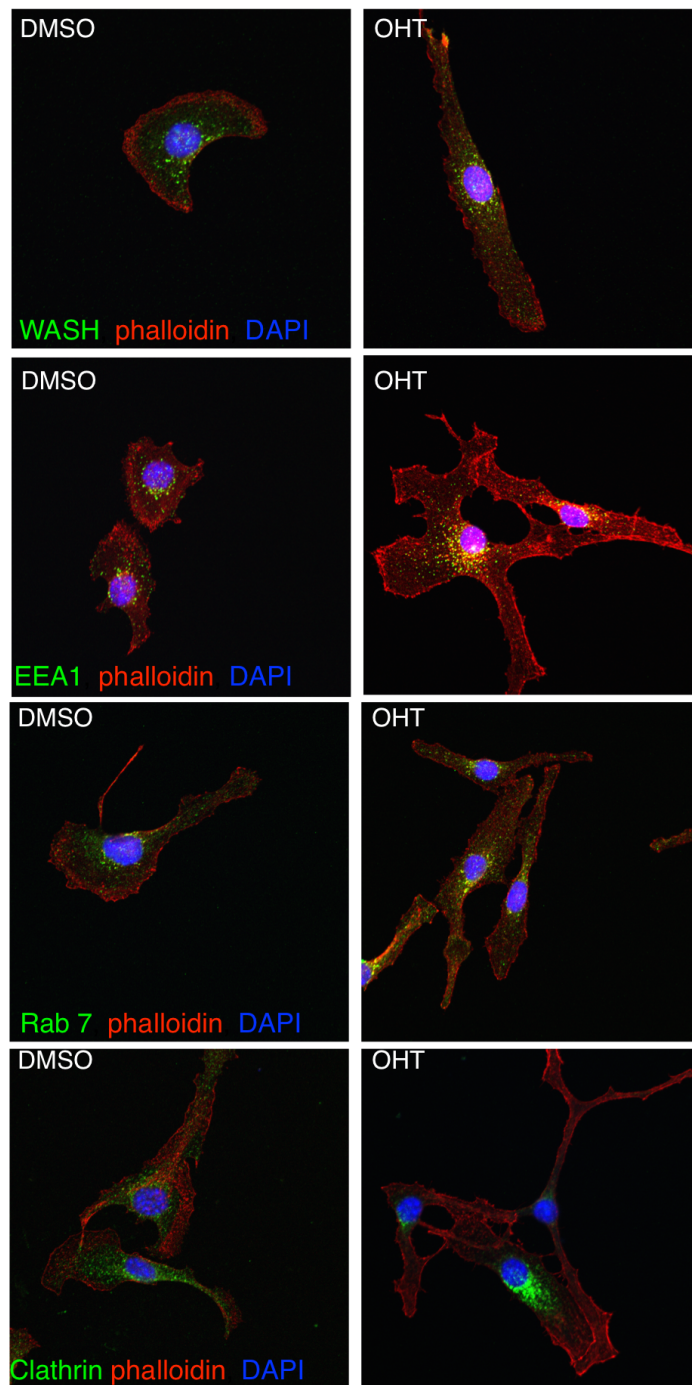


Figure 7.3 Staining for various markers of the vesicular network reveals no gross abnormalities

Confocal imaging of DMSO (left side) or OHT (right side) treated EW7 *Cdc42* f/f Cre-ERT2; *CDKN2*^{-/-} melanocytes, stained with phalloidin (red) to show F-actin and DAPI to highlight the nucleus with vesicular markers WASH, EEA1 (early endosomes), Rab7 (late endosomes) or clathrin (sites of endocytosis) in green.

In addition to this staining, and taking into account the up-regulation of multiple subunits of the V-ATPase complex in our RNA sequencing data, we wanted to investigate the intracellular pH of Cdc42 null melanocytes. We hypothesised that up-regulation of this complex could lead to an increase in the number of protons being pumped across internal membranes, leading to elevated vesicular acidification. We achieved this using the pHrodo green AM intracellular pH indicator (Thermo Fisher). This is a cell soluble fluorogenic probe, which is weakly fluorescent at neutral pH, but increasingly fluorescent as the pH drops. This probe was weakly fluorescent inside DMSO treated melanocytes, but sites of higher fluorescence could be seen inside the cytoplasm, most likely acidic vesicles (Figure 7.4A, top panel). Interestingly, the cytoplasm of OHT treated cells appeared brighter, and large bright clumps could be seen next to the nucleus (Figure 7.4A, bottom panel, green arrows). Preliminary measurements of the average fluorescent intensity of DMSO and OHT treated melanocytes after incubation with pHrodo suggests that Cdc42 null cells have an elevated pH in comparison to control cells (Figure 7.4B).

These preliminary findings suggest that despite up-regulation of genes associated with lysosomal pathways, the vesicular network in Cdc42 null cells is intact. It would be interesting to extend these findings by assessing the protein levels of the lysosomal genes found to be up-regulated, and by performing immunofluorescence staining against LAMP1 (lysosomal-associated membrane protein 1), to assess if the lysosomal network looks normal. In addition, it would be very interesting to further explore the large, acidic compartment highlighted by the pHrodo probe in Cdc42 knockout cells. To do this, these cells could be fixed and co-stained with Golgi, endoplasmic reticulum, V-ATPase and mitochondrial markers. We believe this compartment may be the Golgi. This is an interesting discovery given the emerging roles for Cdc42 at the Golgi, reviewed recently by Farhan et al (Farhan and Hsu, 2016). It is still unclear whether Cdc42 at the Golgi functions primarily to replenish Cdc42 at the plasma membrane, or whether these pools have a coordinating role, but blocking transport from the golgi to the plasma membrane decreases the activity of Cdc42 at the plasma membrane (Baschieri et al., 2014). Cdc42 can polarise transport at the Golgi to favour the anterograde direction by modulating the cargo sorting function of the COPI (Coat protein 1) complex (Park et al., 2015).

It is surprising therefore that the vesicular network appears to be largely unaffected in Cdc42 null melanocytes, however we have not confirmed whether the contents or sorting of these vesicles is altered. To our knowledge, there has not been any work regarding the link between Cdc42 and Golgi acidification. We believe it is possible that the absence of Cdc42 causes an up-regulation and accumulation of the V-ATPase complex in the Golgi, leading to its acidification. This could have drastic knock-on effects for the cells, as proteins would be unable to fold correctly at this level of acidity.

7.2.3 Which pathways link Cdc42 to adhesion dynamics?

One of the main questions arising from this study is which downstream effectors of Cdc42 play a part in controlling adhesion dynamics. Due to Cdc42's major role in controlling cell polarity, actin dynamics and gene expression, it is likely that there are many factors that link Cdc42 to this process. It is possible that Cdc42 controls the localisation and/or activation of key proteins involved in adhesion assembly and maturation. It would be intriguing to investigate the composition of adhesions in Cdc42 knockout cell lines. It would be particularly interesting to explore the cell surface levels of integrins $\alpha 4$ and $\beta 3$ using flow cytometry to discover if their down-regulation at the gene and protein level leads to less incorporation into adhesions. It would also be valuable to analyse melanoblast adhesion in skin explants through fixation and staining. It would be important to define whether controlling integrin expression levels is directly a function of Cdc42, or if this is a compensatory mechanism of the cells to long-term loss of Cdc42. This could be explored by rescuing integrin expression in melanocyte cell lines, or by exploring the effect of activating Cdc42 on integrin levels.

Our preliminary results which suggest that Cdc42 null melanoblasts may have a highly acidic Golgi. This could mean that components essential to build nascent adhesions get stuck or misfolded at this location, and are not transported to distant sites of adhesion in pseudopods.

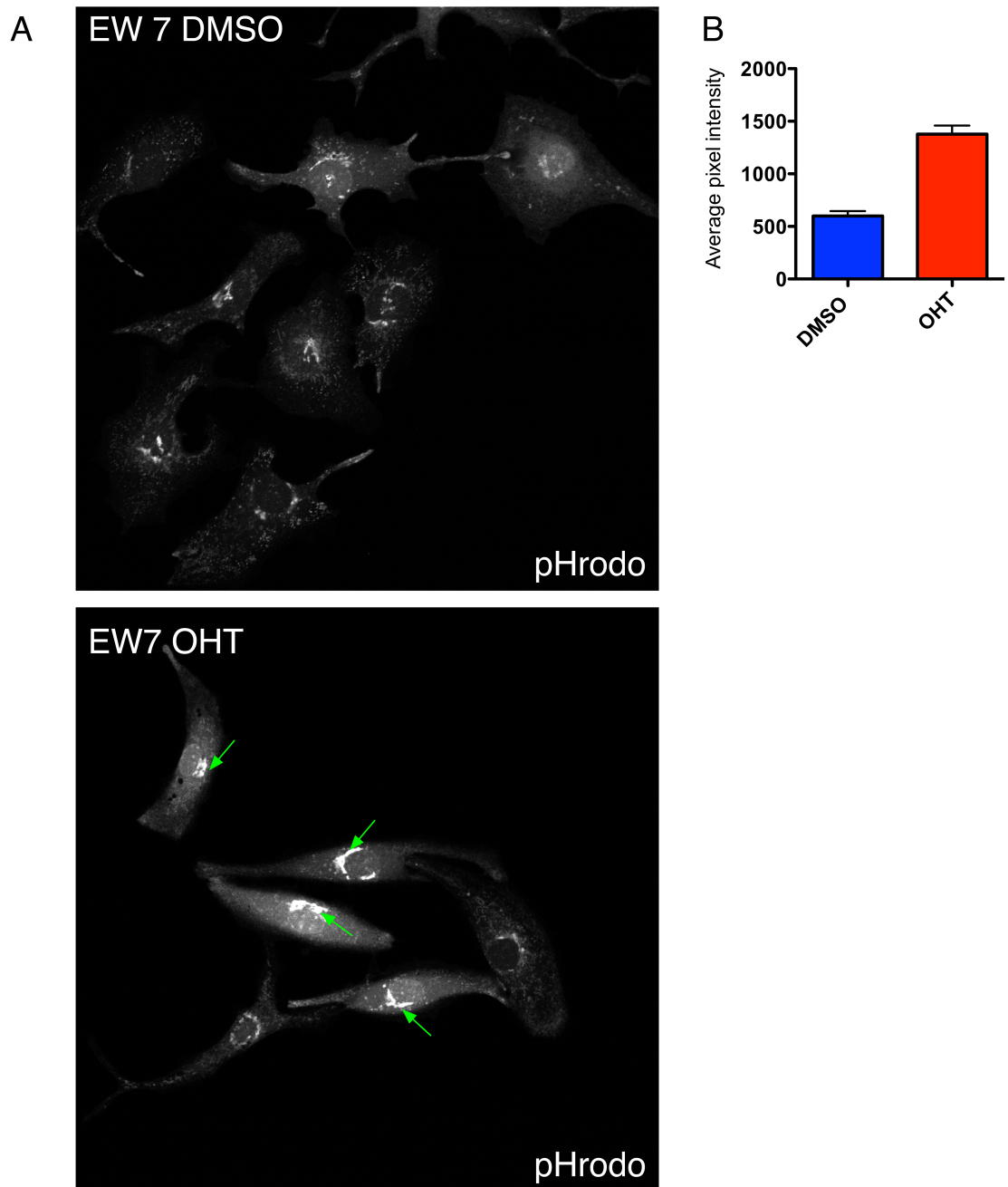


Figure 7.4 Cdc42 null melanocytes have a large, highly acidic compartment and overall have a higher pH than control cells

(A) Confocal images of EW7 *Cdc42* *f/f* Cre-ERT2; *CDKN2*^{-/-} melanocytes treated with DMSO or OHT after 30 minutes incubation with pHrodo green AM intracellular pH indicator. Higher fluorescence indicates acidic conditions, green arrows indicate highly acidic compartments. **(B)** Quantification of the average pixel intensity of DMSO and OHT treated cells in (A) as a read out of cellular pH. Measurements taken from 22 cells (n=1). Graph shows mean + SEM.

7.2.4 Does Cdc42 control invasion *in vivo*?

Our investigations showed that Cdc42 plays a role in the invasion of B16F10 melanoma cells into two different *in vitro* invasion assays. Having gained positive results from this preliminary study, it would be worthwhile extending it further into an *in vivo* melanoma metastasis study. In the absence of a good metastatic model for melanoma metastasis, these cells could initially be injected into the tail veins of mice, and their ability to colonise the lung analysed through histological analysis.

8 References

- ACKERMANN, J., FRUTSCHI, M., KALOULIS, K., MCKEE, T., TRUMPP, A. & BEERMANN, F. 2005. Metastasizing melanoma formation caused by expression of activated N-RasQ61K on an INK4a-deficient background. *Cancer Res*, 65, 4005-11.
- ADAMEYKO, I., LALLEMEND, F., AQUINO, J. B., PEREIRA, J. A., TOPILKO, P., MULLER, T., FRITZ, N., BELJAJEVA, A., MOCHII, M., LISTE, I., USOSKIN, D., SUTER, U., BIRCHMEIER, C. & ERNFORS, P. 2009. Schwann cell precursors from nerve innervation are a cellular origin of melanocytes in skin. *Cell*, 139, 366-79.
- AKSAN, I. & GODING, C. R. 1998. Targeting the microphthalmia basic helix-loop-helix-leucine zipper transcription factor to a subset of E-box elements in vitro and in vivo. *Mol Cell Biol*, 18, 6930-8.
- ALBELDA, S. M., METTE, S. A., ELDER, D. E., STEWART, R., DAMJANOVICH, L., HERLYN, M. & BUCK, C. A. 1990. Integrin distribution in malignant melanoma: association of the beta 3 subunit with tumor progression. *Cancer Res*, 50, 6757-64.
- ASPENSTRÖM, P. 2014. BAR domain proteins regulate Rho GTPase signaling. *Small GTPases*, 5, 7.
- BAILEY, C. M., MORRISON, J. A. & KULESA, P. M. 2012. Melanoma revives an embryonic migration program to promote plasticity and invasion. *Pigment Cell Melanoma Res*, 25, 573-83.
- BASCHIERI, F., CONFALONIERI, S., BERTALOT, G., DI FIORE, P. P., DIETMAIER, W., LEIST, M., CRESPO, P., MACARA, I. G. & FARHAN, H. 2014. Spatial control of Cdc42 signalling by a GM130-RasGRF complex regulates polarity and tumorigenesis. *Nat Commun*, 5, 4839.
- BASTOS, R. N., PENATE, X., BATES, M., HAMMOND, D. & BARR, F. A. 2012. CYK4 inhibits Rac1-dependent PAK1 and ARHGEF7 effector pathways during cytokinesis. *J Cell Biol*, 198, 865-80.
- BEATY, B. T. & CONDEELIS, J. 2014. Digging a little deeper: the stages of invadopodium formation and maturation. *Eur J Cell Biol*, 93, 438-44.
- BERGINSKI, M. E. & GOMEZ, S. M. 2013. The Focal Adhesion Analysis Server: a web tool for analyzing focal adhesion dynamics. *F1000Res*, 2, 68.
- BOUZAHZAH, B., ALBANESE, C., AHMED, F., PIXLEY, F., LISANTI, M. P., SEGALL, J. D., CONDEELIS, J., JOYCE, D., MINDEN, A., DER, C. J., CHAN, A., SYMONS, M. & PESTELL, R. G. 2001. Rho family GTPases regulate mammary epithelium cell growth and metastasis through distinguishable pathways. *Mol Med*, 7, 816-30.
- BRIDGEWATER, R. E., NORMAN, J. C. & CASWELL, P. T. 2012. Integrin trafficking at a glance. *J Cell Sci*, 125, 3695-701.
- CALDERWOOD, D. A. 2004. Integrin activation. *J Cell Sci*, 117, 657-66.
- CHEN, B., BRINKMANN, K., CHEN, Z., PAK, C. W., LIAO, Y., SHI, S., HENRY, L., GRISHIN, N. V., BOGDAN, S. & ROSEN, M. K. 2014. The WAVE regulatory complex links diverse receptors to the actin cytoskeleton. *Cell*, 156, 195-207.
- CHEN, F., MA, L., PARRINI, M. C., MAO, X., LOPEZ, M., WU, C., MARKS, P. W., DAVIDSON, L., KWIATKOWSKI, D. J., KIRCHHAUSEN, T., ORKIN, S. H., ROSEN, F. S., MAYER, B. J., KIRSCHNER, M. W. & ALT, F. W. 2000. Cdc42 is required for PIP(2)-induced actin polymerization and early development but not for cell viability. *Curr Biol*, 10, 758-65.

- CHIRCOP, M. 2014. Rho GTPases as regulators of mitosis and cytokinesis in mammalian cells. *Small GTPases*, 5.
- CHOU, M. M., MASUDA-ROBENS, J. M. & GUPTA, M. L. 2003. Cdc42 promotes G1 progression through p70 S6 kinase-mediated induction of cyclin E expression. *J Biol Chem*, 278, 35241-7.
- CHRISTOFORI, G. & SEMB, H. 1999. The role of the cell-adhesion molecule E-cadherin as a tumour-suppressor gene. *Trends Biochem Sci*, 24, 73-6.
- CHUN, J. S. & JACOBSON, B. S. 1992. Spreading of HeLa cells on a collagen substratum requires a second messenger formed by the lipoxygenase metabolism of arachidonic acid released by collagen receptor clustering. *Mol Biol Cell*, 3, 481-92.
- CHUN, J. S. & JACOBSON, B. S. 1993. Requirement for diacylglycerol and protein kinase C in HeLa cell-substratum adhesion and their feedback amplification of arachidonic acid production for optimum cell spreading. *Mol Biol Cell*, 4, 271-81.
- CHURCH, D. M., SCHNEIDER, V. A., GRAVES, T., AUGER, K., CUNNINGHAM, F., BOUK, N., CHEN, H. C., AGARWALA, R., MCLAREN, W. M., RITCHIE, G. R., ALBRACHT, D., KREMITZKI, M., ROCK, S., KOTKIEWICZ, H., KREMITZKI, C., WOLLAM, A., TRANI, L., FULTON, L., FULTON, R., MATTHEWS, L., WHITEHEAD, S., CHOW, W., TORRANCE, J., DUNN, M., HARDEN, G., THREADGOLD, G., WOOD, J., COLLINS, J., HEATH, P., GRIFFITHS, G., PELAN, S., GRAFHAM, D., EICHLER, E. E., WEINSTOCK, G., MARDIS, E. R., WILSON, R. K., HOWE, K., FLICEK, P. & HUBBARD, T. 2011. Modernizing reference genome assemblies. *PLoS Biol*, 9, e1001091.
- CZUCHRA, A., WU, X., MEYER, H., VAN HENGEL, J., SCHROEDER, T., GEFFERS, R., ROTTNER, K. & BRAKEBUSCH, C. 2005. Cdc42 is not essential for filopodium formation, directed migration, cell polarization, and mitosis in fibroblastoid cells. *Mol Biol Cell*, 16, 4473-84.
- DEAKIN, N. O. & TURNER, C. E. 2008. Paxillin comes of age. *J Cell Sci*, 121, 2435-44.
- DELMAS, V., MARTINOZZI, S., BOURGEOIS, Y., HOLZENBERGER, M. & LARUE, L. 2003. Cre-mediated recombination in the skin melanocyte lineage. *Genesis*, 36, 73-80.
- DEMALI, K. A., BARLOW, C. A. & BURRIDGE, K. 2002. Recruitment of the Arp2/3 complex to vinculin: coupling membrane protrusion to matrix adhesion. *J Cell Biol*, 159, 881-91.
- DEVREOTES, P. & HORWITZ, A. R. 2015. Signaling networks that regulate cell migration. *Cold Spring Harb Perspect Biol*, 7, a005959.
- DURGAN, J., KAJI, N., JIN, D. & HALL, A. 2011. Par6B and atypical PKC regulate mitotic spindle orientation during epithelial morphogenesis. *J Biol Chem*, 286, 12461-74.
- ELBEDIWI, A., VINCENT-MISTIAEN, Z. I., SPENCER-DENE, B., STONE, R. K., BOEING, S., WCULEK, S. K., CORDERO, J., TAN, E. H., RIDGWAY, R., BRUNTON, V. G., SAHAI, E., GERHARDT, H., BEHRENS, A., MALANCHI, I., SANSOM, O. J. & THOMPSON, B. J. 2016. Integrin signalling regulates YAP and TAZ to control skin homeostasis. *Development*, 143, 1674-87.
- ETIENNE-MANNEVILLE, S. 2004. Cdc42--the centre of polarity. *J Cell Sci*, 117, 1291-300.
- ETIENNE-MANNEVILLE, S. & HALL, A. 2001. Integrin-mediated activation of Cdc42 controls cell polarity in migrating astrocytes through PKCzeta. *Cell*, 106, 489-98.
- ETIENNE-MANNEVILLE, S. & HALL, A. 2002. Rho GTPases in cell biology. *Nature*, 420, 629-35.

- ETIENNE-MANNEVILLE, S. & HALL, A. 2003. Cdc42 regulates GSK-3 β and adenomatous polyposis coli to control cell polarity. *Nature*, 421, 753-6.
- ETIENNE-MANNEVILLE, S., MANNEVILLE, J. B., NICHOLLS, S., FERENCZI, M. A. & HALL, A. 2005. Cdc42 and Par6-PKC ζ regulate the spatially localized association of Dlg1 and APC to control cell polarization. *J Cell Biol*, 170, 895-901.
- FAIRN, G. D., HERMANSSON, M., SOMERHARJU, P. & GRINSTEIN, S. 2011. Phosphatidylserine is polarized and required for proper Cdc42 localization and for development of cell polarity. *Nat Cell Biol*, 13, 1424-30.
- FARHAN, H. & HSU, V. W. 2016. Cdc42 and Cellular Polarity: Emerging Roles at the Golgi. *Trends Cell Biol*, 26, 241-8.
- FIDYK, N., WANG, J. B. & CERIONE, R. A. 2006. Influencing cellular transformation by modulating the rates of GTP hydrolysis by Cdc42. *Biochemistry*, 45, 7750-62.
- FISHER, S., BARRY, A., ABREU, J., MINIE, B., NOLAN, J., DELOREY, T. M., YOUNG, G., FENNELL, T. J., ALLEN, A., AMBROGIO, L., BERLIN, A. M., BLUMENSTIEL, B., CIBULSKIS, K., FRIEDRICH, D., JOHNSON, R., JUHN, F., REILLY, B., SHAMMAS, R., STALKER, J., SYKES, S. M., THOMPSON, J., WALSH, J., ZIMMER, A., ZWIRKO, Z., GABRIEL, S., NICOL, R. & NUSBAUM, C. 2011. A scalable, fully automated process for construction of sequence-ready human exome targeted capture libraries. *Genome Biol*, 12, R1.
- FRIEDL, P. & WOLF, K. 2003. Tumour-cell invasion and migration: diversity and escape mechanisms. *Nat Rev Cancer*, 3, 362-74.
- FRITZ, G., BRACHETTI, C., BAHLMANN, F., SCHMIDT, M. & KAINA, B. 2002. Rho GTPases in human breast tumours: expression and mutation analyses and correlation with clinical parameters. *Br J Cancer*, 87, 635-44.
- FRITZ, G., JUST, I. & KAINA, B. 1999. Rho GTPases are over-expressed in human tumors. *Int J Cancer*, 81, 682-7.
- FUCHS, S., HERZOG, D., SUMARA, G., BUCHMANN-MOLLER, S., CIVENNI, G., WU, X., CHROSTEK-GRASHOFF, A., SUTER, U., RICCI, R., RELVAS, J. B., BRAKEBUSCH, C. & SOMMER, L. 2009. Stage-specific control of neural crest stem cell proliferation by the small rho GTPases Cdc42 and Rac1. *Cell Stem Cell*, 4, 236-47.
- GAO, L., BAI, L. & NAN, Q. 2013. Activation of Rho GTPase Cdc42 promotes adhesion and invasion in colorectal cancer cells. *Med Sci Monit Basic Res*, 19, 201-7.
- GARDEL, M. L., SCHNEIDER, I. C., ARATYN-SCHAUS, Y. & WATERMAN, C. M. 2010. Mechanical integration of actin and adhesion dynamics in cell migration. *Annu Rev Cell Dev Biol*, 26, 315-33.
- GENOVA, J. L., JONG, S., CAMP, J. T. & FEHON, R. G. 2000. Functional analysis of Cdc42 in actin filament assembly, epithelial morphogenesis, and cell signaling during *Drosophila* development. *Dev Biol*, 221, 181-94.
- GERSHON, T. R., OPPENHEIMER, O., CHIN, S. S. & GERALD, W. L. 2005. Temporally regulated neural crest transcription factors distinguish neuroectodermal tumors of varying malignancy and differentiation. *Neoplasia*, 7, 575-84.
- GIANNONE, G., DUBIN-THALER, B. J., DOBEREINER, H. G., KIEFFER, N., BRESNICK, A. R. & SHEETZ, M. P. 2004. Periodic lamellipodial contractions correlate with rearward actin waves. *Cell*, 116, 431-43.
- GJOERUP, O., LUKAS, J., BARTEK, J. & WILLUMSEN, B. M. 1998. Rac and Cdc42 are potent stimulators of E2F-dependent transcription capable of promoting retinoblastoma susceptibility gene product hyperphosphorylation. *J Biol Chem*, 273, 18812-8.

- GOEDHART, J., VAN WEEREN, L., HINK, M. A., VISCHER, N. O., JALINK, K. & GADELLA, T. W., JR. 2010. Bright cyan fluorescent protein variants identified by fluorescence lifetime screening. *Nat Methods*, 7, 137-9.
- GOKSOY, E., MA, Y. Q., WANG, X., KONG, X., PERERA, D., PLOW, E. F. & QIN, J. 2008. Structural basis for the autoinhibition of talin in regulating integrin activation. *Mol Cell*, 31, 124-33.
- GOTTA, M., ABRAHAM, M. C. & AHRINGER, J. 2001. CDC-42 controls early cell polarity and spindle orientation in *C. elegans*. *Curr Biol*, 11, 482-8.
- GUPTON, S. L. & WATERMAN-STORER, C. M. 2006. Spatiotemporal feedback between actomyosin and focal-adhesion systems optimizes rapid cell migration. *Cell*, 125, 1361-74.
- HAN, J., LIU, S., ROSE, D. M., SCHLAEPFER, D. D., MCDONALD, H. & GINSBERG, M. H. 2001. Phosphorylation of the integrin alpha 4 cytoplasmic domain regulates paxillin binding. *J Biol Chem*, 276, 40903-9.
- HANAHAH, D. & WEINBERG, R. A. 2000. The hallmarks of cancer. *Cell*, 100, 57-70.
- HARBURGER, D. S. & CALDERWOOD, D. A. 2009. Integrin signalling at a glance. *J Cell Sci*, 122, 159-63.
- HARI, L., BRAULT, V., KLEBER, M., LEE, H. Y., ILLE, F., LEIMEROOTH, R., PARATORE, C., SUTER, U., KEMLER, R. & SOMMER, L. 2002. Lineage-specific requirements of beta-catenin in neural crest development. *J Cell Biol*, 159, 867-80.
- HEASMAN, S. J. & RIDLEY, A. J. 2008. Mammalian Rho GTPases: new insights into their functions from in vivo studies. *Nat Rev Mol Cell Biol*, 9, 690-701.
- HIEMER, S. E., SZYMANIAK, A. D. & VARELAS, X. 2014. The transcriptional regulators TAZ and YAP direct transforming growth factor beta-induced tumorigenic phenotypes in breast cancer cells. *J Biol Chem*, 289, 13461-74.
- HINTON, A., BOND, S. & FORGAC, M. 2009. V-ATPase functions in normal and disease processes. *Pflugers Arch*, 457, 589-98.
- HO, H. Y., ROHATGI, R., LEBENSOHN, A. M., LE, M., LI, J., GYGI, S. P. & KIRSCHNER, M. W. 2004. Toca-1 mediates Cdc42-dependent actin nucleation by activating the N-WASP-WIP complex. *Cell*, 118, 203-16.
- HORTON, E. R., BYRON, A., ASKARI, J. A., NG, D. H., MILLON-FREMILLON, A., ROBERTSON, J., KOPER, E. J., PAUL, N. R., WARWOOD, S., KNIGHT, D., HUMPHRIES, J. D. & HUMPHRIES, M. J. 2015. Definition of a consensus integrin adhesome and its dynamics during adhesion complex assembly and disassembly. *Nat Cell Biol*, 17, 1577-87.
- HUANG DA, W., SHERMAN, B. T. & LEMPICKI, R. A. 2009. Systematic and integrative analysis of large gene lists using DAVID bioinformatics resources. *Nat Protoc*, 4, 44-57.
- HUANG, X. & SAINT-JEANNET, J. P. 2004. Induction of the neural crest and the opportunities of life on the edge. *Dev Biol*, 275, 1-11.
- HUMPHRIES, J. D., BYRON, A. & HUMPHRIES, M. J. 2006. Integrin ligands at a glance. *J Cell Sci*, 119, 3901-3.
- HUMPHRIES, J. D., PAUL, N. R., HUMPHRIES, M. J. & MORGAN, M. R. 2015. Emerging properties of adhesion complexes: what are they and what do they do? *Trends Cell Biol*, 25, 388-97.
- HYTONEN, V. P. & WEHRLE-HALLER, B. 2016. Mechanosensing in cell-matrix adhesions - Converting tension into chemical signals. *Exp Cell Res*, 343, 35-41.
- INSALL, R. H. & MACHESKY, L. M. 2009. Actin dynamics at the leading edge: from simple machinery to complex networks. *Dev Cell*, 17, 310-22.

- ITOH, R. E., KUROKAWA, K., OHBA, Y., YOSHIZAKI, H., MOCHIZUKI, N. & MATSUDA, M. 2002. Activation of rac and cdc42 video imaged by fluorescent resonance energy transfer-based single-molecule probes in the membrane of living cells. *Mol Cell Biol*, 22, 6582-91.
- JACQUEMET, G., HAMIDI, H. & IVASKA, J. 2015. Filopodia in cell adhesion, 3D migration and cancer cell invasion. *Curr Opin Cell Biol*, 36, 23-31.
- JAFFE, A. B., KAJI, N., DURGAN, J. & HALL, A. 2008. Cdc42 controls spindle orientation to position the apical surface during epithelial morphogenesis. *J Cell Biol*, 183, 625-33.
- JOHNSON, D. I. & PRINGLE, J. R. 1990. Molecular characterization of CDC42, a *Saccharomyces cerevisiae* gene involved in the development of cell polarity. *J Cell Biol*, 111, 143-52.
- JOHNSON, E., SEACHRIST, D. D., DELEON-RODRIGUEZ, C. M., LOZADA, K. L., MIEDLER, J., ABDUL-KARIM, F. W. & KERI, R. A. 2010. HER2/ErbB2-induced breast cancer cell migration and invasion require p120 catenin activation of Rac1 and Cdc42. *J Biol Chem*, 285, 29491-501.
- JOHNSON, H. E., KING, S. J., ASOKAN, S. B., ROTTY, J. D., BEAR, J. E. & HAUGH, J. M. 2015. F-actin bundles direct the initiation and orientation of lamellipodia through adhesion-based signaling. *J Cell Biol*, 208, 443-55.
- JOHNSON, J. M., JIN, M. & LEW, D. J. 2011. Symmetry breaking and the establishment of cell polarity in budding yeast. *Curr Opin Genet Dev*, 21, 740-6.
- JORDAN, S. A. & JACKSON, I. J. 2000. MGF (KIT ligand) is a chemokinetic factor for melanoblast migration into hair follicles. *Dev Biol*, 225, 424-36.
- KIM, D., PERTEA, G., TRAPNELL, C., PIMENTEL, H., KELLEY, R. & SALZBERG, S. L. 2013. TopHat2: accurate alignment of transcriptomes in the presence of insertions, deletions and gene fusions. *Genome Biol*, 14, R36.
- KLEIN, O., CLEMENTS, A., MENZIES, A. M., O'TOOLE, S., KEFFORD, R. F. & LONG, G. V. 2013. BRAF inhibitor activity in V600R metastatic melanoma. *Eur J Cancer*, 49, 1073-9.
- KOVAR, D. R. & POLLARD, T. D. 2004. Progressing actin: Formin as a processive elongation machine. *Nat Cell Biol*, 6, 1158-9.
- KRAYNOV, V. S., CHAMBERLAIN, C., BOKOCH, G. M., SCHWARTZ, M. A., SLABAUGH, S. & HAHN, K. M. 2000. Localized Rac activation dynamics visualized in living cells. *Science*, 290, 333-7.
- KUMASAKA, M., SATO, H., SATO, S., YAJIMA, I. & YAMAMOTO, H. 2004. Isolation and developmental expression of *Mitf* in *Xenopus laevis*. *Dev Dyn*, 230, 107-13.
- LANGMEAD, B. & SALZBERG, S. L. 2012. Fast gapped-read alignment with Bowtie 2. *Nat Methods*, 9, 357-9.
- LARUE, L., DE VUYST, F. & DELMAS, V. 2013. Modeling melanoblast development. *Cell Mol Life Sci*, 70, 1067-79.
- LE CLAINCHE, C. & CARLIER, M. F. 2008. Regulation of actin assembly associated with protrusion and adhesion in cell migration. *Physiol Rev*, 88, 489-513.
- LI, A., DAWSON, J. C., FORERO-VARGAS, M., SPENCE, H. J., YU, X., KONIG, I., ANDERSON, K. & MACHESKY, L. M. 2010. The actin-bundling protein fascin stabilizes actin in invadopodia and potentiates protrusive invasion. *Curr Biol*, 20, 339-45.
- LI, A., MA, Y., YU, X., MORT, R. L., LINDSAY, C. R., STEVENSON, D., STRATHDEE, D., INSALL, R. H., CHERNOFF, J., SNAPPER, S. B., JACKSON, I. J., LARUE, L., SANSOM, O. J. & MACHESKY, L. M. 2011. Rac1 drives melanoblast organization during mouse development by orchestrating pseudopod-driven motility and cell-cycle progression. *Dev Cell*, 21, 722-34.

- LI, A., MORTON, J. P., MA, Y., KARIM, S. A., ZHOU, Y., FALLER, W. J., WOODHAM, E. F., MORRIS, H. T., STEVENSON, R. P., JUIN, A., JAMIESON, N. B., MACKAY, C. J., CARTER, C. R., LEUNG, H. Y., YAMASHIRO, S., BLYTH, K., SANSOM, O. J. & MACHESKY, L. M. 2014. Fascin is regulated by slug, promotes progression of pancreatic cancer in mice, and is associated with patient outcomes. *Gastroenterology*, 146, 1386-96 e1-17.
- LIN, R., BAGRODIA, S., CERIONE, R. & MANOR, D. 1997. A novel Cdc42Hs mutant induces cellular transformation. *Curr Biol*, 7, 794-7.
- LISTER, J. A., ROBERTSON, C. P., LEPAGE, T., JOHNSON, S. L. & RAIBLE, D. W. 1999. nacre encodes a zebrafish microphthalmia-related protein that regulates neural-crest-derived pigment cell fate. *Development*, 126, 3757-67.
- LIU, Y., WANG, Y., ZHANG, Y., MIAO, Y., ZHAO, Y., ZHANG, P. X., JIANG, G. Y., ZHANG, J. Y., HAN, Y., LIN, X. Y., YANG, L. H., LI, Q. C., ZHAO, C. & WANG, E. H. 2009. Abnormal expression of p120-catenin, E-cadherin, and small GTPases is significantly associated with malignant phenotype of human lung cancer. *Lung Cancer*, 63, 375-82.
- LOUGHNA, S. & HENDERSON, D. 2007. Methodologies for staining and visualisation of beta-galactosidase in mouse embryos and tissues. *Methods Mol Biol*, 411, 1-11.
- LOVE, M. I., HUBER, W. & ANDERS, S. 2014. Moderated estimation of fold change and dispersion for RNA-seq data with DESeq2. *Genome Biol*, 15, 550.
- LOW, B. C., PAN, C. Q., SHIVASHANKAR, G. V., BERSHADSKY, A., SUDOL, M. & SHEETZ, M. 2014. YAP/TAZ as mechanosensors and mechanotransducers in regulating organ size and tumor growth. *FEBS Lett*, 588, 2663-70.
- MA, Y., LI, A., FALLER, W. J., LIBERTINI, S., FIORITO, F., GILLESPIE, D. A., SANSOM, O. J., YAMASHIRO, S. & MACHESKY, L. M. 2013. Fascin 1 is transiently expressed in mouse melanoblasts during development and promotes migration and proliferation. *Development*, 140, 2203-11.
- MACHACEK, M., HODGSON, L., WELCH, C., ELLIOTT, H., PERTZ, O., NALBANT, P., ABELL, A., JOHNSON, G. L., HAHN, K. M. & DANUSER, G. 2009. Coordination of Rho GTPase activities during cell protrusion. *Nature*, 461, 99-103.
- MACHESKY, L. M., ATKINSON, S. J., AMPE, C., VANDEKERCKHOVE, J. & POLLARD, T. D. 1994. Purification of a cortical complex containing two unconventional actins from *Acanthamoeba* by affinity chromatography on profilin-agarose. *J Cell Biol*, 127, 107-15.
- MACKENZIE, M. A., JORDAN, S. A., BUDD, P. S. & JACKSON, I. J. 1997. Activation of the receptor tyrosine kinase Kit is required for the proliferation of melanoblasts in the mouse embryo. *Dev Biol*, 192, 99-107.
- MACNEVIN, C. J., TOUTCHKINE, A., MARSTON, D. J., HSU, C. W., TSYGANKOV, D., LI, L., LIU, B., QI, T., NGUYEN, D. V. & HAHN, K. M. 2016. Ratiometric Imaging Using a Single Dye Enables Simultaneous Visualization of Rac1 and Cdc42 Activation. *J Am Chem Soc*, 138, 2571-5.
- MARSHANSKY, V. & FUTAI, M. 2008. The V-type H⁺-ATPase in vesicular trafficking: targeting, regulation and function. *Curr Opin Cell Biol*, 20, 415-26.
- MAYER, T. C. 1973. The migratory pathway of neural crest cells into the skin of mouse embryos. *Dev Biol*, 34, 39-46.
- MEDIC, S. & ZIMAN, M. 2009. PAX3 across the spectrum: from melanoblast to melanoma. *Crit Rev Biochem Mol Biol*, 44, 85-97.
- MINDELL, J. A. 2012. Lysosomal acidification mechanisms. *Annu Rev Physiol*, 74, 69-86.

- MITCHISON, T. J. & CRAMER, L. P. 1996. Actin-based cell motility and cell locomotion. *Cell*, 84, 371-9.
- MOASE, C. E. & TRASLER, D. G. 1992. Spotch locus mouse mutants: models for neural tube defects and Waardenburg syndrome type I in humans. *J Med Genet*, 29, 145-51.
- MORREALE, A., VENKATESAN, M., MOTT, H. R., OWEN, D., NIETLISPACH, D., LOWE, P. N. & LAUE, E. D. 2000. Structure of Cdc42 bound to the GTPase binding domain of PAK. *Nat Struct Biol*, 7, 384-8.
- MORT, R. L., HAY, L. & JACKSON, I. J. 2010. Ex vivo live imaging of melanoblast migration in embryonic mouse skin. *Pigment Cell Melanoma Res*, 23, 299-301.
- MORT, R. L., KEIGHREN, M., HAY, L. & JACKSON, I. J. 2014. Ex vivo culture of mouse embryonic skin and live-imaging of melanoblast migration. *J Vis Exp*.
- MORT, R. L., ROSS, R. J., HAINEY, K. J., HARRISON, O. J., KEIGHREN, M. A., LANDINI, G., BAKER, R. E., PAINTER, K. J., JACKSON, I. J. & YATES, C. A. 2016. Reconciling diverse mammalian pigmentation patterns with a fundamental mathematical model. *Nat Commun*, 7, 10288.
- MUINONEN-MARTIN, A. J., SUSANTO, O., ZHANG, Q., SMETHURST, E., FALLER, W. J., VELTMAN, D. M., KALNA, G., LINDSAY, C., BENNETT, D. C., SANSOM, O. J., HERD, R., JONES, R., MACHESKY, L. M., WAKELAM, M. J., KNECHT, D. A. & INSALL, R. H. 2014. Melanoma cells break down LPA to establish local gradients that drive chemotactic dispersal. *PLoS Biol*, 12, e1001966.
- MULLER, D. W. & BOSSERHOFF, A. K. 2008. Integrin beta 3 expression is regulated by let-7a miRNA in malignant melanoma. *Oncogene*, 27, 6698-706.
- NAKAYAMA, A., NGUYEN, M. T., CHEN, C. C., OPDECAMP, K., HODGKINSON, C. A. & ARNHEITER, H. 1998. Mutations in microphthalmia, the mouse homolog of the human deafness gene MITF, affect neuroepithelial and neural crest-derived melanocytes differently. *Mech Dev*, 70, 155-66.
- NISHIMURA, T., YAMAGUCHI, T., KATO, K., YOSHIZAWA, M., NABESHIMA, Y., OHNO, S., HOSHINO, M. & KAIBUCHI, K. 2005. PAR-6-PAR-3 mediates Cdc42-induced Rac activation through the Rac GEFs STEF/Tiam1. *Nat Cell Biol*, 7, 270-7.
- NOBES, C. D. & HALL, A. 1995. Rho, rac, and cdc42 GTPases regulate the assembly of multimolecular focal complexes associated with actin stress fibers, lamellipodia, and filopodia. *Cell*, 81, 53-62.
- NOBES, C. D. & HALL, A. 1999. Rho GTPases control polarity, protrusion, and adhesion during cell movement. *J Cell Biol*, 144, 1235-44.
- NOVAK, A., GUO, C., YANG, W., NAGY, A. & LOBE, C. G. 2000. Z/EG, a double reporter mouse line that expresses enhanced green fluorescent protein upon Cre-mediated excision. *Genesis*, 28, 147-55.
- OCEGUERA-YANEZ, F., KIMURA, K., YASUDA, S., HIGASHIDA, C., KITAMURA, T., HIRAOKA, Y., HARAGUCHI, T. & NARUMIYA, S. 2005. Ect2 and MgcRacGAP regulate the activation and function of Cdc42 in mitosis. *J Cell Biol*, 168, 221-32.
- OLSON, M. F., ASHWORTH, A. & HALL, A. 1995. An essential role for Rho, Rac, and Cdc42 GTPases in cell cycle progression through G1. *Science*, 269, 1270-2.
- OLSON, M. F. & SAHAI, E. 2009. The actin cytoskeleton in cancer cell motility. *Clin Exp Metastasis*, 26, 273-87.
- OPDECAMP, K., NAKAYAMA, A., NGUYEN, M. T., HODGKINSON, C. A., PAVAN, W. J. & ARNHEITER, H. 1997. Melanocyte development in vivo and in neural

- crest cell cultures: crucial dependence on the Mitf basic-helix-loop-helix-zipper transcription factor. *Development*, 124, 2377-86.
- PARK, S. Y., YANG, J. S., SCHMIDER, A. B., SOBERMAN, R. J. & HSU, V. W. 2015. Coordinated regulation of bidirectional COPI transport at the Golgi by CDC42. *Nature*, 521, 529-32.
- PELLETIER, A. J., BODARY, S. C. & LEVINSON, A. D. 1992. Signal transduction by the platelet integrin alpha IIb beta 3: induction of calcium oscillations required for protein-tyrosine phosphorylation and ligand-induced spreading of stably transfected cells. *Mol Biol Cell*, 3, 989-98.
- PETRIE, R. J., KOO, H. & YAMADA, K. M. 2014. Generation of compartmentalized pressure by a nuclear piston governs cell motility in a 3D matrix. *Science*, 345, 1062-5.
- PETRIE, R. J. & YAMADA, K. M. 2016. Multiple mechanisms of 3D migration: the origins of plasticity. *Curr Opin Cell Biol*, 42, 7-12.
- PIAO, S. & AMARAVADI, R. K. 2016. Targeting the lysosome in cancer. *Ann N Y Acad Sci*, 1371, 45-54.
- PICCOLO, S., DUPONT, S. & CORDENONSI, M. 2014. The biology of YAP/TAZ: hippo signaling and beyond. *Physiol Rev*, 94, 1287-312.
- PICKERING, K., ALVES-SILVA, J., GOBERDHAN, D. & MILLARD, T. H. 2013. Par3/Bazooka and phosphoinositides regulate actin protrusion formation during *Drosophila* dorsal closure and wound healing. *Development*, 140, 800-9.
- PLUMMER, R. S., SHEA, C. R., NELSON, M., POWELL, S. K., FREEMAN, D. M., DAN, C. P. & LANG, D. 2008. PAX3 expression in primary melanomas and nevi. *Mod Pathol*, 21, 525-30.
- POLLARD, T. D. & COOPER, J. A. 2009. Actin, a central player in cell shape and movement. *Science*, 326, 1208-12.
- PRAGER-KHOUTORSKY, M., LICHTENSTEIN, A., KRISHNAN, R., RAJENDRAN, K., MAYO, A., KAM, Z., GEIGER, B. & BERSHADSKY, A. D. 2011. Fibroblast polarization is a matrix-rigidity-dependent process controlled by focal adhesion mechanosensing. *Nat Cell Biol*, 13, 1457-65.
- PRICE, L. S., LENG, J., SCHWARTZ, M. A. & BOKOCH, G. M. 1998. Activation of Rac and Cdc42 by integrins mediates cell spreading. *Mol Biol Cell*, 9, 1863-71.
- RAFTOPOULOU, M. & HALL, A. 2004. Cell migration: Rho GTPases lead the way. *Dev Biol*, 265, 23-32.
- RAMSAY, A. G., KEPLER, M. D., JAZAYERI, M., THOMAS, G. J., PARSONS, M., VIOLETTE, S., WEINREB, P., HART, I. R. & MARSHALL, J. F. 2007a. HS1-associated protein X-1 regulates carcinoma cell migration and invasion via clathrin-mediated endocytosis of integrin alphavbeta6. *Cancer Res*, 67, 5275-84.
- RAMSAY, A. G., MARSHALL, J. F. & HART, I. R. 2007b. Integrin trafficking and its role in cancer metastasis. *Cancer Metastasis Rev*, 26, 567-78.
- RATH, S., LIEBL, J., FURST, R., VOLLMAR, A. M. & ZÄHLER, S. 2014. Regulation of endothelial signaling and migration by v-ATPase. *Angiogenesis*, 17, 587-601.
- REBHUN, R. B., CHENG, H., GERSHENWALD, J. E., FAN, D., FIDLER, I. J. & LANGLEY, R. R. 2010. Constitutive expression of the alpha4 integrin correlates with tumorigenicity and lymph node metastasis of the B16 murine melanoma. *Neoplasia*, 12, 173-82.
- REGINENSI, A., SCOTT, R. P., GREGORIEFF, A., BAGHERIE-LACHIDAN, M., CHUNG, C., LIM, D. S., PAWSON, T., WRANA, J. & MCNEILL, H. 2013. Yap- and

- Cdc42-dependent nephrogenesis and morphogenesis during mouse kidney development. *PLoS Genet*, 9, e1003380.
- REYMOND, N., IM, J. H., GARG, R., VEGA, F. M., BORDA D'AGUA, B., RIOU, P., COX, S., VALDERRAMA, F., MUSCHEL, R. J. & RIDLEY, A. J. 2012. Cdc42 promotes transendothelial migration of cancer cells through beta1 integrin. *J Cell Biol*, 199, 653-68.
- RIDLEY, A. J. 2015. Rho GTPase signalling in cell migration. *Curr Opin Cell Biol*, 36, 103-12.
- RIDLEY, A. J. & HALL, A. 1992. The small GTP-binding protein rho regulates the assembly of focal adhesions and actin stress fibers in response to growth factors. *Cell*, 70, 389-99.
- RIEDL, J., CREVENNA, A. H., KESSENBROCK, K., YU, J. H., NEUKIRCHEN, D., BISTA, M., BRADKE, F., JENNE, D., HOLAK, T. A., WERB, Z., SIXT, M. & WEDLICH-SOLDNER, R. 2008. Lifeact: a versatile marker to visualize F-actin. *Nat Methods*, 5, 605-7.
- SAKURAI-YAGETA, M., RECCHI, C., LE DEZ, G., SIBARITA, J. B., DAVIET, L., CAMONIS, J., D'SOUZA-SCHOREY, C. & CHAVRIER, P. 2008. The interaction of IQGAP1 with the exocyst complex is required for tumor cell invasion downstream of Cdc42 and RhoA. *J Cell Biol*, 181, 985-98.
- SCHACHTNER, H., LI, A., STEVENSON, D., CALAMINUS, S. D., THOMAS, S. G., WATSON, S. P., SIXT, M., WEDLICH-SOLDNER, R., STRATHDEE, D. & MACHESKY, L. M. 2012. Tissue inducible Lifeact expression allows visualization of actin dynamics in vivo and ex vivo. *Eur J Cell Biol*, 91, 923-9.
- SCHADENDORF, D., GAWLIK, C., HANEY, U., OSTMEIER, H., SUTER, L. & CZARNETZKI, B. M. 1993. Tumour progression and metastatic behaviour in vivo correlates with integrin expression on melanocytic tumours. *J Pathol*, 170, 429-34.
- SCHMIDT, A. & HALL, A. 2002. Guanine nucleotide exchange factors for Rho GTPases: turning on the switch. *Genes Dev*, 16, 1587-609.
- SCHOLL, F. A., KAMARASHEV, J., MURMANN, O. V., GEERTSEN, R., DUMMER, R. & SCHAFFER, B. W. 2001. PAX3 is expressed in human melanomas and contributes to tumor cell survival. *Cancer Res*, 61, 823-6.
- SERRANO, M., LEE, H., CHIN, L., CORDON-CARDO, C., BEACH, D. & DEPINHO, R. A. 1996. Role of the INK4a locus in tumor suppression and cell mortality. *Cell*, 85, 27-37.
- SERRELS, B., SERRELS, A., BRUNTON, V. G., HOLT, M., MCLEAN, G. W., GRAY, C. H., JONES, G. E. & FRAME, M. C. 2007. Focal adhesion kinase controls actin assembly via a FERM-mediated interaction with the Arp2/3 complex. *Nat Cell Biol*, 9, 1046-56.
- SHIMIZU, Y., ROSE, D. M. & GINSBERG, M. H. 1999. Integrins in the immune system. *Adv Immunol*, 72, 325-80.
- SILVER, D. L., HOU, L. & PAVAN, W. J. 2006. The genetic regulation of pigment cell development. *Adv Exp Med Biol*, 589, 155-69.
- SINHA, S. & YANG, W. 2008. Cellular signaling for activation of Rho GTPase Cdc42. *Cell Signal*, 20, 1927-34.
- SPORN, M. B. 1996. The war on cancer. *Lancet*, 347, 1377-81.
- STEINERT, G., SCHOLCH, S., NIEMIETZ, T., IWATA, N., GARCIA, S. A., BEHRENS, B., VOIGT, A., KLOOR, M., BENNER, A., BORK, U., RAHBARI, N. N., BUCHLER, M. W., STOECKLEIN, N. H., WEITZ, J. & KOCH, M. 2014. Immune escape and survival mechanisms in circulating tumor cells of colorectal cancer. *Cancer Res*, 74, 1694-704.

- STEINGRIMSSON, E., COPELAND, N. G. & JENKINS, N. A. 2004. Melanocytes and the microphthalmia transcription factor network. *Annu Rev Genet*, 38, 365-411.
- SWAMINATHAN, V., FISCHER, R. S. & WATERMAN, C. M. 2016. The FAK-Arp2/3 interaction promotes leading edge advance and haptosensing by coupling nascent adhesions to lamellipodia actin. *Mol Biol Cell*, 27, 1085-100.
- TACHIBANA, M., KOBAYASHI, Y. & MATSUSHIMA, Y. 2003. Mouse models for four types of Waardenburg syndrome. *Pigment Cell Res*, 16, 448-54.
- TADOKORO, S., SHATTIL, S. J., ETO, K., TAI, V., LIDDINGTON, R. C., DE PEREDA, J. M., GINSBERG, M. H. & CALDERWOOD, D. A. 2003. Talin binding to integrin beta tails: a final common step in integrin activation. *Science*, 302, 103-6.
- TAKEDA, K., YASUMOTO, K., TAKADA, R., TAKADA, S., WATANABE, K., UDONO, T., SAITO, H., TAKAHASHI, K. & SHIBAHARA, S. 2000. Induction of melanocyte-specific microphthalmia-associated transcription factor by Wnt-3a. *J Biol Chem*, 275, 14013-6.
- TEILLET, M. A. & LE DOUARIN, N. 1970. [The migration of pigmentary cells studies by the method of heterospecific grafts of neural tube in bird embryo]. *C R Acad Sci Hebd Seances Acad Sci D*, 270, 3095-8.
- THIERY, J. P., ACLOQUE, H., HUANG, R. Y. & NIETO, M. A. 2009. Epithelial-mesenchymal transitions in development and disease. *Cell*, 139, 871-90.
- THOMAS, A. J. & ERICKSON, C. A. 2008. The making of a melanocyte: the specification of melanoblasts from the neural crest. *Pigment Cell Melanoma Res*, 21, 598-610.
- TUCCI, M. G., LUCARINI, G., BRANCORSINI, D., ZIZZI, A., PUGNALONI, A., GIACCHETTI, A., RICOTTI, G. & BIAGINI, G. 2007. Involvement of E-cadherin, beta-catenin, Cdc42 and CXCR4 in the progression and prognosis of cutaneous melanoma. *Br J Dermatol*, 157, 1212-6.
- UNBEKANDT, M. & OLSON, M. F. 2014. The actin-myosin regulatory MRCK kinases: regulation, biological functions and associations with human cancer. *J Mol Med (Berl)*, 92, 217-25.
- VARELAS, X. 2014. The Hippo pathway effectors TAZ and YAP in development, homeostasis and disease. *Development*, 141, 1614-26.
- VEGA, F. M. & RIDLEY, A. J. 2008. Rho GTPases in cancer cell biology. *FEBS Lett*, 582, 2093-101.
- VUORI, K. & RUOSLAHTI, E. 1993. Activation of protein kinase C precedes alpha 5 beta 1 integrin-mediated cell spreading on fibronectin. *J Biol Chem*, 268, 21459-62.
- WANG, J. B., ERICKSON, J. W., FUJI, R., RAMACHANDRAN, S., GAO, P., DINAVAHI, R., WILSON, K. F., AMBROSIO, A. L., DIAS, S. M., DANG, C. V. & CERIONE, R. A. 2010. Targeting mitochondrial glutaminase activity inhibits oncogenic transformation. *Cancer Cell*, 18, 207-19.
- WILKINSON, S., PATERSON, H. F. & MARSHALL, C. J. 2005. Cdc42-MRCK and Rho-ROCK signalling cooperate in myosin phosphorylation and cell invasion. *Nat Cell Biol*, 7, 255-61.
- WINOGRAD-KATZ, S. E., FASSLER, R., GEIGER, B. & LEGATE, K. R. 2014. The integrin adhesome: from genes and proteins to human disease. *Nat Rev Mol Cell Biol*, 15, 273-88.
- WOLF, K., TE LINDERT, M., KRAUSE, M., ALEXANDER, S., TE RIET, J., WILLIS, A. L., HOFFMAN, R. M., FIGDOR, C. G., WEISS, S. J. & FRIEDL, P. 2013. Physical limits of cell migration: control by ECM space and nuclear deformation and tuning by proteolysis and traction force. *J Cell Biol*, 201, 1069-84.

- WONG, S., GUO, W. H. & WANG, Y. L. 2014. Fibroblasts probe substrate rigidity with filopodia extensions before occupying an area. *Proc Natl Acad Sci U S A*, 111, 17176-81.
- WOODHAM, E. F. & MACHESKY, L. M. 2014. Polarised cell migration: intrinsic and extrinsic drivers. *Curr Opin Cell Biol*, 30, 25-32.
- WU, Y. I., FREY, D., LUNGU, O. I., JAEHRIG, A., SCHLICHTING, I., KUHLMAN, B. & HAHN, K. M. 2009. A genetically encoded photoactivatable Rac controls the motility of living cells. *Nature*, 461, 104-8.
- YAJIMA, I., BELLOIR, E., BOURGEOIS, Y., KUMASAKA, M., DELMAS, V. & LARUE, L. 2006. Spatiotemporal gene control by the Cre-ERT2 system in melanocytes. *Genesis*, 44, 34-43.
- YAMAGUCHI, H., LORENZ, M., KEMPIAK, S., SARMIENTO, C., CONIGLIO, S., SYMONS, M., SEGALL, J., EDDY, R., MIKI, H., TAKENAWA, T. & CONDEELIS, J. 2005. Molecular mechanisms of invadopodium formation: the role of the N-WASP-Arp2/3 complex pathway and cofilin. *J Cell Biol*, 168, 441-52.
- YOON, S. O., SHIN, S. & MERCURIO, A. M. 2005. Hypoxia stimulates carcinoma invasion by stabilizing microtubules and promoting the Rab11 trafficking of the alpha6beta4 integrin. *Cancer Res*, 65, 2761-9.
- YU, X., ZECH, T., MCDONALD, L., GONZALEZ, E. G., LI, A., MACPHERSON, I., SCHWARZ, J. P., SPENCE, H., FUTTO, K., TIMPSON, P., NIXON, C., MA, Y., ANTON, I. M., VISEGRADY, B., INSALL, R. H., OIEN, K., BLYTH, K., NORMAN, J. C. & MACHESKY, L. M. 2012. N-WASP coordinates the delivery and F-actin-mediated capture of MT1-MMP at invasive pseudopods. *J Cell Biol*, 199, 527-44.
- ZANCONATO, F., CORDENONSI, M. & PICCOLO, S. 2016. YAP/TAZ at the Roots of Cancer. *Cancer Cell*, 29, 783-803.
- ZHU, X., WANG, J., MORIGUCHI, K., LIOW, L. T., AHMED, S., KAVERINA, I. & MURATA-HORI, M. 2011. Proper regulation of Cdc42 activity is required for tight actin concentration at the equator during cytokinesis in adherent mammalian cells. *Exp Cell Res*, 317, 2384-9.
- ZIEGLER, W. H., LIDDINGTON, R. C. & CRITCHLEY, D. R. 2006. The structure and regulation of vinculin. *Trends Cell Biol*, 16, 453-60.

9 Appendix

Supplementary video 1 Division is extended in Cdc42 null melanoblasts due to a defect in cytokinesis

Movie showing the division of control (Ctl) and Cdc42 null (Cdc42 f/f) melanoblasts in skin explants from rounding up through to the separation of daughter cells. Images taken every 5 minutes, video played at 8 frames per second.

Supplementary video 2 Cdc42 null melanoblasts have an elongated, bipolar morphology and move more slowly through skin explants.

Movie of skin explant from Z/EG^{+/-} expressing embryos at E15.5. Confocal section of control (Ctl) and Cdc42 null (Cdc42 f/f) melanoblasts moving through the epidermal layer of the skin. Images taken 5 minutes, video played at 15 frames per second.

Supplementary video 3 Actin bursts can be seen at the tips of Cdc42 null pseudopods

Movie of lifeact expressing control (Ctl) and Cdc42 null (Cdc42 f/f) melanoblasts moving through the embryo skin epidermis. Orange areas show bursts of actin. Images taken every minute, video played at 8 frames per second

Supplementary video 4 Cdc42 knock-out melanocytes are extended and bipolar and are unable to form lamellipods

Time lapse movies of DMSO or OHT treated Cdc42 f/f Cre-ERT2; CDKN2^{-/-} primary melanocyte cells (EW7) on fibronectin primary melanocyte lines migrating on fibronectin. Images taken every 15 minutes, video played at 8 frames per second.

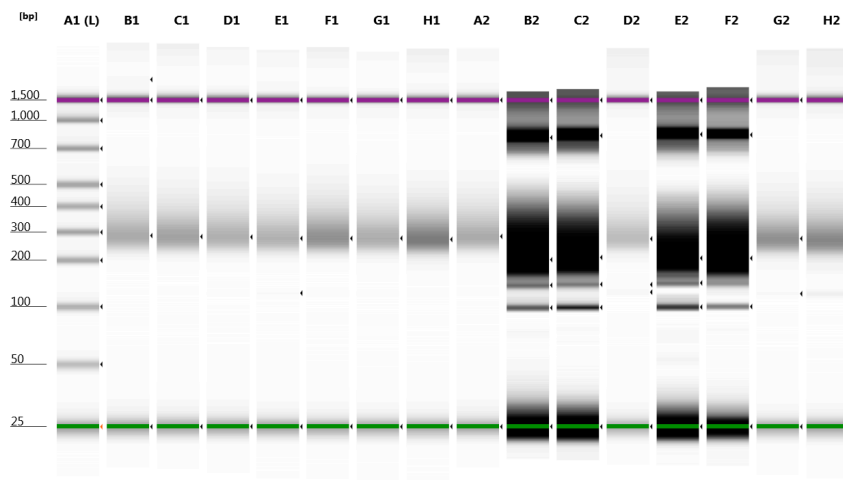
Supplementary video 5 Division is extended in Cdc42 null melanocytes due to a defect in cytokinesis

Time-lapse imaging showing division of DMSO (Ctl) or OHT (Cdc42 f/f) treated Cdc42 f/f Cre-ERT2; CDKN2^{-/-} primary melanocytes (EW7). Division counted from from rounding up through to the separation of daughter cells. Images taken every 15 minutes, video played at 2 frames per second.

RNA Sequencing Quality Check

EW1 EW2.1 DMSO (Repeat1)
 EW2 EW2.1 DMSO (Repeat2)
 EW3 EW2.1 OHT (Repeat1)
 EW4 EW2.1 OHT (Repeat2)
 EW5 EW2.2 DMSO (Repeat1)
 EW6 EW2.2 DMSO (Repeat2)
 EW7 EW2.2 OHT (Repeat1)
 EW8 EW2.2 OHT (Repeat2)

Gel Images

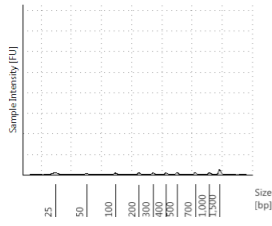


Default image (Contrast 179%), Image is Scaled to view larger Molecular Weight range

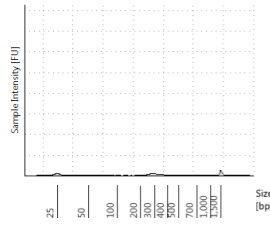
Sample Info

Well	Conc. [ng/ul]	Sample Description	Alert	Observations
A1	21.6	Ladder		Ladder
B1	11.3	EW1		
C1	11.8	EW2		
D1	9.95	EW3		
E1	10.3	EW4		
F1	16.9	EW5		
G1	11.3	EW6		
H1	20.1	EW7		
A2	11.1	EW8		
B2	142	HOM1		
C2	125	HOM2		
D2	9.20	HOM3		
E2	95.3	HOM4		
F2	117	WT1		
G2	15.3	WT2		
H2	16.5	WT3		

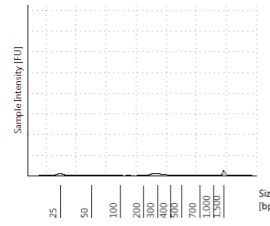
A1: Ladder



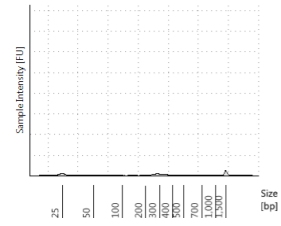
B1: EW1



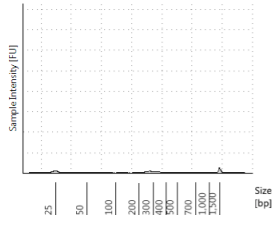
C1: EW2



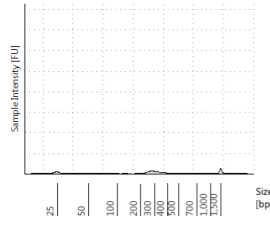
D1: EW3



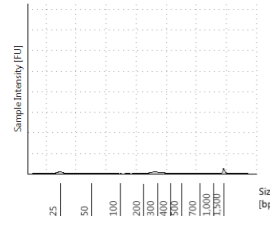
E1: EW4



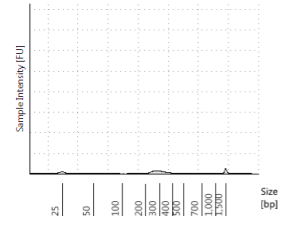
F1: EW5



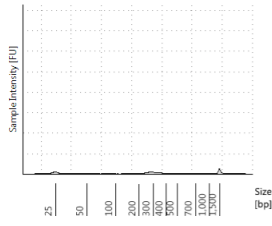
G1: EW6



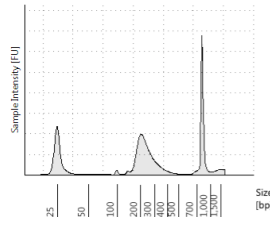
H1: EW7



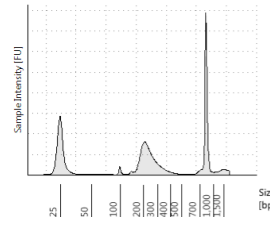
A2: EW8



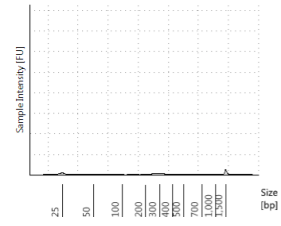
B2: HOM1



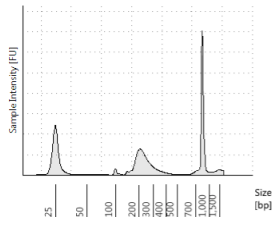
C2: HOM2



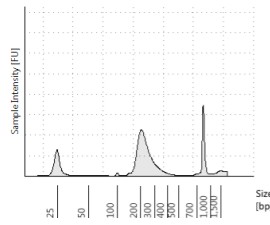
D2: HOM3



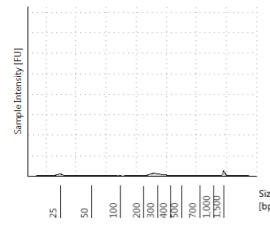
E2: HOM4



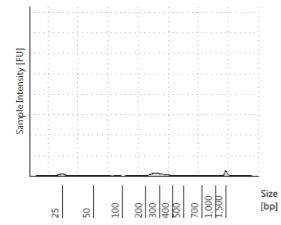
F2: WT1

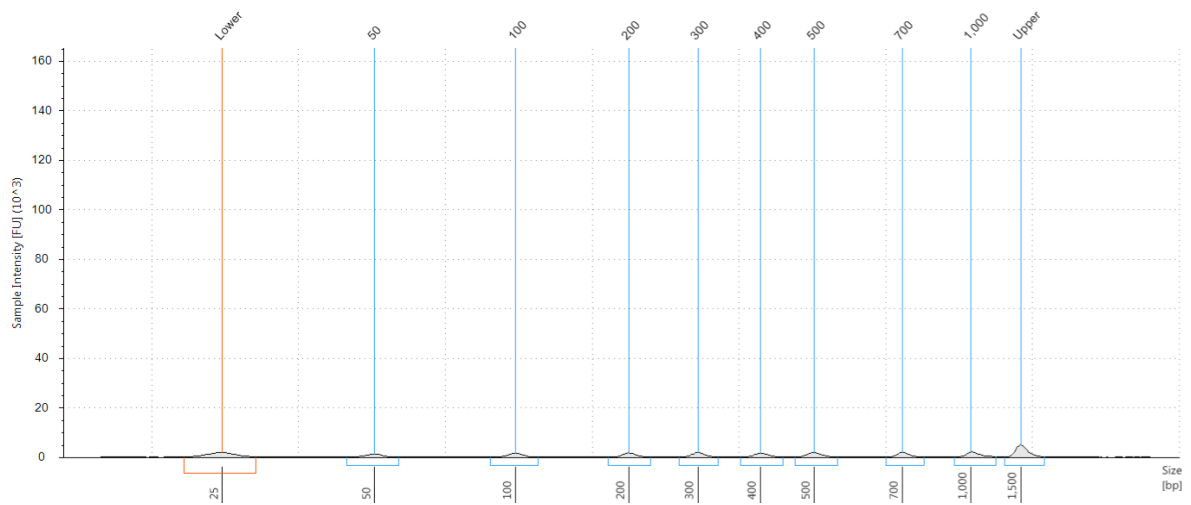


G2: WT2



H2: WT3

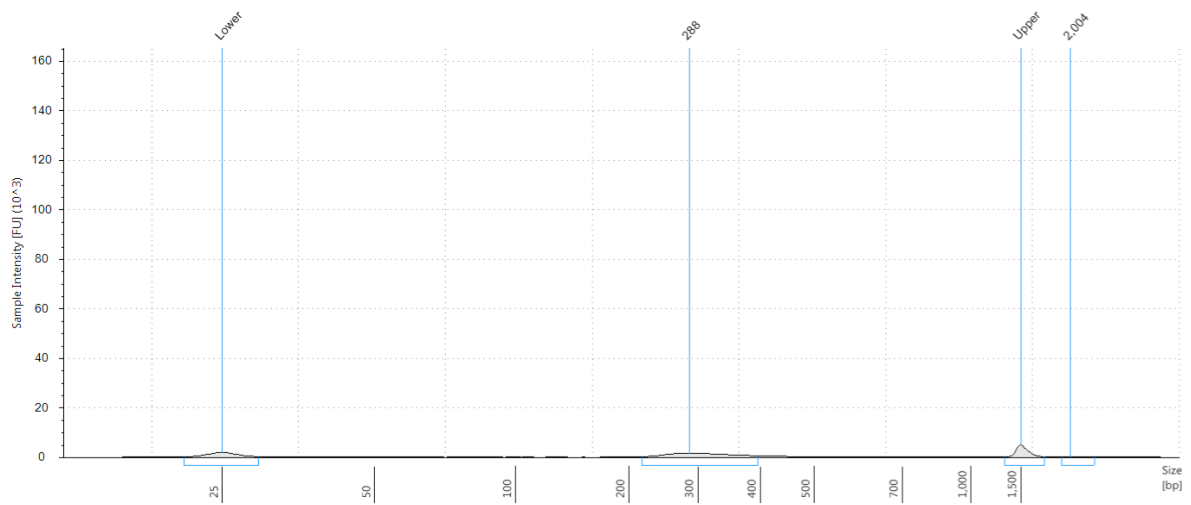


A1: Ladder**Sample Table**

Well	Conc. [ng/ul]	Sample Description	Alert	Observations
A1	21.6	Ladder		Ladder

Peak Table

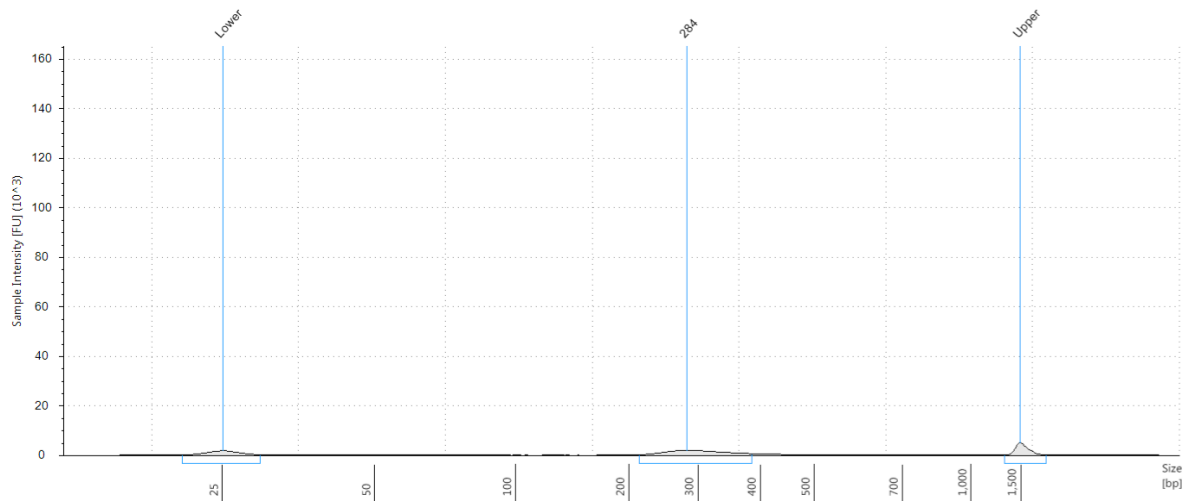
Size [bp]	Calibrated Conc. [ng/ul]	Assigned Conc. [ng/ul]	Peak Molarity [nmol/l]	% Integrated Area	Peak Comment	Observations
25	5.85	-	360	-		Lower Marker
50	2.39	-	73.6	11.09		
100	2.56	-	39.4	11.89		
200	2.64	-	20.3	12.25		
300	2.65	-	13.6	12.28		
400	2.56	-	9.85	11.88		
500	2.92	-	8.97	13.52		
700	2.70	-	5.94	12.52		
1,000	3.14	-	4.83	14.57		
1,500	6.50	6.50	6.67	-		Upper Marker

B1: EW1**Sample Table**

Well	Conc. [ng/ul]	Sample Description	Alert	Observations
B1	11.3	EW1		

Peak Table

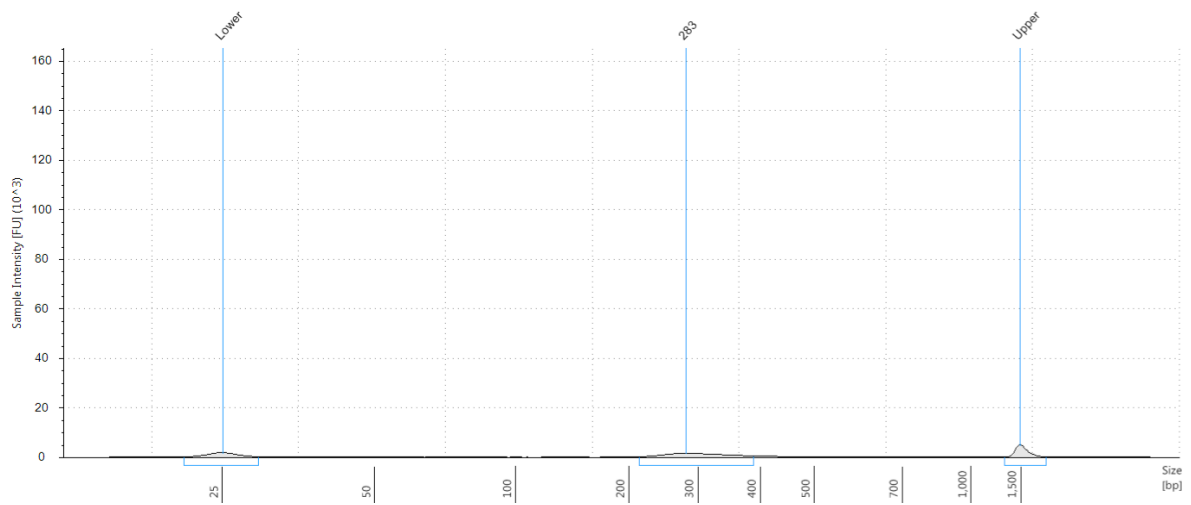
Size [bp]	Calibrated Conc. [ng/ul]	Assigned Conc. [ng/ul]	Peak Molarity [nmol/l]	% Integrated Area	Peak Comment	Observations
25	6.42	-	395	-		Lower Marker
288	11.1	-	59.5	98.25		
1,500	6.50	6.50	6.67	-		Upper Marker
2,004	0.199	-	0.153	1.75		

C1: EW2**Sample Table**

Well	Conc. [ng/ul]	Sample Description	Alert	Observations
C1	11.8	EW2		

Peak Table

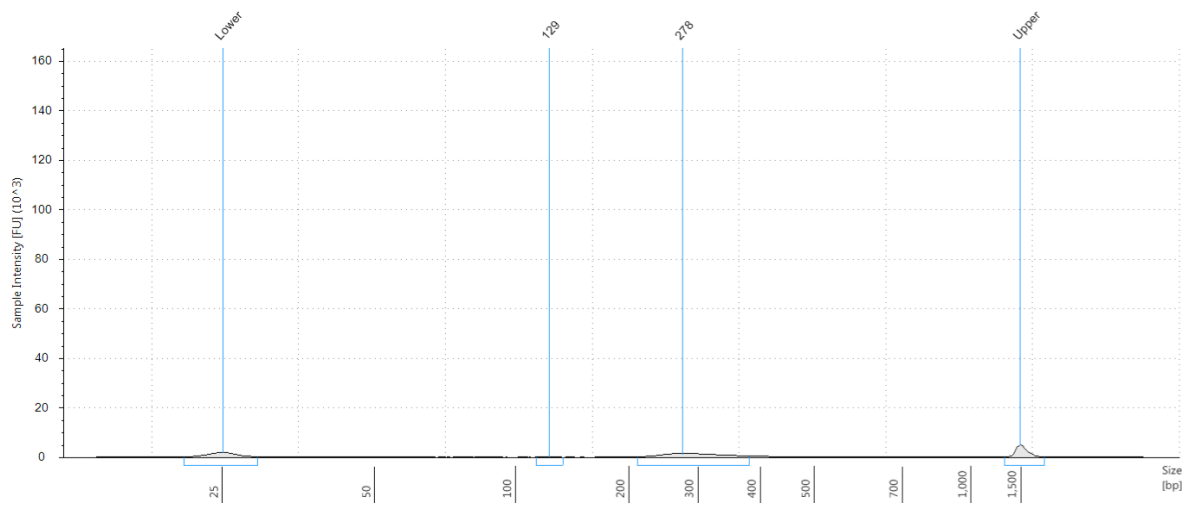
Size [bp]	Calibrated Conc. [ng/ul]	Assigned Conc. [ng/ul]	Peak Molarity [nmol/l]	% Integrated Area	Peak Comment	Observations
25	5.98	-	368	-		Lower Marker
284	11.8	-	64.1	100.00		
1,500	6.50	6.50	6.67	-		Upper Marker

D1: EW3**Sample Table**

Well	Conc. [ng/ul]	Sample Description	Alert	Observations
D1	9.95	EW3		

Peak Table

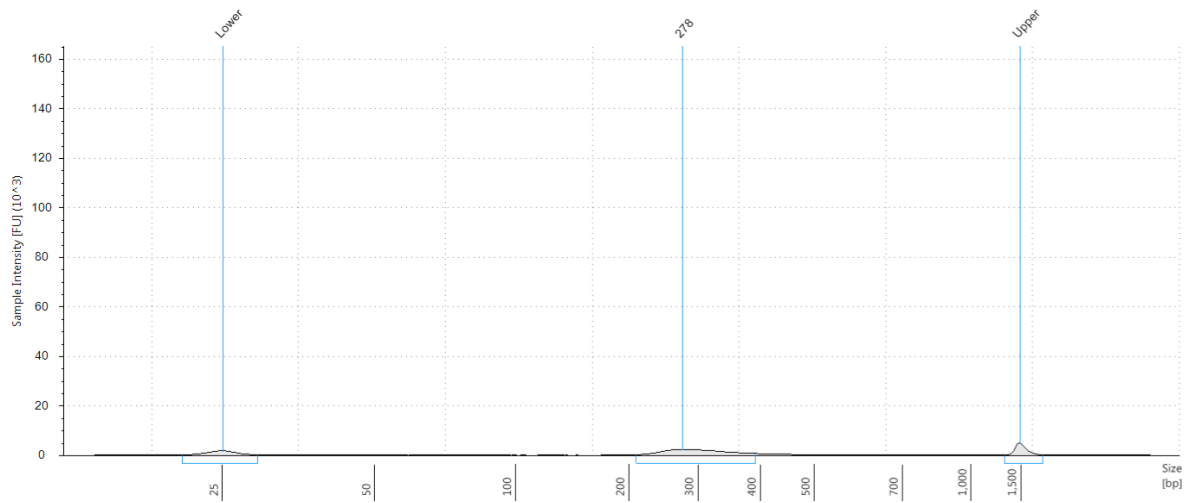
Size [bp]	Calibrated Conc. [ng/ul]	Assigned Conc. [ng/ul]	Peak Molarity [nmol/l]	% Integrated Area	Peak Comment	Observations
25	5.99	-	369	-		Lower Marker
283	9.95	-	54.1	100.00		
1,500	6.50	6.50	6.67	-		Upper Marker

E1: EW4**Sample Table**

Well	Conc. [ng/ul]	Sample Description	Alert	Observations
E1	10.3	EW4		

Peak Table

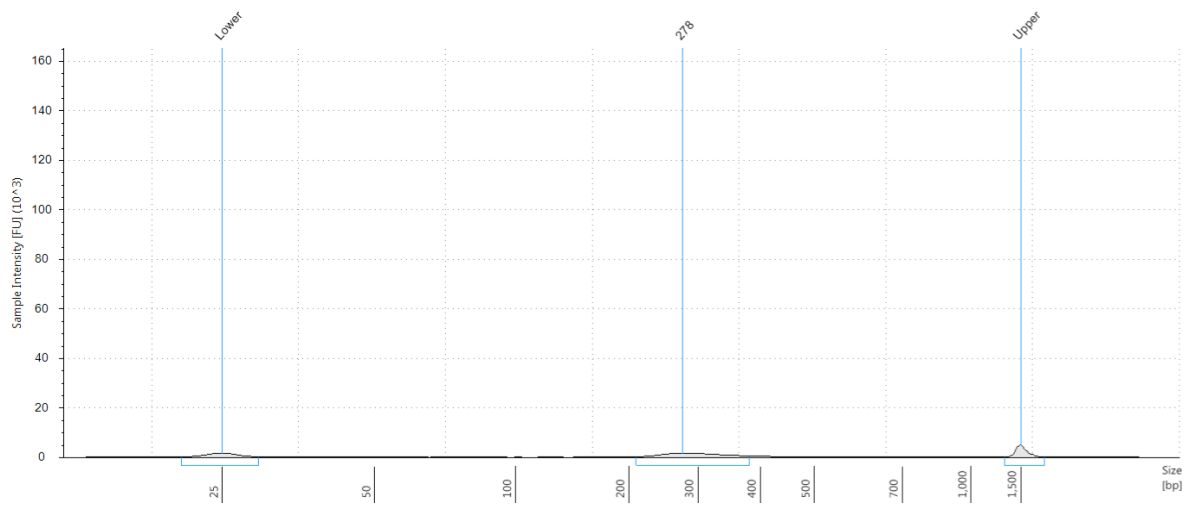
Size [bp]	Calibrated Conc. [ng/ul]	Assigned Conc. [ng/ul]	Peak Molarity [nmol/l]	% Integrated Area	Peak Comment	Observations
25	6.41	-	394	-		Lower Marker
129	0.0766	-	0.911	0.74		
278	10.2	-	56.5	99.26		
1,500	6.50	6.50	6.67	-		Upper Marker

F1: EW5**Sample Table**

Well	Conc. [ng/ul]	Sample Description	Alert	Observations
F1	16.9	EW5		

Peak Table

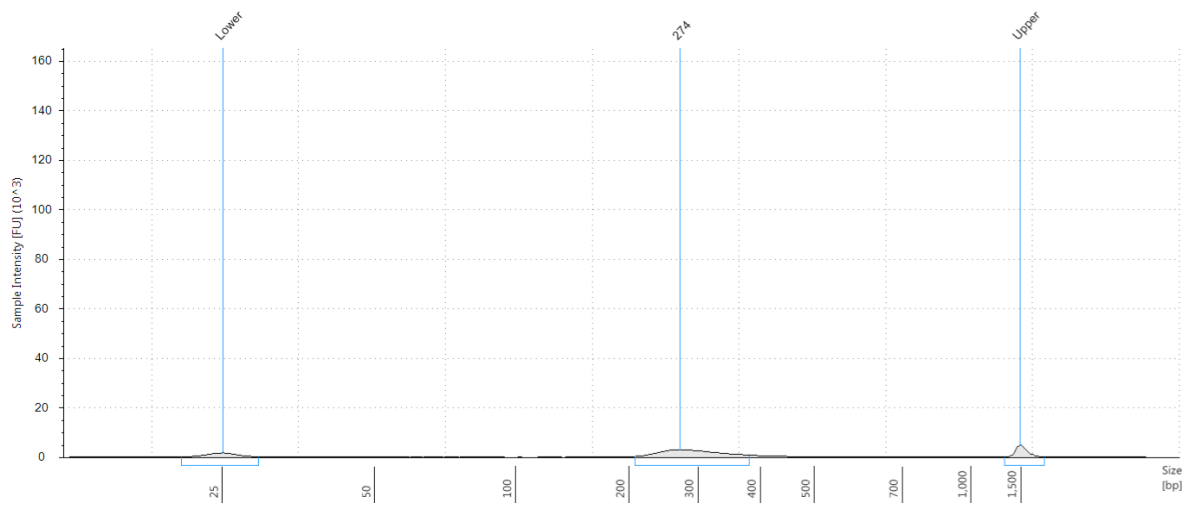
Size [bp]	Calibrated Conc. [ng/ul]	Assigned Conc. [ng/ul]	Peak Molarity [nmol/l]	% Integrated Area	Peak Comment	Observations
25	6.27	-	386	-		Lower Marker
278	16.9	-	93.6	100.00		
1,500	6.50	6.50	6.67	-		Upper Marker

G1: EW6**Sample Table**

Well	Conc. [ng/ul]	Sample Description	Alert	Observations
G1	11.3	EW6		

Peak Table

Size [bp]	Calibrated Conc. [ng/ul]	Assigned Conc. [ng/ul]	Peak Molarity [nmol/l]	% Integrated Area	Peak Comment	Observations
25	6.31	-	388	-		Lower Marker
278	11.3	-	62.3	100.00		
1,500	6.50	6.50	6.67	-		Upper Marker

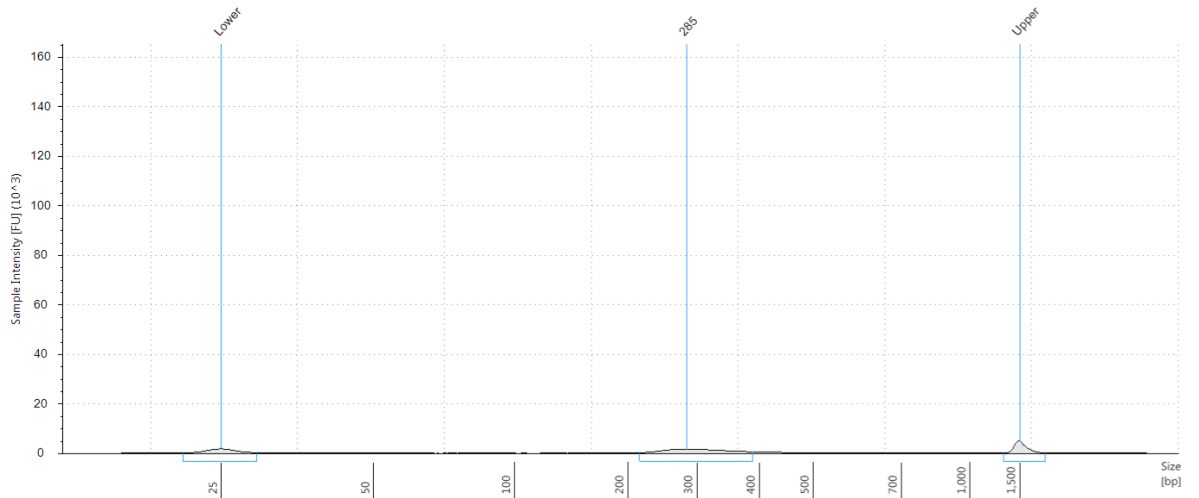
H1: EW7**Sample Table**

Well	Conc. [ng/ul]	Sample Description	Alert	Observations
H1	20.1	EW7		

Peak Table

Size [bp]	Calibrated Conc. [ng/ul]	Assigned Conc. [ng/ul]	Peak Molarity [nmol/l]	% Integrated Area	Peak Comment	Observations
25	6.17	-	380	-		Lower Marker
274	20.1	-	113	100.00		
1,500	6.50	6.50	6.67	-		Upper Marker

A2: EW8



Sample Table

Well	Conc. [ng/ul]	Sample Description	Alert	Observations
A2	11.1	EW8		

Peak Table

Size [bp]	Calibrated Conc. [ng/ul]	Assigned Conc. [ng/ul]	Peak Molarity [nmol/l]	% Integrated Area	Peak Comment	Observations
25	5.81	-	357	-		Lower Marker
285	11.1	-	59.8	100.00		
1,500	6.50	6.50	6.67	-		Upper Marker